Development of a kidney-on-a-chip model for compound screening and transport studies
Vormann, M.K.

Citation
Vormann, M. K. (2021, September 9). *Development of a kidney-on-a-chip model for compound screening and transport studies*. Retrieved from https://hdl.handle.net/1887/3209238

Cover Page

Universiteit Leiden

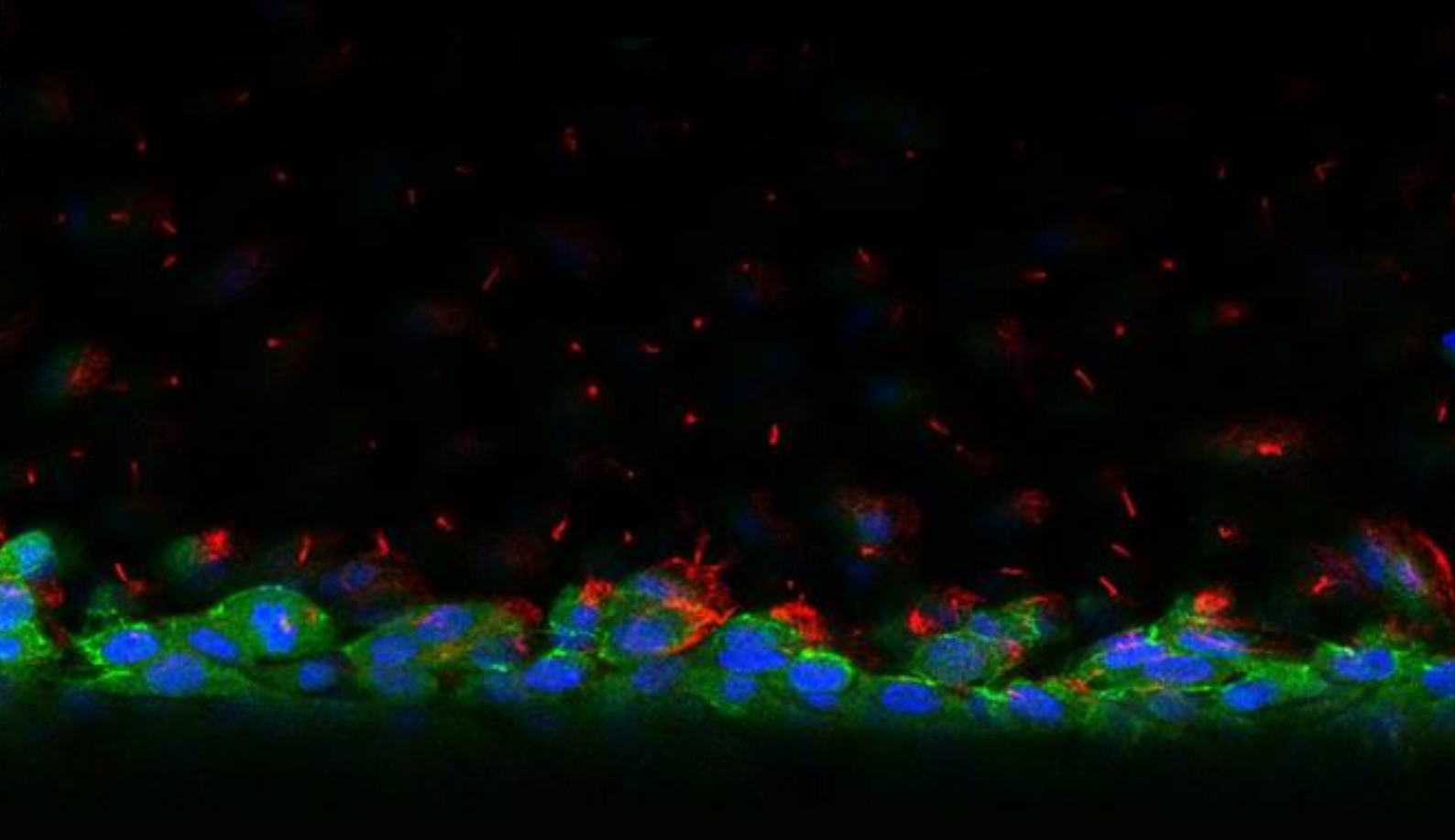**Author**: Vormann, M.K.
Title: Development of a kidney-on-a-chip model for compound screening and transport studies
Issue Date: 2021-09-09

Development of a Kidney-on-a-Chip Model

for Compound Screening and Transport Studies

M.K. Vormann

Development of a Kidney-on-a-Chip Model

for Compound Screening and Transport Studies

Marianne Katharina Vormann

Development of a Kidney-on-a-Chip Model

for Compound Screening and Transport Studies

Proefschrift

ter verkrijging van

de graad van doctor aan de Universiteit Leiden,

op gezag van rector magnificus prof.dr.ir. H. Bijl,

volgens besluit van het college voor promoties

te verdedigen op donderdag 9 september 2021

klokke 10.00 uur

door

Marianne Katharina Vormann

geboren te Gräfelfing in 1986

Promotor:

Prof. Dr. Thomas Hankemeier

Co-Promotor:

Dr. Henriette L. Lanz

Promotiecommissie:

Prof. Dr. H. Irth (chair)

Prof. Dr. J.A. Bouwstra (secretary)

Prof. Dr. R. Masereeuw, Universiteit Utrecht

Prof. Dr. L. Suter-Dick, Fachhochschule Nordwestschweiz

Prof. Dr. B. van de Water, Universiteit Leiden

Prof. Dr. A.J. van Zonneveld, Universiteit Leiden

Content

Chapter 1

Introduction

1

8

Introduction

For safety determination of new drugs, animal studies are still required by the U.S. Food and Drug Administration (FDA) prior to clinical trials on humans [1]. Also, the European Medicines Agency (EMA) and the Japanese Pharmaceuticals and Medical Devices Agency (PMDA) require animal studies before allowing the release of new drugs [2], [3]. However, the EMA recently published a document which includes opportunities for alternatives [2] and since 2013 animal testing is not allowed anymore in Europe in cosmetic products when known ingredients are used [4], [5]. The fact that more than 80% of the drugs which were tested in animal models failed during clinical trials in humans [6] supports the huge impetus to refine and replace animal testing, which is also known as the 3Rs: Replace, Reduce and Refine. The goal of this endeavor is replacing animal testing whenever possible, and reducing the number of animal tests. When strictly necessary, refining animal tests in order to use a minimum amount of experiments and animals is desirable [7]. The reasoning of using animals for drug testing goes back to the declaration of Helsinki 1964, which recommends animal testing when appropriate and when the welfare of animals is respected [8]. The benefits of animal testing are obvious: In animals, drugs can be tested in complete organisms. In several other types of drug testing, such as in cell cultures dishes, testing can only be performed on a single or on several cell types, depending on the culture-possibilities. Animals possess functioning vascular networks which supply the tested organ(s) with nutrients and oxygen. This also has the additional benefit of these vascular networks eliminating waste products. An example of a combination between animal testing and human tissue is when immunodeficient mice can be used for xenografting. Here, human tissue is implanted into an animal model which then has the possibility to vascularize the tissue. These models are known as patient-derived xenografts [9].

Nonetheless, considering the surprisingly huge number of clinical failures which could not have been predicted by animal testing, alternatives need to be investigated as Human cells sometimes respond quite differently to certain substances (medication or cosmetics) than animals cells [10]. Other important reasons why different testing possibilities should be considered are grounded in ethics: not only because of compassion for the animals used for testing but also for humans who participate in clinical trial studies and first patients that receive the new drug [11], [12].

For reducing animal testing primarily in the early stages of pre-clinical testing, 2D cell models have already been used for years [13]. The problem with these 2D models is not difficult to grasp: Cells are cultured on flat plastic or glass surfaces in an environment which does not resemble their natural environment very accurately. In a living organism, cells are encapsulated by a complex network of an extracellular matrix (ECM) in which they grow in close proximity to several other cell types [14].

In this thesis, a 3D *in vitro* model of the kidney will be developed, which should be able to play a big future role in not only the reduction and replacement of animal testing, but also to make medical compound testing more predictable for humans and more cost efficient. The model should be available for pharmaceutical, industry, and academic research to be utilized for studying nephrotoxicity, compound excretion, drug-drug interaction studies, disease modeling, and tests regarding the safety of cosmetics and chemicals.

The importance of the kidney during drug research

Kidney disease is a huge problem in our society which causes many deaths, mainly in hospitalized patients. Each year worldwide around 1.7 million people die of acute kidney injury (AKI) [15]. AKI is characterized as a rapid decrease of the kidney excretory function and urine production [16], [17]. AKI is commonly diagnosed by measuring the concentration of serum urea and creatinine, decreased urine output, or a combination of both to determine the glomerular filtration rate (GFR) [16]. However, the serum creatinine concentration only changes after already half of the GFR is gone, and often renal injury starts before GFR can be measured [16]. To overcome this problem, new biomarkers, such as such as albumin and total protein, neutrophil gelatinase-associated lipocalin (NGAL), and kidney injury molecule 1 (KIM-1), were discovered and are already used for diagnosis. [15], [16]. The use of such markers will eventually lead to an early treatment of AKI and will help to prevent severe cases [15]

AKI is mainly found in one of the four most important structures of the kidneys: the interstitium, the renal blood vessel system, the glomeruli, or the tubules [17]. In this thesis we will focus on the damage to the tubules which can be caused by two major factors: Drug-induced by exogenous and endogenous compounds, and renal ischemia (loss of perfusion) [17].

Around 30% of applied drugs for multiple target conditions relinquish the body unchanged through the kidneys [18] which are therefore vulnerable to (drug-induced) toxicity [19]. Approximately 20% of AKI is induced by drugs in community- and hospital-obtained occurrences. This percentage increases rapidly to more than 60% for older patients [20].To decrease this high rate of cases, compound studies of drug libraries as well as the interactions among drugs need to be studied before a drug is approved to enter the market [21]. Until now only a fraction of potentially nephrotoxic drug candidates are rejected because of nephrotoxicity in pre-clinical studies [21], [22]. Reasons are diverse as the toxicity usually is a result of a combination of factors which involve interaction of the organism with the drugs itself, drug metabolites, and drug–protein conjugates [21]. Elimination of drugs in the kidney is mainly facilitated by membrane transporters. When this pathway is restrained by improperly functioning transporters, drug-transporter interaction, or by drug-drug interaction compounds can accumulate in the cell cytoplasm leading to cellular and tubular damage [23], [24].

In other cases, AKI can be caused due to a comorbidity that disrupts renal perfusion, either because of pre-renal hypoperfusion (e.g. heart failure, hemorrhage) or post-renal obstruction (e.g. cancer, blood clot) [17], [25]. As a result of reduced renal perfusion, the kidney cells suffer from cell damage. Renal ischemia/reperfusion injury (rIRI) initiates a cellular response leading to cell damage, cell death, inflammation, and ultimately AKI [26] [27]. Therefore, assessment of the possibilities of compounds which act in a protecting way during the event of AKI should not be disregarded either.

The diversity of reasons causing AKI makes the requirements for future test platforms complex: Models are needed which need to be predictive for humans, but which also should be available in a high-throughput fashion to test this enormous number of compounds. Both of these conditions require a deeper understanding of the mechanisms of how the kidneys function in order to create a model that can predict the potential of drugs, or drug-drug combinations, to induce AKI.

The kidney

The kidneys are two bean-shaped organs which are found on the left and right side in the retroperitoneal space of the human body. They are responsible for filtering and cleaning the blood from toxic metabolites like urea, uric acid, as well as from (metabolized) drugs. All these compounds are eventually collected in the bladder and removed from the body as urine. Furthermore, the kidneys are responsible for maintaining the homeostasis of the extracellular fluid (pH, sodium, potassium, and calcium concentrations, osmotic pressure), for the regulation of the fluid circulation, and for the production of hormones. The functional units of the kidneys are called nephrons. Each kidney consists of around 1.2 million nephrons, of which each single nephron is able to produce urine as its end product (fig. 1A). Blood capillaries are covered by the Bowman's capsule which is the beginning of the tubular system of the kidneys (fig. 1B). In the glomerulus, blood is mainly filtered from blood cells and proteins by specialized cells called podocytes. In the tubular system behind the glomerulus, further excretion of toxic compounds from the interstitial fluid into the glomerular filtrate takes place. Also, reuptake of water, glucose, nutrients, and electrolytes is a process which happens in the tubular system. These processes make sure the filtrate is concentrated more and more into urine. The filtrate first enters the proximal tubules, then the loop of Henle which is followed by the distal tubule before it flows into the collecting duct and is excreted as urine.

The proximal tubules

Proximal tubules are the part of the nephron where drugs and metabolites are actively eliminated from the body [30]. This pivotal role makes them of high importance during drug development. The proximal tubules are represented by an polarized epithelial layer which functions as a passive and active filter membrane (fig. 2 A).

A

nephron
(figure B)

urine

B

proximal
convoluted tubule
(figure 2A)

Bowman's
capsule

glomerulus

distal
convoluted tubule

peritubular
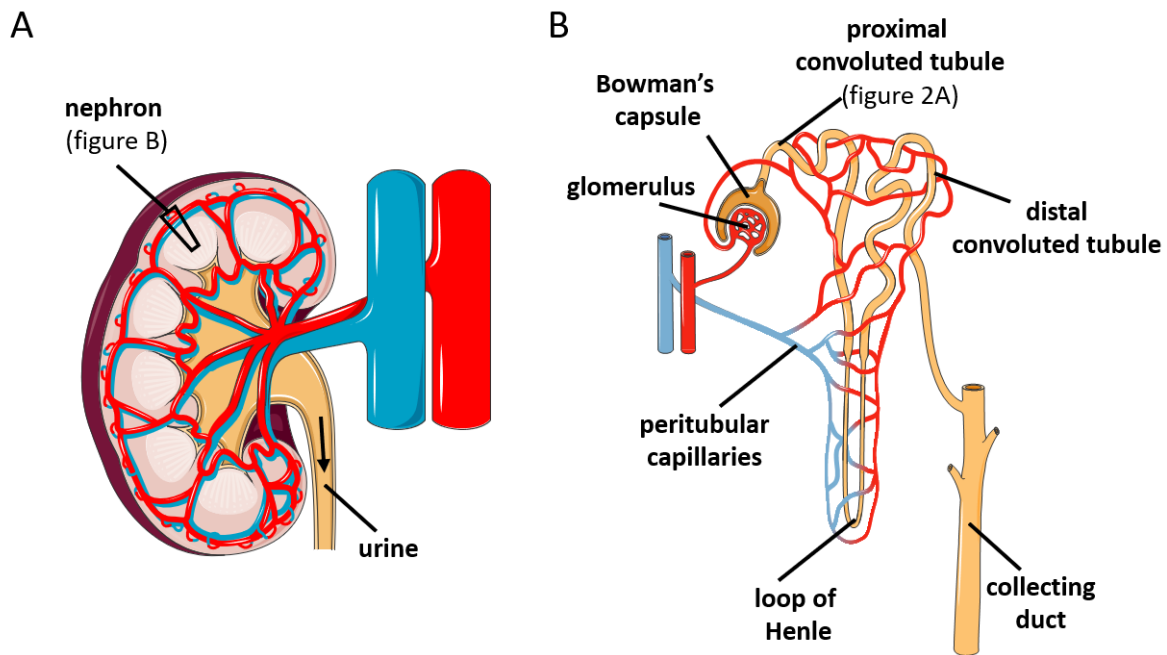capillaries

loop of
Henle

collecting
duct

*Figure 1: Anatomy of the Kidney, nephron, and transport function of the proximal tubule. **A** Sagittal Cross section of one kidney. **B** Schematic of an individual nephron. The proximal tubule is positioned directly behind the glomerulus. Both are located in the cortex, while the rest of the nephron is primarily located in the medulla. Images adapted from* [28] *and produced using templates provided by Servier Medical Art* [29]*.*

The basal side of the proximal tubule attaches to the ECM via its basement membrane and the apical side of the cells faces the tubular lumen. In the proximal tubules approximately 75% of salts and water and up to 100% of organic solutes, such as glucose and amino acids, are reabsorbed. To be able to facilitate this reabsorbing function the luminal surface is covered by a brush boarder packed with microvilli, enlarging the surface in the range of 20-fold [31]. Each cell is endowed with a single primary cilium, which has a sensory function, recognizing flow or mechanical stimulation [32], [33] (fig. 2 A). The proximal tubule cells are connected to each other by tight junctions which facilitate the barrier function of the proximal tubule layer [34].

The transport of most solutes is facilitated by transport proteins which are located on both the apical and basal side of the proximal tubules [23]. These transporters are classified into two main families: transporters of the solute carrier (SLC) family which use an electrochemical gradient and transporters of the ATP binding cassette (ABC) family which are functioning by hydrolyzing ATP to receive the energy needed [28], [37]. SLC transporters are capable of importing or exporting substrates depending on concentration gradients, while most ABC transporters are mainly responsible for the efflux.
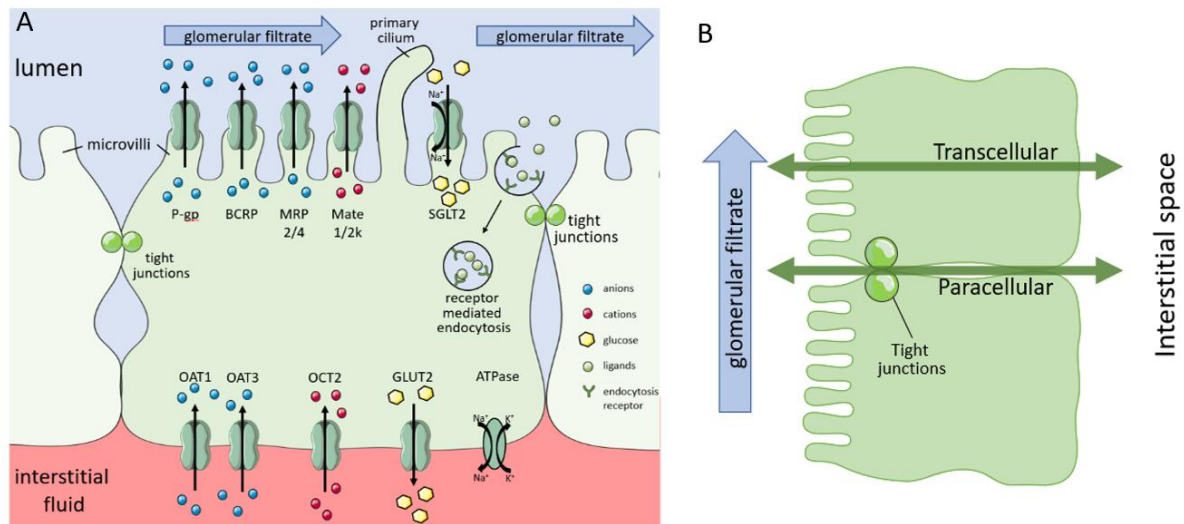
*Figure 2: Mechanisms of compound and fluid and transport between the proximal tubular lumen with the glomerular filtrate and the interstitial space. **A** Via active processes, cells secrete anions (blue) and cations (red) from the interstitial fluid into the cells and emit them out of the cells on the apical side of the cells into the glomerular filtrate. Glucose (yellow) is reabsorbed from the glomerular filtrate and released back into the interstitial fluid. Ligands (green) are reabsorbed by receptor mediated endocytosis. Adapted from* [28], [35]. ***B** Transport mechanisms of the proximal tubule on cellular level showing the difference of transcellular transport and paracellular transport. Adapted from* [36]. *Figures are produced using templates provided by Servier Medical Art* [29]*.*

Reabsorption function of the proximal tubule

Glucose is the main energy supply of the human body. During the filtration of the blood via the glomerulus, glucose is not removed and therefore available in the glomerular filtrate in the same concentration as in the blood. However, almost all the glucose in the filtrate is reabsorbed by the proximal tubules [38]. The proximal tubules therefore play a crucial role regulating the glucose levels in the blood plasma. 90 % of glucose is taken up from the glomerular filtrate into the cell cytoplasm via SLC transporters sodium-glucose transport protein (SGLT/ SLC5A) 2 and 10 % via SGLT1 [38]. Studies using SGLT2 knock out mice show that even though SGLT2 plays a predominant role in the uptake of glucose [39], [40] it seems that sodium-glucose transport protein 1 (SGLT1) can serve as a partial substitute for SGLT2 [40]. Transport via SGLTs has to follow a sodium (Na+) gradient while Na+ and glucose are co-transported across the apical cell membrane [35]. The Na+ concentration gradient is restored via the sodium–potassium pump (Na+/K+-ATPase) which maintains the Na+ and K+ gradient across the cell membrane while hydrolyzing adenosine triphosphate (ATP) [41]. Transport across the basolateral membrane into the interstitial space and the blood stream is facilitated by diffusion glucose transporter (GLUT/ SLC**2**A**2**) 2 [35] (fig. 2A).

Similar to the reabsorption pathway of glucose, amino acids, phosphate, citrate, and lactate are transported by also using Na+ co-transporters of the SLC family to enter the proximal tubule cells

and diffusion via passive transporters back into the bloodstream [42].Re-uptake of nutrients, proteins such as carrier proteins like albumin, and other small bioactive molecules is facilitated via receptor-mediated endocytosis through multi-ligand receptors cubilin and megalin, which are expressed on the apical side of the proximal tubules [28], [43] (fig. 2A).

Reabsorption of water is facilitated via auquaporin-1, the most important water-transporting protein in cell membranes of the kidney proximal tubule [44](fig. 2A). The extensive water reabsorption leads to a high concentration of chloride (Cl) ions in the filtrate. Reabsorption is facilitated by Cl-formate exchangers into the cells followed by diffusion back into the blood stream, before the filtrate leaves the proximal tubule [44].

Renal clearance function

Next to the reabsorption function of the proximal tubules, substances are cleared from the body into the urine. These include waste metabolites, endogenous and exogenous toxins, such as drugs. The epithelial cell membrane of the proximal tubules functions as a selective barrier between the interstitial fluid on the basal side of the cells and luminal fluid on the apical side. The epithelial cells are connected to each other by tight junctions (fig. 2 A). There are two main transport pathways: paracellular transport and transcellular transport (fig. 2 B). As the proximal tubules are not completely leak tight [31], [34], fluids and solutes are not only transported via the transcellular transport, but also paracellular [36] (fig. 2 B). Transcellular transport is mediated across both the apical and basal membrane through the cellular cytoplasm. Most drugs and waste metabolites are eliminated from the body into the pre-urine cells via transcellular transport. Influx via the basal membrane into the cell cytoplasm and efflux into the glomerular filtrate is mediated by different transport mechanisms. Downregulation or variations of the transport function of one of these transport pathways can lead to either drug accumulation in the plasma or in the proximal tubules itself, which makes the proximal tubule cells a target for drug-induced toxicity [30], [37], [45], [46].

[28], [37]The most abundant influx transporters located on the basolateral membrane of the proximal tubules are organic anion transporter 1 (OAT1/SLC22A6), organic anion transporter 3 (OAT3/SLC22A8), and organic cation transporter 2 (OCT2/SLC22A1) (fig. 2 A). Apical secretion into the lumen is facilitated via the P-glycoprotein 1 (P-gp/ABCB1), breast cancer resistance protein (BCRP/ABCG2), multidrug resistance-associated protein 2 (MRP 2/ABCC2) and 4 (MRP 4/ABCC4), and multidrug and toxin extrusion protein 1 (MATE1/SLC47A1) and 2-k (Mate 2-k/SLC47A2) [28]. Influx of organic cation into the cells is generally facilitated via OCT2 and excreted via MATE1 and MATE2k [28]. An example of such an organic cation is the well-known nephrotoxicant cisplatin. The transport function for cisplatin of the MATEs is less potent then the transport function of OCT2, resulting in an accumulation of cisplatin inside of the cells causing nephrotoxicity [23], [46]. Organic anions are typically transported into the cells by OAT1 and OAT3 followed by a release

into the glomerular filtrate via P-gp, BCRP, or MRP2/4. An example of a drug which is eliminated from the body via OAT1 and MRP4 is the antiviral drug tenofovir [47].

The characterization of a functional proximal tubule model

Before being able to perform advanced experiments on *in vitro* systems it is of high importance that the cultures are phenotypically characterized. Throughout this thesis all developed models were analyzed for the characteristics mentioned in the previous chapter using immunofluorescent (IF) stainings. IF utilizes fluorescent-labeled antibodies in order to identify specific target proteins (antigens) in biological tissue [48]. These antibodies can be then visualized using a fluorescent microscope. For the visualization and correct localization of the primary cilia, stainings were performed using an antibody against acetylated tubulin [49]. To detect the microvilli of the epithelial cells an antibody against ezrin was used, as this protein is concentrated in the microvilli [50]. Zonula occludens (ZO)-1, also known as the tight junction protein [51], was used to visualize the barrier formation of the tubules. Next to a visualization of the tight junctions their functionality can be tested using assays which assess the barrier function of the cell layer. A tight barrier formation of proximal tubule layers is important to be able to monitor the effect of compounds on the barrier formation, but it is also crucial when the transport of compounds across the cell layer is assessed. The barrier formations can for example be monitored by studying a fluorescent labeled compound (e.g. a Fluorescein isothiocyanate (FITC) dextran) under the microscope, which was added to the lumen of the tubule. If the dye does not leak through the cell layer of the tubule, the cell barrier can be considered to be leak tight. A good barrier integrity and correct polarization of the tubule is essential for assessing transport and directional toxicity as it allows interrogation and exposure of the apical and basolateral sides independently from one another [31]. Another possibility to assess the barrier function of the proximal tubule layers is by measuring the TransEpithelial/Endothelial Electrical Resistance (TEER). Here, the tightness of the barrier function of the cell layer is assessed by measuring the associated electrical impedance [52]. In addition, assays which can be used to analyze an expected response of the model to certain compound treatments need to be tested or evolved. This can for instance be done using compounds which are known to trigger AKI or inhibit the transport function across the cell barrier. Only when all these examinations are successful, the model can be used for the investigation of a variety of compounds and eventually disease models can be developed.

High-throughput *in vitro* models of the proximal tubule - from 2D to 3D

Up to today the gold standard of *in vitro* models are 2D models, with and without a supporting ECM. These 2D models can be cultured at a large scale in multi-well plates which offer up to 1536 separate identical cell cultures for drug testing. Cells are seeded in these plates and after a few days compound screenings can be performed. This kind of upscaled tests offer important insights in early drug discovery as well as predicting possible drug concentrations in further experiments. However, these systems lack the complexity of the human body as cell monolayers are attached

to (coated) surfaces with their basal side attached to the culture dish (fig. 3A). These models clearly lack the third dimension on the basal side of the cells which, among others, receives all reabsorbed water and glucose in the proximal tubules [53]. Moreover, the proximal tubules play an important role in eliminating drugs into the luminal fluid on the apical side. Therefore, it is crucial for these cultures to be grown in a way that they can be accessed from both the basal and the apical sides. In the last years, a more complex *in vitro* system started to dominate the market: the Transwell® system. Cells in these systems are grown on ECM-coated artificial porous membranes, enabling access to the cell layer from the apical as well as from the basal side [54], [55]. An example of such a culture system can be seen in figure 3B. In Transwell systems, up to 96 cultures can be grown in parallel. This is still a high number of replicates per plate, which means that these systems can be used for high-throughput studies. However, models of proximal tubules cultured on these devices lack the renal proximal tubule typical phenotype and behavior (e.g. correct polarization or significant receptor-mediated transport) which is shown to be a deficiency of shear stress the cells need to experience [56]–[58].
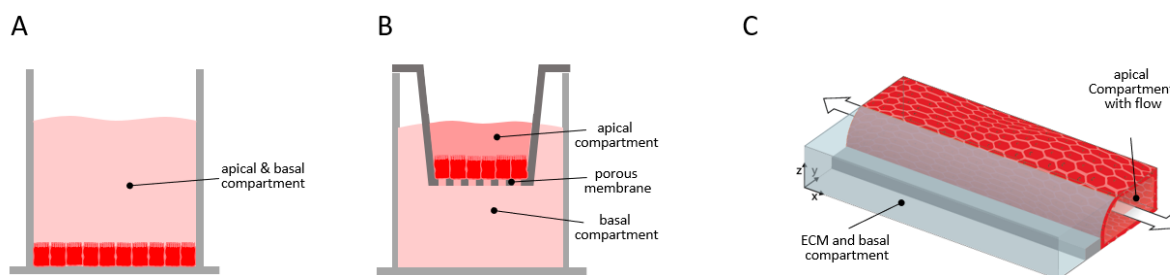

Figure 3: From simple to complex: High-throughput culture systems for proximal tubule epithelial cells based on a standard multiwell plate layout. A Typical 2D culture system in a standard multiwell plate. A monolayer of epithelial cells is grown on a plastic surface of a culture dish. Medium supply is offered from one side (top) only. Slightly more physiologically-relevant models provide a layer of extracellular matrix (ECM) between the cells and the surface. Multiwell plates can offer up to 1536 separate culture chambers. B Transwell® system with up to 96 culture chambers. In a Transwell system, cells are cultured in an insert on top of an ECM-coated porous membrane. This way of culturing enables access to the basal as well as the apical side of the cell layer. C OrganoPlate® 2-lane system containing 96 culture chambers. The OrganoPlate is a newly developed system which enables the possibility to culture epithelial cells against an ECM in a perfused, membrane- free 3D setting.

In 2013 the OrganoPlate® 2-lane (Figure 3C) was launched which enables parallel cultures of up to 96 tissues to be grown in a membrane-free 3D environment with perfusion flow. This system was a breakthrough for culturing endothelial vessels membrane free in a high-throughput fashion against a collagen 1 gel [59]. Though the cells do grow layers against a freestanding ECM, this system was not suitable for culturing proximal tubules, as it lacks the possibility to access the cell layer growing against the ECM from the basal side of the cells. This access is particularly important for the proximal tubules as they actively transport compounds via the cell membrane.

Using microfluidic high-throughput systems for the culture of proximal tubules

In the last decade, a variety of 3D cultured models of proximal tubules has been developed. The majority of these models is cultured in microfluidic channel structures on chip systems. These microfluidic channels can be fabricated using different approaches. Jang et al. [57] for instance, published a model of a kidney-on-a-chip device with cultured renal proximal tubule cells (RPTEC) on a perfused porous polyester membrane microfabricated on a polydimethylsiloxane (PDMS) chip. Fluid sampling can be performed from the apical chamber containing the RPTECs and the adjacent basal chamber. Jang et al. compared their model directly with the Transwell system and could conclude from the results that the presence of flow is crucial for a wide range of physiological functions. Using a model of perfused hollow fibers made of ECM-coated polyethersulfone, Jansen et al. [60] could demonstrate active transport via the OCT2 transporter across the membrane. Homan et al. [56], as well as Weber et al. [58] both used a system where cells from the proximal tubules were successfully grown against an interface of an ECM gel. What all these systems have in common is that the lumen of the proximal tubules could be perfused with exposure to shear stress, the cells were constantly supplied with nutrients and oxygen and waste products were removed. All these models offer access to the basolateral side of the cell membrane, which is of high importance for transport studies across the membrane or independent exposures of the apical or basal cell membrane.

As was discussed in the previous subchapter, one important aspect which all these models lack is the possibility to use these microfluidic systems in a high-throughput fashion similar to the OrganoPlate 2-lane. The patterning of the channel structure on the OrganoPlate is not fixed but can be modified, as long as the design allows access to the channels via the 384 top-well plates. This offers the opportunity to develop different models. One of these models, which offered the high throughput possibilities of the OrganoPlate 2-lane in combination with the possibility of growing tubules with access to the apical and basal side of the cell barrier was the OrganoPlate® 3-lane system. The OrganoPlate 3-lane was developed and continuously improved during the research of this thesis. This development can be also reviewed in more detail in the doctoral thesis by S.J. Trietsch [61].

In short: the OrganoPlate 3-lane (figure 4A) comprises 40 chips (figure 4B) in one platform with a microfluidic channel system that is embedded between two microscope-grade glass plates. Access to this system is enabled via the wells of the top plate. These wells are also functioning as reservoirs, which provide fresh medium and waste product dilution for the cultures in the microfluidic system. For establishing 3D cultures in the chips, a liquefied ECM is added to the middle channel (fig. 4 C). By microfluidic forces, the ECM is guided into the system and patterned via meniscus pinning between the two phaseguides. After polymerization of the ECM, cells are seeded to one of the adjacent channels and medium is added to all wells which are connected to

the perfusion channels. By placing the plate on a rocker platform, perfusion flow through the system is started by passive leveling of the medium (figure 4D).
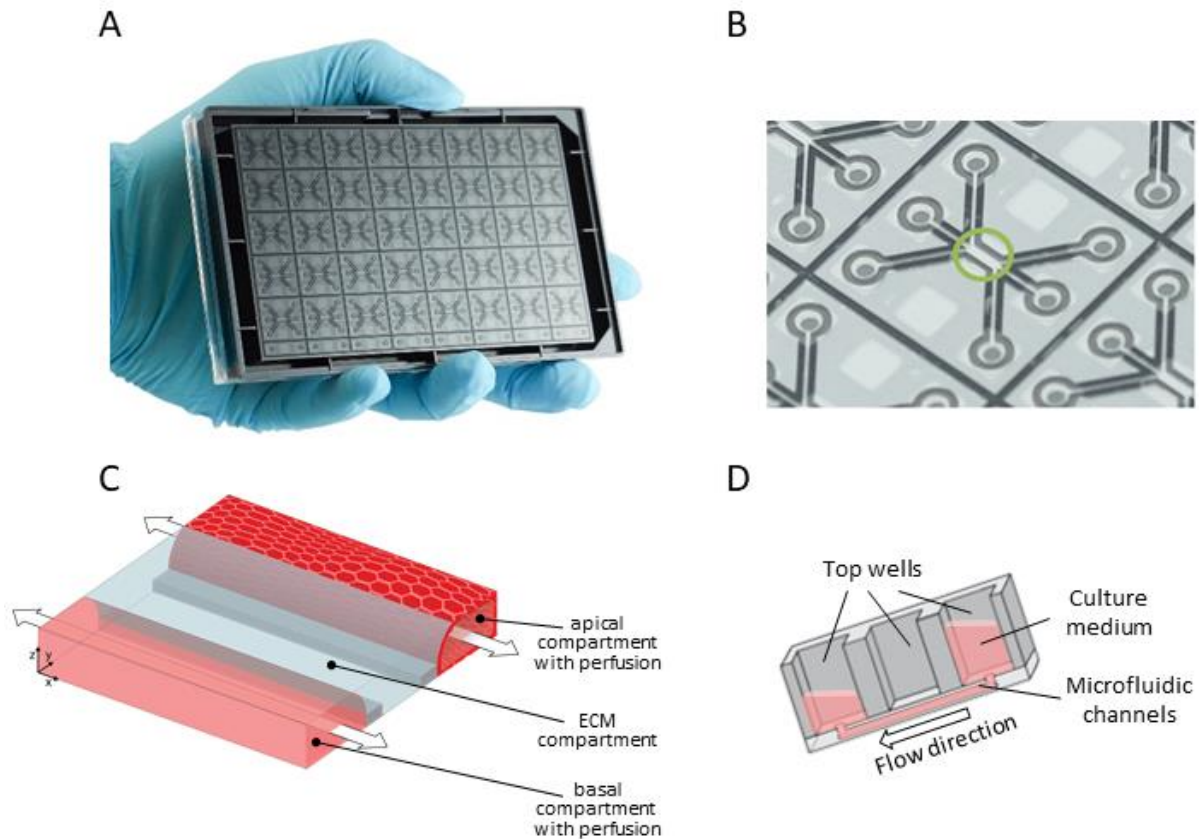
Figure 4: The OrganoPlate® 3-lane. A Bottom view on the modified bottom of the OrganoPlate 3-lane system containing 40 microfluidic cell culture chips embedded in between two microscope grade glass plates. Each single chip can be accessed from the top via the microtiter plate. B Zoom in on one 3-lane chip comprising the three channels in the center (green circle). C Artist impression of the center of the OrganoPlate 3-lane. Channels are divided by small ridges called PhaseGuide (grey). After loading a gel (light blue) in the middle channel, cells (red) are seeded to one of the adjacent channels. After cell attachment, medium is perfused (indicated by white arrows) in both the lumen of the tube and the second perfusion channel (light red). D Side cut view of the top wells connected by one of the microfluidic channels. Perfusion of cell culture medium through the system is created by placing the plate in an angle position on a rocker platform. This results in positioning the wells of the plate on different heights enabling a gravity-driven flow though the channels.

Triggered by the perfusion, monolayers of the epithelial cells grow against the interface with the ECM and the walls of the microfluidic channels until a confluent tubule is grown. These tubules can be used for further experimental studies, including the assessment of the cell barrier against the ECM.

In this thesis the use of the OrganoPlate 3-lane system for the culture of the proximal tubules is described. The 3-lane system offers the possibility to grow proximal tubule cells against an ECM gel. To mimic the tubulointerstitium of the kidney collagen type I, which is one of the most

abundant proteins in the tubulointerstitium of the kidney [62], [63], was used. Cells were seeded into the top channel of the OrganoPlate 3-lane and under bidirectional flow through the perfusion channels confluent tubules were grown. Assays were performed from day 6 to day 10.

Scaling up of the model complexity to a higher physiological relevance: Cocultures of the proximal tubule

The proximal tubules are only one part of the nephron; they are surrounded by a panel of other cell types which also play a role in its function. They interact most closely with endothelial vessels (peritubular capillaries, fig. 1B) which directly provide all compounds that need to be eliminated into the urine via the proximal tubules.

There is a growing number of research papers that describe the importance of adding endothelial cells to the proximal tubule monoculture models. The first papers which demonstrated the benefits of culturing cells in cocultures were already published before 2000. Linas and Repine for example could showed in 1999 [64] that the function of the proximal tubules is controlled by endothelial cells. Aydin et al. demonstrated in 2007 [65] that the human microvascular endothelial cell line HMEC-1 influences the behavior of the renal epithelial cell line HK-2 when grown in a coculture separated by a filter membrane. They measured a significantly higher barrier function of the epithelial cells. Tasnim and Zink in 2011 [66] published that essential transporters of the proximal tubules got upregulated in primary renal proximal tubular cells when cocultured with endothelial cells. Anion transporter OAT 1 showed relative expression levels of a fold change of around 5 when cells were cultured in a coculture compared to the monoculture.

In the studies mentioned above endothelial cells and epithelial cells were cultured in the same system. Mainly Transwell-like systems (fig. 3 B) were used with one cell type cultured on the surface of the bottom compartment and the second cell type on the filter membrane of the top compartment. These systems lacked at least one of two physiological relevant aspects: perfusion flow on the apical sides of both membranes and the correct physical constellation with the basal membranes of each of the structures facing each other.

A handful of systems, which combine both requirements for culturing renal epithelial tubules in a coculture set up with endothelial tubules have been published in recent years (fig. 5).

Vedula et al. [67] developed a device which offers the possibility to culture two different cell types in chambers separated by a polycarbonate membrane under perfusion flow (fig. 5 A). In their device, interaction between both cell types is possible as the membrane is permeable for liquids and solutes, which enables the reabsorption and the transport function across both cell barriers. The membrane itself is topographically-patterned to facilitate tissue organization and function, which they demonstrated by performing a glucose reabsorption study. Rayner et al. [68] (fig. 5 B)
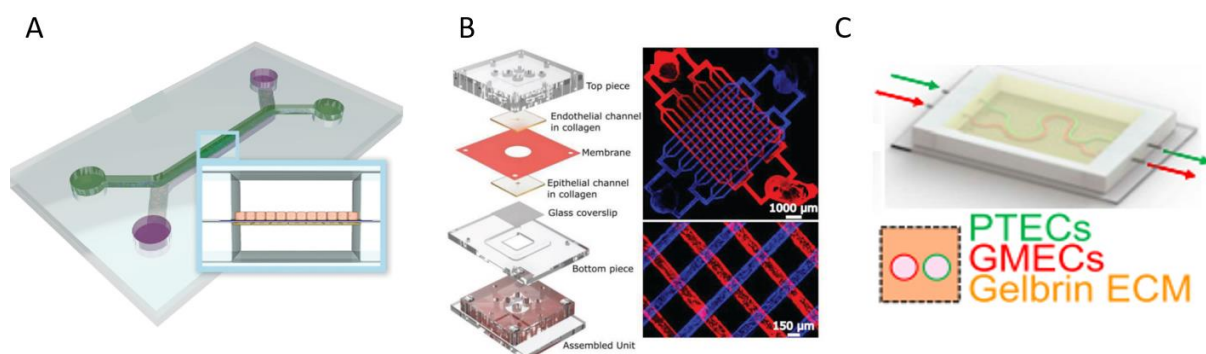
*Figure 5: Microfluidic devices developed for culturing perfused cocultures of renal epithelial tubules and endothelial cells. **A** Vedula et al. developed a device where the two perfused channels (green for RPTEC and purple for the endothelial cells) are separated by a polycarbonate topographically-patterned membrane with pore structure.* [67] ***B** Parallel channel networks of two separately perfused units embedded and separated by a collagen gel only. In one of the two channel networks renal cortical cells were seeded, the other network was utilized for endothelial cells* [68]. ***C** Proximal tubules (PTECs, green) and endothelial cells (GMECs, red) grown in close proximity in a bioprinted ECM network with no artificial barriers present* [69].

and Lin et al. [69] (fig. 5 C) used a similar approach to culture both epithelial and endothelial cells in close proximity by patterning the tubules and vessels inside of an ECM network. Rayner et al. used collagen whereas Lin et al. used a mixture of gelatin and fibrinogen. Both research groups could show that the ECMs were permeable for albumin and glucose by performing successful reabsorption studies. However, so far none of the introduced devices for cocultures can be used in a high throughput fashion which would enable the possibilities to examine the toxicity of broad concentration ranges and compound libraries. Remarkably, Rayner et al. could show that their device is not only suitable for culturing cocultures, but they also already performed triple culture experiments by incorporating pericytes embedded into the ECM [68]. This approach is already a first interesting step in the direction of a complete nephron on a chip as the interstitial cells such as fibroblasts, pericytes, or immune cells are expected to support the regeneration and function of the renal epithelium [70].

Aim and outline of the thesis

Current pre-clinical studies assessing nephrotoxicity lack human-derived *in vitro* models which accurately predict the response of the *in vivo* situation. The aim of the research described in this thesis was to develop a physiologically relevant 3D *in vitro* model of the human renal proximal tubule which combines its physiological complexity with a robust high-throughput organ-on-a-chip system. This proximal-tubule-on-a-chip model should be able to mimic the *in vivo* situation for a variety of applications, such as drug assessment in nephrotoxicity studies, drug-drug interaction studies including drug transport studies, and the assessment of compounds which protect against tubular damage. This thesis focused on the establishment and characterization of such a model and relevant assays. The ultimate aim was to offer a tool for drug research and development of novel medications that is accessible to academia and industry.

In **chapter 2** our aim was to develop a 3D perfused human proximal tubule model that can be used for nephrotoxicity and renal transport assessment. We investigated whether renal proximal tubule cells (RPTEC) can be cultured as tubular structures with correct polarization in the OrganoPlate 3-lane. We elaborated on the need for shear stress, and how fluid flow rate and induced shear stress in the microfluidic channels of the OrganoPlate can be calculated. Furthermore we examined if the model can be used to evaluate the nephrotoxic effect of cisplatin, a drug which is known to show a damaging effect on the proximal tubules *in vivo* as well as *in vitro*. Moreover, our aim of this chapter was to show that the model can be used to study the transport function of the proximal tubule. We demonstrated the transport function using two different approaches: transport of compounds which are taken up into the cells, as well as transepithelial transport assessment across the membrane. In this chapter, a model of the proximal tubule was developed which can be used for drug screening studies and can serve as a solid foundation for further model development of the proximal tubules.

The development of the proximal tubule model described in **chapter 2** was part of the Nephrotube challenge crackIT which was organized by the National Centre for the Replacement Refinement & Reduction of Animals in Research (NC3Rs) [7] and sponsored by GSK, Pfizer, and Roche. The aim of the challenge was to develop a high-throughput, 3D microfluidic platform (Nephroscreen) for the detection of drug-induced nephrotoxicity [71]. In parallel with the work described in **chapter 2**, Vriend et al. [72] developed a screening platform for drug transporter interaction using their conditionally immortalized proximal tubule epithelial cells overexpressing organic anion transporter 1 (ciPTEC-OAT1) seeded in the OrganoPlate. Suter-Dick et al. [73] developed a method which combined the determination of miRNA and the usage of the OrganoPlate system. The aim of **chapter 3** was to develop an advanced proximal tubule on a chip model combining different cell types and readout assays. This was achieved by a joint study of all three research lines within the Nephroscreen to integrate all assays in one platform to study nephrotoxicity induced by known and unknown drugs. Tubules grown in the OrganoPlate were exposed to four model compounds and a panel of eight unknown compounds provided by the sponsor consortium. Proximal tubules grown in the 3-lane system can be used for a complex drug screening combining different cell types with a huge panel of different assays.

In chapter 4 the aim was to investigate whether *in vivo* observations can be replicated with our model developed in **chapter 2** and **chapter 3**. For the study, the effects of the two HIV-medications Stribild and Genvoya on the proximal tubules of the kidney were analyzed. Both drugs contain two different pro-drugs of the known nephrotoxicant tenofovir (Stribild, tenofovir disoproxil (TDF) and Genvoya, tenofovir alafenamide (TAF)) in combination with the same concentrations of Elvitegravir, Cobicistat, and Emtricitabine. In the recent years Stribild was replaced by Genvoya as a result of a better side effect profile. Toxicity of the tenofovir variant used in Genvoya was picked up at only physiologically irrelevant concentrations suggesting that

our model is able to pick up the reduced nephrotoxic effect of TAF compared to TDF. Next, we investigated whether our model is suitable to pick up cumulative toxicity when combining the tenofovir variants with either Elvitegravir, Cobicistat, or Emtricitabine. Additive to super-additive synergistic toxicity could be clearly shown for some combinations, whereas single dosages of each of the compounds showed a lower toxicity.

After using a mono-culture model of proximal tubule cells in **chapters 2** to **4** our aim in **chapter 5** was to explore whether an endothelial vessel alongside the proximal tubule can be added to investigate if AKI induced by ischemia can be studied on this co-culture model. The use of the coculture as an acute kidney injury (AKI) model was characterized by an immunofluorescence staining and validated by a nephrotoxicant study. Subsequently, the ischemic AKI model was developed by exposing the coculture to different ischemic conditions. Two ischemic conditions (condition 1: glucose-free basal medium, static, low oxygen and condition 2: glucose-free basal medium, perfusion, low oxygen) were selected. A co-incubation with potential protective compounds succeeded to show a significant protection against tubular damage after addition of adenosine to the culture medium. This study led to a functional coculture of epithelial tubules and endothelial vessels which can be used to study renoprotective compounds on an ischemic induced AKI model.

In **chapter 6** a general conclusion was given, including a summary of each of the chapters. Finally, this was followed by an outlook on how to address future research on the culture of proximal tubule *in vitro* models.

References

[1]   U.S. Food and Drug Administration, "Investigational New Drug (IND) Application." https://www.fda.gov/drugs/types-applications/investigational-new-drug-ind-application (accessed May 02, 2020).

[2]   European Medicines Agency, "Review and update of EMA guidelines to implement best practice with regard to 3Rs (replacement, reduction and refinement) in regulatory testing of medicinal products – report on actions taken." https://www.ema.europa.eu/en/documents/scientific-guideline/review-update-ema-guidelines-implement-best-practice-regard-3rs-replacement-reduction-refinement_en.pdf (accessed May 02, 2020).

[3]   H. Kojima *et al.*, "Guidance on the Use of Alternative Test Methods for the Safety Assessment of Cosmetics and Quasi-drugs," in *Alternatives to Animal Testing*, vol. 1, Singapore: Springer Singapore, 2019, pp. 63–68. doi: 10.1007/978-981-13-2447-5_8.

[4]   European Commission, "Commission Staff Working Document SEC(2004)1210 - Timetables for the phasing-out of animal testing in the framework of the 7th Amendment to the Cosmetics Directive (Council Directive 76/768/EEC)," *Commission Staff Working Documents*, vol. SEC(2004), 2015.

[5]   "Regulation (EC) No 1223/2009 of the European Parliament and of the Council of 30 November 2009 on cosmetic products," *European Parliament*. https://eur-lex.europa.eu/legal-content/EN/TXT/PDF/?uri=CELEX:02009R1223-20210526&from=EN (accessed Jun. 08, 2021).

[6]   G. A. Van Norman, "Limitations of Animal Studies for Predicting Toxicity in Clinical Trials: Is it Time to Rethink Our Current Approach?," *JACC: Basic to Translational Science*, vol. 4, no. 7, pp. 845–854, 2019, doi: 10.1016/j.jacbts.2019.10.008.

[7]   National Centre for the Replacement Refinement & Reduction of Animals in Reasearch, "The 3Rs." https://www.nc3rs.org.uk/the-3rs (accessed May 02, 2020).

[8]   World Medical Association, "WMA DECLARATION OF HELSINKI – ETHICAL PRINCIPLES FOR MEDICAL RESEARCH INVOLVING HUMAN SUBJECTS." https://www.wma.net/policies-post/wma-declaration-of-helsinki-ethical-principles-for-medical-research-involving-human-subjects/ (accessed May 02, 2020).

[9]   Y. Lai, X. Wei, S. Lin, L. Qin, L. Cheng, and P. Li, "Current status and perspectives of patient-derived xenograft models in cancer research," *Journal of Hematology and Oncology*, vol. 10, no. 1, pp. 1–14, 2017, doi: 10.1186/s13045-017-0470-7.

[10]   P. Gunness, K. Aleksa, K. Kosuge, S. Ito, and G. Koren, "Comparison of the novel HK-2 human renal proximal tubular cell line with the standard LLC-PK1 cell line in studying drug-induced nephrotoxicity," *Canadian Journal of Physiology and Pharmacology*, vol. 88, no. 4, Apr. 2010, doi: 10.1139/Y10-023.

[11]   A. Akhtar, "The Flaws and Human Harms of Animal Experimentation," *Cambridge Quarterly of Healthcare Ethics*, vol. 24, no. 4, pp. 407–419, 2015, doi: 10.1017/S0963180115000079.

[12]   N. Shanks, R. Greek, and J. Greek, "Are animal models predictive for humans?," *Philosophy, Ethics, and Humanities in Medicine*, vol. 4, no. 1, pp. 1–20, 2009, doi: 10.1186/1747-5341-4-2.

[13]   S. K. Doke and S. C. Dhawale, "Alternatives to animal testing: A review," *Saudi Pharmaceutical Journal*, vol. 23, no. 3, pp. 223–229, 2015, doi: 10.1016/j.jsps.2013.11.002.

[14] M. Kapałczyńska *et al.*, "2D and 3D cell cultures – a comparison of different types of cancer cell cultures," *Archives of Medical Science*, vol. 14, no. 4, pp. 910–919, 2018, doi: 10.5114/aoms.2016.63743.

[15] A. Zuk and J. v. Bonventre, "Acute Kidney Injury," *Annual Review of Medicine*, vol. 67, no. 1, pp. 293–307, Jan. 2016, doi: 10.1146/annurev-med-050214-013407.

[16] R. Bellomo, J. A. Kellum, and C. Ronco, "Acute kidney injury," *The Lancet*, vol. 380, no. 9843, pp. 756–766, 2012, doi: 10.1016/S0140-6736(11)61454-2.

[17] D. P. Basile, M. D. Anderson, and T. A. Sutton, "Pathophysiology of acute kidney injury," *Comprehensive Physiology*, vol. 2, no. 2, pp. 1303–1353, 2012, doi: 10.1002/cphy.c110041.

[18] J. Faria, S. Ahmed, K. G. F. Gerritsen, S. M. Mihaila, and R. Masereeuw, "Kidney-based *in vitro* models for drug-induced toxicity testing," *Archives of Toxicology*, vol. 93, no. 12, pp. 3397–3418, 2019, doi: 10.1007/s00204-019-02598-0.

[19] M. A. Perazella, "Renal vulnerability to drug toxicity," *Clinical Journal of the American Society of Nephrology*, vol. 4, no. 7, pp. 1275–1283, 2009, doi: 10.2215/CJN.02050309.

[20] C. a. Naughton, "Drug-Induced Nephrotoxicity," *American Academy of Family Physicians*, vol. 78, no. 6, pp. 743–750, 2008.

[21] A. Astashkina, B. Mann, and D. W. Grainger, "A critical evaluation of *in vitro* cell culture models for high-throughput drug screening and toxicity," *Pharmacology and Therapeutics*, vol. 134, no. 1. pp. 82–106, Apr. 2012. doi: 10.1016/j.pharmthera.2012.01.001.

[22] D. Cook *et al.*, "Lessons learned from the fate of AstraZeneca's drug pipeline: A five-dimensional framework," *Nature Reviews Drug Discovery*, vol. 13, no. 6. Nature Publishing Group, pp. 419–431, 2014. doi: 10.1038/nrd4309.

[23] P. Fisel, O. Renner, A. T. Nies, M. Schwab, and E. Schaeffeler, "Solute carrier transporter and drug-related nephrotoxicity: The impact of proximal tubule cell models for preclinical research," *Expert Opinion on Drug Metabolism and Toxicology*, vol. 10, no. 3. pp. 395–408, Mar. 2014. doi: 10.1517/17425255.2014.876990.

[24] T. Nakamura, A. Yonezawa, S. Hashimoto, T. Katsura, and K. I. Inui, "Disruption of multidrug and toxin extrusion MATE1 potentiates cisplatin-induced nephrotoxicity," *Biochemical Pharmacology*, vol. 80, no. 11, pp. 1762–1767, Dec. 2010, doi: 10.1016/j.bcp.2010.08.019.

[25] K. Makris and L. Spanou, "Acute Kidney Injury: Definition, Pathophysiology and Clinical Phenotypes," *The Clinical biochemist. Reviews*, vol. 37, no. 2, pp. 85–98, 2016, [Online]. Available: https://www.ncbi.nlm.nih.gov/pmc/articles/PMC5198510/

[26] M. Malek and M. Nematbakhsh, "Renal ischemia/reperfusion injury; from pathophysiology to treatment.," *Journal of renal injury prevention*, vol. 4, no. 2, pp. 20–27, 2015, doi: 10.12861/jrip.2015.06.

[27] G. R. Kinsey, L. Li, and M. D. Okusa, "Inflammation in acute kidney injury," *Nephron - Experimental Nephrology*, vol. 109, no. 4, 2008, doi: 10.1159/000142934.

[28] M. J. Wilmer, C. P. Ng, H. L. Lanz, P. Vulto, L. Suter-Dick, and R. Masereeuw, "Kidney-on-a-Chip Technology for Drug-Induced Nephrotoxicity Screening," *Trends in Biotechnology*, vol. 34, no. 2, pp. 156–170, 2016, doi: 10.1016/j.tibtech.2015.11.001.

[29] LES LABORATOIRES SERVIER, "Servier Medical Art." https://smart.servier.com (accessed Nov. 26, 2020).

[30] S. K. Nigam, W. Wu, K. T. Bush, M. P. Hoenig, R. C. Blantz, and V. Bhatnagar, "Handling of drugs, metabolites, and uremic toxins by kidney proximal tubule drug transporters," *Clinical Journal of the American Society of Nephrology*, vol. 10, no. 11, pp. 2039–2049, 2015, doi: 10.2215/CJN.02440314.

[31] K. S. Matlin and M. J. Caplan, "Epithelial Cell Structure and Polarity," in *Seldin and Giebisch's The Kidney*, 5th ed., R. Alpern, M. Caplan, and O. Moe, Eds. Elsevier, 2013, pp. 3–43. doi: 10.1016/B978-0-12-381462-3.00001-0.

[32] F. Lin and L. M. Satlin, "Polycystic kidney disease: The cilium as a common pathway in cystogenesis," *Current Opinion in Pediatrics*, vol. 16, no. 2, pp. 171–176, 2004, doi: 10.1097/00008480-200404000-00010.

[33] V. Raghavan and O. A. Weisz, "Flow stimulated endocytosis in the proximal tubule," *Current Opinion in Nephrology and Hypertension*, vol. 24, no. 4, pp. 359–365, 2015, doi: 10.1097/MNH.0000000000000135.

[34] L. Gonzalez-Mariscal *et al.*, "Tight junction proteins ZO-1, ZO-2, and occludin along isolated renal tubules," *Kidney International*, vol. 57, no. 6, pp. 2386–2402, 2000, doi: 10.1046/j.1523-1755.2000.00098.x.

[35] E. C. Chao and R. R. Henry, "SGLT2 inhibition-A novel strategy for diabetes treatment," *Nature Reviews Drug Discovery*, vol. 9, no. 7, pp. 551–559, 2010, doi: 10.1038/nrd3180.

[36] N. H. García, C. R. Ramsey, and F. G. Knox, "Understanding the role of paracellular transport in the proximal tubule," *News in Physiological Sciences*, vol. 13, pp. 38–43, 1998, doi: 10.1152/physiologyonline.1998.13.1.38.

[37] S. K. Nigam, "What do drug transporters really do?," *Nature Reviews Drug Discovery*, vol. 14, no. 1, pp. 29–44, 2014, doi: 10.1038/nrd4461.

[38] A. Mather and C. Pollock, "Glucose handling by the kidney," *Kidney International*, vol. 79, no. 120, pp. S1–S6, Mar. 2011, doi: 10.1038/ki.2010.509.

[39] V. Vallon *et al.*, "SGLT2 mediates glucose reabsorption in the early proximal tubule," *Journal of the American Society of Nephrology*, vol. 22, no. 1, pp. 104–112, 2011, doi: 10.1681/ASN.2010030246.

[40] T. Rieg *et al.*, "Increase in SGLT1-mediated transport explains renal glucose reabsorption during genetic and pharmacological SGLT2 inhibition in euglycemia," *American Journal of Physiology - Renal Physiology*, vol. 306, no. 2, pp. 188–193, 2014, doi: 10.1152/ajprenal.00518.2013.

[41] S. P. Soltoff, "ATP and the Regulation of Renal Cell Function," *Annual Review of Physiology*, vol. 48, no. 1, pp. 9–31, Oct. 1986, doi: 10.1146/annurev.ph.48.030186.000301.

[42] L. Lin, S. W. Yee, R. B. Kim, and K. M. Giacomini, "SLC transporters as therapeutic targets: Emerging opportunities," *Nature Reviews Drug Discovery*, vol. 14, no. 8. Nature Publishing Group, pp. 543–560, Aug. 01, 2015. doi: 10.1038/nrd4626.

[43] M. L. Eshbach and O. A. Weisz, "Receptor-Mediated Endocytosis in the Proximal Tubule," *Annual Review of Physiology*, vol. 79, no. 1, pp. 425–448, Feb. 2017, doi: 10.1146/annurev-physiol-022516-034234.

[44] S. Nielsen, T.-H. Kwon, H. Dimke, M. Skott, and J. Frøkiær, "Aquaporin Water Channels in Mammalian Kidney," in *Seldin and Giebisch's The Kidney*, 5th ed., R. Alpern, M. Caplan, and O. Moe, Eds. Elsevier, 2013, pp. 1405–1439. doi: 10.1016/B978-0-12-381462-3.00041-0.

[45] V. Vallon, "Tubular Transport in Acute Kidney Injury: Relevance for Diagnosis, Prognosis and Intervention," *Nephron*, vol. 134, no. 3, pp. 160–166, 2016, doi: 10.1159/000446448.

[46] H. Motohashi and K. I. Inui, "Organic cation transporter OCTs (SLC22) and MATEs (SLC47) in the human kidney," *AAPS Journal*, vol. 15, no. 2, pp. 581–588, 2013, doi: 10.1208/s12248-013-9465-7.

[47] J. J. Kohler *et al.*, "Tenofovir renal proximal tubular toxicity is regulated by OAT1 and MRP4 transporters," *Laboratory Investigation*, vol. 91, no. 6, pp. 852–858, 2011, doi: 10.1038/labinvest.2011.48.

[48] K. Im, S. Mareninov, M. F. P. Diaz, and W. H. Yong, "An Introduction to Performing Immunofluorescence Staining," in *Physiology & behavior*, vol. 176, no. 3, 2019, pp. 299–311. doi: 10.1007/978-1-4939-8935-5_26.

[49] I. B. Alieva, L. A. Gorgidze, Y. A. Komarova, O. A. Chernobelskaya, and I. A. Vorobjev, "Experimental model for studing the primary cilia in tissue culture cells," *Biologicheskie Membrany*, vol. 15, no. 6, pp. 716–717, 1998.

[50] M. Berryman, Z. Franck, and A. Bretscher, "Ezrin is concentrated in the apical microvilli of a wide variety of epithelial cells whereas moesin is found primarily in endothelial cells," *Journal of Cell Science*, vol. 105, no. 4, pp. 1025–1043, 1993.

[51] H. Bauer, J. Zweimueller-Mayer, P. Steinbacher, A. Lametschwandtner, and H. C. Bauer, "The Dual Role of Zonula Occludens (ZO) Proteins," *Journal of Biomedicine and Biotechnology*, vol. 2010, pp. 1–11, 2010, doi: 10.1155/2010/402593.

[52] A. Nicolas *et al.*, "High throughput transepithelial electrical resistance (TEER) measurements on perfused membrane-free epithelia," *Lab on a Chip*, vol. 21, no. 9, pp. 1676–1685, May 2021, doi: 10.1039/d0lc00770f.

[53] N. Sánchez-Romero, C. M. S. Schophuizen, I. Giménez, and R. Masereeuw, "*In vitro* systems to study nephropharmacology: 2D versus 3D models," *European Journal of Pharmacology*, vol. 790, pp. 36–45, 2016, doi: 10.1016/j.ejphar.2016.07.010.

[54] M. Hara-Chikuma and A. S. Verkman, "Aquaporin-1 facilitates epithelial cell migration in kidney proximal tubule," *Journal of the American Society of Nephrology*, vol. 17, no. 1, pp. 39–45, 2006, doi: 10.1681/ASN.2005080846.

[55] A. Vinaiphat, K. Charngkaew, and V. Thongboonkerd, "More complete polarization of renal tubular epithelial cells by artificial urine," *Cell Death Discovery*, vol. 4, no. 1, 2018, doi: 10.1038/s41420-018-0112-z.

[56] K. A. Homan *et al.*, "Bioprinting of 3D Convoluted Renal Proximal Tubules on Perfusable Chips," *Scientific Reports*, vol. 6, pp. 1–13, 2016, doi: 10.1038/srep34845.

[57] K. J. Jang *et al.*, "Human kidney proximal tubule-on-a-chip for drug transport and nephrotoxicity assessment," *Integrative Biology (United Kingdom)*, vol. 5, no. 9, pp. 1119–1129, 2013, doi: 10.1039/c3ib40049b.

[58] E. J. Weber *et al.*, "Development of a microphysiological model of human kidney proximal tubule function," *Kidney International*, vol. 90, no. 3, pp. 627–637, 2016, doi: 10.1016/j.kint.2016.06.011.

[59] V. Van Duinen *et al.*, "96 Perfusable Blood Vessels To Study Vascular Permeability *in vitro*," *Scientific Reports*, vol. 7, no. 1, pp. 1–11, 2017, doi: 10.1038/s41598-017-14716-y.

[60] J. Jansen *et al.*, "Human proximal tubule epithelial cells cultured on hollow fibers: Living membranes that actively transport organic cations," *Scientific Reports*, vol. 5, no. November, pp. 1–12, 2015, doi: 10.1038/srep16702.

[61] S. J. Trietsch, "Microfluidic 3D cell culture for high throuput screening," Leiden University, 2017.

[62] C. Alexakis, P. Maxwell, and G. Bou-Gharios, "Organ-specific collagen expression: Implications for renal disease," *Nephron - Experimental Nephrology*, vol. 102, no. 3–4, pp. 71–75, 2006, doi: 10.1159/000089684.

[63] B. Singh, C. Fleury, F. Jalalvand, and K. Riesbeck, "Human pathogens utilize host extracellular matrix proteins laminin and collagen for adhesion and invasion of the host," *FEMS Microbiology Reviews*, vol. 36, no. 6, pp. 1122–1180, 2012, doi: 10.1111/j.1574-6976.2012.00340.x.

[64] S. L. Linas and J. E. Repine, "Endothelial cells regulate proximal tubule epithelial cell sodium transport," *Kidney International*, vol. 55, no. 4, pp. 1251–1258, 1999, doi: 10.1046/j.1523-1755.1999.00360.x.

[65] S. Aydin *et al.*, "Influence of microvascular endothelial cells on transcriptional regulation of proximal tubular epithelial cells," *American Journal of Physiology - Cell Physiology*, vol. 294, no. 2, pp. 543–554, 2008, doi: 10.1152/ajpcell.00307.2007.

[66] F. Tasnim and D. Zink, "Cross talk between primary human renal tubular cells and endothelial cells in cocultures," *American Journal of Physiology - Renal Physiology*, vol. 302, no. 8, pp. 1055–1062, 2012, doi: 10.1152/ajprenal.00621.2011.

[67] E. M. Vedula, J. L. Alonso, M. A. Arnaout, and J. L. Charest, "A microfluidic renal proximal tubule with active reabsorptive function," *PLoS ONE*, vol. 12, no. 10, pp. 1–15, 2017, doi: 10.1371/journal.pone.0184330.

[68] S. G. Rayner *et al.*, "Reconstructing the Human Renal Vascular–Tubular Unit *In vitro*," *Advanced Healthcare Materials*, vol. 7, no. 23, pp. 1–11, 2018, doi: 10.1002/adhm.201801120.

[69] N. Y. C. Lin *et al.*, "Renal reabsorption in 3D vascularized proximal tubule models," *Proceedings of the National Academy of Sciences of the United States of America*, vol. 116, no. 12, pp. 5399–5404, 2019, doi: 10.1073/pnas.1815208116.

[70] H. Castrop, "The Role of Renal Interstitial Cells in Proximal Tubular Regeneration," *Nephron*, vol. 141, no. 4, pp. 265–272, 2019, doi: 10.1159/000496278.

[71] NC3Rs, "Crack It Review 2019," London, 2019.

[72] J. Vriend *et al.*, "Screening of Drug-Transporter Interactions in a 3D Microfluidic Renal Proximal Tubule on a Chip," *AAPS Journal*, vol. 20, no. 5, 2018, doi: 10.1208/s12248-018-0247-0.

[73] L. Suter-Dick *et al.*, "Combining Extracellular miRNA Determination with Microfluidic 3D Cell Cultures for the Assessment of Nephrotoxicity: a Proof of Concept Study," *AAPS Journal*, vol. 20, no. 5, pp. 1–9, 2018, doi: 10.1208/s12248-018-0245-2.

1

Chapter 2

Nephrotoxicity and Kidney Transport Assessment on 3D Perfused Proximal Tubules

MK Vormann, L Gijzen, S Hutter, L Boot, A Nicolas, A van den Heuvel, J Vriend, CP Ng, TTG Nieskens, V van Duinen, B de Wagenaar, R Masereeuw, L Suter-Dick, SJ Trietsch, M Wilmer, J Joore, P Vulto, HL Lanz

2

Abstract

Proximal tubules in the kidney play a crucial role in reabsorbing and eliminating substrates from the body into the urine, leading to high local concentrations of xenobiotics. This makes the proximal tubule a major target for drug toxicity that needs to be evaluated during the drug development process. Here, we describe an advanced *in vitro* model consisting of fully polarized renal proximal tubular epithelial cells cultured in a microfluidic system. Up to forty leak-tight tubules were cultured on this platform, that provides access to the basolateral as well as the apical side of the epithelial cells. Exposure to the nephrotoxicant cisplatin caused a dose-dependent disruption of the epithelial barrier, a decrease in viability, an increase in effluent LDH activity, and changes in expression of tight-junction marker zona-occludence 1, actin and DNA-damage marker H2A.X, as detected by immunostaining. Activity and inhibition of the efflux pumps P-glycoprotein (P-gp) and multidrug resistance protein (MRP) were demonstrated using fluorescence-based transporter assays. In addition, the transepithelial transport function from the basolateral to the apical side of the proximal tubule was studied. The apparent permeability of the fluorescent P-gp substrate rhodamine 123 was decreased by 35% by co-incubation with cyclosporin A. Furthermore, the activity of the glucose transporter SGLT2 was demonstrated using the fluorescent glucose analog 6-NBDG which was sensitive to inhibition by phlorizin. Our results demonstrate that we developed a functional 3D perfused proximal tubule model with advanced renal epithelial characteristics that can be used for drug screening studies.

Introduction

Renal proximal tubules play a crucial role in reabsorbing salt, water, and organic solutes such as glucose from the glomerular filtrate as well as eliminating endogenous and exogenous waste products from the body [1]. The transepithelial transport of substrates and the concentration of xenobiotics in the tubular lumen make the proximal tubule a target for drug-induced toxicity [2].

Currently, preclinical assessment of nephrotoxicity is mainly performed in animal studies. However, due to ethical concerns and the limited translatability of these models to the human situation, *in vitro* modelling is rapidly becoming important for studying solute transport, drug-induced toxicity and disease-related kidney failure [3]. Current-day *in vitro* models typically comprise human renal proximal tubule cells (RPTECs) grown on a permeable membrane support. But, these systems often lack elements such as flow or embedding in an extracellular matrix (ECM) structure and are not compatible with image-based readouts. Moreover, the permeable support membrane is a crucial barrier influencing both transport parameters and physiology of cells.

In recent years, the use of microfluidics has gained significant interest for building human tissue models of enhanced physiological relevance. These techniques, popularly referred to as Organ-on-a-Chip, add flow to cell culture systems, enable gradient formation, facilitate a 3D architecture

of tissues, allow engineering of tissue complexity through layered co-cultures, and are typically compatible with ECM-embedded cultures. Various model systems for the renal proximal tubule have been reported over the past few years [4]–[7]. Although they represent powerful examples of the added value of microfluidics to the realm of *in vitro* kidney modelling, these chips are largely prototypes, yield single data points per chip, require external tube and pump connections for each chip and are typically constructed of materials that absorb hydrophobic compounds [8].

The current challenge is to implement these prototypes into platforms combined with protocols and assays for routine use in an end-user environment [9], [10]. Robust cell culture protocols are needed that can be performed in parallel in order to test dilution series, including several replicates and appropriate controls. Furthermore, the platform needs to be compatible with a range of assays that are typically used in an *in vitro* environment, including fluorescence-based methods, immunohistochemical staining, barrier integrity monitoring, transport studies, viability assays, qRT-PCR, ELISA's and many others. Last but not least, operation of the platform should straightforward to the level that expert microfluidic skills are not required for end-users. Therefore, the organ-on-a-chip platform needs to be compatible with standard lab equipment such as pipets, (confocal) microscopes, plate readers, and other microwell-plate compatible equipment.

In this research, we used the OrganoPlate [11], a microtiter-plate based microfluidic chip platform enabling forty tissues per plate. A proximal tubule-on-a-chip was modeled with renal proximal tubule epithelial cells [12] (RPTEC, SAK 7 clone) grown as perfused tubules against an ECM.

The cells used for this study were developed and characterized by Li et al [12] and showed similar expression levels of several uptake and efflux transporters when compared to human primary proximal tubule cells. The RPTEC line further showed improved uptake and efflux compared to the HK-2 cell line, with a more sensitive detection of nephrotoxicants. Two of the efflux transporters, P-glycoprotein (P-gp) and multidrug resistance-associated protein 4 (MRP4), showed high levels of expression. Furthermore, the morphology of cell monolayers showed a typical cobblestone structure which is important for tight barriers.

After optimization of growth conditions of RPTEC in the OrganoPlate, tubules were analyzed for polarization of the epithelial layer by immunostaining, and barrier integrity through a live fluorescent dye assay. Next, the platform was evaluated for its suitability in studying (trans-epithelial) transport and drug-induced toxicity. The technology can be implemented in every basic cell laboratory with standard laboratory equipment and can be assessed with multiplexed readouts.

Materials and methods

Cell culture

Renal proximal tubule epithelial cells (RPTEC, Kidney PTEC Control Cells, SA7K Clone, Sigma, Germany, MTOX1030) were cultured on PureCol-coated (Advanced BioMetrix, 5005-B, diluted with 1:30 in HBSS (Sigma H6648), 20 min incubation at 37 °C) T75 flasks in MEME alpha Modification (Sigma, M4526) supplemented with RPTEC Complete Supplement (Sigma, MTOXRCSUP), L-glutamine (1.87 mM, Sigma, G7513), Gentamicin (28 µg/ml, Sigma, G1397) and Amphotericin B (14 ng/ml, Sigma, A2942). Cells were incubated in a humidified incubator (37 °, 5 % CO_2), and every 2-3 days, medium was changed. At 90-100 % confluency, cells were washed with HBSS (Sigma, H6648), detached with accutase (Sigma, A6964), pelleted (140 g, 5 minutes), and used for seeding in the OrganoPlate. Cells for experiments were used up to passage 3.

OrganoPlate culture

For all experiments a three-lane OrganoPlate (Mimetas BV, 4003 400B) with a channel width of 400 µm and a height of 220 µm was used. 1.6 µL of extracellular matrix (ECM) gel composed of 4 mg/ml collagen 1 (AMSbio Cultrex 3D Collagen I Rat Tail, Cat. 3447-319 020-01), 100 mM HEPES (Life Technologies, 15630) and 3.7 mg/mL $NaHCO_3$ (Sigma, 320 S5761) was injected into the middle inlet (fig. 1a) of all 40 chips. After a polymerization time of 20 minutes, 20 µL HBSS was added on top of the collagen 1 and the plate was incubated in a humified incubator at 37 °C over night. After polymerization of the ECM, the plate could be also stored in a humified incubator (37 °C) for up to a week. RPTEC were detached and resuspended in medium at a concentration of 10 x 10^6 cells per mL. 2 µL of the cell suspension (20 x 10^3 cells) was injected into each top inlet, followed by an addition of 50 µL medium to the same well. For control chips, 2 µL of medium was injected into the top inlet instead of the cell suspension. Subsequently, the OrganoPlate was placed for 5 hours at an angle of 70 degree into the incubator (37 °C, 5 % CO_2, humidified). After attachment of the cells 50 µL of medium was added to the top outlet, bottom inlet, bottom outlet (fig. 1a), and HBSS on the gel was removed. The OrganoPlate was placed flat in an incubator on an interval rocker platform (+/- 7 degree angle, 8 min interval) enabling a bidirectional flow though the perfusion channels (See fig. 5S). At day 3 antibiotics (gentamycin and amphotericin B) were removed from the medium. Medium was replaced every 2-3 days. 48-hour toxicant exposures were started at day 6, all other experiments were performed at day 7, 8,9, or 10. To show the effect of flow in the system an OrganoPlate was taken off the rocker platform from day 1 to day 4. At day 4 medium was refreshed and the plate was rocked again under same conditions as the control experiments.

Immunohistochemistry

RPTEC tubes were fixed by replacing the medium with 3.7 % formaldehyde (Sigma, 252549) in HBSS (Sigma, 55037C) for 10 minutes. Tubules were washed with washing solution (4 % fetal bovine serum (Gibco, 16140-071) in HBSS) and permeabilized (0.3 % Triton X-100 (Sigma, T8787) in HBSS) for 10 minutes. Next, cells were incubated for 45 minutes in blocking solution (2 % FBS, 2 % bovine serum albumin (BSA) (Sigma, A2153), and 0.1 % Tween 20 (Sigma, P9416) in HBSS).
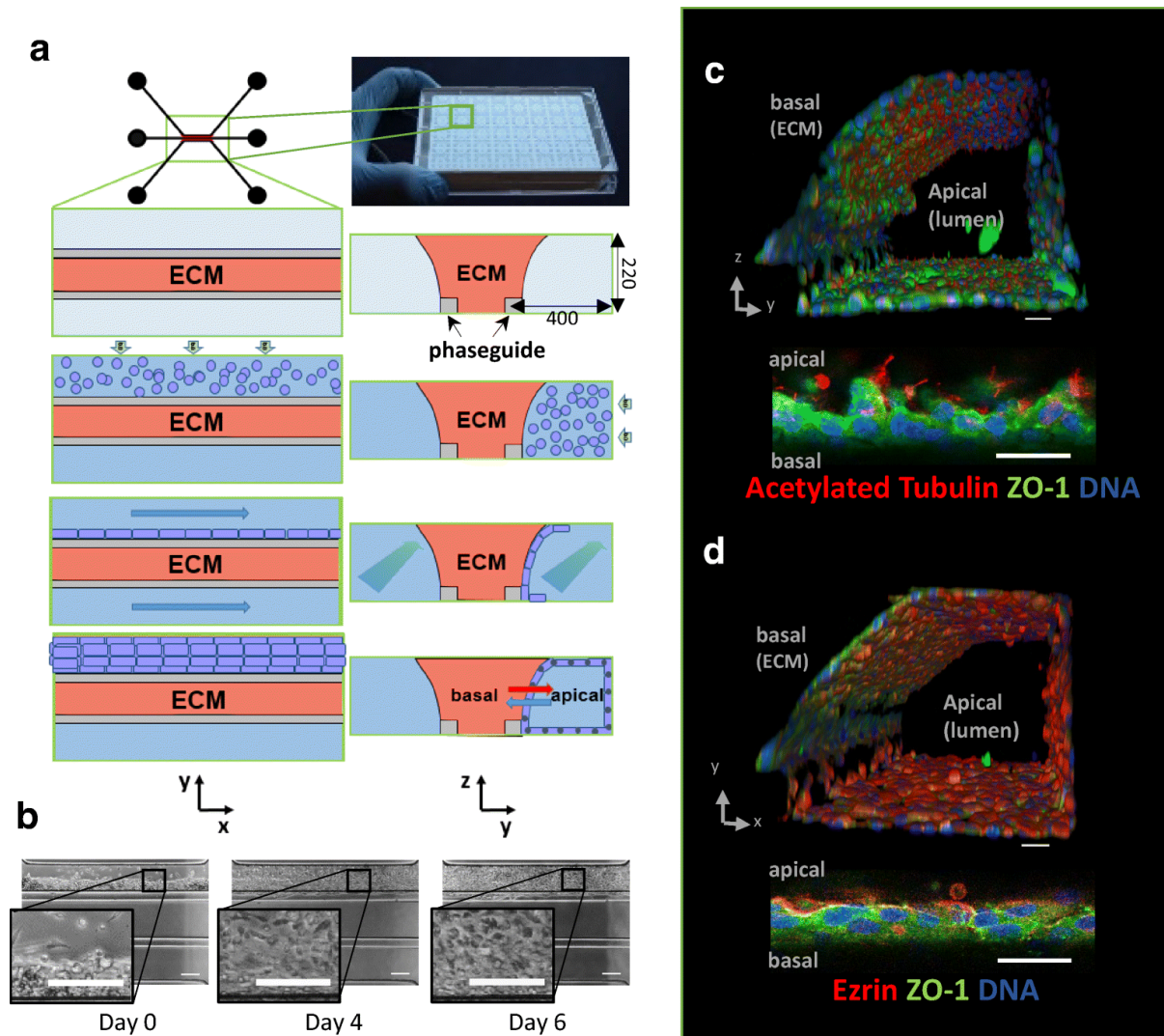

*Figure 1: **Proximal tubule-on-a chip model in the 3-lane OrganoPlate platform. a** Seeding RPTEC against collagen 1: After loading collagen 1 into the middle channel cells were seeded in the adjacent channel. By gravity cells are triggered to attach to the gel. After inducing flow RPTEC start growing a perfused tubular structure. Dimensions of the channels are in µm. **b** Phase contrast images at day 0, day 4, and day 6 after seeding of RPTEC. Images show that RPTEC form a tubular structure in the top channel in 6 days. Scale bar = 200 µm. **c,d** 3D reconstruction images of RPTEC tubules in the OrganoPlate showing a view into the lumen of tubules (apical side). The magnification shows a single z-slice of the cells growing against the ECM. Nuclei in blue. Scale bars = 30 µm. **c** Image of the tubule showing the presence of cilia (acetylated tubulin, red) pointing into the direction of the lumen. The confluent tubules express ZO-1 at the cell borders which confirms the tight junction formation between neighboring epithelial (green). **d** Ezrin expression (red) on the apical side and ZO-1 (green) expression at the cell borders of the tubules shows the correct polarization of the cells.*

Hereafter cells were incubated with the primary antibodies, diluted in blocking solution, for 60 minutes at room temperature. Primary antibodies against Ms-a-ezrin (BD Biosciences, 610602, 1:200), Ms-a-acetylated tubulin (Sigma, T6793, 1:4000), Rb-a-Zonula occludens-1 (ZO-1) (Thermo Fischer, 61-7300, 1:125, rabbit), Rb-a-Phospho-Histone (H2A.X) (Cell Signaling Technology, 9718S, 1:200, rabbit), Mouse isotype (Life technologies, 86599), Rabbit isotype (Life technologies, 86199), were used. Subsequently, cells were washed 3 times with washing solution and then incubated for 30 minutes at room temperature with secondary antibodies Gt-a-Ms IgG (H+L) Alexa Fluor 555 (Life Technologies, A21422,1:250), Gt-a-Rb IgG (H+L) Alexa Fluor 488 (Life Technologies, A32731, 1:250) diluted in blocking solution. After washing the tubules three times, nuclei were stained with DraQ5 (Abcam, ab108410, 1:1000) or Nucblue fixed cell stain (Life Technologies, R37606, 2 drops/mL) or Actin red (Life Technologies, R37112, 2 drops/mL) in the last washing step. Fluorescent images for the 3D reconstructions were taken with the Leica SP5-Sted Confocal Microscope. A z-stack of 220 μm with 2 μm between each image plane was imaged with Alexa 488, Alexa 555 and Alexa 647. Fluorescent images for the analysis of the protein expression after a toxicant exposure were taken with the ImageXpress® Micro Confocal High-Content Imaging System (Molecular Devices). A z-stack of 5 μm between each image plane was imaged with for DAPI, FITC, TRITC and Cy5 channels. A maximum projection was created for depicting the images and a summary projection was used for quantifying the fluorescent intensity of the markers.

Barrier integrity assay

The barrier integrity assay (BI assay) was performed by replacing the medium of the perfusion channel with medium containing 0.5 mg/ml TRITC-dextran (4.4 kDa, Sigma, FD20S) and 0.5 mg/ml FITC-dextran (155 kDa, Sigma, T1287). Next, the plate was imaged every two minutes for 12 minutes with the ImageXpress Micro XLS-C High Content Imaging System (Molecular Devices) at 37 °C. Leakage of the dyes from the apical side of the tube to the basal side into the ECM was measured and the ratio between the basal and the apical was analyzed with Fiji [13]. The labeled dextrans can be washed out after each measurement. The permeability of the membranes was analyzed by measuring the amount of molecules which leaked though the membrane into the adjacent gel lane over time. From these measurements the apparent permeability index (P_{app}: initial flux of a compound through a membrane, normalized by membrane surface area and donor concentration) was calculated by the following formula:

$$P_{app} = \frac{\Delta C_{receiver} \times V_{receiver}}{\Delta t \times A_{barrier} \times C_{donor}} \left(\frac{cm}{s}\right)$$

$\Delta C_{receiver}$ is the measured normalized intensity difference of the ECM to the donor channel (fig. 2b) (value of FL_{ECM}/ value of FL_{perf}) at t_{0min} and t_{10min}, $V_{receiver}$ is the volume of the measured region in the ECM channel (fig. 2b, c; channel height x channel with x channel length = 220 μm x 2304 μm x 204.8 μm = 0.0001 cm^2), Δt is the time difference t_{10min}-t_{0min} = 10 minutes, $A_{barrier}$ (0.0057 cm^2

) is the surface of the ECM interface with the medium channel, and C_{donor} is the donor concertation of the dextran dye (0.5 mg/mL).
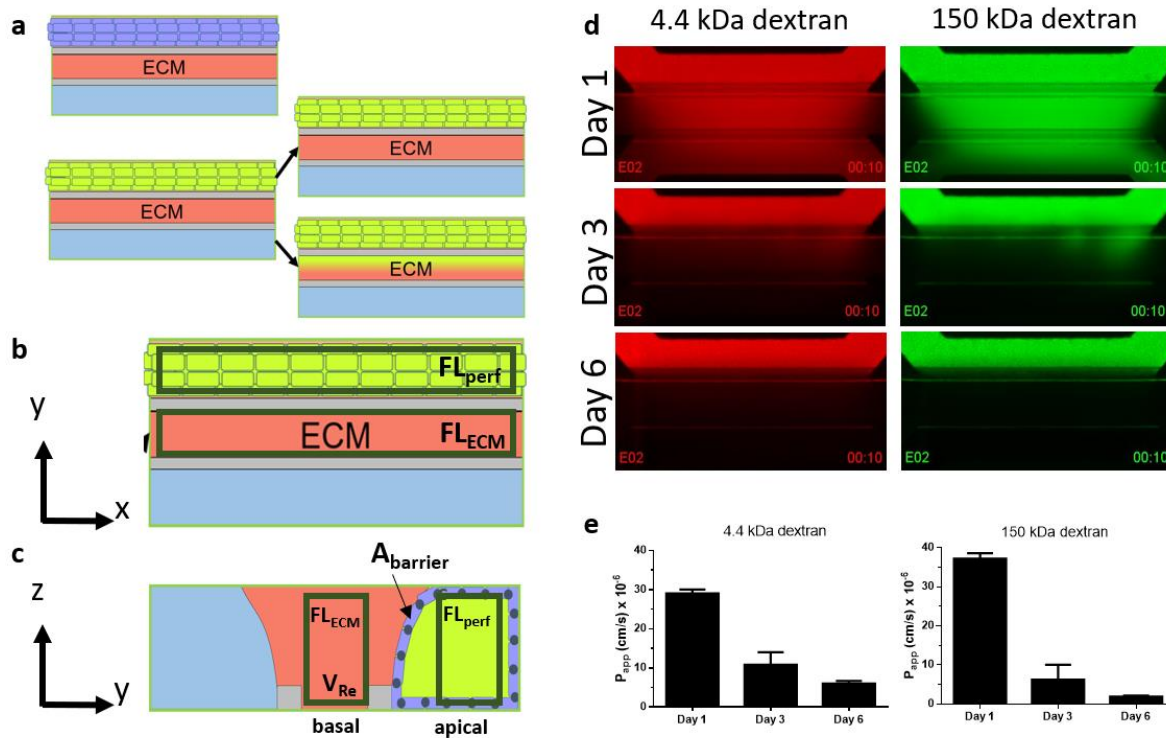
*Figure 2: **Barrier Integrity assay on tubular culture in the 3-lane OrganoPlate platform. a** The barrier integrity of the cell layer against the ECM was examined by perfusing the lumen of the tubule with dextran dyes. In healthy, leak-tight tubules dyes remain in the lumen, whereas in leaky tubules the dye enters the ECM channel. **b** The proportion of dye leaking through the tubule was monitored by measuring the fluorescence of the leaking dye into the gel. The gel channel intensity (FL_{ECM}) was normalized for the intensity of dye in the perfusion channel (F_{Lperf}). **c** Vertical illustration of the dye in the lumen of the tubule. $A_{barrier}$ is the area of the cell layer against the interface, $V_{receiver}$ (V_{re}) is the volume of the ECM behind the barrier which receives the dye. **d** Fluorescent images of the 10 minutes timepoint. Images were taken at day 1, day 3, and day 6 after seeding of RPTEC. At day 1 tubules did not form a barrier yet, whereas at day 3 the barrier is already partially formed. From day 6 the barrier is leak tight. **e** Apparent permeability (P_{app}) of the RPTEC tubules at different days. For all measurements, the same chips were analyzed over time (n=4). Error bars represent the standard deviation.*

Cisplatin exposure

To determine the toxic effect of cisplatin on RPTEC tubules in the OrganoPlate medium of both channels (apical and basal) was replaced at day 6 after seeding with TOX medium (MEME alpha Modification (Sigma, M4526) supplemented with RPTEC Tox Supplement (Sigma, MTOXRTSUP), L-glutamine (1.87 mM, Sigma, G7513)) in the presence of 0, 5, 15, 30, 90, 135, or 270 µM cisplatin (Sigma, P4394, stock: 5 mM in 0.9 % NaCl (Sigma, S7653) in H$_2$0). After 48-hour incubation on the rocker platform phase contrast images were taken and medium was sampled from the top channel. Samples from in- and outlet were pooled and used for the LDH activity assay. Next, tubes

were incubated with WST-8 to determine cell viability. The barrier integrity of the exposed tubules was assessed consecutively of the WST-8 assay. After the exposures and viability measurements, the tubules were fixed with formaldehyde and stained with H2A.X, actin and ZO-1.

Lactate Dehydrogenase Activity Assay

Lactate dehydrogenase (LDH) activity of the samples was determined using the Lactate Dehydrogenase Activity Assay Kit (Sigma, MAK066) according to manufacturer protocol. In short: The medium of the top in- and top outlet was pooled and 2 µL was added in duplicate to a 384 well plate. In parallel a concentration curve of the NADH standard was added. Next, 18µL LDH Assay Buffer was added to all sample wells to bring to an initial volume of 20µl. After a short centrifugation of the plate, 20µl Master Reaction Mix were added to each well and mixed on a horizontal shaker in the plate reader. After one minute, the absorbance was measured at 450 nm. While the plate was incubated it was measured every 2 minutes until the value of the most active sample was higher than that of the highest standard (12.5 nmol/well). For the analysis the LDH activity was determined using the following formula

$$\text{LDH activity} = \frac{\text{B x Sample Dilution Factor}}{(\text{Reaction time}) \text{ x V}}$$

Where B is the amount (nmole) of NADH generated between $t_{initial}$ and t_{final}, the reaction time is $t_{final} - t_{initial}$ (in minutes), and V is the sample volume (in mL) added to the well.

Cell viability (WST-8 assay)

The cell viability of the cells was determined using the Cell Counting Kit – 8 (Sigma, 96992). The WST-8 solution was diluted 1:11 with TOX medium and added to the channels of the OrganoPlate (30 µL in- and outlets). After 18 minutes on the rocker platform and a 2-minute flat incubation, the absorbance in the top in- and outlets was measured with the Multiskan™ FC Microplate Photometer (Thermo scientific) at 450 nm.

Calcein-AM efflux inhibition

Medium in all perfusion channels was replaced with 1 µM calcein-AM (Life technologies, C3099, stock: 1 mM in DMSO) in KHH buffer (Krebs-Henseleit (Sigma, K3753) + 10 mM HEPES (Gibco, 15630) adjusted to pH 7.4) in the presence of 10 µM cyclosporin A (Sigma, 30024, stock: 5 mM in DMSO), 500 µM Digoxin (Fluka, 4599, stock: 100 mM in DMSO), or 0.5% DMSO (Sigma, D8418, vehicle control). After a 60 minutes incubation on the rocker platform chips were washed one time with ice cold KHH buffer. In the next washing step Hoechst 33342 (2 drop/ml, Life Technologies, R37605), 10 µM PSC833 (Sigma, SML0572, stock: 5 mM in DMSO), 10 µM Ko143 (Sigma, K2144, stock: 10 mM in DMSO), and 10 µM MK571 (Sigma, M7571, stock 10 mM in H_2O) were added to the washing solution and the plate was imaged with the ImageXpress® Micro Confocal High-Content Imaging System.

MRP2/4 efflux inhibition

Medium in all perfusion channels was replaced with 1.25 µM CMFDA (Molecular Probes, C7025, stock: 2.5 mM in DMSO) in the presence of 0, 10, 20, and 30 µM MK571 (Sigma, M7571, stock 10 mM in H_2O) in KHH buffer. After 30 minutes incubation on the rocker platform the chips were washed one time with ice cold KHH buffer. In the next washing step Hoechst 33342 (2 drops/ml, Life Technologies, R37605), 10 µM PSC833 (Sigma, SML0572, stock: 5 mM in DMSO), 10 µM Ko143 (Sigma, K2144, stock: 10 mM in DMSO), and 10 µM MK571 (Sigma, M7571) were added to the washing solution and the plate was imaged with the ImageXpress® Micro Confocal High-Content Imaging System.

6-NBDG influx inhibition

Medium in the apical channel (fig. 1) was replaced with OptiHBSS (1/3 Opti-MEM (Gibco, 11058-021), 2/3 HBSS (Sigma, H6648)) containing 500 µM 6-(N-(7-Nitrobenz-2-oxa-1,3-diazol-4-yl)amino)-6-Deoxyglucose (6-NBDG, Molecular Probes, N23106, lot 1704487, stock 10 mM in H_2O) and 0, 20, 100, or 500 µM Phlorizin (Sigma, P3449, stock 200 mM in Ethanol (JT Baker, 8025.2500PE)). All conditions contained 0.25% Ethanol as vehicle control. Medium in the basal channel was replaced with 6-NBDG free medium, concentrations of phlorizin matched apical channel concentrations. After a 30 minutes incubation on the rocker platform cells were washed two times with ice cold OptiHBSS. In the second washing step Hoechst 33342 (2 drops/ml, Life Technologies, R37605) was added to the washing solution and the plate was imaged with the ImageXpress® Micro Confocal High-Content Imaging System.

Image acquisition and analysis of the transport experiments

For the in-cell transport assays plates were imaged with the ImageXpress® Micro Confocal High-Content Imaging System. A z-stack of 220 µm with 10 µm between each image plane was imaged with the FITC and the DAPI channel (fig. S1). The intensity of the FITC signal of the cells growing against the ECM was analyzed with Fiji [13] and corrected for the background and cell number. Treated chips were normalized against vehicle control.

Trans-epithelial transport assay

Medium in the apical channel was replaced with medium containing 20 µM cyclosporin A or 0.4% DMSO. Medium in the basal channel was replaced with TOX medium containing 10 µM Rhodamine 123 (Sigma, 83702, stock: 50 mM in Ethanol) together with 20 µM cyclosporin A or 0.4% DMSO. To determine the concentration of rhodamine 123 a concentration curve was added to unused chips. Tubules were incubated for 5 hours on the rocker platform. After 3 hours and after 5 hours rhodamine 123 concentration was measured by imaging the top inlets with the FITC filter on the ImageXpress Micro XLS-C High Content Imaging Systems. The apparent permeability (P_{app}) was calculated by using the formula

$$P_{app} = \frac{\Delta C_{receiver} \times V_{receiver}}{\Delta t \times A \times C_{donor}} \left(\frac{cm}{s}\right).$$

$C_{receiver}$ is the measured intensity difference in the top wells between t_{3h} and t_{5h}, $V_{receiver}$ is the receiving volume in the reservoirs of the top inlets, t is the time difference t_{5h}-t_{3h} = 2 hours, A is the surface of the ECM interface with the medium channel, and C_{donor} is the donor concertation of 10 µM rhodamine 123.

Flow simulation and experimental verification

The platform described in this work uses a gravity-based perfusion system. The fluid flow rate and induced shear stress in the microfluidic channels of the OrganoPlate was estimated using a numerical model simulated in Python (Python Software Foundation, USA). This model calculates the induced pressure difference between two volumes of fluid, which are present in two microtiter plate wells that are connected by a microfluidic channel. The numerical model is described in more detail in the supplementary information. To validate the numerical model the gravity driven flow in the OrganoPlate, absorption was sequentially measured at 494 nm using a Fluorescein solution (Sigma, 46960, 10 µg/ml in water). For the verification a 9603200B OrganoPlate (2-lane plate with 120 x 200 µm, w x h channels) was used. The FITC solution was added to the channel system with 50 µL in each in- and outlet. After tilting the plate at a set angle the fluorescence of both wells was measured and compared with the associated simulated volumes.

Statistics and data analysis

Images were analyzed using Fiji [13]. Data analysis was performed using Excel (Microsoft office 2016) and GraphPad Prism (GraphPad Software Inc., version 6.07). Error bars represent the standard deviation. Data were analyzed using one- way ANOVA followed by a Dunnett multiple comparison test which compares all treated chips to the control chips. Comparisons of two groups were done using the t-test. A p-value of < 0.05 was considered to be significant. At least 3 technical replicates per data point were obtained.

Results

Development of a proximal tubule-on-a-chip

The platform we used to develop perfused 3D proximal tubules was the 3-lane version of the OrganoPlate (fig. 1a). The top part of this plate is a standard 384-well plate with a modified glass bottom. In the bottom of the OrganoPlate, 40 microfluidic chips are embedded. One chip consists of three 400-µm-wide and 220-µm-high channels separated by ridges, the phaseguides [14]. First, an extracellular matrix (ECM) gel was loaded to the middle channel of the OrganoPlate. The liquefied ECM entered the channels by capillary action and did not overflow to the adjacent channel through meniscus pinning on the phaseguide. The ECM is free-standing, allowing interrogation of the epithelial barrier function without interference of an artificial membrane. For the seeding procedure, a single cell suspension of RPTEC was added to one of the adjacent channels and cells could attach to the ECM by placing the plate on its side, in vertical position (fig.

1a). After attachment of the cells, the plate was placed flat on a rocking platform. By positioning the in- and outlets of one chip on different heights, liquid flow was induced through the channels by leveling between the reservoirs (fig. S5a). Fluid flows are bidirectional and pulsatile. Flow profiles have been simulated and experimentally verified (fig. S5b). The change in fluorescence due to flow of FITC solution between wells showed a high correlation with the associated simulated volumes. Results show that mean flow rates of 2.02 µL/min could be achieved with a mean shear of 0.13 dyne/cm^2 (fig. S5 c,d).

The seeding and culture conditions for proximal tubules-on-a-chip based on RPTEC cells were optimized by testing different settings for parameters, such as seeding density, ECM composition, medium composition, and perfusion height and angle. Figure 1b shows optimal tube formation of RPTEC over time. As seen in figure S3 the flow is crucial for the tubule formation. Without any flow, tubule formation is not possible. In figure S4 the long-term viability of the RPTEC in the OrganoPlate is depicted. RPTEC are stable in the OrganoPlate up to day 11. After this time period, cells start invading the ECM which makes barrier dependent assays impossible. Therefore, it was decided to perform all assays from day 6 to day 10.

Proximal Tubules-on-a-chip form polarized tight barriers
RPTEC tubules were cultured in the OrganoPlate for 7-10 days. As depicted in figure 1c, RPTEC formed a tubular structure with cells lining the ECM (curved part of the tubule) and the walls of the channel, thus having an open, perfused lumen. Confluent tubules formed tight-junctions as visualized by the zona-occludence 1 tight junction (ZO-1) expression [15], and display primary cilia visualized by acetylated tubulin staining [16]. A single cilium per cell was observed, located at the apical side of the cell layer pointing towards the lumen of the tubule (fig. 1c,d). The tubules were also stained for Ezrin [17] that was expressed on the luminal side of the tubule (fig. 1d). It is thus confirmed that the tubes are polarized in a correct manner, with the lumen being the apical side (corresponding to the pre-urine side in an *in vivo* situation) and the basal side being against the extracellular matrix (corresponding to the blood side in and *in vivo* situation).

Subsequently, the integrity of the epithelial barrier was investigated. To this end, a fluorescently labeled dextran was administered to the lumen of the tube. Leakage of the fluorescent dextran from the perfusion channel into the gel compartment was monitored and quantified in order to have a measure for the integrity of the epithelial cell monolayer (fig. 2a-c). To monitor the tubule formation over several days, a higher molecular weight dextran (150 kDa FITC) and a lower molecular weight dextran (4.4 kDa TRITC) were used and leakage was assessed at day 1, 3, and 6 days after seeding. At day 1, no barrier formation could be detected, whereas at day 3 the tubes were partly leak-tight. At day 6, the tubules were fully leak-tight for both dyes (fig 2d). After quantification of the signal at day 6, the calculated P$_{app}$ (apparent permeability) of the tubules were 6 x 10^{-6} cm/s for the 4.4 kDa dextran and 2 x 10^{-6} cm/s for the 150 kDa dextran (fig. 2e). A good barrier integrity of the tubule is crucial for assessing transport and directional toxicity as it

allows interrogation and exposure of the apical and basolateral sides in independently from one another.

The proximal tubule-on-a-chip allows nephrotoxicity assessment

Next, kidney tubules were assessed for toxicity response to cisplatin. Cisplatin is an anti-cancer drug, which is used for the treatment of tumors of the lung, ovary, testicles, and head and neck [18]. The main route of the excretion of cisplatin is via the proximal tubules, which leads to a higher accumulation of the drug in the cells compared to other organs [19]. Kidney tubules were exposed six days after seeding for 48 hours to cisplatin at concentrations ranging from 5 to 270 µM. The toxic effect of cisplatin on the proximal tubules was determined through multiplexing several assays: phase contrast imaging, barrier integrity assessment, WST-8 viability measurement, LDH release and immunohistochemical staining of tight junctions, DNA damage and cytoskeleton integrity. The morphology of the tubules was analyzed by phase contrast imaging and visually started to change at 270 µM cisplatin concentration, at lower concentrations no significant differences were observed (fig. 3a). Cisplatin showed a dose-dependent disruption of the barrier integrity of the tubes as determined by leakage of fluorescent dextran 4.4 kDa and 150 kDa (fig 3b,c) with a matching increase in calculated P_{app} for both the small and large dextran (fig. 3d).

In addition to measuring the impairment of the barrier integrity of the tubules, the cell viability was assessed using the live cell enzymatic activity WST-8 assay. A decrease in cell viability was observed at cisplatin concentrations of 30 µM and higher, which was reduced to approximately 76% compared to the vehicle control at the highest concentration of 270 µM (fig. 3e). Consistent with this, a significant increase in LDH (lactate dehydrogenase) release into the lumen was detected at cisplatin concentrations of 30 µM and higher (fig. 3f). Immunohistochemical analysis of the exposed tubules further confirmed the toxicity of cisplatin. At concentrations of 30 µM and higher, cisplatin caused increased DNA-damage (detected by H2A.X DNA-damage marker staining [20], Fig. 3g,h) and reduced expression of ZO-1 protein in the tight junctions (fig. 3g and 3j). Changes in the actin cytoskeleton were observed from 5 µM onwards (fig. 3g,i).

Active substrate transport across the epithelial membrane

The kidneys play a crucial role in eliminating drugs and metabolic waste products through excretion into the urine [21]. Many compounds require active transport by dedicated enzymes, the efficiency of which can be compromised by different drugs [2], [22].

To study the transporter functionality of kidney tubules in the OrganoPlate, calcein-AM and CMFDA were used to monitor P-gp and MRPs, respectively. These two transporters, that transport substrates into the apical lumen, are from the ATP-binding cassette family of transporters. P-gp mainly transports cationic as well as unconjugated xenobiotics whereas MRP is responsible for removing conjugated compounds from the body [22], [23].
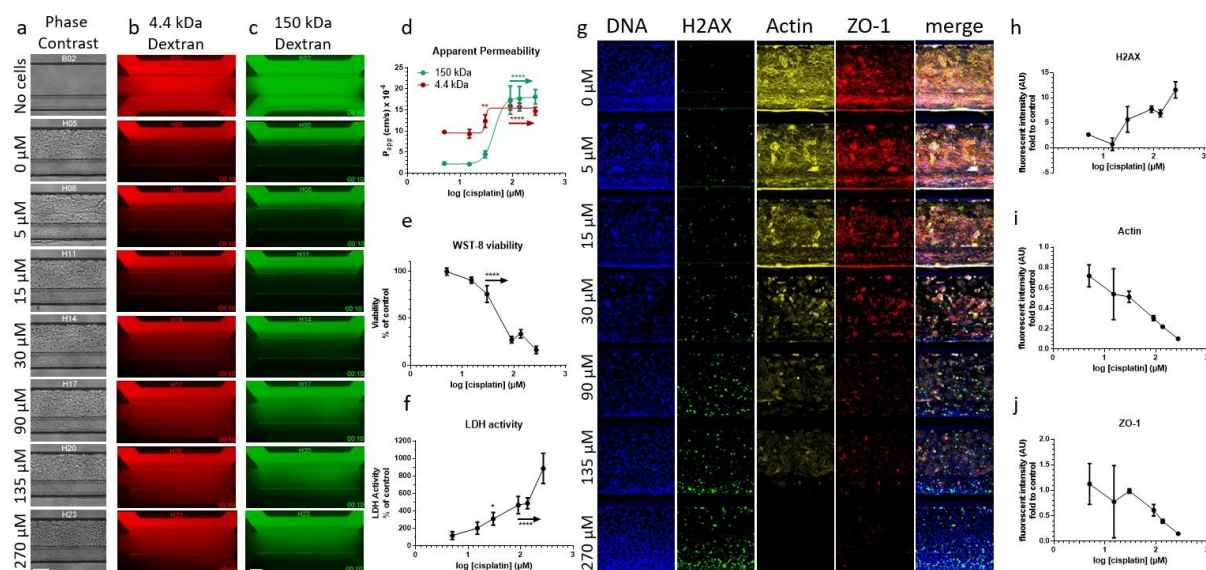
Figure 3: Toxicant readouts after 48 hours cisplatin exposure*. a visual break down of the tube after 48h treatment at highest concentrations. Scale bar = 100 µm. b-c Perfusion of the lumen in the top channel with a lower sized dextran dye of 4.4 kDa and a higher sized dextran dye of 150 kDa. From a concentration of 90 µM the ECM behind the barrier is filled with dye, whereas at concentrations of 5 µM and 15 µM no difference compared to vehicle control can be seen. Scale bar = 200 µm. d For quantification of the barrier function the apparent permeability (Papp) was calculated. For both dextran sizes a significant increase of the Papp could be detected from 90 µM (p<0.0001) compared to vehicle control. e To quantify viability of the cells a WST-8 assay was used. WST-8 is reduced by the cells to an orange formazan product which can be measured with an absorbance reader at 450 nm. Viability was significantly reduced (p<0.0001) from 30 µM compared to vehicle control. f LDH activity in the medium indicated the number of dead cells. The LDH assay detected, similar to the WST-8 assay a significant effect of cisplatin from 30 µM (p<0.05). g Maximum projections or the Immunostaining against H2A.X (DNA damage), actin (cytoskeleton) and ZO-1 (tight junction marker). Scale bar = 200 µm. h-j Fluorescent intensity analysis of the summary projections of DNA damage marker H2A.X, actin cytoskeleton marker, and tight junction marker ZO-1. The intensity of all three markers is corrected for the background and nuclei count. Graphs show data of 3 chips per condition. Error bars represent the standard deviation.*

Calcein-AM is a substrate for P-gp which is often used to assess the functionality of the transporter [23]. Cell tracker reagent 5-chloromethylfluorescein diacetate (CMFDA) is a compound for the MRP transporters [24]. Both compounds enter the cells passively and are converted inside of the cells to the green fluorescent dyes calcein and GS-MF, respectively [23], [25]. Cyclosporin A is an inhibitor of the P-gp transporter, whereas digoxin, which is a medication used to treat various heart conditions, is a substrate for P-gp [2] (fig. 4a). MK571 is an inhibitor of the MRPs [2] (fig 4d).

To measure the influence of compounds on transport activity in the proximal tubule-on-a-chip we set up fluorescent substrate-based activity assays (fig. S1). For the analysis of the uptake of fluorescence inside of the cells lining the ECM, a z-stack of the tubule was imaged, and planes of the desired area are selected (fig. S1e). After removal of the signal from out-of-focus cells, stacks were compressed, and the signal was integrated (fig. S1f).
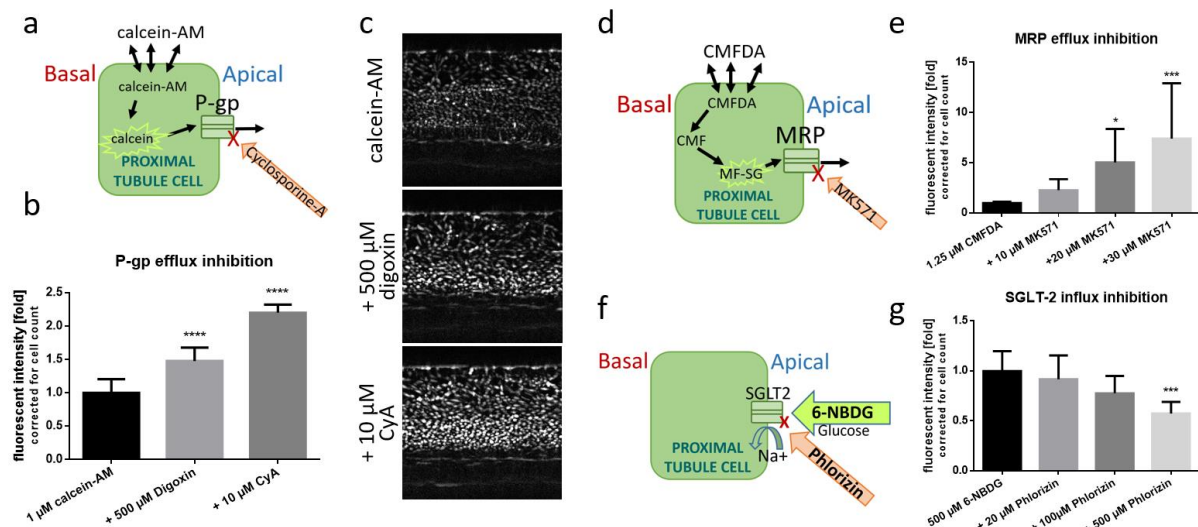
Figure 4: **Evaluation of P-gp, MRP and SLGT2 transporter activity in proximal tubule-on-a-chip. a** *When the non-fluorescent calcein-AM enters the cell membrane esterases in the cytoplasm cleave the acetoxymethyl (AM) ester group, which results in fluorescent calcein. Calcein-AM is pumped out of the cell by the P-glycoprotein-transporter (P-gp).* **b** *Inhibition of calcein-AM efflux: RPTEC were incubated for one hour with 1 µM calcein-AM ± inhibitors. 10 µM cyclosporin A showed the highest inhibitory effect followed by 500 µM digoxin.* **c** *Z-Projections of representative images of the calcein-AM exposed RPTEC area. A higher fluorescent signal could be observed in the presence of transport inhibitors. Scale bar = 200 µm.* **d** *Similar to calcein-AM non-fluorescent CMFDA enters the cells passively. Inside the cells CMFDA is transformed to fluorescent MRP substrate GS-MF.* **e** *Dose-dependent efflux inhibition of GS-MF by MK571 resulted in a significant increase of fluorescent signal inside the cells.* **f** *Influx of fluorescent glucose analog 6-NBDG is inhibited by phlorizin. 6-NBDG influx is mediated by the sodium dependent SGLT2 transporter.* **g** *6-NBDG influx into RPTEC was significantly inhibited by 500 µM phlorizin and a dose dependent trend was observed when inhibited with 20 and 100 µM phlorizin. **: p<0.01 ***: p<0.001 and ****: p<0.0001 one-way Anova with Dunnett's comparison test. Each of the three graphs shows combined data of two independent experiments with 2-5 chips per condition. Error bars represent the standard deviation.*

As both dyes enter the cells passively, RPTEC tubules were exposed to the dyes as well as their respective inhibitors from the apical as well as basal side. A 2.2 ± 0.1 or 1.5 ± 0.2 fold increase in calcein accumulation was observed after co-incubation with cyclosporin A or digoxin, respectively, confirming P-gp activity as both drugs competitively interact with the efflux pump (fig. 4b-c). To monitor MRP-function, an efflux inhibitor cocktail of PSC833, MK571 and Ko143 was used to avoid redundancy of other transporters [23]. A dose-dependent inhibition of GS-MF efflux was observed upon increasing MK571 concentrations, as shown in Figure 4e, confirming MRP activity.

In addition to the efflux transporters, the glucose uptake by the sodium-glucose linked transporter SGLT2 [26], [27] was evaluated using the fluorescent glucose analogue 6-NBDG [28]. SGLT2-mediated influx from tubular lumen into the cells was sensitive to inhibition by the SGLT inhibitor phlorizin [29] (fig. 4f-g). This confirms the presence and activity of the SGLT2 transporter.

The proximal tubule-on-a-chip allows transepithelial transport assessment

To further examine the capability of transepithelial transport across the epithelium of the 3D perfused proximal tubules, the flux of rhodamine123 from the basolateral to the apical compartment was assessed. Rhodamine123 is a substrate of P-gp and its transport was analyzed in absence and presence of the transport inhibitor cyclosporin A [30].
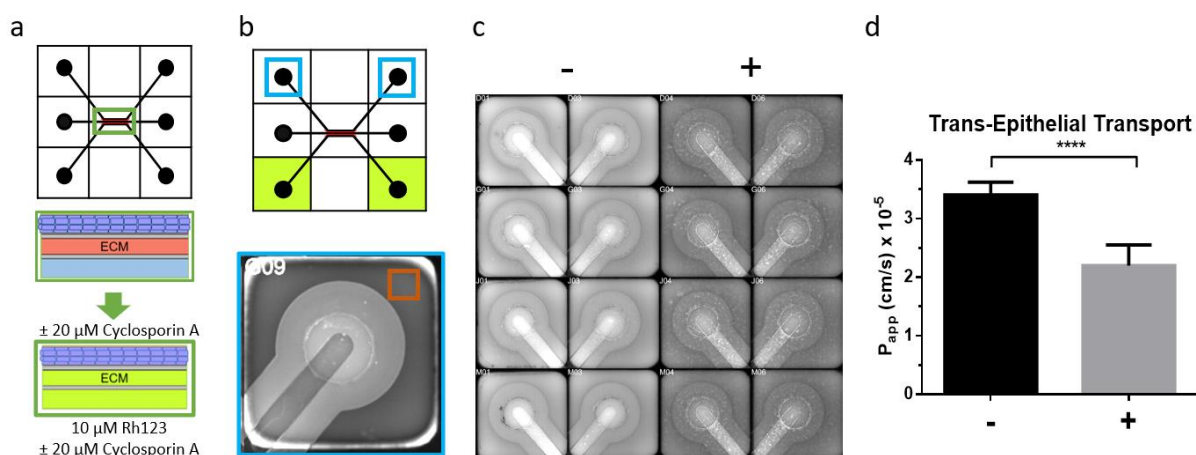

Figure 5: Transepithelial transport of rhodamine 123. a 10 μM rhodamine 123 was added solely to the basal side of the tubule with or without 20 μM cyclosporin A present at both sides of the tube. b After 3 and 5 hours images were taken from the inlets guiding to the lumen of the tubule (blue squares: measured wells). The intensity above the glass bottom of the wells was measured (orange square: area selection). To determine the concentration of rhodamine 123 in the top wells, spiked samples were added to empty chips on the same plate and analyzed. The resulting concentrations were used to calculate the Papp of the transport of rhodamine 123. c Images of the top in- and outlets or the OrganoPlate show the apical fluorescent signals after 5-hour incubation of rhodamine 123 on the basal side of the tubule. A decreased fluorescent signal was observed after co-incubation with cyclosporin A, as shown in the top inlets. -: without transport inhibition, +: with 20 μM cyclosporin A addition (apical and basal). d A significant decrease in Papp was observed when adding rhodamine 123 together with 20 μM cyclosporin A. ****: p<0.0001. Data are combined from two independent experiments with 5-9 chips per plate and per condition. Error bars represent the standard deviation.

The experimental set-up is shown in Figure 5a-b. Rhodamine123 was administered to the basal perfusion channel and measured in the perfusion medium on the apical side. In order to have a highest signal-to-noise ratio, the fluorescent signal was measured in apical-side in- and outlet, where the liquid column was largest. Inhibition of transport by cyclosporine A reduced fluorescence signal in the apical-side in- and outlets as shown by representative images in Figure 5c. It is known that cyclosporin A has a toxic effect on the kidney. Therefore, its effect on the barrier integrity was assessed. It was found that a concentration of 20 μM cyclosporin A was determined as safe as transport inhibitor, supported by the absence of an effect on barrier integrity (fig. S2). The P_{app} of rhodamine123 changed from $3.4*10^{-5} \pm 0.1*10^{-5}$ cm/s without inhibitor to $2.2*10^{-5} \pm 0.1*10^{-5}$ cm/s with cyclosporin A, indicating (inhibition of) active transport (fig. 5d). This is a clear demonstration that transepithelial transport can be assessed in the system.

Discussion & Outlook

We reported the development of a functional proximal tubule-on-a-chip model which can be implemented for routine assessment of kidney toxicity and drug-drug interaction studies. The OrganoPlate platform allows parallel culture and assessment of 40 independent kidney tubules. This is important in toxicological studies or in compound testing as it allows for proper controls, replica's and dilutions series. Induction of flow is realized by passive leveling on an interval rocker system, which is an easy to use alternative to complex pump solutions. Other than the rocking platform, no further specialized lab equipment is needed. As the format of the platform is a standard microtiter layout of a 384 well plate it is fully compatible with most readers, microscopes and robot handling equipment. The platform is fully pipet operated and media changes as well as reagent additions are non-invasive. Physiologically relevance of the system is enhanced by culturing epithelial cells directly against an extracellular matrix mimic in a manner that is free of artificial membranes, under application of perfusion flow and by mimicking the 3D morphology.

A critical aspect in the concept is the selective patterning of extracellular matrix in the chips. In order to do this surface tension techniques have been employed that allow selective ECM priming using pipetting means only. As a consequence thereof, only part of the tube is exposed to the ECM (curved part).

This does not hamper the measurement results as the barrier and the rhodamine transport assay exclusively consider the cell layer against the extracellular matrix. Other systems are known from literature that have full ECM embedment [31], however, such systems come at the cost of throughput and ease of handling, as it is impossible to create a lumen in an ECM gel with pipetting steps only.

Similar choices were made with respect to the dimensions of the proximal tubule. In this study the diameter of the tubules are 400 µm, which is significantly larger than the *in vivo* proximal tubules (approximately 60 µm [32]). However, the choice for larger dimensions allowed a greater sensitivity of assays, particularly those that are executed off chip.

We showed the multiplexing assays in a microfluidic format. The barrier integrity could be monitored in real time by adding a reporter dye. In parallel cellular enzymatic activity (WST-8) and LDH release could be measured. All three assays yielded a similar result to cisplatin exposure, indicating the robustness of the model. Immunohistochemical staining was also used in a multiplex manner for assessment of the effect of cisplatin on the tight junctions (ZO-1), cytoskeleton (actin) and DNA damage (H2A.X). Although some showed higher sensitivity than the live assays, the stains represent an end-point assay and require much more effort to execute properly. Moreover, only a limited number of stains could be multiplexed in the same model, requiring replica's to be used for different analyses.

The multiplexed live assays used for acute kidney toxicity detection here are compatible with chronic toxicity assessments. For example the barrier integrity assays was previously used to study 5-days exposure of gut tubules to toxicants [33]. Non-invasive assays are important to study chronic effects of drugs that only exert negative effects after prolonged use. The proximal tubule model developed here together with multiplexed assays and the possibility for repeated dosing of the model allows for future longitudinal studies.

In this publication we used the microfluidic system for growing tubular structures. In addition to that, other cell types can be embedded into the ECM. An example of functional 3D networks of neurons and glia embedded in the ECM of one channel with an adjacent medium channel is shown by Wevers et al. [34] and Lanz et al. studied the behavior of breast cancer cells grown in an ECM [35]. The method of culturing cells embedded in the ECM can be easily combined with the model presented here: instead of culturing the RPTEC against a pure ECM, supporting cells can be added into the ECM. In addition to this the complexity of the model could be further increased by growing an endothelial tubule in the basal-side perfusion channel. Ultimately, we aim to combine endothelium, fibroblasts and podocytes to have a fully functional kidney-on-a-chip model.

We showed two different possibilities to monitor the transport of the proximal tubules. First, we measured and analyzed the signal of compounds retained by the cells lining the ECM layer. Second, we showed feasibility of transepithelial transport studies on the RPTEC containing tubules using the fluorescent substrate, rhodamine123. Both types of experiments show clear transporter functionality, whereas the latter is the most complex functional assay. We have not assessed organic anion transporter (OAT) expression by the RPTEC used in this study, but 2D evaluation by Suter-Dick [36] showed no response to Tenofovir, indicating absence of the OAT1 transporter. This limits the use of the cell line for assessment of transport of organic ions. To compensate for this, we also implemented a cell line over expressing the organic anion transporter 1 (ciPTEC, [37]). In future work we will compare the performance of both cell models in response to a range of blinded compounds.

For future studies, transport capabilities will be shown also for non-fluorescent substrates. To achieve this goal, radiolabeled compounds or mass spectrometry can be used to analyze and quantify transport. In this manner a much wider range of compounds and transporter functionality can be investigated. These off-plate assays will require sampling of the perfusate instead of the microscope-based read outs used here. The use of microfluidic chips requires limited amounts of cells and medium, which is positive in the light of use of valuable materials with restricted access. However, for certain analysis methods the small sample volumes could be limiting. Detection of transported compounds will depend on the sensitivity of the analysis method (e.g. mass spectrometry). Other off-plate analyses as e.g. qRT-PCR are feasible through pooling of chip lysates. Such functional assays will be of great support for *in vitro* to *in vivo* extrapolation.

In summary we developed a user-friendly, functional kidney-on-a-chip model that can be used to study the effect of compounds in 40 parallel cultured renal tubules. The tubules could be assessed for barrier function by fluorescent imaging and multiplexed with a range of assays including viability, LDH leakage and immunohistochemical staining. In addition, transporter activity was shown by means of transport inhibition studies for both substrate uptake, as well as transcellular transport. The functionality of the platform in combination with the ease of handling and decent throughput makes this a useful platform for studying nephrotoxicity, compound excretion, drug-drug interaction studies and disease mechanisms.

Acknowledgements

Regarding originality and conflict of interest

This publication contains original work. The authors M.K. Vormann, L.Gijzen, S. Hutter, L.Boot, A.Nicolas, A. vd Heuvel, B. de Wagenaar, J. Joore, P.Vulto, and H.L. Lanz are or were employees of Mimetas B.V. This affiliation is declared. The OrganoPlate® is a registered trademark of MIMETAS BV.

References

[1]   Lauralee Sherwood, *Human Physiology: From Cells to Systems*. Brooks Cole, 1997.

[2]   K. M. Morrissey, S. L. Stocker, M. B. Wittwer, L. Xu, and K. M. Giacomini, "Renal Transporters in Drug Development," *Annu. Rev. Pharmacol. Toxicol.*, vol. 53, no. 1, pp. 503–529, 2013.

[3]   M. J. Wilmer, C. P. Ng, H. L. Lanz, P. Vulto, L. Suter-Dick, and R. Masereeuw, "Kidney-on-a-Chip Technology for Drug-Induced Nephrotoxicity Screening," *Trends Biotechnol.*, vol. 34, no. 2, pp. 156–170, 2016.

[4]   K. A. Homan *et al.*, "Bioprinting of 3D Convoluted Renal Proximal Tubules on Perfusable Chips," *Sci. Rep.*, vol. 6, pp. 1–13, 2016.

[5]   E. M. Vedula, J. L. Alonso, M. A. Arnaout, and J. L. Charest, "A microfluidic renal proximal tubule with active reabsorptive function," *PLoS One*, vol. 12, no. 10, pp. 1–15, 2017.

[6]   K. J. Jang *et al.*, "Human kidney proximal tubule-on-a-chip for drug transport and nephrotoxicity assessment," *Integr. Biol. (United Kingdom)*, vol. 5, no. 9, pp. 1119–1129, 2013.

[7] Y. Qu *et al.*, "A nephron model for study of drug-induced acute kidney injury and assessment of drug-induced nephrotoxicity," *Biomaterials*, vol. 155, pp. 41–53, 2018.

[8] B. J. van Meer *et al.*, "Small molecule absorption by PDMS in the context of drug response bioassays," *Biochem. Biophys. Res. Commun.*, vol. 482, no. 2, pp. 323–328, 2017.

[9] V. van Duinen, S. J. Trietsch, J. Joore, P. Vulto, and T. Hankemeier, "Microfluidic 3D cell culture: From tools to tissue models," *Curr. Opin. Biotechnol.*, vol. 35, pp. 118–126, 2015.

[10] A. Junaid, A. Mashaghi, T. Hankemeier, and P. Vulto, "An end-user perspective on Organ-on-a-Chip: Assays and usability aspects," *Curr. Opin. Biomed. Eng.*, vol. 1, pp. 15–22, 2017.

[11] S. J. Trietsch, G. D. Israëls, J. Joore, T. Hankemeier, and P. Vulto, "Microfluidic titer plate for stratified 3D cell culture," *Lab Chip*, vol. 13, no. 18, pp. 3548–3554, 2013.

[12] S. Li *et al.*, "Development and Application of Human Renal Proximal Tubule Epithelial Cells for Assessment of Compound Toxicity," *Curr. Chem. Genomics Transl. Med.*, vol. 11, no. 1, pp. 19–30, Feb. 2017.

[13] J. Schindelin *et al.*, "Fiji: An open-source platform for biological-image analysis," *Nat. Methods*, vol. 9, no. 7, pp. 676–682, 2012.

[14] P. Vulto, S. Podszun, P. Meyer, C. Hermann, A. Manz, and G. A. Urban, "Phaseguides: A paradigm shift in microfluidic priming and emptying," *Lab Chip*, vol. 11, no. 9, pp. 1596–1602, 2011.

[15] B. R. Stevenson, J. D. Siliciano, M. S. Mooseker, and D. A. Goodenough, "Identification of ZO-1: a high molecular weight polypeptide associated with tight junction (zonula occludens) in a," *J. Cell Biol*, vol. 103, no. September, pp. 755–766, 1986.

[16] V. Raghavan and O. A. Weisz, "Flow stimulated endocytosis in the proximal tubule," *Curr. Opin. Nephrol. Hypertens.*, vol. 24, no. 4, pp. 359–365, 2015.

[17] M. Berryman, Z. Franck, and A. Bretscher, "Ezrin is concentrated in the apical microvilli of a wide variety of epithelial cells whereas moesin is found primarily in endothelial cells," *J. Cell Sci.*, vol. 105, no. 4, pp. 1025–1043, 1993.

[18] G. Giaccone, "Clinical perspectives on platinum resistance," *Drugs*, vol. 59, no. SUPPL. 4, pp. 9–17, 2000.

[19] G. S. Oh *et al.*, "Cisplatin-induced kidney dysfunction and perspectives on improving treatment strategies," *Electrolyte Blood Press.*, vol. 12, no. 2, pp. 55–65, 2014.

[20] L. J. Kuo and L.-X. Yang, "Gamma-H2AX - a novel biomarker for DNA double-strand breaks.," *In vivo*, vol. 22, no. 3, pp. 305–9, 2008.

[21] R. Masereeuw and F. G. M. Russel, "Regulatory pathways for ATP-binding cassette transport proteins in kidney proximal tubules," *AAPS J.*, vol. 14, no. 4, pp. 883–894, 2012.

[22] K. M. Giacomini *et al.*, "Membrane transporters in drug development," *Nat. Rev. Drug Discov.*, vol. 9, no. 3, pp. 215–236, 2010.

[23] P. Caetano-Pinto, M. J. Janssen, L. Gijzen, L. Verscheijden, M. J. G. Wilmer, and R. Masereeuw, "Fluorescence-Based Transport Assays Revisited in a Human Renal Proximal Tubule Cell Line," *Mol. Pharm.*, vol. 13, no. 3, pp. 933–944, 2016.

[24] S. E. Jenkinson, G. W. Chung, E. van Loon, N. S. Bakar, A. M. Dalzell, and C. D. A. Brown,

"The limitations of renal epithelial cell line HK-2 as a model of drug transporter expression and function in the proximal tubule.," *Pflugers Arch.*, vol. 464, no. 6, pp. 601–611, 2012.

[25] H. Lindenmaier, M. Becker, W. Haefeli, and J, "Interaction of progestins with the human multidrug resistance-associated protein 2 (MRP2)," *Drug Metab.*, vol. 33, no. 11, pp. 1576–1579, 2005.

[26] I. S. Wood and P. Trayhurn, "Glucose transporters (GLUT and SGLT): expanded families of sugar transport proteins," *Br. J. Nutr.*, vol. 89, no. 1, pp. 3–9, 2003.

[27] V. Vallon *et al.*, "SGLT2 mediates glucose reabsorption in the early proximal tubule," *J. Am. Soc. Nephrol.*, vol. 22, no. 1, pp. 104–112, 2011.

[28] D. W. Jung, H. H. Ha, X. Zheng, Y. T. Chang, and D. R. Williams, "Novel use of fluorescent glucose analogues to identify a new class of triazine-based insulin mimetics possessing useful secondary effects," *Mol. Biosyst.*, vol. 7, no. 2, pp. 346–358, 2011.

[29] J. R. L. Ehrenkranz, N. G. Lewis, C. R. Kahn, and J. Roth, "Phlorizin: A review," *Diabetes. Metab. Res. Rev.*, vol. 21, no. 1, pp. 31–38, 2005.

[30] F. J. Sharom, "The P-glycoprotein multidrug transporter," *Gen. Pharmacol.*, vol. 27, no. 8, pp. 1283–1291, 2011.

[31] E. J. Weber *et al.*, "Development of a microphysiological model of human kidney proximal tubule function," *Kidney Int.*, vol. 90, no. 3, pp. 627–637, 2016.

[32] H.-G. Liebich, *Funktionelle Histologie der Haussäugetiere und Vögel: Lehrbuch und Farbatlas für Studium und Praxis*, 5th ed. Stuttgard: Schattauer, 2010.

[33] S. J. Trietsch *et al.*, "Membrane-free culture and real-time barrier integrity assessment of perfused intestinal epithelium tubes," *Nat. Commun.*, vol. 8, no. 1, pp. 1–7, 2017.

[34] N. Wevers *et al.*, "3D networks of iPSC-derived neurons and glia for high-throughput neurotoxicity screening," *Toxicol. Lett.*, vol. 258, p. S157, 2016.

[35] H. L. Lanz *et al.*, "Therapy response testing of breast cancer in a 3D high-throughput perfused microfluidic platform," *BMC Cancer*, vol. 17, no. 1, p. 709, 2017.

[36] L. Suter-Dick *et al.*, "Combining Extracellular miRNA Determination with Microfluidic 3D Cell Cultures for the Assessment of Nephrotoxicity: a Proof of Concept Study," *AAPS J.*, vol. 20, no. 5, pp. 1–9, 2018.

[37] J. Vriend *et al.*, "Screening of Drug-Transporter Interactions in a 3D Microfluidic Renal Proximal Tubule on a Chip," *AAPS J.*, vol. 20, no. 5, 2018.

2

Supplementary Material
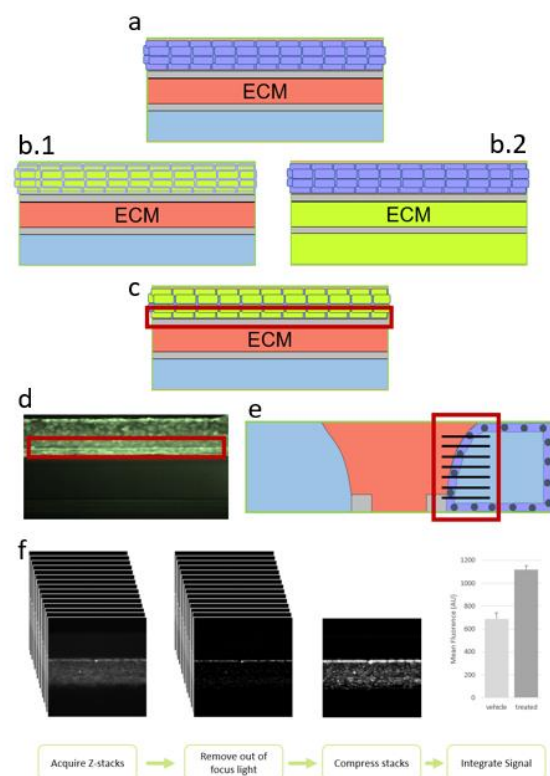
Supplementary figure S1: Cellular transport assay. a *Perfused tubules in the top channel of the OrganoPlate.* ***b*** *Exposure of the tubule with a fluorescent compound either transported through influx transporters into cells, or by efflux transporters out of cells. Both transport mechanisms can be inhibited by specific inhibitors.* ***b.1*** *Apical exposure with fluorescent compound from the apical side (inside of the tubule).* ***b.2*** *Basal exposure from the basal side of the tubule.* ***c*** *Self-fluorescent compounds need to be washed out of the ECM, whereas compounds which are only fluorescent in the cells can be measured without washing. Compound retention in the cells is measured in the cells against the ECM surface (red square).* ***d*** *Fluorescent image of a tube with a green fluorescent compound retained in the cells.* ***e*** *Vertical illustration of the area imaged for the analysis. The black stripes indicate the planes of the z-stack images.* ***f*** *Image analysis: z-stack of the tubule is acquired, and the out of focus light is removed. Subsequently the stack is compressed, and the intensity of the image is measured. After blocking the transport of the compound, the nuclei of the cells are stained and the FITC signal is corrected for the nuclei count.*
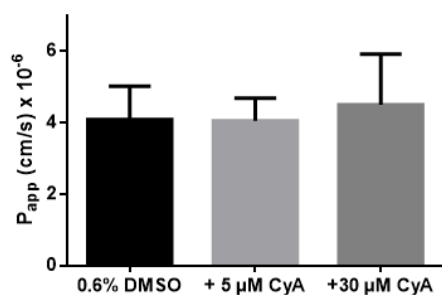
Supplementary figure S2: Apparent permeability (Papp) after cyclosporin A exposure. RPTEC tubules were exposed for 24 hours to 5 µM and 30 µM cyclosporin A. Both concentrations did not show a significant increase of the Papp after exposure. Each error bar represents the standard deviation of 4-5 chips.

a

b
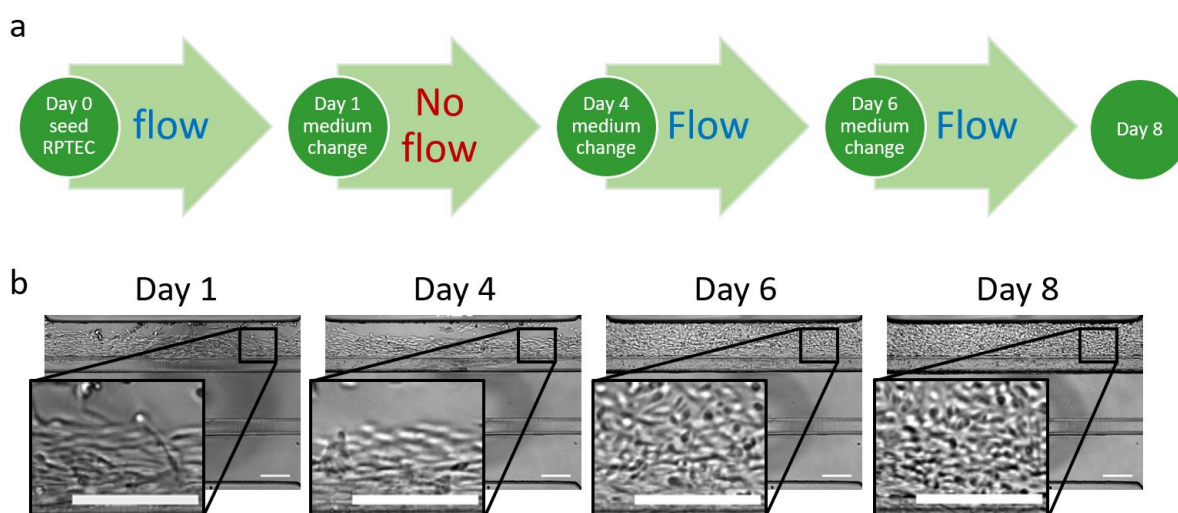
Supplementary figure S3: Importance of flow for tube formation. a Tubules were seeded and kept on the rocker platform for 24h hours. From day 1 to day 4 no flow was applied. The plate was placed back on the rocker platform from day 4 to 8. b Culturing the tubules without flow resulted in a lack of tubule formation at day 4 compared to the standard condition with flow (see fig. 1b). After reintroduction of flow the tube formation process recovered which resulted in a fully-grown tubule at day 8 (instead of day 6 as shown in fig. 1b). Scalebars = 200 µm.
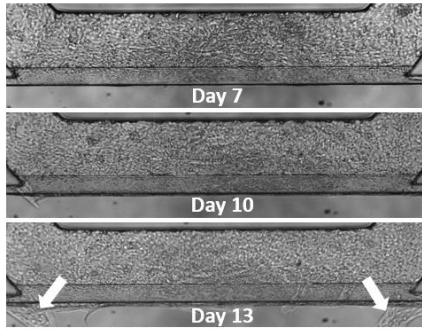
Supplementary figure S4: Stability of RPTEC tubules in the OrganoPlate. *RPTEC tubules are stable up to day 11. After this time period RPTEC start invading the ECM and the tubules are not leak tight anymore. Therefore, experiments should be performed during day 6 and day 11.*
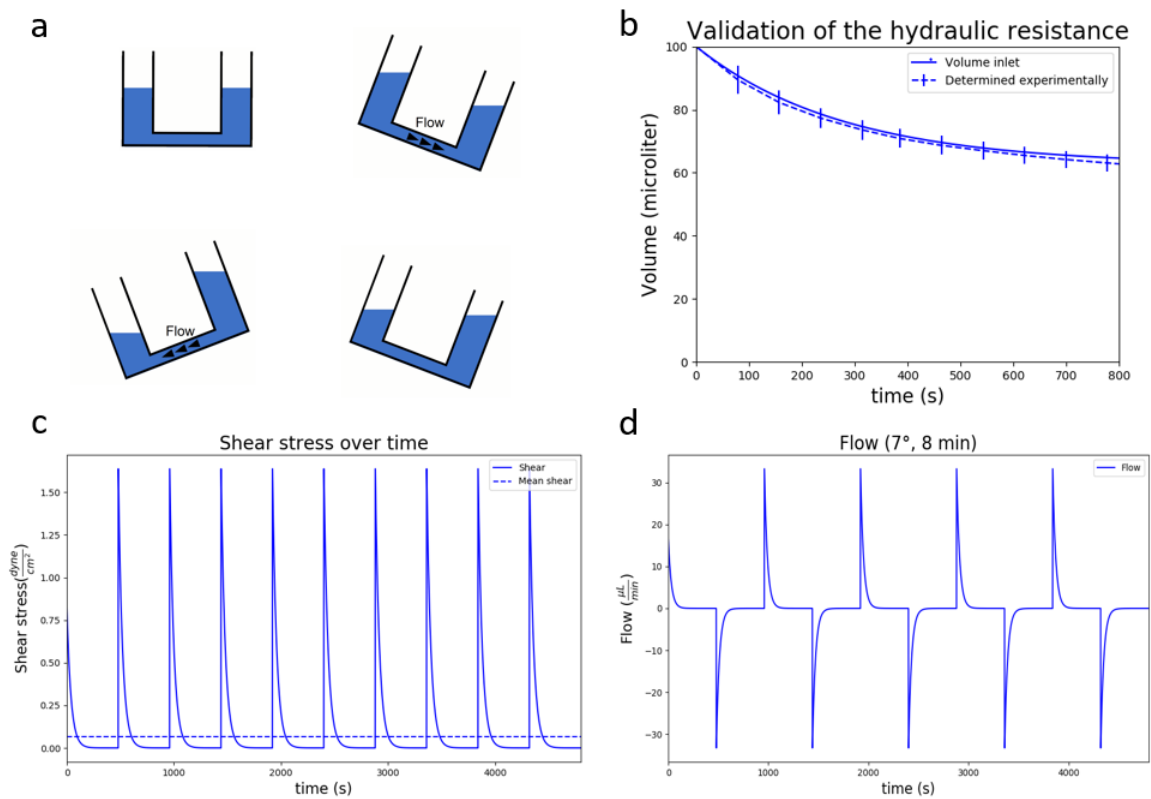
Supplementary figure S5: Validation of the hydraulic resistance. *a Schematic of how the flow is generated in the system. The OrganoPlate was placed in an incubator on an interval rocker platform (+/- 7 degree angle, 8 min interval) enabling a bidirectional flow though the perfusion channels. By placing one inlet to the microfluidic system higher than the other inlet gravity-based perfusion can take place. When the liquid levels in connected wells the plate is tilted and the liquid flows into the opposite direction. b Empirical validation of a numerical model of gravity drive flow in an OrganoPlate. Change in fluorescence due to flow of FITC solution between wells in a 9603200B OrganoPlate (2-lane plate with 120 x 200 µm, w x h channels) (Solid line) showed high correlation with the associated simulated volumes (dashed line). c Sheer stress in the microfluidic channel over time simulated for the 3-lane OrganoPlate with 400 µm wide channels. d Simulated flow rate over time calculated for the microfluidic channel of the 3-lane OrganoPlate with 400 µm wide channels.*

Supplementary Information

Flow rate and sheer stress

The platform described in this work uses a gravity-based perfusion system. When the liquid levels in connected wells are level, no difference in potential energy exists between the two wells, since the gravitational pull on the both volumes of fluid is identical, and no pressure difference exists between the two wells (fig. S5 a).

By periodically tilting a well plate with microfluidically connected wells, a height difference is imposed between the liquid levels in connected wells. The resulting pressure difference causes a fluid flow and associated shear stress.

The fluid flow rate and induced shear stress in the microfluidic channels of the OrganoPlate can be estimated using a numerical model simulated in Python (Python Software Foundation, USA). This model calculates the induced pressure difference between two volumes of fluid, which are present in two microtiter plate wells that are connected by a microfluidic channel. This pressure difference induces a fluid flow, with a flow rate that depends on the hydrodynamic resistance of the microfluidic channel and the fluid properties. This numerical model will be described in more detail below.

When a microfluidic chip is fully seeded, the inlet and outlet well of the perfusion channel are both filled with identical volume (50 μL). When the microtiter plate is levelled (0°) and both volumes are equal, an equilibrium is present: the gravity-induced pressure of both volumes of fluid is identical. The pressure, which is caused by the gravitational pull on a volume of fluid, is calculated by:

$$P = \frac{mg}{A} = \frac{\rho V g}{A} = \rho g h$$

In which pressure P (Pa) is calculated by dividing the weight of the fluid by the surface area of the microfluidic well. The weight is calculated by multiplying mass m (kg) with the gravitational constant g (9.81 m/s^2 or N·m^2/kg^2). Since m can be calculated by multiplying volume V (m^3) with fluid density ρ (kg/m^3), the pressure is calculated by ρgh.

Now, the induced pressure of both volumes of fluid can be calculated. When the microtiter plate is tilted under a certain angle (e.g. 7°), the induced pressure of both volumes is different, resulting in a pressure difference. This difference results in the flow of fluid, whom flow rate can be calculated by:

$$Q = \frac{\Delta P}{R_h}$$

In which flow rate Q (m^3/s) is calculated by dividing the pressure difference ΔP (Pa) by the R_h (kg/(m^4·s)). This resistance is calculated by:

$$R_h = \frac{12\mu L}{wh^3(1 - 0.630h/w)}$$

In which w is the width (m) of the microfluidic channel, h the height of the channel (m), μ the fluid dynamic viscosity (0.001 kg/(m·s) or Pa·s), L the channel length (m) and R_h is the hydrodynamic resistance (kg/(m^4·s))) of a channel with a rectangular cross-section (valid when h < w). This is validated by sequentially measuring the absorption at 494 nm of a 10 μg/ml Fluorescein in water (fig. S5 b). As the volume in the well changes over time, the absorption changes correspondingly. Now, this flow rate can be used to calculate the shear stress, which is exerted on the cells in the perfusion channel. This shear stress τ (Pa) is calculated by:

$$\tau[i] = \frac{6\mu Q[i]}{wh^2}$$

The flow of liquid from one well to the other reduces the difference in liquid level height and thus reduces pressure and flow rate. Numerical integration is used to approximate the flow and resulting shear stress and flow rate over time (fig. S5 c,d) for the settings used in this research.

2

Chapter 3

Implementation of a Human Renal Proximal Tubule on a Chip for Nephrotoxicity and Drug Interaction Studies

MK Vormann*, J Vriend*, HL Lanz, L Gijzen, A van den Heuvel, S Hutter, J Joore, SJ Trietsch, C Stuut, TTG Nieskens, JGP Peters, D Ramp, M Caj, FGM Russel, B Jacobsen, A Roth, S Lu, JW Polli, AA Naidoo, P Vulto, R Masereeuw, MJ Wilmer, L Suter-Dick

*Authors contributed equally

3

Abstract

Proximal tubule epithelial cells (PTEC) are susceptible to drug-induced kidney injury (DIKI). Cell-based, two-dimensional (2D) *in vitro* PTEC models are often poor predictors of DIKI, probably due to the lack of physiological architecture and flow. Here, we assessed a high throughput, 3D microfluidic platform (Nephroscreen) for the detection of DIKI in pharmaceutical development. This system was established with four model nephrotoxic drugs (cisplatin, tenofovir, tobramycin and cyclosporin A) and tested with eight pharmaceutical compounds. Measured parameters included cell viability, release of lactate dehydrogenase (LDH) and N-acetyl-β-D-glucosaminidase (NAG), barrier integrity, release of specific miRNAs, and gene expression of toxicity markers. Drug-transporter interactions for P-gp and MRP2/4 were also determined. The most predictive read outs for DIKI were a combination of cell viability, LDH and miRNA release. In conclusion, Nephroscreen detected DIKI in a robust manner, is compatible with automated pipetting, proved to be amenable to long-term experiments, and was easily transferred between laboratories. This proof-of-concept-study demonstrated the usability and reproducibility of Nephroscreen for the detection of DIKI and drug-transporter interactions. Nephroscreen it represents a valuable tool towards replacing animal testing and supporting the 3Rs (Reduce, Refine and Replace animal experimentation).

Introduction

Renal proximal tubules are susceptible to drug-induced kidney injury (DIKI) [1], which can be a dose-limiting factor in pharmacotherapy and lead to kidney failure in patients. Up to 14–26% of acute kidney injury cases are caused by DIKI [2], [3], [4]. This clinical observation is in stark contrast to the low number of drug candidates, 2% of total, that fail in preclinical development due to nephrotoxicity [5]. This disparity demonstrates the need for better clinically predictive models for nephrotoxicity for use in discovery and early development. Screening-friendly, human-relevant *in vitro* test systems will also help replace animal studies in drug discovery and contribute to the 3 Rs (Replacement, Reduction and Refinement of animal studies). One third of drugs and drug candidates tested are (partially) excreted via the urine following dosing to humans [6], [7]. Active secretion of xenobiotics in the kidney takes place mainly via the proximal tubule epithelial cell (PTEC) of the nephron [8]. A polarized monolayer of PTECs, joined by characteristic epithelial tight junctions, separates the vasculature on the basolateral side from the tubular fluid on the apical side and regulates solutes and water by active transport mechanisms.

In recent years, three-dimensional (3D) microfluidic *in vitro* models of PTECs, also referred to as proximal tubule-on-a-chip, gained significant interest as predictive platforms for nephrotoxicity in drug development [9]. Currently employed in vitro two-dimensional (2D) PTEC models lack important *in vivo* characteristics, such as cell-extracellular matrix (ECM) interaction and fluid shear stress (FSS), which limits their relevance and predictivity with regards to nephrotoxicity [1],

[9], [10]. Renal proximal tubule-on-a-chip showed improved characteristics, such as increased tight-junction formation (ZO-1 expression), and increased number of cilia and microvilli at the apical membrane [11], [12]. Features like albumin uptake and increased P-glycoprotein (P-gp) activity in renal proximal tubule-on-a-chip, and nephrotoxicity induced by cisplatin showed close resemblance with *in vivo* observations [11], [12].

Implementation of renal proximal tubules-on-a-chip in large-scale nephrotoxicity screening is limited due to the complexity and low throughput of most models, often consisting of one chip connected to pumps to generate flow [11], [12]. Furthermore, most renal proximal tubules-on-a-chip described lack basolateral and apical compartments or make use of a two-compartmental model separated by cells cultured on a semi-permeable membrane ignoring cell-ECM interaction [12]. Choice of renal cell source is another important factor in the proximal tubule-on-a-chip. Although freshly isolated primary PTECs show more physiological characteristics in a nephrotoxicity screening proximal tubule-on-a-chip model [13], availability of primary PTECs limits the throughput of this model. Using immortalized renal PTECs would not only overcome this problem but would also enhance reproducibility across different laboratories [13].

This study aimed to assess a high throughput, 3D-microfluidic platform (Nephroscreen) for the detection of drug-induced nephrotoxicity: This platform was specifically designed to fulfill requirements of pharmaceutical companies and promote alternative methods to animal testing in support of the 3Rs. Nephroscreen was first challenged with four selected model human nephrotoxic drugs (cisplatin, tenofovir, tobramycin and cyclosporin A) that affect the proximal tubule. This was complemented with eight additional compounds provided by three pharmaceutical companies for evaluation in a blinded manner. The data were generated at several laboratories to ensure that the platform is robust and transferable.

In Nephroscreen we combined a microfluidics platform with suitable cell lines and appropriate assays. An automatable, microfluidic plate consisting of multiple chips, the OrganoPlate, was combined with renal PTEC cell lines, exposed to FSS induced through passive levelling by gravity [14, [15], [16]. The chosen cells, conditionally immortalized PTEC overexpressing OAT1 (ciPTEC-OAT1) or pseudo-immortalized renal PTEC (RPTEC), are able to establish a polarized epithelium expressing functional transporters [15], [16]. The ciPTEC-OAT1 has been engineered to overexpress OAT1, in addition to other transporters, such as P-gp and OCT2, expressed in the parental ciPTEC line [17], [18]. Therefore, they are an ideal cell line to study the toxicity of substances requiring transport into the cell via these transporters. RPTEC, on the other hand, were chosen due to their performance in establishing leak-tight epithelial barriers. Thus, both implemented cell lines show different, complementary strengths that were exploited by measuring suitable endpoints: ciPTECs were utilized for cytotoxicity, biomarker, and transporter activity measurements while RPTECs performed very well in functional assays such as barrier function.

Cellular damage was studied using various read-outs, such as enzymatic production of formazan (WST-8 assay), indicator of cell viability and release of lactate dehydrogenase (LDH) and N-acetyl-β-D-glucosaminidase (NAG), measures for membrane integrity. Molecular markers of cellular stress included extracellular levels of specific miRNAs: mir34a, mir21, mir192, and mir29a [14], [15], as well as gene expression of heme oxygenase 1: HMOX1 and neutrophil gelatinase-associated lipocalin: NGAL [19]. Functional parameters for the epithelial monolayer consisted of barrier integrity testing as well as interactions with P-gp and multidrug resistance-associated proteins 2 and 4 (MRP2/4) [15], [16].

This study was part of the NC3Rs (https://www.nc3rs.org.uk/) crackIT challenge Nephrotube, launched to generate predictive, animal free-systems for the detection of nephrotoxicity. The results showed the potential of the Nephroscreen for predictive, animal free-detection of nephrotoxicity and drug-transporter interactions.

Materials and Methods

Experimental Workflow: Multi-laboratory Collaboration

The combination of assays described previously [14], [15], [16], used towards a functional Nephroscreen, were performed in laboratories at the School of Life Sciences, University of Applied Sciences Northwestern Switzerland in Muttenz, Switzerland (lab B), the department of Pharmacology and Toxicology, Radboud University Medical Center, Nijmegen, The Netherlands (lab N) and Mimetas, Leiden, The Netherlands (lab L). Transferability, robustness and reproducibility of Nephroscreen was established by performing experimental procedures in the three laboratories using two renal cell lines (ciPTEC and RPTEC). The experimental workflow is depicted in Fig. 1. For cell viability assessment, tubules of both cell lines were cultured and then exposed to nephrotoxicants for 24 or 48 h (lab L), Measurement of cell viability included enzymatic production of formazan using WST-8 (Lab L), LDH release (lab N) and gene expression of toxicity markers (lab L and N). In addition, RPTEC were tested for their barrier function (Lab L). In lab N, the effect of the nephrotoxicants on the transporter functionality of P-gp and MRP2/4 was assessed in ciPTEC-OAT1. The release of selected miRNAs (mir-21, -29a, −34a and −192) and secretion of the enzyme N-acetyl-β-D-glucosaminidase (NAG) in ciPTEC-OAT1 were measured in lab B.

Cell Culture

CiPTEC-OAT1 cells (Cell4Pharma, Oss, NL) were cultured in T75 flasks in a 1:1 mixture of Dulbecco's modified Eagle's medium and nutrient mixture F-12 without phenol red (DMEM-F12, Gibco, ThermoFisher Scientific, Carlsbad, USA, 11039-021) supplemented with insulin-transferrin-sodium selenite media supplement (Sigma-Aldrich, I1884, insulin 5 µg/mL; transferrin 5 µg/mL; sodium selenite 5 ng/mL), 36 ng/mL hydrocortisone (Sigma-Aldrich, H0135), 10 ng/mL epidermal growth factor (Sigma-Aldrich, E9644), 40 pg/mL 3-iodothyronine (Sigma-Aldrich, T5516),

10% v/v fetal bovine serum (FBS, Gibco, 16140-071 or Greiner Bio-One, Alphen aan den Rijn, The Netherlands, 758093), and 1% v/v penicillin/streptomycin (P/S, Sigma-Aldrich, P4333), referred to as ciPTEC complete medium.
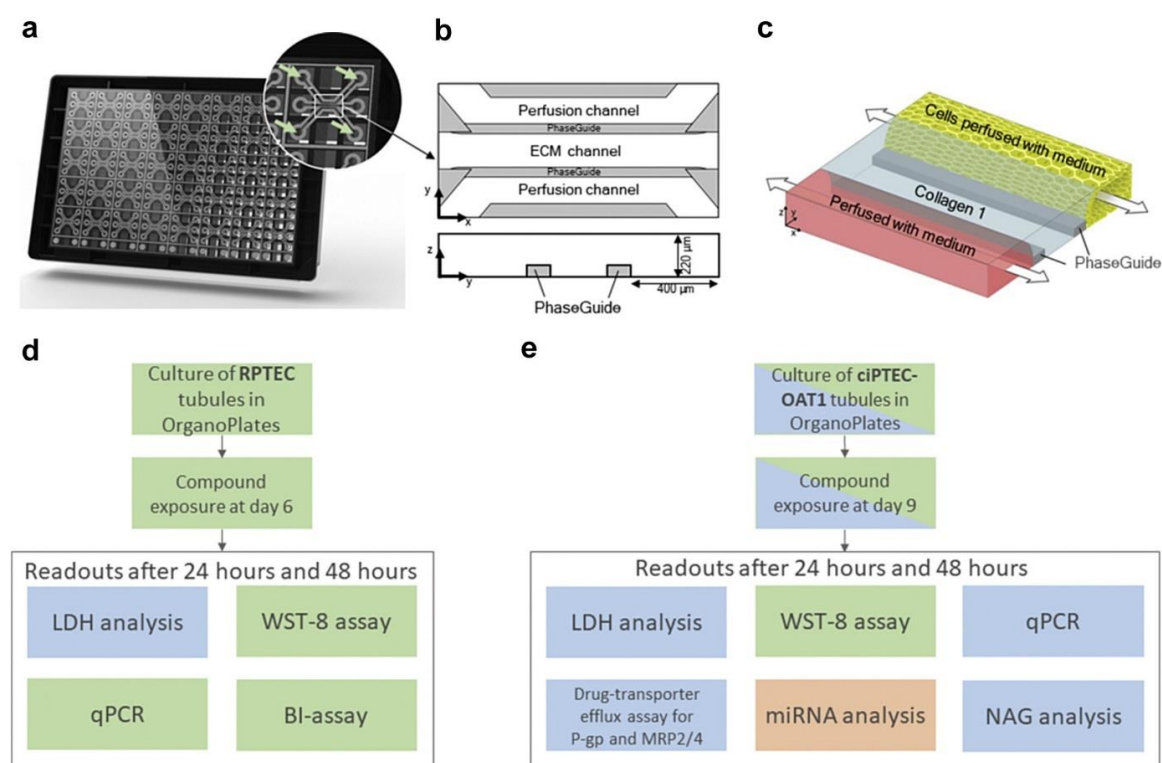

Figure 1: Overview of the microfluidics platform, the cell culture, exposure, and read-out methods performed on ciPTEC-OAT1 tubules and RPTEC tubules. *(a) Image of the back side of the OrganoPlate 3-lane. The microfluid network is positioned in-between a glass sandwich of two microscope grade glass plates which are attached to the bottom of a standard 384 titer well plate. Access to the microfluidic system is facilitated via the top wells. One OrganoPlate comprises in total 40 chips as 8 "wells" compose one chip. Green arrows indicate the inlets used for compound dosing. (b) Schematic of one chip presenting two perfusion channels and the extracellular matrix (ECM) channel in the middle. Channels are divided by 55 μm high ridges called PhaseGuide (grey bars) with act as pressure barriers. (c) Artist impression of one chip. The chip was loaded with collagen 1 (blue) to the ECM channel and proximal tubule cells (yellow) were seeded to the top channel. After cell attachment medium was added to both perfusion channels and perfusion was started (indicated by white arrows). (d) and (e) Flow charts indicating the culture of RPTEC and ciPTEC-OAT1, respectively. Each cell line was cultured following optimized conditions before exposure to compounds for 24 and 48 h. (d) Readouts for RPTEC included lactate dehydrogenase (LDH)-release, cell viability assay using WST-8 assay, determination of barrier integrity (BI) and collection of total RNA for quantitative PCR (qPCR). (e) Readouts for ciPTEC-OAT1 included lactate dehydrogenase (LDH)-release, N-acetyl-β-d-glucosaminidase (NAG) release, cell viability assay using WST-8 assay, determination of drug-transporter efflux assay, collection of release RNA for miRNA determination, and collection of total RNA for quantitative PCR (qPCR). Assays were performed and optimized in three laboratories and the obtained results are colour coded: Lab B, orange, Lab L (green), Lab N (blue).*

Cells were incubated in a humidified incubator (33 °C, 5% v/v CO_2) and every 2–3 days ciPTEC complete medium was changed. At 90–100% confluency cells were washed with HBSS (Sigma-

Aldrich, H6648 or Gibco, 14025-100), detached with accutase (Sigma-Aldrich, A6964), pelleted (200-300×g, 5 min), and used for passaging (10,000–20,000 cells/cm^2) or for seeding in the OrganoPlate. Cells were used for experiments between passage 52 and 65.

RPTEC cells (Kidney PTEC Control Cells, SA7K Clone, Sigma-Aldrich, Schnelldorf, Germany, MTOX1030) were seeded in T75 cell culture flasks coated with PureCol (Advanced BioMetrix, 5005-B, diluted 1:30 in cold Hank's balanced salt solution (HBSS, Sigma-Aldrich, H6648), 20-min incubation at 37 °C) in MEME alpha Modification (Sigma-Aldrich, M4526) supplemented with RPTEC Complete Supplement (Sigma-Aldrich, MTOXRCSUP), *L*-glutamine (1.87 mM, Sigma-Aldrich, G7513), Gentamicin (28 μg/mL, Sigma-Aldrich, G1397) and Amphotericin B (14 ng/mL, Sigma-Aldrich, A2942), referred to as RPTEC complete medium. Cells were incubated in a humidified incubator (37 °C, 5% v/v CO_2) and every 2–3 days RPTEC complete medium was changed. At 90–100% confluency cells were washed with HBSS, detached with accutase (Sigma-Aldrich, A6964), pelleted (140×g, 5 min), and used for seeding in the OrganoPlate. Cells for experiments were used up to passage 3.

OrganoPlate Culture

For all experiments, plates were seeded as described in our previous work [14, [15], [16]. Biefly, a three-lane OrganoPlate (Mimetas BV, 4003 400B, Fig. 1) with a channel width of 400 μm and a height of 220 μm was loaded with 1.6–2 μL of ECM gel composed of 4 mg/mL collagen I (AMSbio Cultrex 3D Collagen I Rat Tail, 3447-020-01), 100 mM HEPES (Life Technologies, ThermoFisher Scientific, 15630), and 3.7 mg/mL sodium bicarbonate (Sigma-Aldrich, 320 S5761) to the middle inlet of all 40 chips. After polymerization of the ECM, HBSS was added on top of the collagen I and the plate was incubated in a humidified incubator (37 °C, 5% v/v CO_2) overnight. RPTEC or ciPTEC-OAT1 were detached from culture flasks and resuspended at a concentration of 10×10^6 cells per mL in RPTEC complete medium or 20×10^6 cells per mL in ciPTEC complete medium, respectively. Of the cell suspension, 2 μL was injected into each top inlet, followed by an addition of 50 μL medium to the same well. For control chips, no cell suspension was added. Subsequently, the OrganoPlate was placed for 4 h at an angle of about 75° into a humidified incubator (37 °C, 5% v/v CO_2 for RPTEC or 33°, 5% v/v CO_2 for ciPTEC-OAT1). After attachment of the cells, which was confirmed by light microscopy, 50 μL medium was added to the top outlet, bottom inlet and bottom outlet. The OrganoPlate was placed flat in an incubator (37 °C, 5% v/v CO_2 for RPTEC or 33 °C, 5% v/v CO_2 for ciPTEC-OAT1) on an interval rocker platform (±7° angle, 8 min interval) enabling a bidirectional flow though the perfusion channels. At day 3, antibiotic free medium was used to refresh the medium in the chips, and the ciPTEC-OAT1 plates were transferred to a humidified incubator (37 °C, 5% v/v CO_2).

Compound Exposure

Cells were exposed for 24 or 48 h to four model nephrotoxicants and eight blinded compounds following the general experimental design depicted in Fig. 1. The selection of the test concentrations was based on doses where toxicological effects were seen *in vivo* and on preliminary cytotoxicity data in 2D obtained with ciPTEC-OAT1. Briefly, cells were seeded in 96-well flat-bottom plates at 35000 cells/cm², maintained until confluency, subsequently exposed for 24 or 48 h to a concentration range of each of the compounds diluted in ciPTEC complete medium and viability was determined (WST-8 assay). For Nephroscreen testing, a low and a high toxicity concentrations were selected. In absence of detectable toxicity, the two highest concentrations were chosen (data not shown). Detailed solvent, dilutions, and culture conditions for each substance are described in Table S1, while data on previous studies used for the determination of potential test concentrations are listed in Table S2, together with relevant toxicity information disclosed after data acquisition and analysis of data had been completed. For compounds R1 and R2, additional experiments including more concentrations and additional time points were performed in lab B. For R1, cells were exposed for 48 h and for R2, cells were exposed for 11 days, with medium changes every 2–3 days.

Using a pipette, 50 µL of the model compounds (cisplatin, tenofovir, tobramycin and cyclosporin A) or the eight blinded compounds (G1, G2 and G3; R1, R2 and R3; and P1 and P2) diluted in medium were dosed via each of the 4 inlets guiding to the microfluidic channels (details in Fig. 1). Medium from both the apical and basolateral perfusion channels was refreshed before exposure to the nephrotoxicants. For RPTEC, the exposure was started at day 6 and dilutions of nephrotoxicants were prepared in TOX medium (MEME alpha Modification (Sigma-Aldrich, M4526) supplemented with RPTEC Tox Supplement (Sigma-Aldrich, MTOXRTSUP), *L*-glutamine (1.87 mM, Sigma-Aldrich, G7513). For ciPTEC-OAT1, cells were exposed on day 9 and dilutions of nephrotoxicants were prepared in ciPTEC complete medium.

WST-8 Assay

Cell viability was determined using the Cell Counting Kit-8 (WST-8, Sigma-Aldrich, 96992) as described previously [14, [15]. Briefly, the WST-8 solution was diluted with ciPTEC complete medium or RPTEC TOX medium (ciPTEC-OAT1 or RPTEC respectively) and added to the channels of the OrganoPlate. After 20–60 min, absorbance was measured at 450 nm with a Multiskan™ FC Microplate Photometer (ThermoFisher Scientific) or with a Benchmark Plus microplate spectrophotometer (Bio-Rad, Veenendaal, The Netherlands). Viability was expressed as % of the control.

LDH Activity in Medium

LDH activity in the culture medium is a measure for membrane integrity. Medium was collected on ice after compound exposure and stored at −80 °C until further processing. After thawing, LDH activity was measured using an activity assay kit (Sigma-Aldrich, MAK066), following the

manufacturer's protocol. In brief, 5 μL per sample was added to a flat bottom 96-well plate. In addition, a calibration curve using a NADH (1.25 mM) standard was prepared. Assay buffer was added to a final volume of 50 μL per well and then a master reaction mix was added per well (1:1, v/v). After 3 min, absorbance was measured at 450 nm on a Benchmark Plus microplate spectrophotometer (Bio-Rad) every 5 min until absorbance measured in a sample was higher than the highest level of NADH in the calibration curve (12 nmol/well). Extracellular LDH activity was expressed as mU/mL.

NAG Measurement in Medium

The levels of β-N-acetylglucosaminidase (NAG) in supernatant are a measure for membrane integrity and are also used as a biomarker of kidney damage *in vivo*. They were determined using the NAG-Assay Kit (BioVision, K733-100), following provider's instructions. Briefly, 30 μL of the supernatant (cell culture medium) where adjusted to a volume of 70 μL with NAG assay buffer in a 96-well plate. To this, 55 μL substrate where added and incubated for 30 min at 37 °C, followed by the addition of 25 μL stop solution. After another 10 min at 37 °C, absorbance was measured at 400 nm in a Flexstation 3 (Molecular Devices). Absorbance of a standard dilution series of pNP (0–20 nmol of pNP/well) was measured in parallel and used for the calculations. Extracellular NAG activity was calculated (mU/mL) and expressed as % of the control.

Barrier Integrity Assay

The barrier integrity assay was performed as previously published on RPTEC [15]. Briefly, the medium of the perfusion channel (apical side of the cells) was replaced with RPTEC TOX medium containing 0.5 mg/mL tetramethylrhodamine (TRITC)-dextran (4.4 kDa, Sigma-Aldrich, FD20S) and 0.5 mg/mL fluorescein isothiocyanate (FITC)-dextran (150 kDa, Sigma-Aldrich, T1287). Subsequently, plates were imaged with the ImageXpress Micro XLS-C High Content Imaging System (Molecular Devices). Leakage of the dyes from the lumen (apical compartment) to the basal compartment into the ECM was measured over time, and the ratio between the basal and the apical compartment was analyzed with Image J version 1.51n [20]. From these measurements, the apparent permeability index (P_{app}) was calculated as previously described [15], using the following formula:

$$P_{app} = \frac{\Delta C_{receiver} \times V_{receiver}}{\Delta t \times A_{barrier} \times C_{donor}} \left(\frac{cm}{s}\right)$$

$\Delta C_{receiver}$ is the measured normalized intensity difference of the ECM to the donor channel (apical compartment) at t_{0min} and t_{10min}, $V_{receiver}$ is the volume of the measured region in the ECM channel (0.0001 cm^2), Δt is the time difference (10 min), $A_{barrier}$ is the surface of the ECM interface with the medium channel (0.0057 cm^2), and C_{donor} is the donor concertation of the dextran dyes (0.5 mg/mL).

Gene Expression of Toxicity and Nephrotoxicity Markers

Total intracellular RNA was isolated from cells harvested from perfusion channels in the OrganoPlate using the RNeasy Micro Kit (Qiagen, Venlo, The Netherlands) as previously described [16]. Complementary DNA (cDNA) was synthesized with Moloney Murine Leukemia Virus (M-MLV, Promega, M1705) reverse transcriptase, according to the manufacturer's protocol. Gene expression levels of heme oxygenase 1 (HMOX1) and neutrophil gelatinase-associated lipocalin (NGAL), encoded by the lipocalin-2 (LCN2), were measured using quantitative PCR (qPCR) with GADPH as reference. TaqMan Universal PCR Master Mix (Life Technologies, 4304437) and gene specific primer-probe sets (HMOX1: Hs01110250_m1, LCN2: Hs01008571_m1 and GAPDH: Hs99999905_m1) were purchased from Applied Biosystems (ThermoFisher Scientific). The real-time PCR was carried out using a fluorometric thermal cycler (Qiagen, Rotor-Gene Q 3000 or Celtic Diagnostics, Corbett research PCR Rotorgene 6000). The PCR program consisted of 10 min of initial denaturation at 95 °C followed by 45 cycles of 15 s at 95 °C and 1 min at 60 °C. Fluorescence was detected at the end of each cycle at 510 nm (excitation 470 nm). Ct values were determined using the second derivative method. For each sample, dCt was calculated using Ct values of the gene of interest and the housekeeping gene (GAPDH). Treatment induced differential gene expression was calculated using the -ddCts -(dCt treatment-dC tcontrol) and fold changes as 2^{-ddCt}.

Detection of miRNAs in Medium

Total RNA was extracted from 80 μL supernatant using the miRNeasy® Serum/Plasma Kit (Qiagen, 217184) following the manufacturer's protocol. miRNAs were reverse-transcribed using the TaqMan® MicroRNA Reverse Transcription Kit (Applied Biosystems®, 4366596) and the miRNA-specific stem-loop primers for the miRNAs-21, -34a, −29a and −192 (Applied Biosystems™, TaqMan microRNA Assays #002438, #000426, #002112, and #000491, respectively). The reaction mix was prepared according to the manufacturer's instructions for a final reaction volume of 10 μL with 3 μL RNA extract. The conditions for reverse transcription were set for 30 min at 16 °C followed for 30 min at 42 °C and 5 min at 85 °C.

The real-time PCR was carried out using a fluorometric thermal cycler (Qiagen, Rotor-Gene Q 3000 or Celtic Diagnostics, Corbett research PCR Rotorgene 6000). The reaction mix contained TaqMan® Fast Advanced Master Mix 1x (Applied Biosystems™, 4444557), TaqMan microRNA Assay primer 1x (Applied Biosystems™) and 1.3 μL cDNA in a final reaction volume of 20 μL. The PCRs were run at 95 °C for 20 s followed by 40 cycles of 1 s at 95 °C and 20 s at 60 °C. All extracted RNAs were analyzed in technical duplicates; Ct-values of these two measurements were averaged and considered a single value.

Drug Transporter Assays

Drug-transporter interactions with P-gp and MRP2/4 were studied in ciPTEC-OAT1 using calcein-acetoxymethyl (calcein-AM, 2 µM, Life Technologies, C1430) and 5-chloromethylfluorescein diacetate (CMFDA, 1.25 µM, Life Technologies, C7025), respectively [16], [21]. Both calcein-AM, a P-gp substrate, and CMFDA are permeable to the cell membrane and are intracellularly metabolized into calcein or glutathione-methylfluorescein (GS-MF), substrates for MRP2/4. PSC833 (10 µM, Tocris, Bristol, UK, 4042/1) was used as model inhibitor for P-gp, included as positive control for inhibition in each experiment. Transport of calcein and GS-MF is by MRP2/4, P-gp and BCRP and therefore, a mixture of PSC833 (10 µM), MK571 (10 µM, Sigma-Aldrich, M7571) and KO143 (10 µM, Sigma-Aldrich, K2144) was used to selectively inhibit efflux, again as positive control [21]. Stocks of calcein-AM, CMFDA, PSC833 and KO143 were dissolved in DMSO (Sigma-Aldrich, D5879), MK571 was dissolved in milli-Q water. Test compounds were dissolved as described in Table S1. Work solutions were prepared in freshly-prepared Krebs-Henseleit buffer (Sigma-Aldrich, K3753), supplemented with 10 mM HEPES (Sigma-Aldrich, H3375) at pH 7.4, referred to as KHH. All conditions contained a final concentration of DMSO of 0.6% v/v. Perfusion channels were washed with 50 µL in the medium-channel inlet and outlet and then perfused twice with KHH. Cells were incubated with calcein-AM and CMFDA with or without the presence of model inhibitors or nephrotoxicants at 37 °C for 1 h. Next, efflux was arrested using PSC833 (10 µM), MK571 (10 µM) and KO143 (10 µM) in cold (4 °C) KHH. Perfusion during washing and incubation was ensured by adding 80 µL or 20 µL to the medium-channel inlet and outlet, respectively.

Intracellular accumulation of calcein and GS-MF in ciPTEC-OAT1 in the OrganoPlate was measured in situ on a spinning disk confocal Becton Dickinson (BD) Pathway 855 high-throughput microscope (BD Bioscience, Breda, The Netherlands). A × 10 objective was used with excitation and emission filters set at 488 nm and 520 nm, respectively. Subsequently, bright-field images of each chip were acquired. Fluorescence intensity was determined at the ECM-medium interface in Image J. Intensity per chip was then normalized to fluorescence measured in vehicle in same experiment.

Data Analysis

Data are presented as mean ± SD for at least three chips (n = 3–5) per condition, unless stated otherwise. Statistics were performed using GraphPad Prism version 8 (San Diego, CA, USA). Data was found to be significantly different compared to medium control or corresponding vehicle if $p < 0.05$ using a one-way ANOVA followed by a Tukey's multi comparison post hoc test.

Results

Robustness of the System

Cisplatin, tenofovir, cyclosporin A and tobramycin have previously been shown to cause mild to severe cytotoxicity in confluent monolayers of ciPTEC-OAT1 in a 96-well plate [14]. In our work, cell viability was measured upon a 48-h exposure to cisplatin (5 and 30 µM), tenofovir (15.6 and 1000 µM), cyclosporin A (5 and 30 µM), and tobramycin (7.5 and 15 mM) in ciPTEC-OAT1 in the OrganoPlate at three different research sites. At the chosen concentrations, these nephrotoxicants caused a significant reduction in cell viability (Fig. 2) and increased LDH release for tobramycin and cyclosporin A at the highest concentrations tested (Figure S2). As depicted in Fig. 2, we observed similar effects in viability of ciPTEC-OAT1 at all three laboratories, in line with earlier findings reported by lab B [14]. The other PTEC line used in the Nephroscreen, RPTEC, showed decreased viability, assessed with WST-8 and LDH-release, after exposure to tobramycin only, thus appeared to be less sensitive than ciPTEC-OAT1 (Figure S2). ciPTEC-OAT1 exposed to tenofovir in the compound screen showed a higher viability compared to the vehicle control when exposed to the low concentration but a significant loss in viability at 1000 µM (Fig. 2).
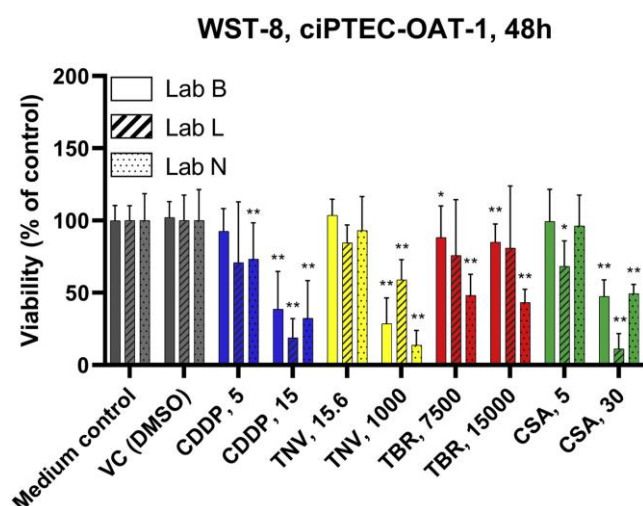

Figure 2: Side to side comparison of viability data received from the WST-8 assay. *Data are from three different labs, performed at FHNW (Lab B), Mimetas (lab L), or at department of Pharmacology and Toxicology, Radboud University Medical Center (lab N). In each site, 1–3 independent experiments with 2–6 replicates (chips) were analyzed. Abbreviations: CDDP, cisplatin; CSA, cyclosporin A; DMSO, dimethyl sulfoxide; TBR, tobramycin; TNV, tenofovir; WST-8, 2-(2-methoxy-4-nitrophenyl)-3-(4-nitrophenyl)-5-(2,4-disulfophenyl)-2H-tetrazolium, monosodium salt; VC, vehicle control. #: in lab L slightly different concentrations for tenofovir were used, 15 µM instead 15.6 µM and 1215 µM instead of 1000 µM. Statistically significant compared to corresponding vehicle: $*p < 0.05$, $**p < 0.01$.*

Assessment of Cytotoxicity and Tubular Damage

Based on the data generated with the model nephrotoxicants, we performed experiments to ascertain the potential nephrotoxicity of eight test substances. These compounds were provided by the pharmaceutical companies GlaxoSmithKline (GSK), Roche and Pfizer in a blinded manner,

referred to as unknown nephrotoxicants, and named as G1, G2 and G3 for compounds provided by GSK, R1, R2 and R3 for compounds provided by Roche, and P1 and P2 for compounds provided by Pfizer.

In a first step, cell viability in confluent monolayers of ciPTEC-OAT1 in 2D was assessed to determine appropriate starting concentrations of the unknown nephrotoxicants in the OrganoPlate (data not shown). Cytotoxicity parameters provided a consistent picture and showed reduced cell viability (WST-8) and increased LDH release caused by five of the unknown nephrotoxicants (G1, G3, R1, R3, P2) in both cell lines tested (Fig. 3a–h). NAG release was only determined in ciPTEC-OAT1 and yielded concordant results (Fig. 3i and j). In general, toxicity was more marked after 48 h than after 24 h exposure. Interestingly, G2 increased cellular production of formazan in RPTECs, while R2 increased this production in ciPTEC-OAT1. The sensitivity of both PTEC cell lines to the treatments was, however, comparable.

In addition to cytotoxicity measurements, the impact of treatments on the functionality of the tubular epithelial layer (i.e. barrier integrity in RPTEC in the OrganoPlate) was determined by assessing the apparent permeability to the low-molecular weight marker dextran-TRITC (4.4 kDa) and high-molecular weight marker dextran-FITC (155 kDa). Impaired barrier function was observed after exposure to tobramycin, and five test substances (G1, G3, R1, R3 and P2). The latter were the same five compounds that caused a decrease in cell viability. The effects were generally more marked after 48 h than after 24 h exposure (Fig. 4).

Drug-Transporter Interactions

Drug-transporter interaction with P-gp and MRP2/4 is another important feature that can result in high intracellular concentrations in PTEC leading to renal toxicity of substances. Drug-transporter interactions were determined in ciPTEC-OAT1 as stable expression of these drug transporters has been previously confirmed in this model [16]. For MRP2/4, interactions were found for cyclosporin A, G2, G3 and P2 (Fig. 5a and c). Cyclosporin A, G3, P1 and P2 resulted in interactions for P-gp (Fig. 5b and d). It is interesting to note that the compound G2 clearly impaired MRP2/4 transport but did not cause any cytotoxicity based on other assays performed, suggesting competition for transport solely.

miRNA-Release

Released miRNAs can act as biomarkers of toxicity that are detectable in cell culture medium before other toxicity biomarkers. The medium of the cells treated with the eight blinded compounds was collected after 24 h of exposure and levels of four selected miRNAs determined as described in materials and methods. Most tested compounds led to increases in the miRNA panel at both tested concentrations (Fig. 6a–d). Exceptions to this assessment were compounds G2 and R2 that did not cause significantly increased release of any of the tested miRNA into the medium. Interestingly, compound R3 led to an increase in all four miRNAs at the lowest tested

concentration (25 µM) while the cells treated with 100 µM did not show changes in miRNA release.

Specific Exposures to Compounds R1 and R2

Due to the lack of toxicity observed in most parameters with compound R2 and to the high concentrations required to elicit a response with R1, tailor-made subsequent experiments were planned in discussion with the sponsors, who knew the identity of the compounds. To this end, ciPTEC-OAT1 in the OrganoPlate were exposed to several concentrations (ranging between 15 and 1000 µM) of R1 and R2 for 48 h and 11 days, respectively. At 48 h, compound R1 showed a dose dependent loss in viability assessed with the WST-8 assay with an EC50 of 214.5 and 277.3 µM (results from two independent experiments). This toxicity was accompanied by a dose dependent induction of HMOX1 (Fig. 7a and b). The results confirm that concentrations ≥ ~100 µM lead to toxicity with an EC50 214 and 277 µM (two independent experiments), whereas HMOX1 expression levels increased in a concentration-dependent manner from a concentration of 62.5 µM (≥2-fold induction; Fig. 7). R1 did not lead to any change in expression of NGAL or in NAG released into the medium (Fig. 7b and c). Based on information provided by the sponsors, compound R2 was additionally tested after long-term (11 days) of incubation. Cytotoxicity assay at 11 days showed a decrease in cell viability with an EC50 of 367.5 and 267.4 µM (results from two independent experiments) (Fig. 8a). As with compound R1, HMOX1 expression increased in a dose dependent manner from a concentration of 30.25 µM (≥2-fold induction; Fig. 8b). The compound, however, did not cause an increase in NGAL expression or led to a release of NAG release into the medium at any of the tested time points (48 hours or 11 days of exposure, Fig. 7b and c).

a
WST-8, ciPTEC-OAT1, 24h
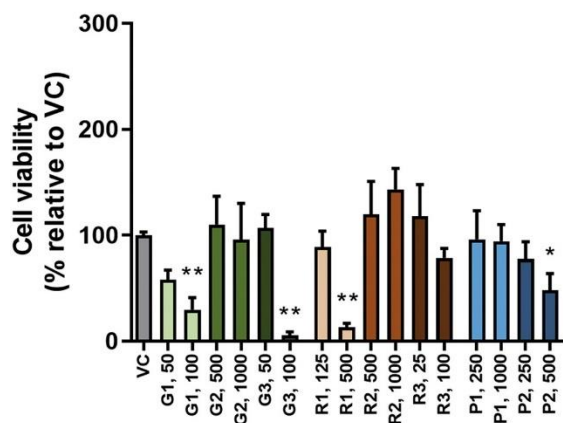
b
WST-8, ciPTEC-OAT1, 48h
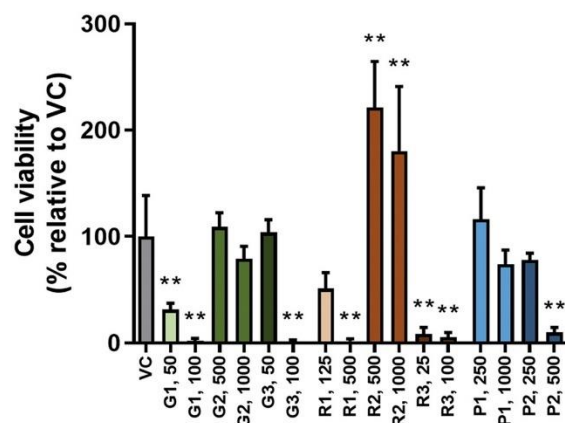
c
WST-8, RPTEC, 24h
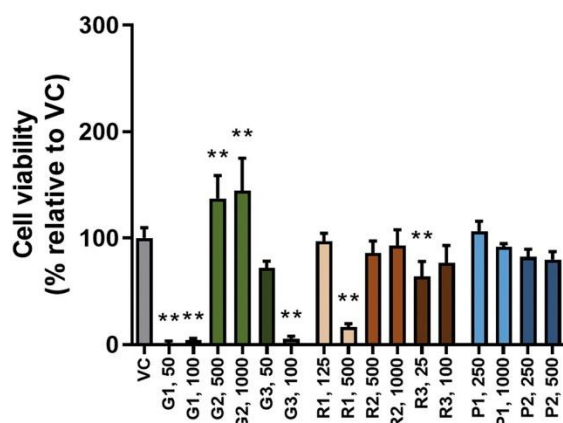
d
WST-8, RPTEC, 48h
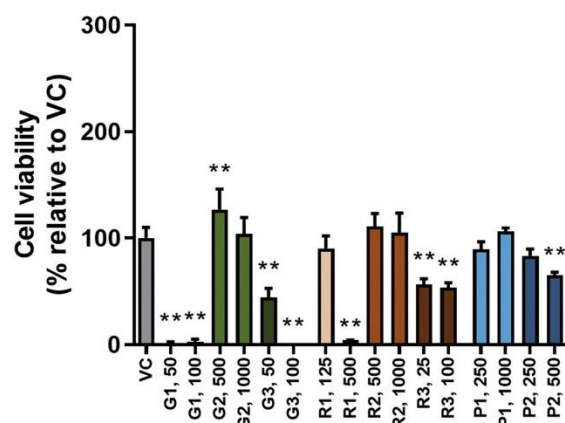
e
LDH activity, ciPTEC-OAT1, 24h

f
LDH activity, ciPTEC-OAT1, 48h

g

LDH activity, RPTEC, 24h

h

LDH activity, RPTEC, 48h

i

NAG, ciPTEC-OAT1, 24h

j
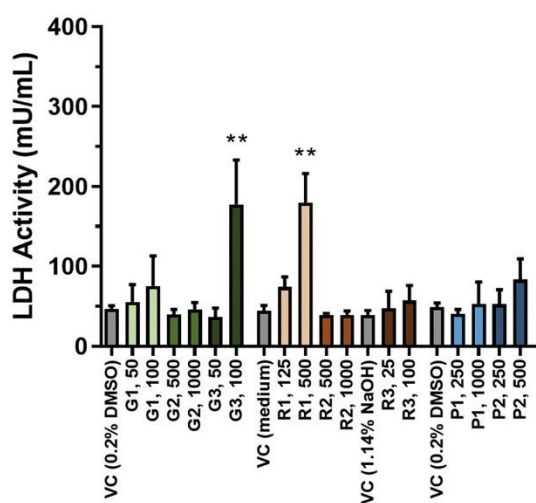
NAG, ciPTEC-OAT1, 48h
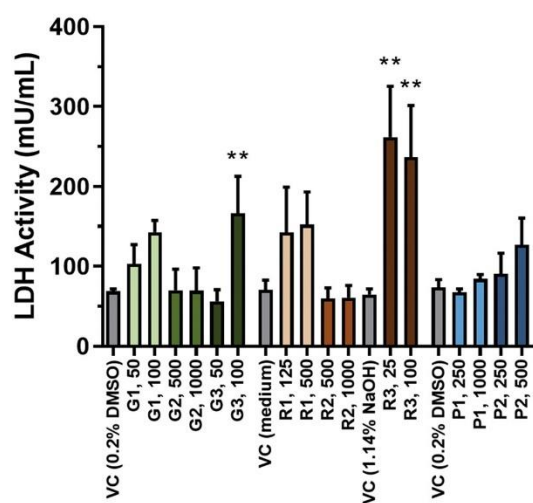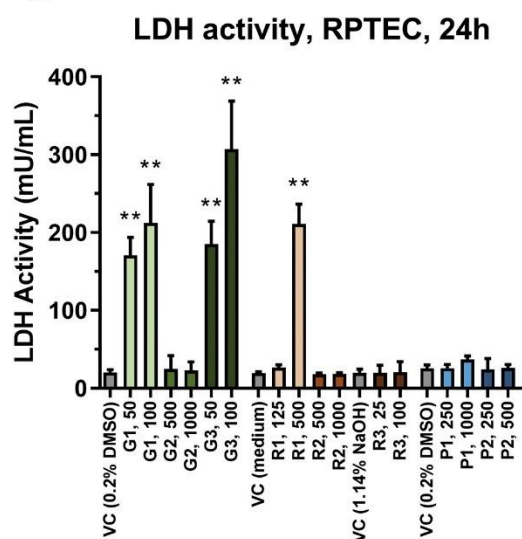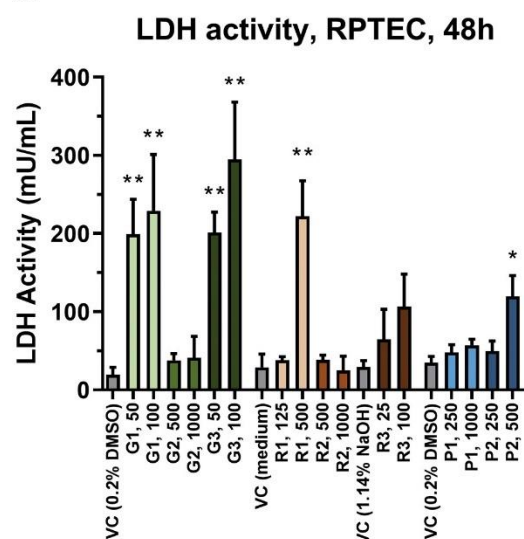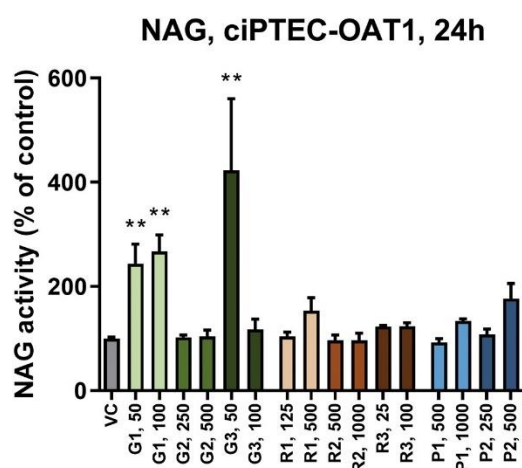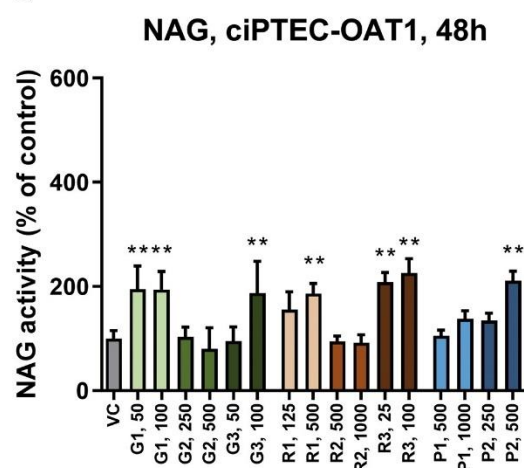
Figure 3: Cell viability and lactate dehydrogenase (LDH) release in compound screen. (a) Cell viability in ciPTEC-OAT1 after 24 h and (b) 48 h exposure. (c) Cell viability in RPTEC after 24 h and (d) 48 h exposure. (e) Release of LDH, as measure of membrane integrity, in ciPTEC-OAT1 after 24 h or (f) 48 h exposure. (g) LDH release in RPTEC after 24 h or (h) 48 h exposure. (i) N-acetyl-β-d-glucosaminidase (NAG) release by ciPTEC-OAT1 treated with sponsor compounds screen after 24 h (i) and 48 h (j) exposure. Abbreviations: VC, vehicle control; WST-8, 2-(2-methoxy-4-nitrophenyl)-3-(4-nitrophenyl)-5-(2,4-disulfophenyl)-2H-tetrazolium, monosodium salt; DMSO, Dimethyl sulfoxide; NaOH, Sodium hydroxide. Statistically significant compared to corresponding vehicle: ∗p < 0.05, ∗∗p < 0.01.

a

Barrier Integrity, 4.4 kDa, 24h
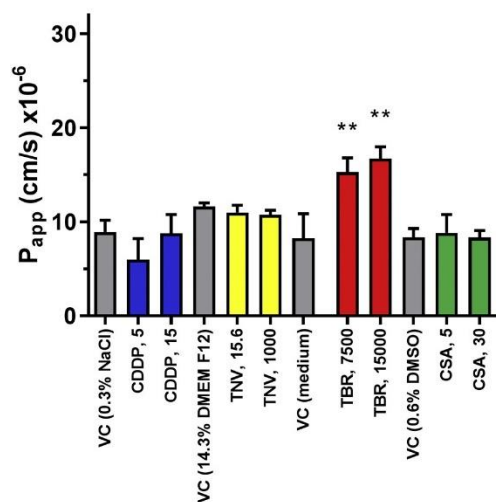
b

Barrier Integrity, 4.4 kDa, 48h
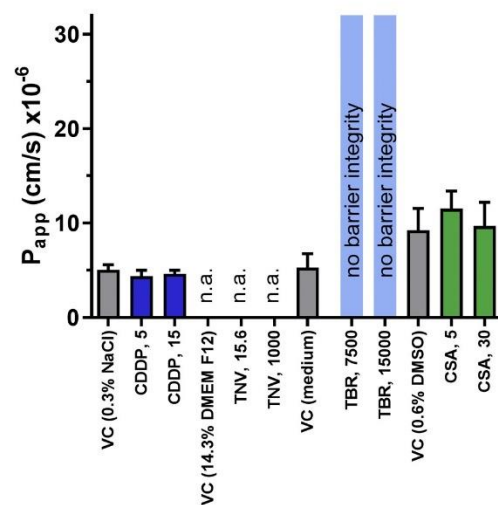
c

Barrier Integrity, 150 kDa, 24h

d
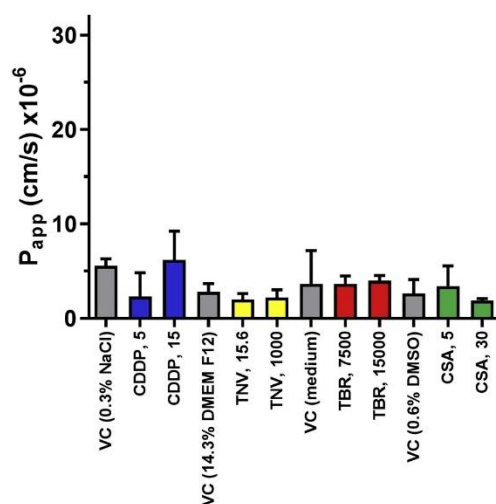
Barrier Integrity, 150 kDa, 48h

e
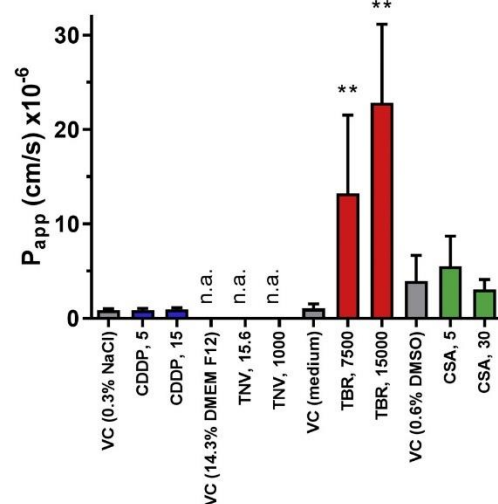
Barrier Integrity, 4.4 kDa, 24h

f
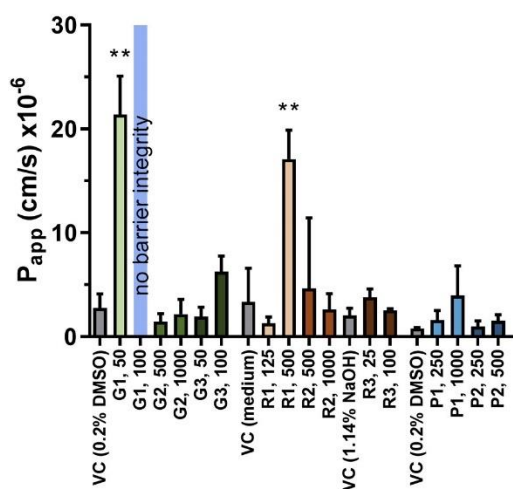
Barrier Integrity, 4.4 kDa, 48h
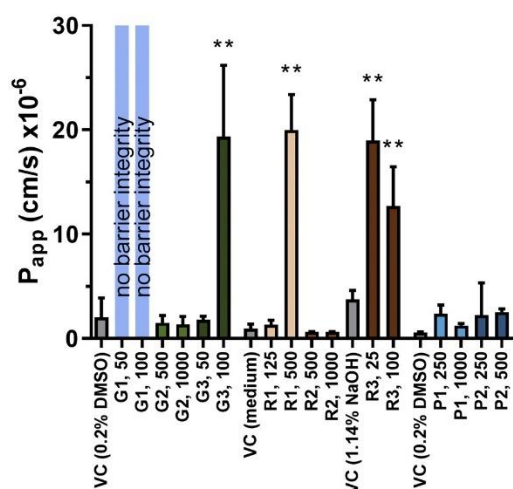
Figure 4: Barrier integrity of RPTEC tubules. *(a) Leakage of high-weight molecular marker (155 kDa) fluorescein isothiocyanate (FITC)-dextran after 24 h or (b) 48 h of exposure to model nephrotoxicants. (c) Leakage of low-weight molecular marker (4.4 kDa) tetramethylrhodamine (TRITC)-dextran after 24 h or (d) 48 h of exposure to model nephrotoxicants cisplatin (CDDP), tenofovir (TNV), tobramycin (TBR) and cyclosporin A (CSA). (e) Leakage of FITC-dextran after 24 h and (f) 48 h of exposure to unknown nephrotoxicants. (g) Leakage of TRITC-dextran after 24 h or (h) 48 h of exposure to unknown nephrotoxicants. Abbreviations: D-F12, Dulbecco's modified Eagle's medium and nutrient mixture F-12; VC, vehicle control; Papp, apparent permeability; DMSO, Dimethyl sulfoxide; NaOH, Sodium hydroxide; kDa, kilodaltons; n.a., not available. Statistically significant compared to corresponding vehicle: ∗p < 0.05, ∗∗p < 0.01.*

a GS-MF

b Calcein-AM

c GS-MF

d Calcein-AM
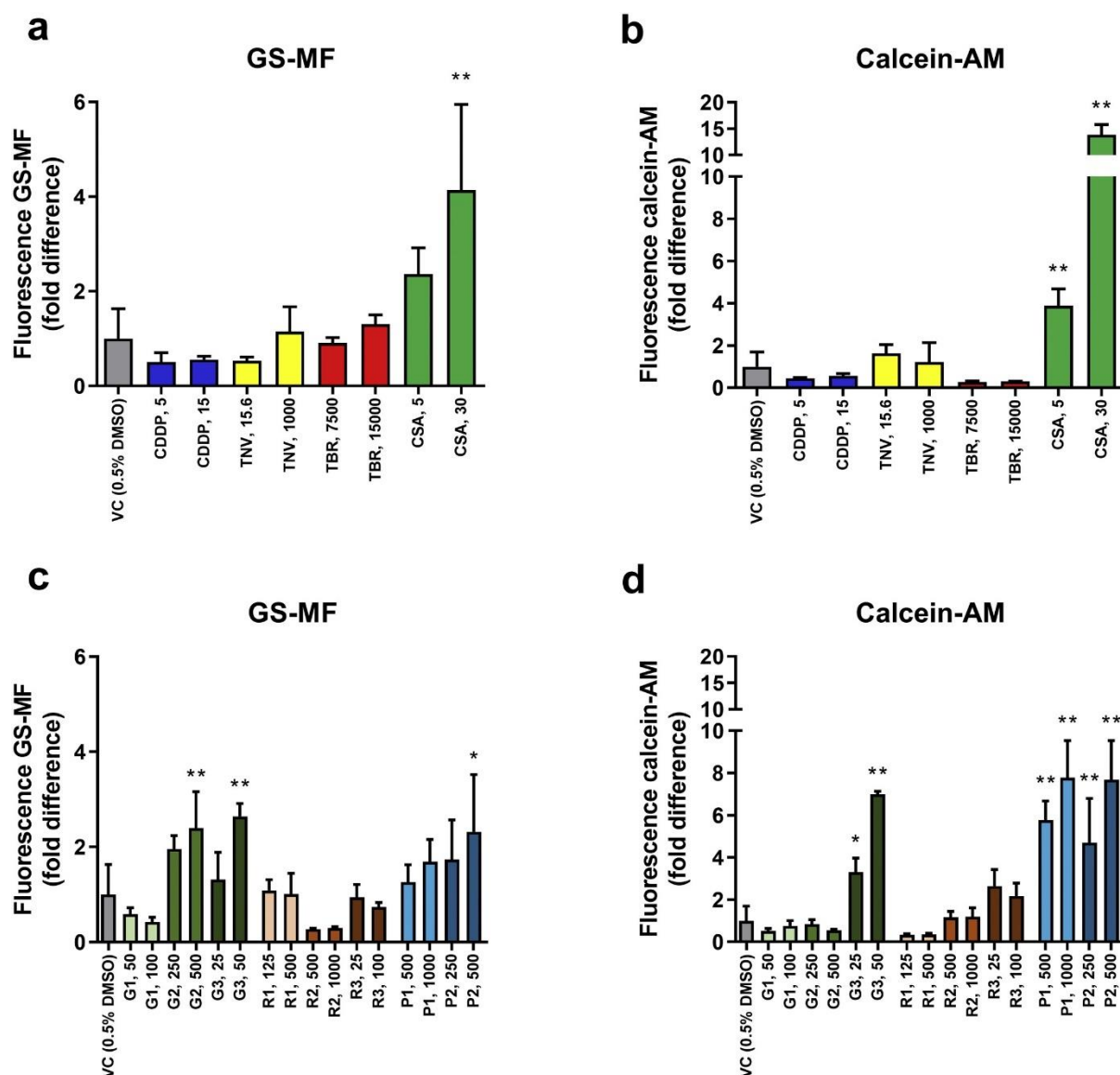
Figure 5: Drug-transporter interaction at multidrug resistance protein 2/4 (MRP2/4) and P-glycoprotein (P-gp) in ciPTEC-OAT1 after co-incubation with compounds at 37 °C for 1 h followed by arresting of efflux with PSC833, MK571 and KO143 (all 10 μM). For model nephrotoxicants cisplatin (CDDP), tenofovir (TNV), tobramycin (TBR) and cyclosporin A (CSA) (a) interactions at MRP2/4 and (b) P-gp and for unknown nephrotoxicants (c) interactions at MRP2/4 and (d) P-gp. Abbreviations: GS-MF, Glutathione methylfluorescein; AM, acetoxymethyl; VC, vehicle control; DMSO, Dimethyl sulfoxide. Statistically significant compared to corresponding vehicle: ∗p < 0.05, ∗∗p < 0.01.
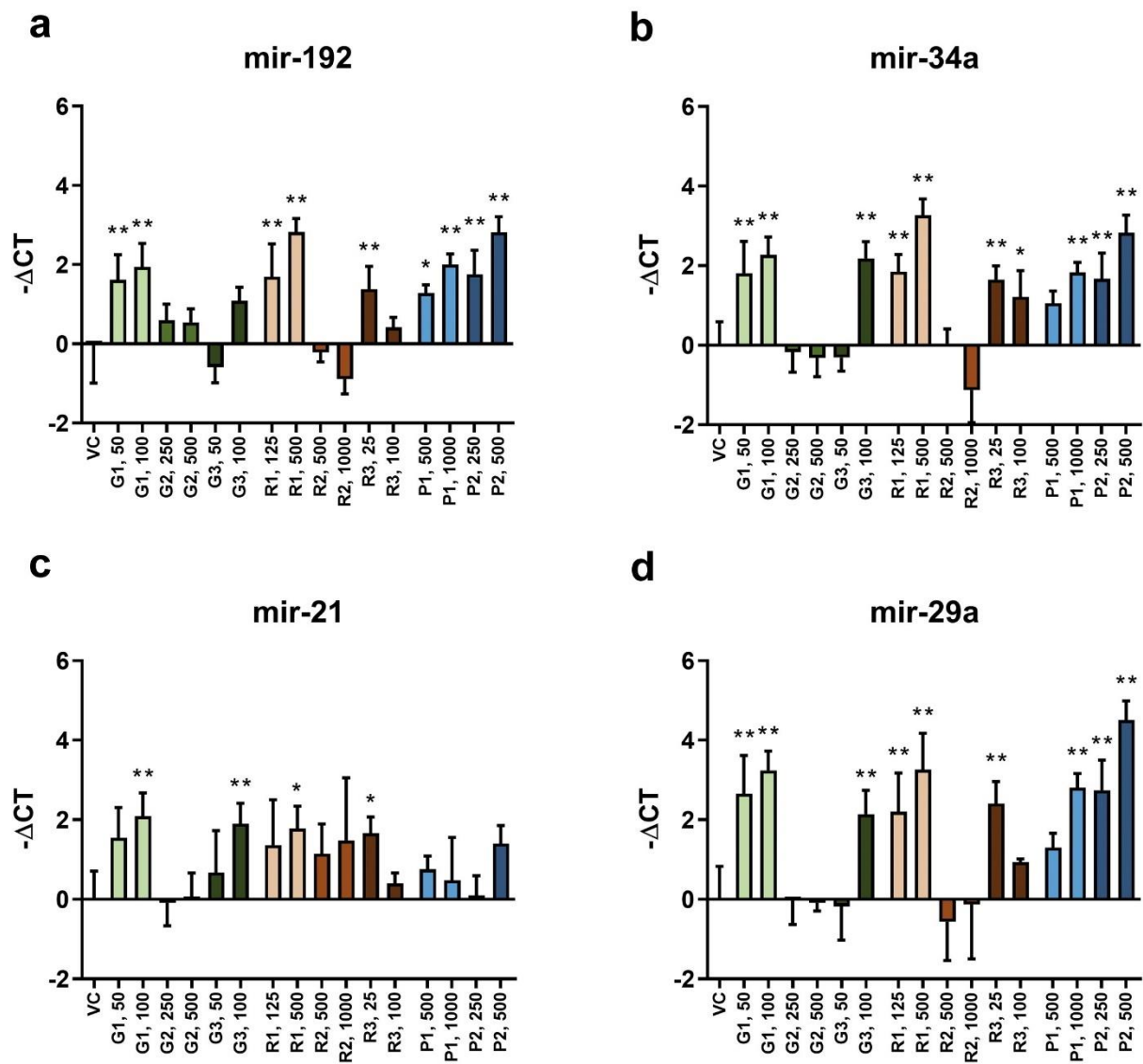
Figure 6: Release into the medium of mir-192 (a), mir-34a (b), mir-21 (c) and mir-29a (d) after 24 h exposure of ciPTEC-OAT1 to sponsor compounds. *Data are represented as Delta CT values in comparison with the vehicle control (VC). Statistically significant compared to corresponding vehicle: *p < 0.05, **p < 0.01.*
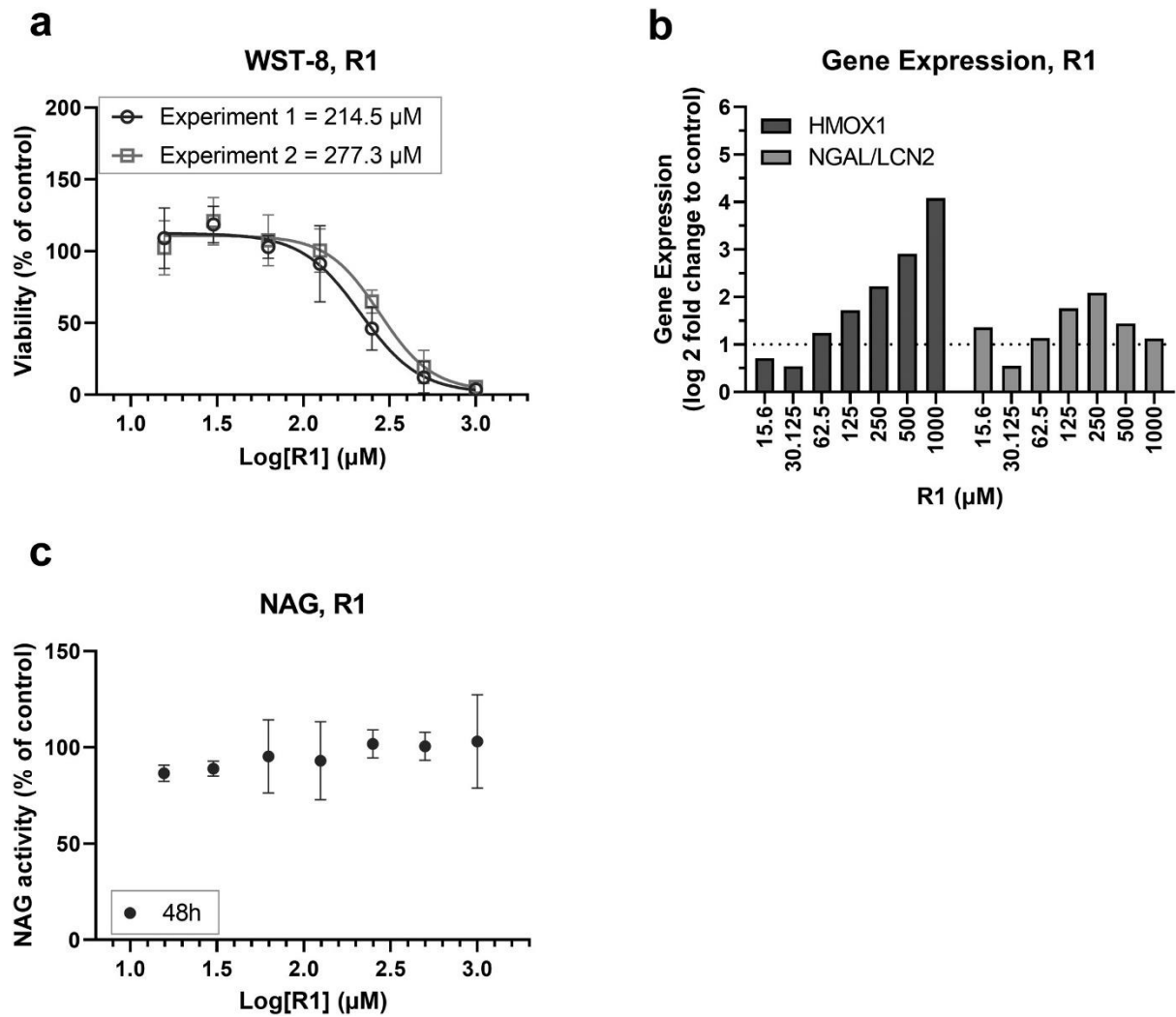
Figure 7: Exposure of ciPTEC-OAT1 to R1 (Colistin). *Data represent cell viability with the IC50 value of each experiment. (a), Gene expression of toxicity markers (b) and release of NAG into the medium after 48 h (c). Abbreviations: HMOX1, heme oxygenase (decycling) 1; LCN2, Lipocalin-2 (LCN2); NGAL, oncogene 24p3 or neutrophil gelatinase-associated lipocalin; NAG, N-acetyl-ß-d-glucosaminidase.*
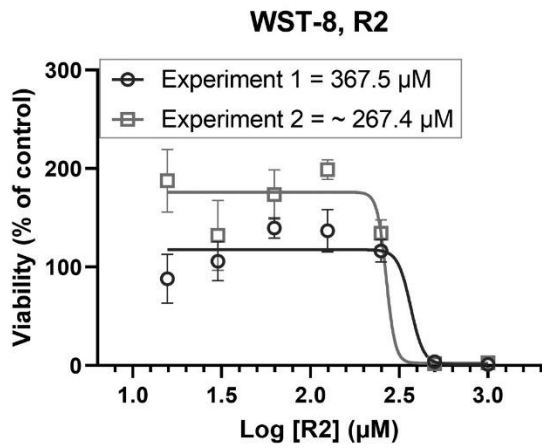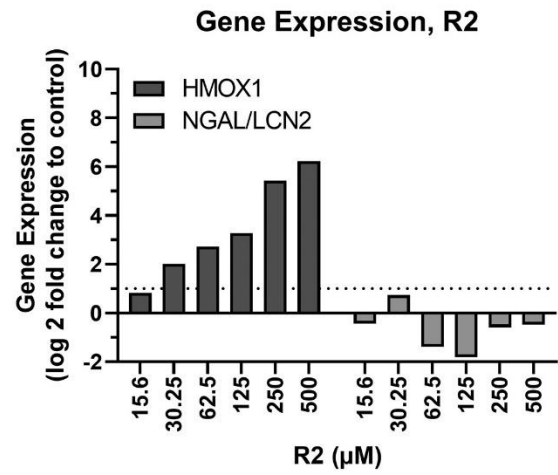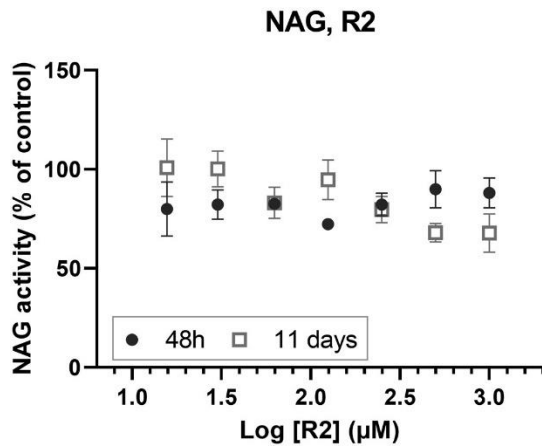
Figure 8: Exposure of ciPTEC-OAT1 to R2 (Cefepime) for 48 h and 11 days. *Data represent cell viability. (a), Gene expression of toxicity markers (b) and release of NAG into the medium after 48 h (circles) and 11 days (squares) (c). Abbreviations: HMOX1, heme oxygenase (decycling) 1; LCN2, Lipocalin-2 (LCN2); NGAL, oncogene 24p3 or neutrophil gelatinase-associated lipocalin; NAG, N-acetyl-ß-d-glucosaminidase.*

Discussion

We demonstrated the use of Nephroscreen, a proximal tubule-on-a-chip platform for the screening of nephrotoxicity and drug-transporter interactions. The robustness and transferability of this platform, a key requirement for broad implementation in industry, was established by the highly comparable results obtained at three different sites as depicted in Fig. 2. Two human renal cell lines, ciPTEC-OAT1 and RPTEC, were exposed to two concentrations of each substance (four model nephrotoxicants and eight blinded compounds) at two exposure times (24 and 48 h). Subsequently, tailor-made assays were performed for two of the compounds (R1, colistin and R2, cefepime), exposing ciPTEC-OAT1. Experimental procedures were carried out in three different laboratories as depicted in Fig. 1, following established standard operating procedures (SOPs).

Concordant with the goal of the study, Nephroscreen was specifically designed to fulfill requirements of pharmaceutical companies. In pre-clinical toxicity studies, multiple drug candidates, typically up to 200 compounds, are assessed *in vitro* and/or *in vivo* in animal experimentation [22]. In this study, we implemented well-characterized PTEC lines, considered relevant for nephrotoxicity and drug-transporter interaction studies, as potential alternatives to animal experimentation [14], [15], [16], [17], [18], [23], [24]. Supply and reproducibility (low batch-to-batch variability) of these commercially available cells are guaranteed. The PTECs were cultured in the OrganoPlate, generating a proximal tubule-on-a-chip consisting of 40 chips on a 384-well microtiter plate format [15]. This model enables the culture of the cells as a tubular structure kept under flow, without the use of support membranes. Perfusion was generated by passive leveling resulting in a bidirectional, oscillating flow allowing significant levels of shear stress circumventing the use of pumps [15], [25]. The diameter of the tubule (approximately 400 μm) is larger than in the human proximal tubule. However, it represents a useful model that allows the long-term culture of polarized cell layers against the ECM with significant barrier function [15].

Effect of the treatments on the PTECs was determined by measuring functional and biochemical parameters. Functional parameters focused on the capacity of compounds to interact with transporters and to impair barrier function. Membrane drug transporters are an important characteristic of PTECs and expression and activity of transporters have been demonstrated previously [6], [17], [18], [24]. Differences in response towards toxicant exposures between ciPTEC-OAT1 and RPTEC could be explained by different expression levels of drug transporters. For instance, ciPTEC-OAT1, but not RPTEC, functionally express OAT1. This explains the lack of sensitivity of RPTEC towards tenofovir, as this substance requires the OAT1 transporter for cellular uptake [18], [24]. Epithelial barrier function is also a key functional parameter, as a leaky epithelium is often an indicator of impaired kidney function, previously demonstrated in this model [15].

Regarding biochemical parameters, cell viability, LDH release and gene expression of toxicity markers were determined on both PTEC lines to assess the effect of the compounds. For ciPTEC-OAT1, assays for drug-transporter interaction, NAG release and miRNA secretion were also performed [14],[16], while RPTEC tubules were more suitable for the assessment of barrier integrity [15]. Cell viability, as measured by enzymatic production of formazan (WST-8 assay), and cell membrane integrity, determined by LDH release into the medium, performed well as *in vitro* markers for cytotoxicity, although with different kinetic profiles (Table 1, Figure S2). In ciPTECs, leakage of NAG into the medium displayed a slightly higher sensitivity in detecting the totoxicity caused by compounds G1 and P2 than LDH release (Fig. 3), but a larger data set would be necessary to corroborate this claim. Decreased barrier integrity was almost always coupled with decreased cell viability and increased LDH release. Thus, we assume that the loss of barrier integrity was directly associated with increased cytotoxicity (Table 1).

The four model nephrotoxicants (cisplatin, tenofovir, tobramycin, cyclosporin A) assessed in this study elicited a response in at least four of the end-point read-outs (Figure S2, Table 1), in agreement with previous results [26], [27], [28], [29], [30]. Furthermore, our data show that cyclosporin A interacts with P-gp, corroborating that Nephroscreen results reflect its known P-gp inhibition [31]. Nephrotoxicity of tobramycin, on the other hand, could only be observed at concentrations that were up to 1500-fold higher than plasma concentrations generally found in patients (0.01 mM) [30]. This is probably due to the low expression of cubilin and megalin receptors in ciPTEC-OAT1 [17], [32], [33] a limitation that needs to be taken into consideration for compounds known to be dependent on this cellular uptake mechanism. During the second phase of the study, eight substances selected and provided by the sponsors were assessed in a blinded manner.

1000 µM and unpublished *in vitro* results with PTEC toxicity at concentrations >500 µM (Table S2).

The ideal set-up for a screening tool requires short-term incubation in order to generate results quickly. Our results show that for most compounds, exposure during 24 and 48 h suffices to detect compound-induced damage to renal tubular cells. However, as demonstrated with the results obtained with R2, the developed platform can also be implemented as a second tier assay for selected substances of interest that may require subchronic or chronic exposure. The sensitivity and specificity of Nephroscreen cannot be determined as only a small set of test compounds was included. Future testing should expand the number of compounds and include compounds with other toxicity target organs (non-nephrotoxic) as well as non-toxic compounds to further characterize the model. Also, side-by-side comparison with conventional 2D cell cultures may be performed to achieve direct comparison and therefore show the value in this model over more simple models. Other proximal tubule-on-a-chip models have, however, demonstrated that 3D microfluidic models increase *in vivo* physiology and sensitivity of PTECs towards nephrotoxicant

exposure [11], [12], [13]. Additional future improvements could include the corroboration and systematic assessment of HMOX-1 induction as an earlier biomarker and its implementation as a FRET-based assay for HMOX1 expression [19]. The implementation of cell lines expressing more types of functional transporters relevant, such as ciPTEC-OAT1/OAT-3 could also be envisaged [18]. Moreover, data on additional compounds could support the creation of intelligent decision algorithms to evaluate the multiparametric data provided by Nephroscreen in an unbiased manner.

Preliminary knowledge such as clinical data (for R1, R2, R3) or *in vivo* toxicity data were provided by sponsors after the Nephroscreen data collection and analysis had been finalized. The compound concentrations selected and applied to Nephroscreen unveiled nephrotoxic potential at concentrations that are considered relevant for toxicological assessment (Table S2). For R1, R2, and R3 there is clinical data available; these compounds are used at very high concentrations and administered parenterally, so that a high systemic exposure is reached in patients. For the other blinded compounds, there is no clinical data but preclinical data on at least one animal species show that the exposure (Cmax) at which nephrotoxicity was observed in a subset of the animals was slightly lower, but in a similar range to that eliciting a positive flag in Nephroscreen. In our experimental set-up, prediction of nephrotoxic liability was highest when combining results of cell viability, LDH release, and miRNA release. Additional functional effects of the compounds were uncovered by the drug-transport interaction measurements. The majority of the unknown nephrotoxicants (G1, G3, R1, R2, R3, P1, and P2) resulted in toxicity detected by at least one of the parameters or in drug-transporter interactions. Interestingly, an interaction at MRP2/4 was observed for G2, despite the lack of toxicity. This could be explained by the fact that G2-induced nephrotoxicity was only observed upon long-term exposure *in vivo* (one month, highest tested dose) as compared to short-term (up to 48 h) exposure tested in Nephroscreen. The compound P1 showed a particularly mild effect on Nephroscreen, as it only led to increased levels of miRNAs (mir192, mir29a, and mir34a) in the medium and an interaction at P-gp, without causing cytotoxicity. This is consistent with the existing animal data showing that this vasopressin 1-a antagonist caused tubular degeneration/regeneration only in female rats treated with a high dose (125 mg/kg/day) for two weeks.

Table 1: Overview Read-Outs Nephrotoxicity and Renal Drug-Transporter Interactions Assessed in This Nephrotoxicant Screening.

	Conc. (μM)	ciPTEC-OAT1					RPTEC		
		Cell Viability	LDH Release	Drug-Transporter Interaction	NAG Activity	miRNA Release	Cell Viability	LDH Release	Barrier Integrity
CDDP	5								
	15	↓ 48 h							
TNV	15.6	↑ 48 h							
	1000	↓ 48 h							
TBR	7500							↑ 48 h	4.4 kDa: ↓ 24 h 150 kDa: ↓ 48 h
	15000	↓ 48 h	↑ 24 h				↓ 48 h	↑ 48 h	4.4 kDa: ↓ 24 h 150 kDa: ↓ 48 h
CSA	5	↓ 48 h		P-gp					
	30	↓ 48 h	↑ 24 h	MRP2/4, P-gp					
G1	50	↓ 24 h			↑ 24 h	mir-34a, mir-29a, mir-192	↓ 24 h	↑ 24 h	4.4 kDa: ↓ 24 h 150 kDa: ↓ 24 h
	100	↓ 24 h			↑ 24 h	mir-21, mir-34a, mir-29a, mir-192	↓ 24 h	↑ 24 h	4.4 kDa: ↓ 24 h 150 kDa: ↓ 24 h
G2	250			MRP2/4			↓ 24 h		
	500						↓ 24 h		
	1000								
G3	25			P-gp					
	50	↓ 24 h		MRP2/4, P-gp	↑ 24 h	mir-21, mir-34a, mir-29a	↓ 48 h	↑ 24 h	4.4 kDa: ↓ 48 h
	100				↑ 48 h	mir-34a, mir-29a, mir-192	↓ 24 h	↑ 24 h	4.4 kDa: ↓ 24 h 150 kDa: ↓ 48 h
R1	125								
	500	↓ 24 h	↑ 24 h		↑ 48 h				4.4 kDa: ↓ 24 h 150 kDa: ↓ 24 h
R2	500	↓ 24 h	↑ 24 h			mir-21, mir-34a, mir-29a, mir-192	↓ 24 h	↑ 24 h	
	1000	↑ 48 h							
R3	25	↓ 48 h	↑ 48 h		↑ 48 h	mir-21, mir-34a, mir-29a, mir-192	↓ 24 h		4.4 kDa: ↓ 48 h 150 kDa: ↓ 48 h
	100	↓ 48 h	↑ 48 h		↑ 48 h	mir-34a	↓ 48 h		4.4 kDa: ↓ 48 h 150 kDa: ↓ 48 h
P1	250			P-gp		mir-192			
	500			P-gp					
	1000			P-gp		mir-34a, mir-29a, mir-192			
P2	250			MRP2/4, P-gp	↑ 48 h	mir-34a, mir-29a, mir-192	↓ 48 h	↑ 48 h	4.4 kDa: ↓ 48 h
	500	↓ 24 h				mir-34a, mir-29a, mir-192			

For cell viability, LDH release, drug-transporter interaction, and barrier integrity: ↑ represents significant increased effect observed compared to corresponding vehicle, ↓ represents significant decreased effect observed compared to corresponding vehicle. CDDP, cisplatin; CLDN2, claudin-2; Conc., concentration; CSA, cyclosporin A; FITC, fluorescein isothiocyanate; LDH, lactate dehydrogenase; MRP2/4, multidrug resistance-associated proteins 2 and 4; P-gp, P-glycoprotein; TBR, tobramycin; TNV, tenofovir; TRITC, tetramethylrhodamine.

In the last phase of this study, tailor-made experiments were performed including expanded concentration ranges of two compounds after their identities had been uncovered: R1 (colistin) and R2 (cefepime). For R1 (colistin) we repeated the cytotoxicity assay and determined gene expression of HMOX-1 and NGAL, as well as the release of NAG in the medium. The EC50 for cytotoxicity obtained in this experiment was in line with the results of the first round of experiments (~200 µM). The *in vitro* cytotoxicity of colistin has been reported by others in the high micromolar range, around 690 µM.34 Preliminary gene expression data, however, uncovered a dose-dependent increase in HMOX-1 from a concentration of 30 µM (>2-fold induction). Transcriptional upregulation of heme oxygenase-1 is a well-known indicator of cellular stress in several cells and tissues, including PTECs and may be a more sensitive biomarker of toxicity [19], [26]. This was also supported by the long-term (11 days) exposure of the Nephroscreen to R2 (cefempime). Cefepime had an EC50-value for cytotoxicity of approximately 300 µM, while the concentration-dependent transcriptional induction of HMOX-1 was observed at concentrations from of 62 µM (>2-fold induction). These results also show that a long-term exposure is required for this compound, as the short-term experiment failed to show toxicity up to a concentration of 1000 µM and unpublished *in vitro* results with PTEC toxicity at concentrations >500 µM (Table S2).

The ideal set-up for a screening tool requires short-term incubation in order to generate results quickly. Our results show that for most compounds, exposure during 24 and 48 h suffices to detect compound-induced damage to renal tubular cells. However, as demonstrated with the results obtained with R2, the developed platform can also be implemented as a second tier assay for selected substances of interest that may require subchronic or chronic exposure. The sensitivity and specificity of Nephroscreen cannot be determined as only a small set of test compounds was included. Future testing should expand the number of compounds and include compounds with other toxicity target organs (non-nephrotoxic) as well as non-toxic compounds to further characterize the model. Also, side-by-side comparison with conventional 2D cell cultures may be performed to achieve direct comparison and therefore show the value in this model over more simple models. Other proximal tubule-on-a-chip models have, however, demonstrated that 3D microfluidic models increase *in vivo* physiology and sensitivity of PTECs towards nephrotoxicant exposure [11], [12], [13]. Additional future improvements could include the corroboration and systematic assessment of HMOX-1 induction as an earlier biomarker and its implementation as a FRET-based assay for HMOX1 expression [19]. The implementation of cell lines expressing more types of functional transporters relevant, such as ciPTEC-OAT1/OAT-3 could also be envisaged [18]. Moreover, data on additional compounds could support the creation of intelligent decision algorithms to evaluate the multiparametric data provided by Nephroscreen in an unbiased manner.

Conclusion

An advanced screening tool is needed to increase speed, reduce costs and animal testing while assessing the potential nephrotoxicity of new drug candidates. Taken together, our results indicate that Nephroscreen, consisting of a microfluidic organ-on-a-chip system coupled with a multiparametric biomarker analysis is able to identify potential nephrotoxicants. Nephroscreen is a reliable medium-throughput, standardized, automatable system that proved efficacious in identifying nephrotoxicants and provided insights into their mode of toxicity.

Conflicts of Interest

This publication contains original work. The authors Marianne K. Vormann, Henriëtte L. Lanz, Linda Gijzen, Angelique van den Heuvel, Simon Hutter, Jos Joore, Sebastiaan J. Trietsch, and Paul Vulto are or were employees of Mimetas B.V. This affiliation is declared. The OrganoPlate® is a registered trademark of MIMETAS BV. Martijn Wilmer and Frans Russel are co-inventors on patent EP2010/066792 "Novel conditionally immortalized human proximal tubule cell line expressing functional influx and efflux transporters" assigned to Radboud University Medical Center and commercialized through Cell4Pharma.com, for which Martijn Wilmer acts as scientific advisor.

Acknowledgements

References

[1]   Soo JY, Jansen J, Masereeuw R, Little MH 2018. Advances in predictive *in vitro* models of drug-induced nephrotoxicity. Nat Rev Nephrol 14(6):378-393.

[2]   Uchino S, Kellum JA, Bellomo R, Doig GS, Morimatsu H, Morgera S, Schetz M, Tan I, Bouman C, Macedo E, Gibney N, Tolwani A, Ronco C, Beginning, Ending Supportive Therapy for the Kidney I 2005. Acute renal failure in critically ill patients: a multinational, multicenter study. JAMA 294(7):813-818.

[3]   Hoste EA, Bagshaw SM, Bellomo R, Cely CM, Colman R, Cruz DN, Edipidis K, Forni LG, Gomersall CD, Govil D, Honore PM, Joannes-Boyau O, Joannidis M, Korhonen AM, Lavrentieva A, Mehta RL, Palevsky P, Roessler E, Ronco C, Uchino S, Vazquez JA, Vidal Andrade E, Webb S, Kellum JA 2015. Epidemiology of acute kidney injury in critically ill patients: the multinational AKI-EPI study. Intensive Care Med 41(8):1411-1423.

[4]   Mehta RL, Pascual MT, Soroko S, Savage BR, Himmelfarb J, Ikizler TA, Paganini EP, Chertow GM, Program to Improve Care in Acute Renal D 2004. Spectrum of acute renal failure in the intensive care unit: the PICARD experience. Kidney Int 66(4):1613-1621.

[5]   Guengerich FP 2011. Mechanisms of drug toxicity and relevance to pharmaceutical development. Drug Metab Pharmacokinet 26(1):3-14.

[6]   Morrissey KM, Stocker SL, Wittwer MB, Xu L, Giacomini KM 2013. Renal transporters in drug development. Annu Rev Pharmacol Toxicol 53:503-529.

[7]   Varma MV, Feng B, Obach RS, Troutman MD, Chupka J, Miller HR, El-Kattan A 2009. Physicochemical determinants of human renal clearance. J Med Chem 52(15):4844-4852.

[8]   Ivanyuk A, Livio F, Biollaz J, Buclin T 2017. Renal Drug Transporters and Drug Interactions. Clin Pharmacokinet 56(8):825-892.

[9]   Wilmer MJ, Ng CP, Lanz HL, Vulto P, Suter-Dick L, Masereeuw R 2016. Kidney-on-a-Chip Technology for Drug-Induced Nephrotoxicity Screening. Trends Biotechnol 34(2):156-170.

[10]   Tiong HY, Huang P, Xiong S, Li Y, Vathsala A, Zink D 2014. Drug-induced nephrotoxicity: clinical impact and preclinical *in vitro* models. Mol Pharm 11(7):1933-1948.

[11]   Homan KA, Kolesky DB, Skylar-Scott MA, Herrmann J, Obuobi H, Moisan A, Lewis JA 2016. Bioprinting of 3D Convoluted Renal Proximal Tubules on Perfusable Chips. Sci Rep 6:34845.

[12]   Jang KJ, Mehr AP, Hamilton GA, McPartlin LA, Chung S, Suh KY, Ingber DE 2013. Human kidney proximal tubule-on-a-chip for drug transport and nephrotoxicity assessment. Integrative biology : quantitative biosciences from nano to macro 5(9):1119-1129.

[13]   Sakolish C, Weber EJ, Kelly EJ, Himmelfarb J, Mouneimne R, Grimm FA, House JS, Wade T, Han A, Chiu WA, Rusyn I 2018. Technology Transfer of the Microphysiological Systems: A Case Study of the Human Proximal Tubule Tissue Chip. Sci Rep 8(1):14882.

[14]   Suter-Dick L, Mauch L, Ramp D, Caj M, Vormann MK, Hutter S, Lanz HL, Vriend J, Masereeuw R, Wilmer MJ 2018. Combining Extracellular miRNA Determination with Microfluidic 3D Cell Cultures for the Assessment of Nephrotoxicity: a Proof of Concept Study. AAPS J 20(5):86.

[15] Vormann MK, Gijzen L, Hutter S, Boot L, Nicolas A, van den Heuvel A, Vriend J, Ng CP, Nieskens TTG, van Duinen V, de Wagenaar B, Masereeuw R, Suter-Dick L, Trietsch SJ, Wilmer M, Joore J, Vulto P, Lanz HL 2018. Nephrotoxicity and Kidney Transport Assessment on 3D Perfused Proximal Tubules. AAPS J 20(5):90.

[16] Vriend J, Nieskens TTG, Vormann MK, van den Berge BT, van den Heuvel A, Russel FGM, Suter-Dick L, Lanz HL, Vulto P, Masereeuw R, Wilmer MJ 2018. Screening of Drug-Transporter Interactions in a 3D Microfluidic Renal Proximal Tubule on a Chip. AAPS J 20(5):87.

[17] Adler M, Ramm S, Hafner M, Muhlich JL, Gottwald EM, Weber E, Jaklic A, Ajay AK, Svoboda D, Auerbach S, Kelly EJ, Himmelfarb J, Vaidya VS 2016. A Quantitative Approach to Screen for Nephrotoxic Compounds *In vitro*. J Am Soc Nephrol 27(4):1015-1028.

[18] Schindelin J, Arganda-Carreras I, Frise E, Kaynig V, Longair M, Pietzsch T, Preibisch S, Rueden C, Saalfeld S, Schmid B, Tinevez JY, White DJ, Hartenstein V, Eliceiri K, Tomancak P, Cardona A 2012. Fiji: an open-source platform for biological-image analysis. Nat Methods 9(7):676-682.

[19] Caetano-Pinto P, Janssen MJ, Gijzen L, Verscheijden L, Wilmer MJ, Masereeuw R 2016. Fluorescence-Based Transport Assays Revisited in a Human Renal Proximal Tubule Cell Line. Mol Pharm 13(3):933-944.

[20] Sakolish CM, Esch MB, Hickman JJ, Shuler ML, Mahler GJ 2016. Modeling Barrier Tissues *In vitro*: Methods, Achievements, and Challenges. EBioMedicine 5:30-39.

[21] Fedecostante M, Westphal KGC, Buono MF, Sanchez Romero N, Wilmer MJ, Kerkering J, Baptista PM, Hoenderop JG, Masereeuw R 2018. Recellularized Native Kidney Scaffolds as a Novel Tool in Nephrotoxicity Screening. Drug Metab Dispos 46(9):1338-1350.

[22] Li S, Zhao J, Huang R, Steiner T, Bourner M, Mitchell M, Thompson DC, Zhao B, Xia M 2017. Development and Application of Human Renal Proximal Tubule Epithelial Cells for Assessment of Compound Toxicity. Curr Chem Genom Transl Med 11:19-30.

[23] Nieskens TT, Peters JG, Schreurs MJ, Smits N, Woestenenk R, Jansen K, van der Made TK, Roring M, Hilgendorf C, Wilmer MJ, Masereeuw R 2016. A Human Renal Proximal Tubule Cell Line with Stable Organic Anion Transporter 1 and 3 Expression Predictive for Antiviral-Induced Toxicity. AAPS J 18(2):465-475.

[24] Wilmer MJ, Saleem MA, Masereeuw R, Ni L, van der Velden TJ, Russel FG, Mathieson PW, Monnens LA, van den Heuvel LP, Levtchenko EN 2010. Novel conditionally immortalized human proximal tubule cell line expressing functional influx and efflux transporters. Cell and tissue research 339(2):449-457.

[25] van Duinen V, van den Heuvel A, Trietsch SJ, Lanz HL, van Gils JM, van Zonneveld AJ, Vulto P, Hankemeier T 2017. 96 perfusable blood vessels to study vascular permeability *in vitro*. Sci Rep 7(1):18071.

[26] Ozkok A, Edelstein CL 2014. Pathophysiology of cisplatin-induced acute kidney injury. Biomed Res Int 2014:967826.

[27] Jafari A, Khalili H, Dashti-Khavidaki S 2014. Tenofovir-induced nephrotoxicity: incidence, mechanism, risk factors, prognosis and proposed agents for prevention. Eur J Clin Pharmacol 70(9):1029-1040.

[28]   Ramamoorthy H, Abraham P, Isaac B 2014. Mitochondrial dysfunction and electron transport chain complex defect in a rat model of tenofovir disoproxil fumarate nephrotoxicity. J Biochem Mol Toxicol 28(6):246-255.

[29]   Mingeot-Leclercq MP, Tulkens PM 1999. Aminoglycosides: nephrotoxicity. Antimicrob Agents Chemother 43(5):1003-1012.

[30]   Schentag JJ, Lasezkay G, Cumbo TJ, Plaut ME, Jusko WJ 1978. Accumulation pharmacokinetics of tobramycin. Antimicrob Agents Chemother 13(4):649-656.

[31]   Polli JW, Wring SA, Humphreys JE, Huang L, Morgan JB, Webster LO, Serabjit-Singh CS 2001. Rational use of *in vitro* P-glycoprotein assays in drug discovery. J Pharmacol Exp Ther 299(2):620-628.

[32]   Vriend J, Peters JGP, Nieskens TTG, Škovroňová R, Blaimschein N, Schmidts M, Roepman R, Schirris TJJ, Russel FGM, Masereeuw R, Wilmer MJ 2020. Flow stimulates drug transport in a human kidney proximal tubule-on-a-chip independent of primary cilia. Biochim Biophys Acta Gen Subj 1864(1):129433.

[33]   Sun Y, Goes Martini A, Janssen MJ, Garrelds IM, Masereeuw R, Lu X, Danser AHJ 2020. Megalin: A Novel Endocytic Receptor for Prorenin and Renin. Hypertension 75(5):1242-1250.

[34]   Roberts KD, Azad MA, Wang J, Horne AS, Thompson PE, Nation RL, Velkov T, Li J 2015. Antimicrobial Activity and Toxicity of the Major Lipopeptide Components of Polymyxin B and Colistin: Last-line Antibiotics against Multidrug-Resistant Gram-negative Bacteria. ACS Infect Dis 1(11):568-575.

3
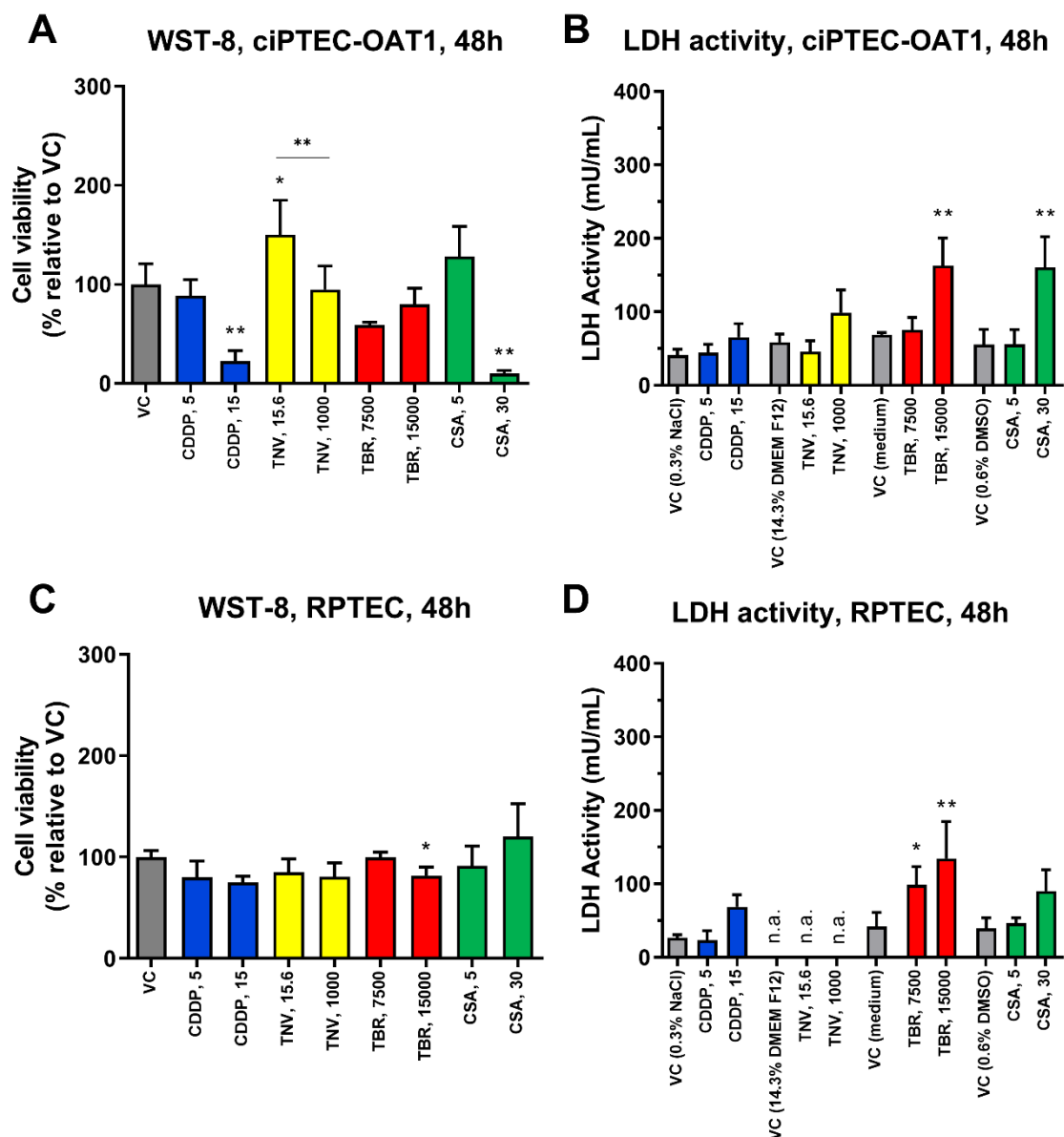
Figure S1: Release of lactate dehydrogenase (LDH) (B, D)) and Cell Viability (A, C) *upon exposure to model nephrotoxicants cisplatin (CDDP), tenofovir (TNV), tobramycin (TBR) and cyclosporin A (CSA) in ciPTEC-OAT1 after 48 hours. Abbreviations: D-F12, Dulbecco's modified Eagle's medium and nutrient mixture F-12; WST-8, 2-(2-methoxy-4-nitrophenyl)-3-(4-nitrophenyl)-5-(2,4-disulfophenyl)-2H-tetrazolium, monosodium salt; HMOX1, heme oxygenase (decycling) 1; LDH, lactate dehydrogenase; DMSO, Dimethyl sulfoxide; VC, vehicle control; n.a., not available. Statistically significant compared to corresponding vehicle: *p<0.05, **p<0.01.*

Table S1: Test compounds used to study nephrotoxicity and renal drug-transporter interactions

Compound	Supplier, catalog no.	Compound exposure toxicity assessment				3D fluorescent efflux assays		
		Vehicle	Stock conc. (mM)	Final vehicle conc. (v/v)	Exposure conc. (mM)	Vehicle	Stock conc. (mM)	Exposure conc. (mM)
CDDP	Sigma-Aldrich, P4394	0.9% NaCl in H₂O (lab L), PTEC CM (lab N)	5 (lab L), 1.5 (lab N)	0.3% (lab L)	0.005, 0.015	DMSO	15	0.005, 0.015
TNV	Santa Cruz, 204335	Culture medium (lab L), HBSS (lab N)	7 (lab L), 5 (lab N)	-	0.0156, 1	HBSS	5	0.0156, 1
TBR	Sigma-Aldrich, T1783	Culture medium (lab L), PTEC SFM (lab N)	100	-	7.5, 15	KHH	100	7.5, 15
CSA	Sigma-Aldrich, 30024	DMSO	5 (lab L), 40 (lab N)	0.6% (lab L), 0.08% (lab N)	0.005, 0.03	DMSO	40	0.005, 0.03
G1	Blinded, GSK	DMSO	50	0.2%	0.05, 0.1	DMSO	50	0.05, 0.1
G2	Blinded, GSK	DMSO	500	0.1%	0.25, 0.5	DMSO	500	0.25, 0.5
G3	Blinded, GSK	DMSO	500	0.02%	0.025, 0.05, 0.1	DMSO	50	0.025, 0.05

3

R1	Blinded, Roche	Culture medium	10	-	0.125, 0.5	KHH	10	0.125, 0.5
R2	Blinded, Roche	Culture medium	100	-	0.5, 1	KHH	100	0.5, 1
R3	Blinded, Roche	Milli-Q + 11.4% v/v 1 M NaOH	100	0.1%	0.025, 0.1	Milli-Q + 11.4% v/v 1 M NaOH	100	0.025, 0.1
P1	Blinded, Pfizer	DMSO	500	0.2%	0.25, 1	DMSO	500	500, 1000
P2	Blinded, Pfizer	DMSO	500	0.1%	0.25, 0.5	DMSO	500	0.25, 0.5

CDDP, cisplatin; Conc., concentration; CSA, cyclosporin A; D-F12, Dulbecco's modified Eagle's medium and nutrient mixture F-12; DMSO, dimethyl sulfoxide; HBSS, Hank's balanced salt solution; KHH, Krebs-Henseleit buffer supplemented with HEPES (10 mM); PTEC CM, proximal tubule epithelial cell complete medium; PTEC SFM, proximal tubule epithelial cell serum-free medium; TBR, tobramycin; TNV, tenofovir

Table S2 Overview of available *in vitro* and *in vivo* data of blinded nephrotoxicants

Compound	Previous studies	Reference
G1	Oral dose studies in monkeys (14 days): kidney weights and kidney to body ratios for males dosed at 1500 mg G1 R-enantiomer/kg/day where higher than those for the controls. Especially one animal was particularly high. Mottled and irregular surface was observed in one male kidney; and pallor in one female kidney at 1500 mg/kg/day R-enantiomer. Renal tubular nephritis occurred in two males given 1500 mg/kg/day of G1 R-enantiomer. C_{max} of R-enantiomer at highest dose 6.9 µM (2.5 µg/mL). Nephroscreen flag: 50 µM	Sponsor
G2	Oral toxicity study in rats (1 month): one male and one female died at day 3, two males on day 4. Highest dose of 200 mg/kg/day was lowered to 150 mg/kg/day on day 4. Tubular necrosis associated with tubular regeneration and interstitial mononuclear cell infiltration was noted in three males at the highest dose. One additional animal exhibited serum chemistry changes associated with renal tubular lesions. Thirteen male rats and 17 female rats with similar dosing regimen survived to the end of the study. C_{max} at highest dose in male was 18 µg/mL (45 µM) and in female 41 µg/mL (103 µM). Oral toxicity study in Beagle dogs (1 month): dose at 0.5, 3 or 20 mg/kg/day. Both kidneys at highest dose in males were reduced in size, correlated with reduced weight and tubular degeneration/regeneration (in 2 out of 3 males) and glomerulosclerosis. C_{max} at highest dose in male was14 µg/mL (35 µM) and in female 15 µg/mL (37.5 µM). Nephroscreen flag: MRP interaction, 250 µM	Sponsor

3

G3	Oral gavage dose range-finding study in rats (7 days): inclusions in epithelial cells lining collecting ducts of papilla, crystals in the collecting ducts. Some animals presented with basophilia of tubules in the cortex and degeneration/regeneration of the medullary epithelium. Some animals (both male and female) presented with tubule dilation. Increases in plasma creatinine concentrations (mild to moderate). C_{max} in male was 2 µg/mL (4.6 µM) and in female 4.5 µg/mL (10.4 µM).	Sponsor
	Oral study in minipig (7 days): 100 or 300 mg/kg/day, once daily; or 1000mg/kg/day up to 3 days (severe clinical signs – animals were killed). Pallor and enlargement of the kidney; dilated tubules, interstitial inflammation/fibrosis in all areas of the kidney, crystals in lumen consistent with obstructive nephropathy. Increased plasma levels of urea and sCr. C_{max} in male was 19.4 µg/mL (45 µM) and in female 3.5 µg/mL (8 µM).	
	Nephroscreen flag: 50 µM	
R1
Colistin (antibiotic)	Colistin undergoes extensive renal tubular reabsorption (up to 80%) upon glomerular filtration. Most of the filtered colistin is retained in the body. Clinical use leads to plasma concentrations of approximately 2 mg/L (approx. 1.7 µM) following i.v. administration of 250 mg/day. Colistin increases tubular epithelial barrier permeability and causes cell swelling, cell lysis, resulting in acute tubular necrosis. Conventional 2D human primary PTECs were susceptible for toxicity at 100 µM.	[1], [2]
	Nephroscreen flag: 250 µM/ 62 µM	
R2
Cefepime
(cephalosporin antibiotic)	Cefepime accumulates in PTECs where it can form crystals and induces necrotic cell death. It is clinically administered at high doses (up to 9 g/day, parenterally). Conventional 2D human primary PTECs were susceptible to high concentrations (500-1000 µM) and after prolonged treatment (several days).	[3]
	Nephroscreen flag: 500 µM/ 62 µM	

R3	Zoledronat (bisphosphonate drug class)	Zoledronat (zoledronic acid) is excreted unmetabolized via the kidney. It is administered clinically at doses of 4 mg/day, i.v. . A relationship exists between peak levels of zoledronic acid in the blood and renal toxicity since renal damage declines when the dose is reduced. *In vitro* toxicity documented in a rat renal cell line (NRK- 52E at 100 μM), human primary cells (100 μM) and in a renal cell line (HK-2 at 1000 μM). Nephroscreen flag: 25 μM	[4]-[7]
P1	*Vasopressin 1a antagonist*	*In vitro* toxicity found in human liver cell line THLE at > 300 μM. In a rat study (2 weeks), females showed tubular degeneration/regeneration at highest dose (125 mg/kg/day). The renal cortex and the outer and inner stripes of the outer medulla were affected. This finding was most suggestive of damage to the proximal tubules but also, to a lesser extent, distal nephron segments, and correlated with slight increases in urinary protein. Proteinuria was most likely the result of decreased resorption of low molecular weight proteins from the proximal convoluted tubule, secondary to tubular damage. C_{max} was (both in male and female) 14.6 μM. Nephroscreen flag: 250 μM	Sponsor
P2	*Prostaglandin E2 receptor anatagonist*	*In vitro* toxicity found in human liver cell line THLE at > 262 μM. In a rat study (2 weeks), male and female rats were treated with mid dose (50 mg/kg) or high dose (250 mg/kg). In female rats, 1 out of 10 rats at mid dose and all rats at high dose showed renal tubular degeneration in the pars recta, while males were unaffected. Levels of KIM-1 in tissue and urine were elevated, while levels of BUN and sCr remained normal. Full recovery was observed on cessation of dosing. It is noteworthy that AUC in male rats at 50 and 250 mg/kg on day 14 was 6 and 8 times lower, respectively, than those achieved in females at the same dose level based on the free unbound drug fraction. C_{max} was (both in male and female) 1.5 mM, unbound fraction was 55.8 μM. Nephroscreen flag: 250 μM	Sponsor

2D, two-dimensional, AUC, area under the curve; BUN, blood urea nitrogen; Cmax, maximum serum concentration; HK-2, human kidney-2; KIM-1, kidney injury molecule-1; NRK- 52E, normal rat kidney-52E; PTEC, proximal tubule epithelial cell; sCr, serum creatinine; THLE, transformed human liver epithelial

3

References

[1]   Ordooei Javan A, Shokouhi S, Sahraei Z 2015. A review on colistin nephrotoxicity. Eur J Clin Pharmacol 71(7):801-810.

[2]   Plachouras D, Karvanen M, Friberg LE, Papadomichelakis E, Antoniadou A, Tsangaris I, Karaiskos I, Poulakou G, Kontopidou F, Armaganidis A, Cars O, Giamarellou H 2009. Population pharmacokinetic analysis of colistin methanesulfonate and colistin after intravenous administration in critically ill patients with infections caused by gram-negative bacteria. Antimicrob Agents Chemother 53(8):3430-3436.

[3]   Elsayed MG, Elkomy AA, Gaballah MS, Elbadawy M 2014. Nephrotoxicity of cefepime: A new cephalosporin antibiotic in rats. J Pharmacol Pharmacother 5(1):33-38.

[4]   Markowitz GS, Fine PL, Stack JI, Kunis CL, Radhakrishnan J, Palecki W, Park J, Nasr SH, Hoh S, Siegel DS, D'Agati VD 2003. Toxic acute tubular necrosis following treatment with zoledronate (Zometa). Kidney Int 64(1):281-289.

[5]   Luhe A, Kunkele KP, Haiker M, Schad K, Zihlmann C, Bauss F, Suter L, Pfister T 2008. Preclinical evidence for nitrogen-containing bisphosphonate inhibition of farnesyl diphosphate (FPP) synthase in the kidney: implications for renal safety. Toxicol *In vitro* 22(4):899-909.

[6]   Bergner R, Siegrist B, Gretz N, Pohlmeyer-Esch G, Kranzlin B 2015. Nephrotoxicity of ibandronate and zoledronate in Wistar rats with normal renal function and after unilateral nephrectomy. Pharmacol Res 99:16-22.

[7]   Verhulst A, Sun S, McKenna CE, D'Haese PC 2015. Endocytotic uptake of zoledronic acid by tubular cells may explain its renal effects in cancer patients receiving high doses of the compound. PLoS One 10(3):e0121861.

Chapter 4

Drug-Drug Interaction Study on a Proximal-Tubule-on-a-Chip

MK Vormann, L Boot, HL Lanz

4

Introduction

Renal proximal tubules play a huge role in the elimination of waste products and drugs from the body and are known to be a common target of drug induced toxicity [1]. Tenofovir (TFV) is such an antiretroviral drug of which drug-related nephrotoxicity is widely accepted [2]. TFV is a nucleotide reverse transcriptase inhibitor in the treatment of human immunodeficiency viruses (HIV) and Hepatitis B infected patients [2]. It is transformed by intracellular phosphorylation into the active metabolite tenofovir diphosphate. This metabolite is then incorporated into the viral deoxyribonucleic acid (DNA) where it functions as a DNA-chain terminator [3]. TFV itself is not membrane permeable, thus not suitable for oral administration and needs to be delivered as a prodrug [4] (fig. 1). Since 2012 the prodrug tenofovir disoproxil fumarate (TDF) has been used to treat HIV in combination with the antiretroviral agents elvitegravir, cobicistat, and emtricitabine in the single-tablet regimen Stribild [5]. However, TDF has now been replaced by a newly developed prodrug of TFV: tenofovir alafenamide (TAF). TAF is delivered for the treatment of HIV with the same three antiretroviral agents and available for patients since 2015 under the trade name Genvoya [6]. Measured by revenue Genvoya was the most used HIV medication in 2017 and 2018 [7]. The main reason why TDF was replaced by TAF is the limited risk for nephrotoxicity and reduced loss of bone mineral density [8]. In our recent work we were already able to show the toxicity of TFV on proximal tubule cells, however the prodrugs TDF and TAF were never tested in our model before (chapter 3, [9]).

In this study, it is investigated whether one or both of the TFV prodrugs have a toxic effect on the proximal tubule cells. Also, we wanted to investigate if any of the TFV-combined antiretroviral compounds are nephrotoxic by themselves or amplify the toxic effect while co-incubated with the TFV prodrugs.

TDF is unstable when in contact with blood plasma where it quickly undergoes hydrolysis into TFV [3], [10] (fig. 1). Only a small part of the drug is therefore taken up by the HIV target cells with high levels of TFV remaining in the blood plasma [4]. The newly developed prodrug TAF has a higher stability when in contact with plasma than TDF resulting in a superior efficiency of HIV-target cell delivery. This results in a higher antiviral activity and reduced dosage compared to TDF [4], [11], [12]. When patients switched from Stribild (which contains TDF) to Genvoya (which contains TAF) patients suffered less adverse kidney-related side effects [13].

The elimination of TFV from the blood plasma is mediated via glomerular filtration and secretion via the renal proximal tubule. It is actively transported through the influx transporters organic anion transporter (OAT) 1 and 3, and efflux transporter multi-drug resistance protein (MRP) 4 into the pre-urine [10], [14], [15]. Imbalance of the transporters can result in increased concentrations of TFV in the proximal tubule cells causing a high likeliness for drug-drug-interaction (DDI) [2], [16]. When TFV accumulates in the proximal tubule cells, disruption and inflammation of the

mitochondria in the proximal tubule can be observed [16]. Both prodrugs of TFV are co-administered with three other active compounds, namely elvitegravir, cobicistat, and emtricitabine.
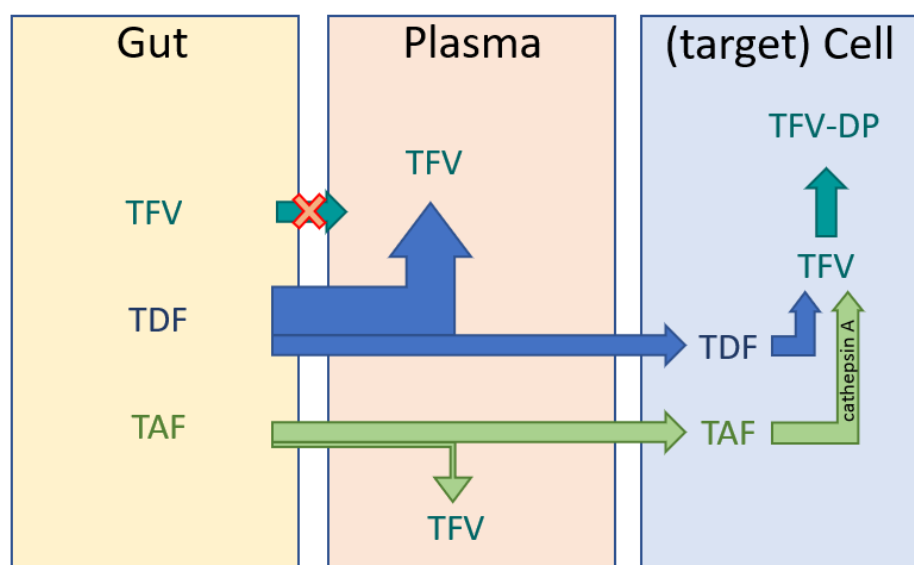
Figure 1: Comparison of the conversion pathways of tenofovir (TFV), tenofovir disoproxil fumarate (TDF), and tenofovir alafenamide (TAF) into the active metabolite tenofovir diphosphate (TFV-DP), a nucleotide reverse transcriptase inhibitor. TFV itself is not membrane permeable and is delivered orally by the prodrugs TDF or TAF. TDF is unstable when in contact with blood plasma where it quickly undergoes hydrolysis into TFV, resulting in a fraction of the delivered TDF entering the target cells. TAF on the contrary is stable and converted mainly intracellularly by cathepsin A into TFV. Adapted from [3], [4].

Emtricitabine is, similar to TFV, a reverse transcriptase inhibitor which prevents the virus from replicating itself [17]. In combination with TFV it showed a high anti-HIV activity [18]. Elvitegravir reduces the ability of the HIV-1 virus to replicate by preventing the insertion of viral DNA into the host cell [19]. This effect is enhanced by cobicistat, a cytochrome P-450 (CYP) 3A inhibitor, which extends Elvitegravir's time window, requiring one dose per day only [19].

Emtricitabine is thought to be eliminated similarly to TFV via glomerular filtration and active tubular secretion [17]. Although extensive research has been carried out on active tubular secretion of TFV, only a few studies exist which study the renal elimination process of emtricitabine and its possible role in DDI. Experimental data suggest that emtricitabine could be a substrate for multidrug and toxin extrusion protein 1 (Mate 1) [20], one of the efflux transporters of proximal tubule cells.

Around 95% of elvitegravir is recovered in feces and less than 7% in urine, indicating mainly hepatobiliary excretion of elvitegravir [21], [22]. In addition no metabolites of elvitegravir are detected in the urine indicating that elvitegravir is unlikely to cause a nephrotoxic event on its own [22].

Cobicistat, a booster for elvitegravir, was introduced on the market to replace ritonavir, because it is associated with reduced DDI [23]. Administration of cobicistat can lead to increased serum creatinine concentrations which are most probably a result of its inhibition potential of the multidrug and toxin extrusion protein–mediated efflux of creatinine [23], [24]. However, renal elimination of cobicistat happens only to a fraction of the compound, most is eliminated through feces [21].

Until today only a few *in vitro* studies exist which were used to pick up nephrotoxic effects of TFV on proximal tubule cells after individual dosing of TFV [25], [26], and even fewer in combination with elvitegravir, cobicistat, emtricitabine [24]. Considering the low number of studies and models which are described in literature, there is an urgent need for more research for potential test platforms which are able to detect nephrotoxic effects, especially in combinatorial drug exposures. This requires a minimal level of throughput of the testing system. The experimental work presented here further analyzes the toxicity of the two different TFV variants TDF and TAF. In our research we will study the toxicity of all single compounds of both drug combinations as well as potential drug interactions by combining each of the TFV prodrugs with each of the co-administrated compounds.

We will test the five compounds individually and in combination on our recently developed kidney-on-a-chip platform in the OrganoPlate 3-lane system (chapter 2, [27]). We could already assess that this kidney-on-a-chip model can be used as a reliable screening platform which is able to pick up nephrotoxic effects of known and unknown nephrotoxicants (chapter 2, [27] and chapter 3, [9]). In this study we will use renal proximal tubule cells where we could not measure any toxic effect after exposure to mono doses of TFV. Primarily we want to investigate whether one or both of the TFV prodrugs do have a toxic effect on these proximal tubule cells indicating a potential other elimination pathway than TFV. Furthermore, the three compounds co-administrated with the TFV prodrugs are not known to be eliminated via the anion pathway and therefore could show a toxic effect to the cells, as the cation pathway (if used by the compounds) was shown to be present in our model including the elimination via efflux transporter P-glycoprotein. Moreover, we wanted to investigate if any of the compounds does lead to damage in the proximal tubules or potentially amplifies the toxic effect when co-incubated with the TFV prodrugs.

Here we describe the use of a kidney-on-a-chip platform to test the effect of single administrated compounds as well as drug combinations. The model which we use enables compound assessment on 40 parallel cultured renal tubules. The platform is combined with a range of assays including the analysis of lactate dehydrogenase (LDH) activity in the medium as a measure of cell death, viability assays, fluorescence-based barrier integrity monitoring, and immunohistochemical staining of DNA damage marker H2AX. The technology can be used for high

throughput DDI studies which can be used to determine the effects or interaction of drugs on the kidney.

Methods

Cell culture

Proximal tubules were cultured in accordance with the protocols developed previously [27]. In short, renal proximal tubule epithelial cells (RPTEC; Kidney PTEC Control Cells, SA7K Clone, Sigma, Germany, MTOX1030, cultured in the supplier's medium) were seeded at passage 3 to the top channel in the OrganoPlate® 3-lane (*4003 400B*, MIMETAS, the Netherlands) against collagen 1 (composed of 4 mg/mL collagen 1 (AMSbio Cultrex 3D Collagen I Rat Tail, Cat. 3447-319 020-01), 100 mM HEPES (Life Technologies, 15630), and 3.7 mg/mL NaHCO3 (Sigma, 320 S5761)). The OrganoPlate was placed on a rocker platform (OrganoFlow®, MI-OFPR-L, Mimetas) in the incubator (37 °C, 5% CO2) at an angle of 7 degrees and a rotation interval of 8 minutes to enable perfusion though the channels.

Toxicant exposure

At day 6 after seeding of RPTEC to the OrganoPlate, medium of the top and the bottom channel was replaced by TOX medium (Minimum Essential Medium Eagle, Sigma-Aldrich, M4526, supplemented with RPTEC Tox Supplement, Sigma Aldrich, MTOXRTSUP) containing the compounds and/or the vehicle control. Cultures were exposed for 48 hours (see Table 1 for all compound information and concentrations). All compounds were dissolved in Dimethyl sulfoxide (DMSO, Sigma-Aldrich, D8418, vehicle control) according to the supplier's (*MedChemExpress*) recommendations.

The highest concentration which was tested for each of the compounds was dependent on the final DMSO concentration in the exposure medium which was set at 0.5%. This made ensured that in the follow up experiments combinations of the compounds could be tested at DMSO concentrations up to 1%. Concentrations higher than 1% DMSO have been shown to influence results strongly (data not shown). Concentrations were used at a quarter-log dilution range with 9 concentrations (including 0 µM). In follow-up experiments, combinations of each of the three compounds were tested in combination with the two prodrugs of TFV. The first combination was chosen at a concentration which did not show a toxic effect on the tubules of the mono-exposures, whereas in the second combination preferably at least one of the two compounds had shown a toxic effect.

Table 1: Compound information. All ordered at MedChemExpress and dissolved in DMSO.

Compound	Order number	Stock concentration (mM)	Highest experimental concentration in concentration curve (µM)
Tenofovir disoproxil fumarate (TDF)	HY-13782	10	50
Tenofovir alafenamide (TAF)	HY-15232A	60	300
Emtricitabine (Em)	HY-17427	40	200
Elvitegravir (El)	HY-14740	10	50
Cobicistat (Co)	HY-10493	35	175

Furthermore, the drugs were tested in the same ratio as used in the prescribed medication, which was not possible for TAF, as the concentration of TAF would have been too low to show any effect. The TAF concentration was kept around the level on which it was just toxic and combined with the other three compounds in a way to not exceed 1 % DMSO. The chosen concentrations of the combinations can be found in Table 2.

Table 2: Compound concentrations used for the combinations of the drugs. TDF: Tenofovir disoproxil fumarate, TAF: Tenofovir alafenamide fumarate, Em: Emtricitabine, El: Elvitegravir, Co: Cobicistat.

Drug brand name	Low concentration combination (µM)	High concentration combination (µM)
Stribild	74.4 TDF & 35.5 Em	92.0 TDF & 44.0 Em
Stribild	18.6 TDF & 8.9 El	27.0 TDF & 31.0 El
Stribild	8.0 TDF & 15.9 Co	27.7 TDF & 55.2 Co
Genvoya	287.6 TAF & 6.0 Em	575.2 TAF & 13.0 Em
Genvoya	176.0 TAF & 8.9 El	456.4 TAF & 23.0 El
Genvoya	314.9 TAF & 15.9 Co	515.4 TAF & 45.0 Co

LDH assay

The lactate dehydrogenase (LDH) activity assay was performed as previously described [27]. In short: For the analysis of the LDH activity, medium from the wells guiding to the apical side of the tubule was analyzed using a Lactate Dehydrogenase Activity Assay kit (Sigma, MAK066). For the study of the concentration curves the LDH assay was analyzed according to the supplier's recommendations, whereas for the combination screen LDH activity was measured at the same time point for all combinations to be able to directly compare the data.

WST-8 assay (Viability)

To analyze the viability of the cells the cell counting kit-8 (Sigma, 96992) was used as previously described [27]. In short: The 2-(2-methoxy-4-nitrophenyl)-3-(4-nitrophenyl)-5-(2,4-disulfophenyl)-2H-tetrazolium, monosodium salt (WST-8) buffer was diluted 1:11 in medium and added to both perfusion channels of each chip. After a 20-minute incubation on the rocker, absorbance was measured at 450 nm in the in-and outlets with access to the lumen of the proximal tubule and averaged per chip.

BI assay

For the assessment of the apparent permeability index (P_{app}) of the tubules a barrier integrity assay was performed as previously described [27]. In short: Medium containing 0.5 mg/ml TRITC Dextran 4.4 kDa (Sigma, FD20S) and 0.5 mg/ml FITC Dextran 150 kDa (Sigma, T1287) was added to the lumen of the tubule and leakage out of the tubule into the ECM compartment was measured using a fluorescent microscope (Molecular devices) and analyzed using ImageJ [28].

Immunostaining

The barrier integrity assay was followed by a fixation with 3.7% formaldehyde after which an immunostaining was performed as previously described [27]. Markers Rb-a-Phospho-Histone (H2AX, DNA damage, Cell signaling technology, 9718S, 1:200), actin (skeleton of the cells, Life technologies, R37112, 2 drops/ml buffer), and acetylated tubulin (primary cilia and tubulin structures, Sigma, T6793, 1:4000) in combination with a DNA staining (Hoechst 3342, Invitrogen, H3570, 1:2000) were analyzed.

Statistics

Data analysis was performed using GraphPad Prism (GraphPad Prism, version 9.0.0 (121)). Data were analyzed using one-way ANOVA followed by a Tukey's multiple comparison test which compares each result with each other result. A p value of < 0.05 was considered to be significant.

Results

HIV-patients are commonly treated with Genvoya which replaced Stribild in recent years. Both are tenofovir prodrug-containing medications and are supplied as pills which contain a combination of active, antiretroviral compounds, namely emtricitabine, elvitegravir and cobicistat, and one of the two prodrugs of TFV, TAF or TDF, respectively.

The proximal-tubule-on-a-chip can be used to determine renal toxicity

Proximal tubules were seeded to the top channel of the OrganoPlate 3-lane (fig. 2 A-D). First, collagen 1 was loaded to the middle channel. After polymerization of the collagen 1 proximal tubule, cells were seeded to the top perfusion channel. Next, medium was added to the top wells guiding to the channel system and the OrganoPlate was placed on an interval rocker, enabling perfusion. At day 6 tubules were mature and leak tight and toxicant exposures could be started

[27]. To determine the renal toxicity of the test compounds, medium of both perfusion channels was replaced by medium containing the compounds or vehicle control and the OrganoPlate was placed again for 48 hours on the interval rocker.
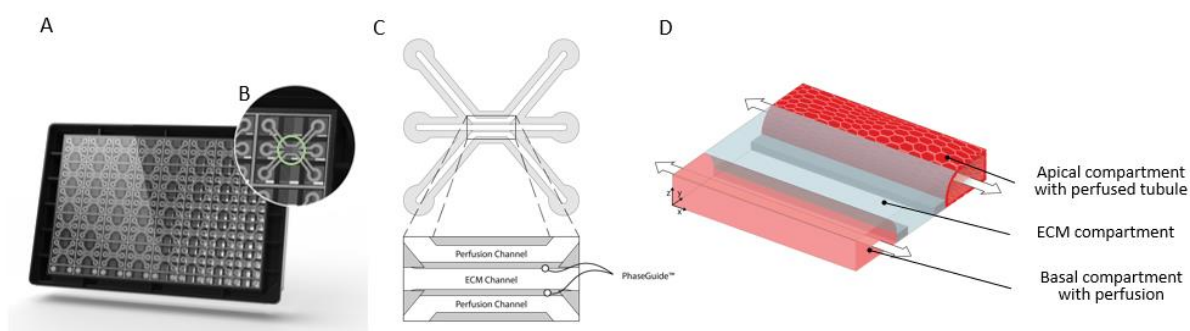

Figure 2: Proximal tubule-on-a-chip model in the OrganoPlate 3-lane platform. *A The top part of the OrganoPlate is a standard 384-well microtiter plate with 40 microfluidic chips embedded into a modified glass bottom. B Zoom-in on one chip with three channels convene in the center of the chip (green circle). C Schematic of the OrganoPlate 3-lane channel system. The three channels are 400 µm wide and 200 µm high and divided by 50 µm high phaseguides which function as liquid pressure barriers. D 3D artist impression of one chip. The chip was loaded with collagen 1 (light blue) to the ECM channel and proximal tubule cells (red) were seeded to the top perfusion channel. After cell attachment medium (light red) was added to both perfusion channels and perfusion was started (indicated by white arrows). For exposures medium of both perfusion channels was replaced by medium containing the compounds or vehicle control.*

Exposure to the TFV prodrugs TDF and TAF

The toxicity of each TFV prodrug was tested by exposing the tubules to a dose range of a quarter-log concentration curve. The starting concentrations can be found in Table 1. The effect of the drugs on the proximal tubules was measured in three different ways in a multiplexed fashion: 1) the loss of tubular barrier integrity (P_{app}), 2) the loss of cellular membrane integrity (LDH), and 3) the reduction in enzymatic activity (viability).

The integrity of the tubular barrier after the exposure can be measured through determining the apparent permeability (P_{app}). Increasing values indicate a loss of the barrier function [27], [29]. Both TDF and TAF did not show damage of the cell connections after the exposure (fig. 3 A,B). The viability assay used for this study determines dehydrogenase activity as a measure for cell number [30] and the LDH activity assay measures the content of the enzyme LDH that is released into the cell culture medium upon damage to the plasma membrane [31]. In line with the barrier integrity assay no effect of TDF could be measured in both assays (fig. 3 C-F). TAF did not have an influence on the viability either, however a significant increase of LDH activity in the medium to 180% of the control could be measured.
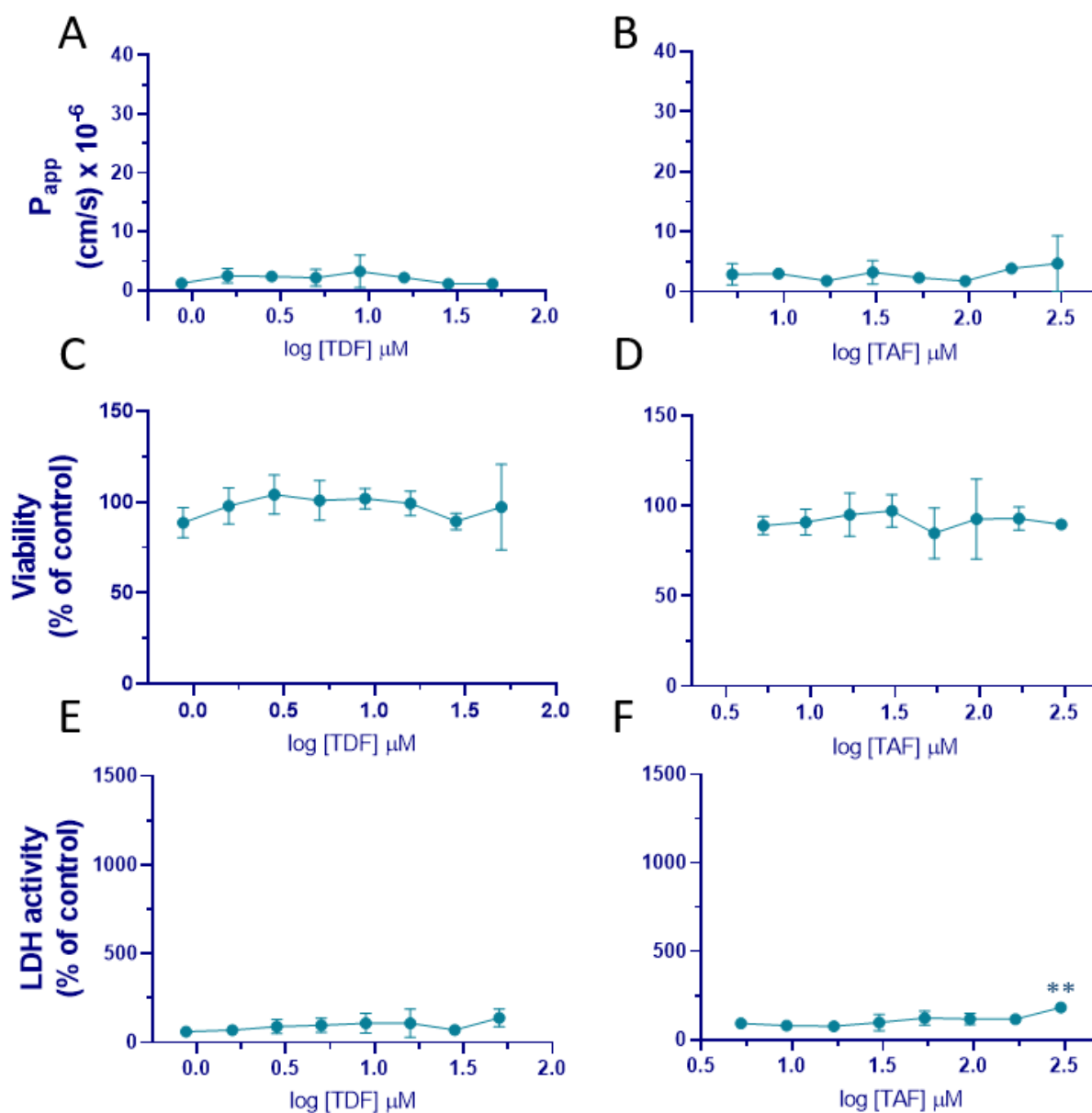
Figure 3: Exposure of RPTEC for 48 hours to concentration curves of the tenofovir prodrugs TDF (A, C, E) and TAF (B, D, F). *Data represent the P_{app} of a 150 kDa dextran (A, B),), the cell viability measured using a WST-8 assay (C, D), and the LDH activity in the medium (E, F). Abbreviations: P_{app}: apparent permeability; LDH: Lactate dehydrogenase; TDF: tenofovir disoproxil fumarate; TAF: tenofovir alafenamide fumarate. 3-5 chips per measure point. Data represent the mean with standard deviation. Data were compared to the lowest concentration of the corresponding compounds, *: $p<0.05$; **$p<0.01$.*

High concentrations of elvitegravir and cobicistat caused damage to the proximal tubules

Next to the TFV prodrugs TDF and TAF the same readouts were performed on the three co-administrated compounds. Emtricitabine had no effect on the barrier at the concentrations tested (fig. 4 A). For both elvitegravir and cobicistat a loss in barrier integrity could be measured for the two highest concentrations, 28 µM, 50 µM and 98 µM, 175 µM, respectively (fig. 4 B,C). The barrier loss was highest for cobicistat, at 30 x 10^{-6} cm/s compared to 23 x 10^{-6} cm/s for elvitegravir.

No loss of viability could be measured when cells were exposed to emtricitabine (fig. 4 D). When exposed to elvitegravir only the highest concentration (50 µM) showed a rapid loss in viability (fig. 4 E), whereas the pattern of cobicistat was more comparable to the barrier integrity assay with the last two concentrations showing a rapid loss in viability (fig. 4 F).
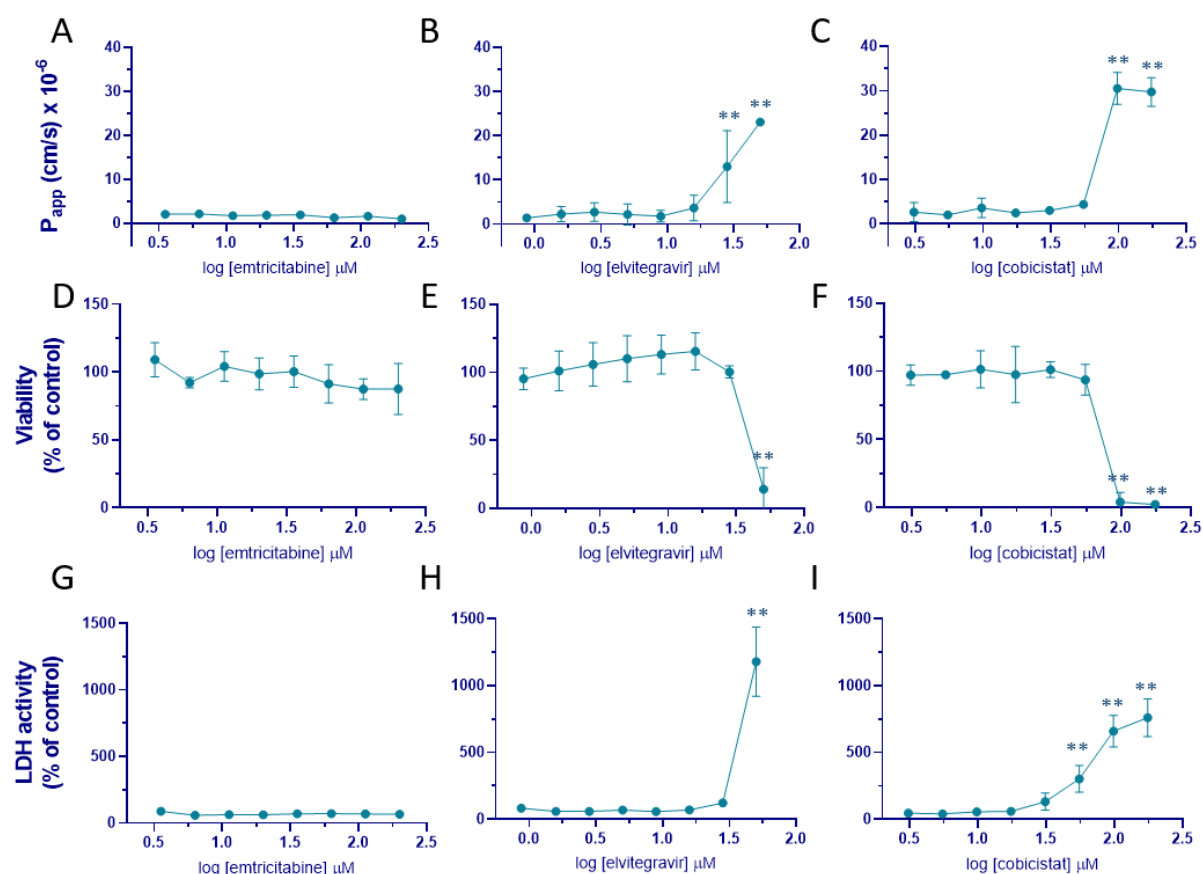
Figure 4: Exposure of RPTEC tubules for 48 hours to dose ranges of emtricitabine (A, D, G), elvitegravir (B, E, H), and cobicistat (C, F, I). Data represent the P_{app} of a 150 kDa fitc dextran (A-C), the cell viability measured using a WST-8 assay (D-F), and the LDH activity in the medium (G-I). Abbreviations: P_{app}: apparent permeability; LDH: Lactate dehydrogenase; n= 3-5 chips per measure point. Data represent the mean with standard deviation. Data were compared to the lowest concentration of the corresponding compounds, *: p<0.05; **p<0.01.

In line with the barrier integrity and the viability assay, exposure to emtricitabine did not result in any release of LDH, whereas the highest concentration of elvitegravir, 50 µM, led to a sudden increase of more than 1000 % release of LDH into the culture medium, similar to the measured effect in the viability assay where also only the highest concentration showed an effect. For cobicistat, LDH activity rose more gradually from a concentration starting at 55 µM to about 750% at the highest concentration of 175 µM (fig. 4 D-F).

Interestingly, the damaging effects of elvitegravir and cobicistat were measured for the lowest active concentrations in different assays. While the initial damage of elvitegravir was detected

with the barrier assay, cobicistat caused first release of LDH into the medium before an effect was detected by other assays.

DDIs can be picked up by the proximal-tubule-on-a-chip model

The highest concentration of the quarter-log dilution range was set to a DMSO concentration of 0.5%. In the drug interaction study a DMSO concentration of up to 1% was tolerated as this was the highest concentration which did not influence the behavior of RPTEC during a 48-hour exposure in previously performed experiments (data not shown). The first combination was chosen at a concentration which did not show a toxic effect on the tubules, whereas in the second combination preferably at least one of the two compounds did show a toxic effect. To not exceed 1% DMSO some of the compounds could not be tested at the highest possible concentration, since all drugs were tested at the same ratio as used in the prescribed medication. The chosen concentrations of the drug combinations can be found in Table 2.

From each drug combination the compounds were also tested alone and in combination, while the vehicle concentration was kept the same. The same readouts as for the dose analysis were chosen and in addition a fourth readout was added, which analyzed the occurrence DNA damage by immunostaining for a DNA damage marker H2AX [32].

Figure 5 provides the experimental data of TDF combined with each of the compounds emtricitabine (fig. 5 A,D,G,K), elvitegravir (fig. 5 B,E,i,L), and cobicistat (fig. 5 C,F,J,M).

Emtricitabine did not have a damaging effect on the proximal tubules in any of the assays: neither alone nor in co-incubation with TDF.

An effect of elvitegravir could be detected at its highest concentration (31.0 μM) in all assays, though no drug interaction with TDF (27 μM) could be measured, except a slight increase of DNA damage when dosed together.

Cobicistat caused a damaging effect on the apparent permeability (a 5-fold change compared to vehicle, fig. 5 C), the viability (reduced to 70%, fig. 5 F), the LDH release (a 8-fold change, fig. 5J), and the DNA damage staining (increase to around 350%, fig. 5M) when exposed to the higher concentration (55.2 μM). When co-administered with TDF an enhanced damaging effect could be measured in the barrier integrity assay, leading to complete loss of the barrier function, a reduction to 20% of the viability and an increased signal of the fluorescent intensity to 2000% compared to the vehicle control. A moderate effect of TDF addition could be measured in the LDH assay where the effect on LDH release was 1.3 times higher compared to an exposure to cobicistat only.

Figure 5: Exposure of RPTEC to combinations of the single components of the drugs co-incubated with TDF. *A,D,G,K co-incubation of TAF with emtricitabine (em), B,E,i,L Co-incubation of TAF with elvitegravir (el)), C,F.J,M co-incubation of TAF with cobicistat (co). A-C P_{app} measured with a fluorescent barrier integrity assay. D-F Viability measured with a WST-8 assay. G-J Analysis of LDH activity in the medium. K-M Fluorescent intensity of the H2AX immunofluorescence staining which is an antibody which detects DNA damage. Abbreviations: VC: vehicle control; P_{app}: apparent permeability; LDH: Lactate dehydrogenase; TDF: tenofovir disoproxil fumarate; Em: Emtricitabine; El: Elvitegravir; Co: Cobicistat. 3-5 chips per measure point. Data represent the mean with standard deviation. Data were compared to the vehicle control (VC) when not indicated differently by horizontal bars. ns: not significant; *: p<0.05; **p<0.01.*
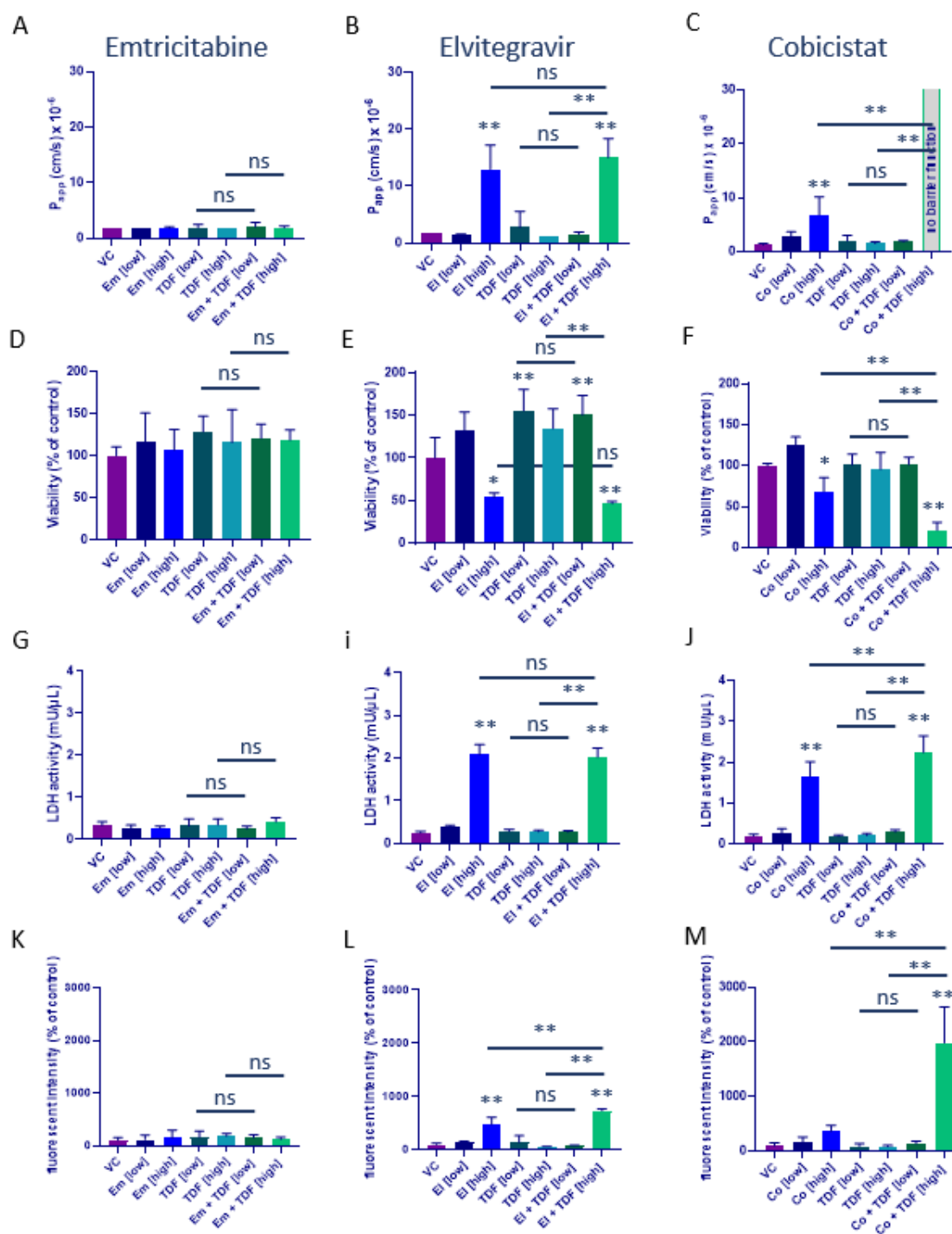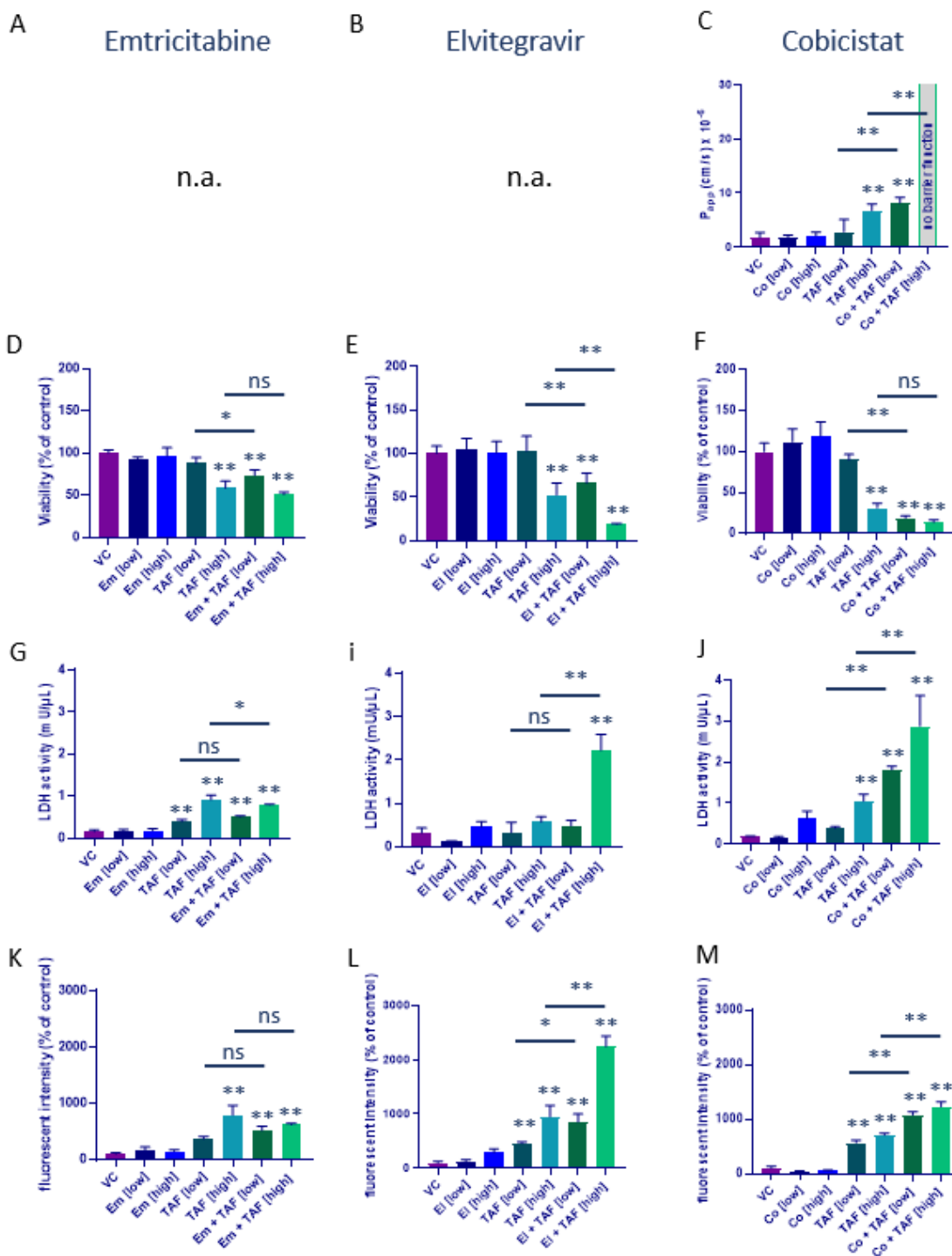
Figure 6: Exposure of RPTEC to combinations of the single components of the drugs co-incubated with TAF. **A,D,G,K** co-incubation of TAF with emtricitabine (em), **B,E,i,L** Co-incubation of TAF with elvitegravir (el)), **C,F,J,M** co-incubation of TAF with cobicistat (co). **A-C** P_{app} measured with a fluorescent barrier integrity assay. **D-F** Viability measured with a WST-8 assay. **G-J** Analysis of LDH activity in the medium. **K-M** Fluorescent intensity of the H2AX immunofluorescence staining which is an antibody which detects DNA damage. Abbreviations: VC: vehicle control; P_{app}: apparent permeability; LDH: Lactate dehydrogenase; TAF: tenofovir alafenamide fumarate; Em: Emtricitabine; El: Elvitegravir; Co: Cobicistat; n.a.: data not available. 3-5 chips per measure point. Data represent the mean with standard deviation. Data were compared to the vehicle control (VC) when not indicated differently by horizontal bars. ns: not significant; *: p<0.05; **p<0.01.

The experimental data of TAF combined with each of the compounds emtricitabine (fig. 6 A,D,G,K), elvitegravir (fig. 6 B,E,i,L), and cobicistat (fig. 6 C,F,J,M) is provided in figure 6.

When TAF was tested at a higher concentration than tested during the dose range study, TAF showed a toxic effect in all assays when exposed to concentrations above 300 µM (fig. 6). This observation was in line with the results of the dose range study (fig. 3), where a moderate effect of 300 µM TAF was seen in the LDH assay.

Similar to the exposure with TDF, little or no effect of emtricitabine was measured when co-exposed with TAF. In the viability assay a slight decreased viability could be measured during co-exposure of TAF (low) mono dose compared to TAF (low) + emtricitabine (fig. 6 D). This effect was not measured with any of the other assays. However, an opposite mild effect of the combination of TAF (high) + emtricitabine was measured in the LDH activity assay (fig. 6 G). These mild effects indicate that emtricitabine and TAF do not enhance each other in damaging the proximal tubules.

The combination of elvitegravir and TAF did enhance the damage on the tubules when dosed together at both the low (176.0 µM TAF and 8.9 µM elvitegravir) and the high (456.4 µM TAF and 23.0 µM elvitegravir) combinations which could be measured in all readouts with one exception: the combination of TAF 176.0 µM (low) + elvitegravir 8.9 µM did not increase the LDH activity (fig. 6 i), though an effect was detected with the viability assay (fig. 6 E) and the DNA damage staining (fig. 6 L).

Exposure to cobicistat alone did not show any damaging effect to the proximal tubules at both chosen doses of 15.9 µM (low) and 45 µM (high). For TAF 314 µM (low) a damaging effect could only be detected in the DNA staining (fig. 6 M), whereas an effect of the higher dose (515.4 µM) could be measured in all assays (fig. 6 C,F,J,M). When cobicistat and TAF were combined, an enhanced damaging effect could be observed with all assays for the low and the high doses of the combinations, which in the barrier integrity assay led to a complete loss of the barrier function.

In summary, these results show that elvitegravir and cobicistat have a damaging effect on the proximal tubules. When TAF was tested at a higher concentration (above 300 µM) than tested during the dose range study, TAF caused a moderate toxic effect in all assays. Interaction of compounds leading to increased damage could be seen when cobicistat and TDF were exposed in the same cocktail. A strong effect of TAF when exposed together with elvitegravir or cobicistat could be measured with all readout assays.

Discussion

The present study was focused on assessing whether we can use our proximal tubule-on-a-chip model (fig. 2) in a DDI study using a panel of multiplexed assays to examine the toxicity of mono and combinatorial dosages of HIV-targeting drugs. Increased toxicity could be clearly shown when

combining compounds, whereas single compound exposure showed a lower level of toxicity on the proximal tubules.

Mono doses of TDF did not show any damaging effect for a concentration up to 92 µM (fig. 3, 5). In our study we exposed the cells in a medium containing around 1% fetal bovine serum (TOX medium). Callebaut et al. showed that TDF is mostly converted to TFV when in contact with serum [3]. We presume that in our study TDF was converted into TFV as well after dilution in TOX medium. TFV toxicity in literature ranges from 10 µM in OAT1 (over-) expressing cells to no toxic events measurable in human RPTEC at concentrations even above 4 mM [24]–[26] (Table 3).

Table 3: IC50 values after TFV exposure in human proximal tubule cell sources with and without stable transporter expression

Cell source	Stable transporter expression	IC 50 after TFV exposure (µM)	Reference
Human RPTEC		> 1000, > 4000	[9], [24]
ciPTEC-OAT1	OAT1	189	[25]
HEK293T-OAT1	OAT1	10, 78	[26], [24]
HEK293T-OAT1/MRP4	OAT1 and MRP4	299	[24]

Considering that TDF is converted into TFV when in contact with serum it is likely that the damaging molecular concentration of TDF will be similar to the damaging molecular concentration of TFV. In the current study TDF was not tested above 100 µM. Most likely TDF was not tested at its actual toxic concentration. However, we used human RPTEC without OAT transporters which, similarly to the human RPTEC used by Stray et al. [24] and us [9], did not show a cytotoxic response when exposed to TFV. Further research can be undertaken to investigate if there is a damaging effect of TDF measurable after exposure in serum-free medium. Moreover, it is recommended to dissolve the TFV prodrugs in an aqueous solutions (for example (serum free) culture medium) to be able to test the compound at higher concentrations, without exceeding the maximum vehicle concentration of DMSO.

In contrast to TDF, a damaging effect of TAF on the proximal tubules could be detected from values of 300 µM and higher (fig. 3 and 6) for the individual dosing and a value of 176 µM when dosed in combination with elvitegravir. These concentrations fall into the dose ranges which were reported by us (chapter 3, [9]) and are slightly above the concentrations other groups reported (Table 3) when exposing proximal tubules cells to TFV. TAF is thought to be stable when in contact with blood plasma [3] and not a compound for OAT1 transport as it enters cells passively [15]. Our findings support the outcome of these studies, since the exposure to TAF resulted in

nephrotoxic damage at similar concentrations as TFV when exposed to cells expressing anion transporter OAT 1.

In the present study we wanted to examine if, next to the TFV prodrugs, one of the additive compounds had a toxic or enhancing toxic effect on the proximal tubules when combined with the TFV variants. In the following couple of paragraphs the possible toxicity and toxicity-enhancing effects of different compounds are discussed, using the results of this research.

Emtricitabine did not show a toxic effect on the proximal tubules (fig. 4, 5, 6). This is in line with existing literature, where no direct toxic effect of emtricitabine on human RPTEC is found [24]. Even though it is thought that emtricitabine is eliminated similarly to TFV via glomerular filtration and active tubular secretion, we can suggest from our results that the clearance pathways are most probably not the same, because co-incubation of emtricitabine and TFV did not show any interaction in the used readouts.

Elvitegravir did not have an enhancing effect on the cytotoxicity when dosed in combination with TDF (fig. 5). When dosed together with TAF, elvitegravir strongly enhanced the damaging effect (fig. 6). Most interestingly, neither elvitegravir nor TAF increased the LDH activity in the medium individually. When the two were combined at high concentrations, super-additive synergistic effects occurred with increased LDH activity to more than 450%. This result could be somewhat surprising, as elvitegravir is not believed to affect the kidneys but is mainly eliminated via hepatobiliary excretion [22]. It is likely that if this elimination pathway is not available, exposure to high concentrations of elvitegravir does cause damage to the renal cells.

Cobicistat is transported via the cation pathway (influx via OCT2, efflux via mate 1), whereas TFV is transported via the anion pathway (influx via OAT 1/3 and efflux via MRP4) [10], [24], [33]. As we were able to detect damage of drugs transported via the cation pathway previously [27], it is possible that if cobicistat is having a damaging effect on the proximal tubules this effect would be measured. When cobicistat was dosed at concentrations of 55 µM, mild damaging effects were measured. When cobicistat was dosed at 55 µM in combination with 27.7 µM TDF (which by itself did not show any damaging effect) increased damage on the tubules could be measured with all assays. Similar results could be detected when cobicistat was dosed together with TAF (fig. 6). Here, an increase in cytotoxicity was measured for the low dosed combinations as well as the highly concentrated combinations. Therefore, it can be concluded that the combination of TFV and cobicistat at high molecular concentrations leads to enhanced cytotoxicity in the proximal tubule cells.

In the next paragraph the possible interaction of cobicistat with TFV will be discussed. Cobicistat is generally well tolerated by patients and has limited known side effects. In both drug cocktails cobicistat is used as a CYP 3A inhibitor for elvitegravir. Elvitegravir is predominantly metabolized by CYP3A with a short half-life [23]. When elvitegravir is co-formulated with cobicistat the

elimination of elvitegravir is prolonged, allowing an administration once per day [22]. TFV is not known to be an CYP inhibitor/enhancer or being metabolized by CYP3A enzymes [34] as TFV is eliminated via the urine unchanged [35]. It is likely that the increased damage on the proximal tubules which we observed cannot be attributed to an accumulation of TFV in the cells after a delayed metabolism when dosed together with cobicistat. Another possible explanation may be that at high concentrations of cobicistat, TFV can enter the cells by other pathways than the OAT1 transport which is lacking in RPTEC. In a study by Stray et al. [24] the potential of cobicistat to influence the pharmacology of TFV was assessed. They found that cobicistat did not interact with the transport of TFV by OAT1, but they could detect a minor inhibitory effect of cobicistat on OAT3 transport. However, they suggested that this effect was unlikely to be clinically relevant as most TFV transport in the proximal tubules is mediated by OAT1. Next to the influx via OAT1 they also assessed the efflux transporter MRP4. In our recent work we were able to confirm the presence of MRP mediated efflux in our model [27]. Stray et al. could show that MRP4 mediated efflux is sensitive to cobicistat in serum-free medium. However, this effect was eliminated when they performed the experiments in serum-containing medium. In our study we used much higher concentrations of both TFV and cobicistat. Therefore, it could be possible that not all cobicistat was eliminated in the presence of serum (1% in the exposure medium) and was able to inhibit MRP4 efflux, resulting in higher concentrations of both TFV and cobicistat in the cells leading to an increase in damage when combining the drugs.

The study we performed does have some important limitations, which actually can guide future research. First, when comparing the concentrations of the compounds in the culture medium to the maximum clinically observed concentrations in plasma, those which showed a toxic effect in our *in vitro* model were higher than reported *in vivo* [36], [37]. Thus, to be able to translate our results to the *in vivo* situation, further research on our *in vitro* model needs to be performed. Starting with pharmacokinetic modeling to determine drug concentrations and combinations to be tested [38], many aspects would need to be optimized and standardized: the culture of the model itself, the assays and the readout methods, exposure concentrations, and exposure duration. Eventually these data can be used in *in silico* models to accurately predict the *in vivo* situation [39], [40].

Another limitation in this study is that a commercially available cell source was used which does not express all crucial transporters which are responsible for (part of) the transport of some of the tested compounds. Nonetheless, we were able to show that TFV delivered in the form of prodrug TAF has a cytotoxic effect on our proximal tubule model at concentrations similar to exposure of OAT1-expressing cells when exposed to TFV. In the combination studies additive or even synergistic damaging effects on the proximal tubules were detected. Using an even broader panel of assays and a second cell source with OAT1 expression would be a fruitful area for further work.

One last limitation in this study which affected the results significantly was that in the combination study TAF was used in much higher concentrations than would have been adequate when trying to resemble the ratio of TAF to co-administered compounds in Genvoya. In Genvoya, the molecular concentration of TAF is only a fraction of the three other compounds. Here it would be interesting to re-design the initial experiments by dissolving the compounds in, if possible, aqueous solutions to be able to test the compounds at the correct ratios.

Although we know that the concentrations used in this study were too high to be physiologically relevant, we could show that the proximal-tubule-on-a-chip platform is a suitable tool that can be used to study the effect of drugs and drug combinations on the kidney.

Conclusion

The present study was designed to determine if the proximal tubule-on-a-chip can be used to study compound panels and toxicity-enhancing effects when compounds are co-administered. To this end different read-out assays were used to study the toxicity of the drugs. We could show that particularly the combination of the assays can lead to a more complete picture of the compound's toxicity. For some compounds, their earliest toxicity can be identified in the barrier integrity assay because they damage the cell connections first, other compounds affect the cell membrane initially, resulting in an increase of LDH activity in the medium. The findings of this investigation complement those of earlier published data (chapter 2, [27] and chapter 3, [9]), where also the combination of assays offered a broader picture on the toxicity mechanism. For future studies it could be of high interest to combine the assays from all studies.

In recent years, Stribild, which contains the tenofovir (TFV) prodrug tenofovir disoproxil fumarate (TDF) was replaced by Genvoya which contains the prodrug tenofovir alafenamide (TAF). TAF is thought to be taken up by cells passively, whereas TDF is converted into TFV in the presence of serum containing medium and then enters cells via anion transporter OAT1. The model used in this research is lacking transporter OAT1 and did not show a response to TFV exposure in previous studies [9]. However, the present results could show that TAF, when tested individually, is cytotoxic at similar molecular concentrations compared to the exposure concentrations of TFV when exposed to cells containing the OAT1 transport mechanism (chapter 3, [9]), while no cytotoxic effect was detected with TDF. From these results we can conclude that TAF enters cells passively, whereas TDF converts into TFV and is dependent on active anion transport to accumulate inside the cells and cause cytotoxicity.

TAF is administered in Genvoya at a fraction of TDF in Stribild (10 mg and 300 mg, respectively, [41], [42]). When TAF was dosed at the correct ratio compared to the toxic concentration of TFV, no toxicity was measured in the present study. We can therefore conclude that our experiments

confirmed that the new drug combination (Genvoya) using TAF instead of TDF does have a decreased potential for adverse kidney-related side effects, supporting the results seen clinically.

In the present study the combination of TAF and the other three antiretroviral agents was not dosed at the correct ratio as used in Genvoya because this would exceed the concentration of solvent DMSO. At correct ratios TAF could have been tested only at a fraction of the concentration found toxic in the mono dose study. An obvious area for future research could start by focusing on testing the drugs used in Genvoya at the concentrations which resemble the ratio of TAF to co-administered compounds in Genvoya. Doing this would grant a better model which can be used to mimic the influence of TAF and its co-administered compounds on the results.

In most research which study the effect of TFV and its prodrugs, they are tested individually. Our results indicate that elvitegravir as well as cobicistat also affected the proximal tubule cells. We suggest that in future studies TFV and its prodrugs should be tested in combination with the drugs with which they will be co-administered. However, during *in vitro* experiments some of the drugs might be incorrectly dosed, as *in vivo* they would be metabolized quickly by the liver or cleared via the gut. To overcome this problem a possible solution could be to connect the present model with a liver-on-the-chip system [43] and/or a gut-on-a-chip system [29], [44]. Or, include pharmacokinetic modeling to choose proper concentrations for experiments.

We were able to show that the proximal-tubule-on-a-chip model can serve as a steppingstone for future DDI studies. Our platform is able to distinguish which processes are affected first by the different drug (combinations) and pick up synergistic (additive and super-additive) effects of co-administered drugs. Moreover, the platform can be potentially used to assess if these synergistic effects are relevant or not when used in combination with pharmacogenetic modeling.

References

[1]   S. K. Nigam, W. Wu, K. T. Bush, M. P. Hoenig, R. C. Blantz, and V. Bhatnagar, "Handling of drugs, metabolites, and uremic toxins by kidney proximal tubule drug transporters," *Clinical Journal of the American Society of Nephrology*, vol. 10, no. 11, pp. 2039–2049, 2015, doi: 10.2215/CJN.02440314.

[2]   J. J. Kohler *et al.*, "Tenofovir renal proximal tubular toxicity is regulated by OAT1 and MRP4 transporters," *Laboratory Investigation*, vol. 91, no. 6, pp. 852–858, 2011, doi: 10.1038/labinvest.2011.48.

[3]   C. Callebaut, G. Stepan, Y. Tian, and M. D. Miller, "*In vitro* virology profile of tenofovir alafenamide, a novel oral prodrug of tenofovir with improved antiviral activity compared to that of tenofovir disoproxil fumarate," *Antimicrobial Agents and Chemotherapy*, vol. 59, no. 10, pp. 5909–5916, 2015, doi: 10.1128/AAC.01152-15.

[4]   A. S. Ray, M. W. Fordyce, and M. J. M. Hitchcock, "Tenofovir alafenamide: A novel prodrug of tenofovir for the treatment of Human Immunodeficiency Virus," *Antiviral Research*, vol. 125, pp. 63–70, 2016, doi: 10.1016/j.antiviral.2015.11.009.

[5] U.S. Food & Drug Administration, "Drug Approval Package, Stribild, Fixed Dose," 2012. https://www.accessdata.fda.gov/drugsatfda_docs/nda/2012/203100Orig1s000TOC.cfm#:~:text =Approval Date%3A 08%2F27%2F2012 (accessed Oct. 29, 2020).

[6] U.S. Food & Drug Administration, "GENVOYA (elvitegravir, cobicistat, emtricitabine, and tenofovir alafenamide) fixed-dose combination tablet.," 2015. https://www.accessdata.fda.gov/drugsatfda_docs/nda/2015/207561Orig1s000Approv.pdf (accessed Oct. 29, 2020).

[7] Statista, "Selected top HIV/AIDS drugs worldwide based on revenue from 2016 to 2018," *Statista*, 2019. https://www.statista.com/statistics/273434/revenue-of-the-worlds-most-important-aids-drugs/ (accessed Oct. 29, 2020).

[8] E. De Clercq, "Role of tenofovir alafenamide (TAF) in the treatment and prophylaxis of HIV and HBV infections," *Biochemical Pharmacology*, vol. 153, pp. 2–11, Jul. 2018, doi: 10.1016/j.bcp.2017.11.023.

[9] M. K. Vormann *et al.*, "Implementation of a Human Renal Proximal Tubule on a Chip for Nephrotoxicity and Drug Interaction Studies," *Journal of Pharmaceutical Sciences*, pp. 1–14, 2021, doi: 10.1016/j.xphs.2021.01.028.

[10] A. S. Ray *et al.*, "Mechanism of active renal tubular efflux of tenofovir," *Antimicrobial Agents and Chemotherapy*, vol. 50, no. 10, pp. 3297–3304, 2006, doi: 10.1128/AAC.00251-06.

[11] T. K. Novick, M. J. Choi, A. Z. Rosenberg, B. A. McMahon, D. Fine, and M. G. Atta, "Tenofovir alafenamide nephrotoxicity in an HIV-positive patient," *Medicine*, vol. 96, no. 36, p. e8046, Sep. 2017, doi: 10.1097/MD.0000000000008046.

[12] X. Liu and G. Pan, Eds., *Drug Transporters in Drug Disposition, Effects and Toxicity*, vol. 1141. Singapore: Springer Singapore, 2019. doi: 10.1007/978-981-13-7647-4.

[13] P. E. Sax *et al.*, "Tenofovir Alafenamide Vs. Tenofovir Disoproxil Fumarate in Single Tablet Regimens for Initial HIV-1 Therapy," *JAIDS Journal of Acquired Immune Deficiency Syndromes*, vol. 67, no. 1, pp. 52–58, Sep. 2014, doi: 10.1097/QAI.0000000000000225.

[14] Y. Uwai, H. Ida, Y. Tsuji, T. Katsura, and K. I. Inui, "Renal transport of adefovir, cidofovir, and tenofovir by SLC22A family members (hOAT1, hOAT3, and hOCT2)," *Pharmaceutical Research*, vol. 24, no. 4, pp. 811–815, 2007, doi: 10.1007/s11095-006-9196-x.

[15] R. A. Bam, S. R. Yant, and T. Cihlar, "Tenofovir alafenamide is not a substrate for renal organic anion transporters (OATs) and does not exhibit OAT-dependent cytotoxicity," *Antiviral Therapy*, vol. 19, no. 7, pp. 687–692, 2014, doi: 10.3851/IMP2770.

[16] J. J. Kohler *et al.*, "Tenofovir renal toxicity targets mitochondria of renal proximal tubules," *Laboratory Investigation*, vol. 89, no. 5, pp. 513–519, 2009, doi: 10.1038/labinvest.2009.14.

[17] L. M. Bang and L. J. Scott, "Emtricitabine: An Antiretroviral Agent for HIV infection," *Drugs*, vol. 63, no. 22, pp. 2413–2424, 2003, doi: 10.2165/00003495-200363220-00003.

[18] K. Borroto-Esoda, J. E. Vela, F. Myrick, A. S. Ray, and M. D. Miller, "*In vitro* evaluation of the anti-HIV activity and metabolic interactions of tenofovir and emtricitabine," *Antiviral Therapy*, vol. 11, no. 3, pp. 377–384, 2006.

[19] J. L. Olin, L. M. Spooner, and O. M. Klibanov, "Elvitegravir/cobicistat/emcitrabine/ténofovir disoproxil (fumarate de) en association dans un seul comprimé pour le traitement de l'infection

par le VIH," *Annals of Pharmacotherapy*, vol. 46, no. 12, pp. 1671–1677, 2012, doi: 10.1345/aph.1R468.

[20]   J. Reznicek, M. Ceckova, L. Cerveny, F. Müller, and F. Staud, "Emtricitabine is a substrate of MATE1 but not of OCT1, OCT2, P-gp, BCRP or MRP2 transporters," *Xenobiotica*, vol. 47, no. 1, pp. 77–85, 2017, doi: 10.3109/00498254.2016.1158886.

[21]   D. J. Cada, S. Torres, T. L. Levien, and D. E. Baker, "Elvitegravir/Cobicistat/Emtricitabine/Tenofovir disoproxil fumarate tablets," *Hospital Pharmacy*, vol. 48, no. 1, pp. 48–56, 2013, doi: 10.1310/hpj4801-48.

[22]   S. Ramanathan, A. A. Mathias, P. German, and B. P. Kearney, "Clinical pharmacokinetic and pharmacodynamic profile of the HIV integrase inhibitor elvitegravir," *Clinical Pharmacokinetics*, vol. 50, no. 4, pp. 229–244, 2011, doi: 10.2165/11584570-000000000-00000.

[23]   B. M. Shah, J. J. Schafer, J. Priano, and K. E. Squires, "Cobicistat: A New Boost for the Treatment of Human Immunodeficiency Virus Infection," *Pharmacotherapy: The Journal of Human Pharmacology and Drug Therapy*, vol. 33, no. 10, pp. 1107–1116, Oct. 2013, doi: 10.1002/phar.1237.

[24]   K. M. Stray *et al.*, "Evaluation of the effect of cobicistat on the *in vitro* renal transport and cytotoxicity potential of tenofovir," *Antimicrobial Agents and Chemotherapy*, vol. 57, no. 10, pp. 4982–4989, 2013, doi: 10.1128/AAC.00712-13.

[25]   T. T. G. Nieskens *et al.*, "A Human Renal Proximal Tubule Cell Line with Stable Organic Anion Transporter 1 and 3 Expression Predictive for Antiviral-Induced Toxicity," *AAPS Journal*, vol. 18, no. 2, pp. 465–475, 2016, doi: 10.1208/s12248-016-9871-8.

[26]   X. Zhang, R. Wang, M. Piotrowski, H. Zhang, and K. L. Leach, "Intracellular concentrations determine the cytotoxicity of adefovir, cidofovir and tenofovir," *Toxicology in vitro*, vol. 29, no. 1, pp. 251–258, 2015, doi: 10.1016/j.tiv.2014.10.019.

[27]   M. K. Vormann *et al.*, "Nephrotoxicity and Kidney Transport Assessment on 3D Perfused Proximal Tubules," *AAPS Journal*, vol. 20, no. 5, pp. 1–11, 2018, doi: 10.1208/s12248-018-0248-z.

[28]   J. Schindelin *et al.*, "Fiji: An open-source platform for biological-image analysis," *Nature Methods*, vol. 9, no. 7, pp. 676–682, 2012, doi: 10.1038/nmeth.2019.

[29]   S. J. Trietsch *et al.*, "Membrane-free culture and real-time barrier integrity assessment of perfused intestinal epithelium tubes," *Nature Communications*, vol. 8, no. 1, pp. 1–7, 2017, doi: 10.1038/s41467-017-00259-3.

[30]   H. Tominaga *et al.*, "A water-soluble tetrazolium salt useful for colorimetric cell viability assay," *Analytical Communications*, vol. 36, no. 2, pp. 47–50, 1999, doi: 10.1039/a809656b.

[31]   C. Legrand *et al.*, "Lactate dehydrogenase (LDH) activity of the number of dead cells in the medium of cultured eukaryotic cells as marker," *Journal of Biotechnology*, vol. 25, no. 3, pp. 231–243, 1992, doi: 10.1016/0168-1656(92)90158-6.

[32]   L. J. Kuo and L. X. Yang, "γ-H2AX- A novel biomaker for DNA double-strand breaks," *In vivo*, vol. 22, no. 3, pp. 305–310, 2008.

[33]   E. I. Lepist *et al.*, "Contribution of the organic anion transporter OAT2 to the renal active tubular secretion of creatinine and mechanism for serum creatinine elevations caused by cobicistat," *Kidney International*, vol. 86, no. 2, pp. 350–357, 2014, doi: 10.1038/ki.2014.66.

[34]   Gilead Sciences, "VIREAD® (tenofovir disoproxil fumarate) Tablets Patient Information," 2005.

[35]   B. P. Kearney, J. F. Flaherty, and J. Shah, "Tenofovir disoproxil fumarate: Clinical pharmacology and pharmacokinetics," *Clinical Pharmacokinetics*, vol. 43, no. 9, pp. 595–612, 2004, doi: 10.2165/00003088-200443090-00003.

[36]   C. M. Perry, "Elvitegravir/Cobicistat/Emtricitabine/Tenofovir Disoproxil Fumarate Single-Tablet Regimen (Stribild®): A Review of Its Use in the Management of HIV-1 Infection in Adults," *Drugs*, vol. 74, no. 1, pp. 75–97, Jan. 2014, doi: 10.1007/s40265-013-0158-4.

[37]   J. M. Custodio *et al.*, "Pharmacokinetics and Safety of Tenofovir Alafenamide in HIV-Uninfected Subjects with Severe Renal Impairment," *Antimicrobial Agents and Chemotherapy*, vol. 60, no. 9, pp. 5135–5140, Sep. 2016, doi: 10.1128/AAC.00005-16.

[38]   C. Perry, G. Davis, T. M. Conner, and T. Zhang, "Utilization of Physiologically Based Pharmacokinetic Modeling in Clinical Pharmacology and Therapeutics: an Overview," *Current Pharmacology Reports*, vol. 6, no. 3, pp. 71–84, 2020, doi: 10.1007/s40495-020-00212-x.

[39]   B. Feng, J. L. LaPerle, G. Chang, and M. V. Varma, "Renal clearance in drug discovery and development: Molecular descriptors, drug transporters and disease state," *Expert Opinion on Drug Metabolism and Toxicology*, vol. 6, no. 8, pp. 939–952, 2010, doi: 10.1517/17425255.2010.482930.

[40]   S. Polak, "*In vitro* to human *in vivo* translation – pharmacokinetics and pharmacodynamics of quinidine," *ALTEX*, vol. 30, no. 3, pp. 309–318, 2013, doi: 10.14573/altex.2013.3.309.

[41]   Gilead Sciences, "STRIBILD® (elvitegravir, cobicistat, emtricitabine, and tenofovir disoproxil fumarate) tablets, for oral use - prescribing information," 2012.

[42]   Gilead Sciences, "GENVOYA® (elvitegravir, cobicistat, emtricitabine, and tenofovir alafenamide) tablets, for oral use - prescribing information," 2015.

[43]   K. M. Bircsak *et al.*, "A 3D microfluidic liver model for high throughput compound toxicity screening in the OrganoPlate®," *Toxicology*, vol. 450, no. August 2020, p. 152667, 2021, doi: 10.1016/j.tox.2020.152667.

[44]   E. Naumovska *et al.*, "Direct on-chip differentiation of intestinal tubules from induced pluripotent stem cells," *International Journal of Molecular Sciences*, vol. 21, no. 14, pp. 1–15, 2020, doi: 10.3390/ijms21144964.

4

4

Chapter 5

Modelling and Prevention of Acute Kidney Injury Through Ischemia and Reperfusion in a Combined Human Renal Proximal Tubule/Blood Vessel-on-a-Chip.

MK Vormann, LM Tool, M Ohbuchi, L Gijzen, R van Vught, T Hankemeier, F Kiyonaga, T Kawabe, T Goto, A Fujimori, P Vulto, HL Lanz & K Tetsuka

5

Significance Statement

Renal ischemia/reperfusion injury (rIRI) is one of the major causes associated with tubular damage leading to acute kidney injury (AKI). In this study we modelled rIRI-induced AKI *in vitro* in a reconstituted human renal proximal tubule-on-a-chip with endothelial vessels through the control of ischemic parameters (i.e. oxygen, nutrients, and flow). The ischemic conditions had a detrimental effect on the proximal tubule, that was significantly amplified by subsequent reperfusion. Adenosine was shown to protect from disruption of epithelial cells and caspase 3/7 activation. As the platform is amenable to screening, this model will support pathophysiological research as well as drug discovery.

Abstract

Background Renal ischemia/reperfusion injury (rIRI) is one of the major causes of acute kidney injury (AKI). While animal models are suitable for investigating systemic symptoms of AKI they are limited in translatability. Human *in vitro* models are crucial in giving mechanistic insights into rIRI, however, they miss out on crucial aspects as reperfusion injury and the multi tissue aspect of AKI.

Methods We advanced the current renal proximal tubule-on-a-chip model to a coculture model with a perfused endothelial vessel separated by an extracellular matrix (ECM). The coculture was characterized for its three-dimensional structure, protein expression, and response to nephrotoxins. Then, rIRI was captured through control of oxygen levels, nutrient availability, and perfusion flow settings. Injury was quantified through morphological assessment, caspase 3/7 activation, and cell viability.

Results The combination of low oxygen, reduced glucose, and interrupted flow was potent to disturb the proximal tubules. This effect was strongly amplified upon reperfusion. Endothelial vessels were less sensitive to the ischemia-reperfusion parameters. Adenosine treatment showed a protective effect on the disruption of the epithelium and on the caspase 3/7 activation.

Conclusions A human *in vitro* rIRI model was developed using a coculture of a proximal tubule and blood vessel on-a-chip, which was used to characterize the renoprotective effect of adenosine. The robustness of the model and assays in combination with the throughput of the platform make it ideal to advance pathophysiological research and enable the development of novel therapeutic modalities.

Introduction

Acute kidney injury (AKI) is a severe medical problem with a high mortality rate. Every year around 1.7 million people die of AKI worldwide [1], [2]. Since the kidney is responsible for eliminating waste products from the blood it encounters high concentrations of xenobiotics and is therefore

vulnerable for (drug-induced) toxicity [3], [4]. In the kidney, renal proximal tubule epithelial cells (RPTEC) express many ATP-dependent transporters and play important roles in re-absorption of essential nutrients. RPTEC have a high energy demand to drive active transporters, and renal blood flow supplies the required oxygen [5], [6]. Patients with a disrupted renal flow, either because of pre-renal hypoperfusion (e.g. heart failure, hemorrhage) or post-renal obstruction (e.g. cancer, blood clot) also suffer from AKI [3], [7]. Renal ischemia/reperfusion injury (rIRI) causes a loss of function and cell damage of the proximal tubule structure, ultimately leading to AKI [8]–[10]. Recently, AKI has been extensively researched as a symptom following SARS-CoV-2 infection [11].

For investigating the pathophysiology of rIRI and drug screening for AKI, animal models are widely used to capture systemic symptoms of AKI [12]. However, here a significant species difference between animal and human is observed [13]. Not all drug candidates that showed efficacy in animal models showed efficacy in AKI treatment in clinical trials. *In vitro* cellular models are also applied for elucidation of rIRI/AKI mechanistic insights [14]. Unfortunately, traditional 2D culture settings of RPTEC lack their typical structure and their associated functionality [15], [16]. *In vitro* experiments do allow for a controlled environment, allowing manipulation of specific variables, and enabling higher reproducibility [14] . Finally, replacement of animal models is expected to reduce costs and time, as well as increase the throughput and predictability [17], [18].

Human cellular models can be valuable tools for tackling rIRI and discovery of AKI preventive agents [19]. *In vitro* rIRI models have been reported that enable induction of hypoxia by chemical induction, enzymatic induction, or anaerobic chambers [14]. However, additional parameters are important to comprehensively mimic ischemia-inducing insults [20]. Loss of nutrients, loss of flow, and buildup of waste products, as well as the reset of all parameters upon reperfusion can cause damage and should be included in rIRI modelling. Recent advances in tissue engineering and microfluidic cell culture techniques have made significant progress in modelling key aspects of human organs *in vitro* [15]. For example, a 3D model of the proximal tubule comprising perfusion flow was established in a microfluidic chip setup [21]–[24]. Application of shear stress to the apical side is important as it regulates tight-junction and polarized transporter localization [25]–[28]. We have previously reported a human proximal tubule on-a-chip model comprised of 40 perfused proximal tubules grown against an extracellular matrix (ECM) [24]. We showed the utility of this model for assessing kidney toxicity, drug-drug interaction, and transporter function [24], [29], [30].

In this study, we developed an advanced model to study rIRI comprising a perfused 3D proximal tubule adjacent to a 3D perfused blood vessel. The proximal tubule and blood vessel are separated by a collagen 1 surrogate extracellular matrix (ECM). We characterized the culture using immunostaining for cell type specific markers and ensured correct polarization. We then validated the response to nephrotoxicants. We modelled rIRI by adjusting culture parameters

such as oxygen concentration, perfusion flow, and nutrients like glucose, followed by a return to normal culture conditions. Finally, we assessed the protective potential of adenosine, nicotinamide, and N-acetylcysteine (NAC) that have been reported to prevent rIRI in animal models [31]–[35]. We foresee that this new human rIRI model will provide a springboard for the development of preventative or curative treatments for ischemic AKI.

Materials and Methods

Cell culture

Human renal Proximal Tubule Epithelial Cells (RPTEC, Kidney PTEC Control Cells, SA7K Clone, Sigma-Aldrich, MTOX1030) were cultured on PureCol-coated (Advanced BioMetrix, 5005-B, diluted with 1:30 in HBSS (Sigma H6648), 20 min incubation at 37 °C) T75 flasks (Corning, 431464U) in MEME alpha Modification (Sigma, M4526) supplemented with RPTEC Complete Supplement (Sigma, MTOXRCSUP), L-glutamine (1.87 mM, Sigma, G7513), Gentamicin (28 µg/ml, Sigma, G1397) and Amphotericin B (14 ng/ml, Sigma, A2942). Cells were incubated in a humidified incubator (37 °C, 5 % CO_2) and medium was changed every 2-3 days. At 90-100 % confluency, cells were washed with HBSS, detached with accutase (Sigma, A6964), neutralized with culture medium, pelleted (140 g, 5 minutes), and used for seeding in the OrganoPlate. Cells were used up to passage 3.

Human umbilical vein endothelial cells (HUVEC, Lonza, C2519A) were cultured on surface treated T75 (Thermo Scientific, 156499) flasks in MV2 complete medium (Endothelial Cell Medium MV2, Promocell, C-22022) supplemented with Supplement Mix Endothelial Cell Growth Medium MV2 (Promocell, C-39226), and 1% Pen/Strep (Sigma, P4333). Cells were incubated in a humidified incubator (37 °C, 5 % CO_2) and medium was changed every 2-3 days. At 90-100 % confluency, cells were washed with HEPES-BSS (Lonza, CC-5022), detached with 0.025% Trypsin-EDTA (1X) solution (Lonza, CC-5012), neutralized with Trypsin Neutralizing Solution (Lonza, CC-5002), pelleted (200 g, 5 minutes), and used for seeding in the OrganoPlate. Cells were used up to passage 9.

Establishment of the RPTEC-HUVEC coculture

For all experiments, the OrganoPlate® 3-lane (Mimetas BV, 4003 400B) was used. Figure 1a shows a photograph of the bottom of the OrganoPlate, demonstrating the 40 microfluidic channel networks, glued to a standard 384-well plate. A zoom in on a single chip highlights the region of interest where three microfluidic channels join in the center (green circle, Fig. 1b). The 3 channels are separated by PhaseGuides, which are small ridges that prevent overflow between adjacent channels through meniscus pinning [36] (Fig. 1c, grey bars).

As a starting point for the seeding, we took the RPTEC monoculture protocol as previously described [24] and introduced a seeding procedure for an endothelial vessel alongside the RPTEC tubule (Fig. 1 d-f). In short, 2 µL of a liquefied ECM gel composed of 4 mg/ml collagen I was loaded

into the middle inlet of all 40 chips and let to polymerize (Fig. 1d step 1). The following day RPTECs were seeded against the gel to the top channel and allowed to adhere (Fig. 1d step 2). After attachment of the cells, medium was added and the OrganoPlate was placed in an incubator on an interval rocker platform (Mimetas BV, MI-OFPR-L) (+/- 7 degree angle, 8 minute interval) enabling a passive, bidirectional flow though the perfusion channels (Fig. 1d step 3).

HUVEC were added to the bottom channel of the microfluidic chip on day 2 (Fig. 1d step 4). HUVEC were detached as described above and re-suspended in MV2 complete medium at a concentration of 10 x 10^6 cells per ml. Medium from all bottom in- and outlets was aspirated, and the plate was turned 180° resulting in RPTEC tubes sitting in the bottom. 2 μL of the HUVEC cell suspension was added to the (new) top left inlet. Subsequently, 1 μL was aspirated via the outlet from the top channel to guide HUVEC though the system. The OrganoPlate was placed on its side at an angle of 75° to let the HUVEC attach to the ECM. After an incubation time of 60 minutes, medium from both channels was switched to coculture medium (50% CellBiologics complete human endothelial cell medium (basal medium with the growth factor supplement kit (H1168)) and 50% RPTEC complete medium). Perfusion was applied again resulting in fully grown tubules of RPTEC and HUVEC at day 6 (Fig. 1c, 1d step 5). Cocultures were used for experiments up to day 12. The timeline of coculture seeding was determined in an optimization study (data not shown) with RPTEC seeded on day 0, and HUVEC on day 2 (Fig. 1 d-f).

Immunohistochemistry

Cocultures were fixed by replacing the medium with 3.7% formaldehyde (Sigma, 252549) in HBSS (Sigma, 55037C) for 10 minutes. Tubules were washed with washing solution (4% fetal bovine serum (Gibco, 16140-071) in HBSS) and permeabilized (0.3% Triton X-100 (Sigma, T8787) in HBSS) for 10 minutes. Next, cultures were incubated for 45 minutes in blocking solution (2% FBS, 2% bovine serum albumin (BSA) (Sigma, A2153), and 0.1% Tween 20 (Sigma, P9416) in HBSS). Hereafter cultures were incubated with the primary antibodies, diluted in blocking solution, for 60 minutes at room temperature. Primary antibodies against Ms-a-ezrin (BD Biosciences, 610602, 1:200), Ms-a-acetylated tubulin (Sigma, T6793, 1:4000), Rb-a-Zonula occludens-1 (ZO-1) (Thermo Fischer, 61-7300, 1:125) and Rb-a-VE-cadherin (Abcam, Ab33168, 1:1000) were used. Subsequently, cultures were washed twice with washing solution for 5 minutes each and then incubated for 30 minutes at room temperature with secondary antibodies Gt-a-Ms IgG (H+L) Alexa Fluor 555 ((Thermo Scientific , A21422,1:250) and Gt-a-Rb IgG (H+L) Alexa Fluor 488 ((Thermo Scientific, A32731, 1:250) diluted in blocking solution. After washing the tubules two times for 5 minutes, nuclei were stained with Hoechst 33342 (Thermo Fisher Scientific, H3570, 1:2000) in the last washing step. Fluorescent images for the 3D reconstructions were taken with the ImageXpress® Micro Confocal High-Content Imaging System (Molecular Devices). A z-stack of 220 μm with 2 μm between each image plane was acquired for DAPI, FITC, and TRITC channels. 3D reconstructions and maximum projections were created using ImageJ [37].
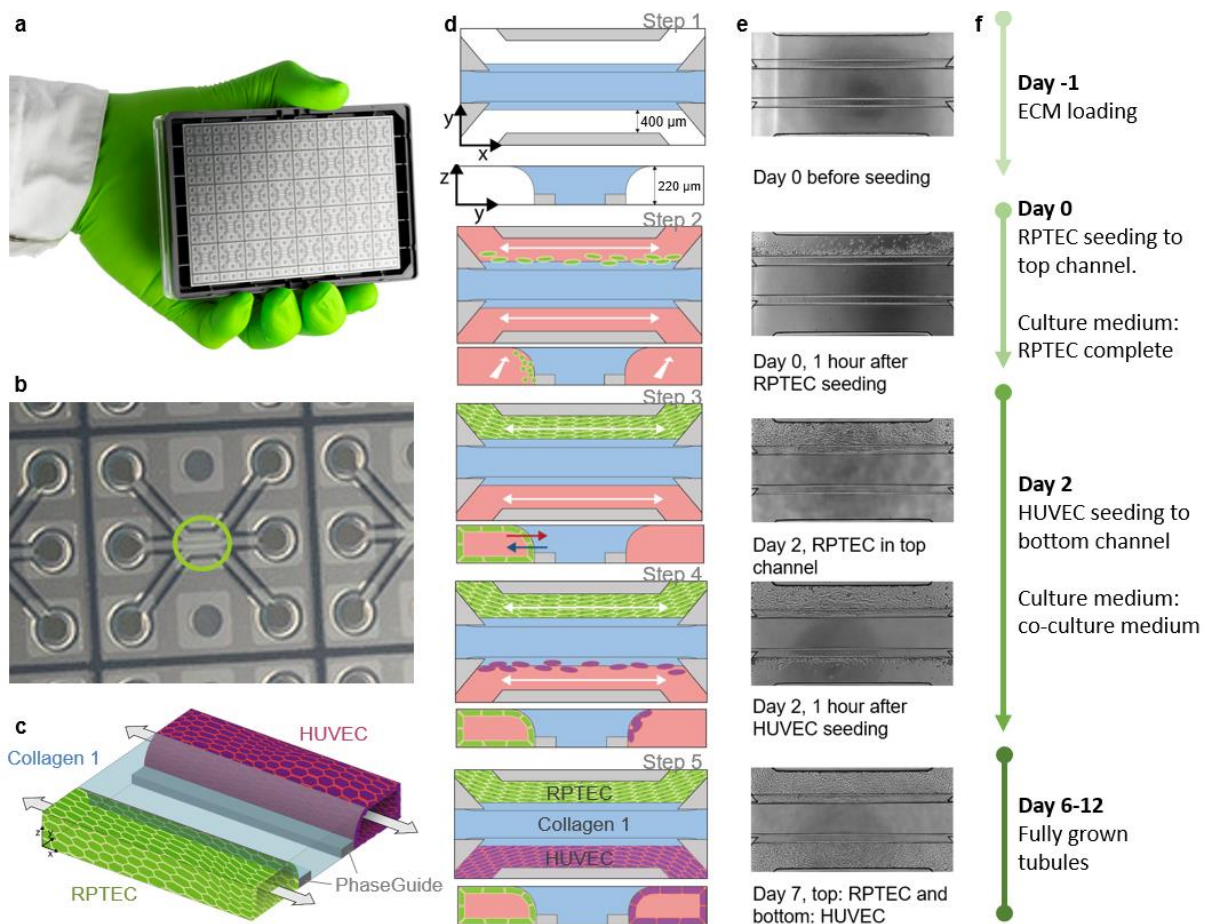
Figure 1: Overview of the seeding method of the RPTEC/HUVEC coculture in the OrganoPlate 3-lane.
a Photograph of the bottom-side of the culture platform showing 40 microfluidic channel networks underneath a 384-well plate. b Zoom-in on a single microfluidic channel network comprising three channels that join in the center (green circle). c 3D artist impression of the center of a chip, where two tubules are cultured in the two lateral channels (green and purple) along an ECM gel in the middle channel (light blue). Two phaseguides (grey bars) define the positioning of the ECM gel leading to the three-lane stratified profile. d Artist impression in horizontal projection and vertical cross section, e associated phase-contrast images and f timeline for setting up the coculture. Pictures show a single chip and formation of the tubular structures at day 0, 3, and 7.

Nephrotoxicant exposure

Cultures were exposed to a concentration range of cisplatin, tobramycin and cyclosporin A (CysA) [38] (Table 1). Staurosporine (10 µM), a well-known apoptosis inducer [39], was included as a positive control, and dexamethasone (30 µM) [40] as a negative control. On day 6 medium of both channels was replaced with coculture medium complemented with a nephrotoxicant, the positive or the negative control (Table 1). Following a 48-hour incubation on the rocker platform, medium was sampled from the top wells connected to the RPTEC tubules. Samples from in- and outlet were pooled and used for the lactate dehydrogenase (LDH) activity assay. Tubules were thereafter incubated with WST-8 buffer diluted in medium to determine viability. Phase-contrast and fluorescent images were acquired using the ImageXpress XLS Micro HCI system (Molecular

Devices) to assess the morphology of the cells and their nuclei. Moreover, activation of caspase 3/7 activity was visualized.

Table 1: Nephrotoxic compounds used for validation of the model.

Compound	catalog no. (Sigma-Aldrich)	Solvent	Final vehicle conc. (v/v)	Highest concentration
Cisplatin	P4394	0.9% NaCl in H_2O	5.4%	270 µM
Tobramycin	T1783	Culture medium	-	50 mM
Cyclosporin A	30024	DMSO	0.6%	60 µM
Staurosporine	S4400	DMSO	0.1%	10 µM
Dexamethasone	D4902	DMSO	0.1%	30 µM

Fluorogenic caspase-3/7 assay and nuclei staining

For acquiring live cell images of cells undergoing caspase-3/7 mediated apoptosis, culture medium was replaced with medium containing Caspase-3/7 Green Apoptosis Assay Reagent (dilution 1:1000, Sartorius, #4440). After a 1.5-hour incubation at 37°C, 21% O2, 5% CO2 on the rocker platform a z-stack of 220 µm with 5 µm between each image plane was acquired for FITC using the ImageXpress® Micro Confocal High-Content Imaging System (Molecular Devices) with a 10x objective. The plate was thereafter fixated as described previously [24] and nuclei were stained with Hoechst 33342 and imaged again for DAPI. One maximum projection per chip was created for both, DAPI and FITC using ImageJ.

Lactate dehydrogenase activity assay

LDH activity of the samples was determined using the Lactate Dehydrogenase Activity Assay Kit (Sigma, MAK066) according to manufacturer protocol. In short, the medium of the top in- and top outlet or bottom in- and bottom outlet was pooled for RPTEC or HUVEC, respectively. 2 µL was added in duplicate to a black 384 well plate with a glass bottom. Next, 18 µL LDH assay buffer was added to all sample wells to add up to an initial volume of 20 µL. In parallel, a concentration curve of the NADH standard was added. After a short centrifugation step, 20µl Master Reaction Mix was added to each well. After one minute, the absorbance was measured with the Multiskan™ FC Microplate Photometer (Thermo scientific) at 450 nm every 2 minutes for 6 minutes. Background subtraction was performed using the results of cell-free chips exposed to medium without any additives. The LDH activity was determined using the following formula:

$$\text{LDH activity } (nmol/min/ml) = \frac{\text{nmol NADH x sample dilution factor}}{\text{reaction time } (min) \text{ x sample volume } (mL)}$$

Cell viability (WST-8 assay)

The viability of the cells was determined using the Cell Counting Kit – 8 (Sigma, 96992). The WST-8 solution was diluted 1:11 with coculture medium and added to both perfusion channels of one chip (30 µL in- and outlets). After an 18-minute incubation at 37°C and 5% CO2 on the rocker platform and a 2-minute static incubation, the absorbance in the top in- and outlets was measured with the Multiskan™ FC Microplate Photometer (Thermo scientific) at 450 nm. For background subtraction measurements from cell-free chips were used.

Modeling renal ischemia and renal reperfusion

Renal ischemia was modelled on the OrganoPlate cocultures by exposing the cultures to low oxygen (5% O2), and/or low glucose and nutrient availability, and/or no perfusion. This was compared to a normoxic culture: atmospheric O_2 of 21%, coculture medium, and perfusion. Eight different setups were tested (Table 2).

Table 2: Conditions used to model Ischemia. N=normoxia, L=low oxygen, P=perfusion, S=static, +glu=coculture medium, -glu=DMEM w/o glucose.

Condition (abbreviation)	Oxygen Tension	Perfusion	Glucose and nutrient availability
N+P+glu	Normoxia (21% O_2)	Yes (rocker)	Coculture medium
N+P-glu	Normoxia (21% O_2)	Yes (rocker)	DMEM w/o glucose
N+S+glu	Normoxia (21% O_2)	No (static)	Coculture medium
N+S-glu	Normoxia (21% O_2)	No (static)	DMEM w/o glucose
L+P+glu	Low oxygen (5% O_2)	Yes (rocker)	Coculture medium
L+P-glu	Low oxygen (5% O_2)	Yes (rocker)	DMEM w/o glucose
L+S+glu	Low oxygen (5% O_2)	No (static)	Coculture medium
L+S-glu	Low oxygen (5% O_2)	No (static)	DMEM w/o glucose

On day 6 of the coculture, ischemic conditions were induced. For low oxygen, cultures were placed in a low oxygen incubator (5% CO_2, 37°C, 5% O_2). Perfusion was stopped by removing the plates from the rocker-platform. For low nutrient cultures the medium was changed to DMEM without glucose (Gibco #11966-025). The cultures were exposed to combinations of the ischemic conditions for 24 hours, after which medium was sampled for the LDH assay and phase-contrast images were acquired. To model renal ischemic reperfusion injury, the exposure was followed by a reperfusion of the cultures for another 24 hours in normoxic conditions. Subsequently, medium

was sampled for LDH assay, WST-8 viability was determined, phase-contrast images were acquired, and the cultures were stained for DNA and caspase-3/7 activation.

Assessment of potential protective compounds

Prevention of ischemic damage during exposure and reperfusion of the cultures was assessed upon addition of adenosine, nicotinamide and NAC during exposure and reperfusion to the culture medium of both channels (Table 3). For testing possible protecting effects of the co-incubation with the three compounds, cultures were exposed to the selected ischemic conditions L+P-glu and L+S-glu and compared to the N+P+glu control. The experiment was executed with an ischemia exposure time of 12 hours or 24 hours, both followed by 24-hour reperfusion. LDH activity samples and phase-contrast images were acquired after the exposure and after reperfusion. WST-8 viability assay and DNA and caspase-3/7 staining were performed after reperfusion only. Staurosporine (10µM) was used as positive control for the viability assays.

Table 3: Protective compounds tested to prevent cell damage during renal ischemia and reperfusion.

Compound	Supplier, catalog no.	Solvent	Stock conc. (mM)	Exposure conc. (mM)
Adenosine	Sigma, A4036	1M NH$_4$OH (heated) Sigma, 09859	180	1
Nicotinamide	Sigma, N0636	milliQ	1000	10
N-acetylcysteine	Sigma, A9165	milliQ	500	1

Real time imaging

On day 6 of culture, the plate was placed in the EVOS® FL Auto Imaging System (Life Technologies, 5% CO$_2$, 37°C, humidified) and incubated static in DMEM without glucose medium under 5% O$_2$ (L+S-glu) for 24 hours to mimic an ischemic event. Phase-contrast and FITC images were acquired every 32 minutes for 24 hours. Hereafter, the plate was reperfused with nutrient-rich coculture medium in normoxia (21% O2) and perfusion was reinstated by placing the EVOS FL Auto Imaging System on a rocker platform (7 degree angle, 8 minute interval) for another 24-hours, while phase-contrast and FITC images were acquired every 32 minutes. During the exposure and reperfusion, cultures were co-incubated with or without 1 mM adenosine. To monitor the activation of caspase 3/7 the caspase-3/7 green apoptosis assay reagent was added to the medium (1:1000).

Data analysis and statistics

Images were processed using ImageJ [37]. Data analysis was performed using Excel (Microsoft office 365 Business) and GraphPad Prism (GraphPad Software Inc., version 8.4.2). Error bars represent the standard deviation. One-way ANOVA was used for statistical analysis between groups followed by Tukey's multiple comparisons test. A log(y) transformation was used to normalize the data if indicated by Anderson-Darling test or Brown Forsythe test of variances. In case of negative values, data was transformed using log(y+1). A p-value of < 0.05 was considered as significant.

Results

A perfused coculture of epithelial tubules and endothelial vessels was established in a microfluidic chip.

Figure 1 illustrates the setup for the perfused coculture of a human renal proximal tubule-on-a-chip and a blood vessel. RPTEC are cultured in the OrganoPlate 3-lane system against a collagen 1 ECM mimic and formed a tubular structure upon application of perfusion flow. At the same time a blood vessel was grown from HUVECs against the ECM on the other side. The 3-lane stratified setup is achieved by patterning a collagen 1 gel in the center of the chip using capillary pinning barriers called phaseguides [36].

Figure 2 shows immunohistochemical stainings of the coculture model from a top view (a, d, g) and a 3D bird's eye view (c, f, i). Tight junctions were confirmed through ZO-1 expression (Fig. 2a-f, green) [41]. Acetylated tubulin staining showed one primary cilium per cell on the luminal side for both cell types, (Fig. 2 a-c, g-i, red) [42], [43]. Epithelial marker and brush border protein Ezrin [44] was exclusively located on the apical side of the RPTEC layer (Fig. 2 d-f, red). Endothelial adherence junction protein VE-cadherin [45] was expressed by the endothelial cells at the cell borders (Fig. 2 g-i, green).

A 3D reconstruction of the coculture obtained by confocal microscopy showed that RPTEC and HUVEC adhered to the ECM in the central channel and grew to confluency after 6 and 4 days, respectively (Fig. 2 c, f, i). A view on the cross-section of both structures showed lumen formation on both sides of ECM, with the basal sides of the membranes facing each other.

The perfused 3D renal proximal tubule and blood vessel-on-a-chip is sensitive to nephrotoxicants.

Next, we assessed the response of the model to cisplatin, tobramycin, and CysA after 48-hours exposure. Phase-contrast imaging showed rounded-up and clustered cells for high concentrations of cisplatin and tobramycin, whereas the morphology of the culture upon CysA exposure remained normal for all concentrations (Fig. 3a).
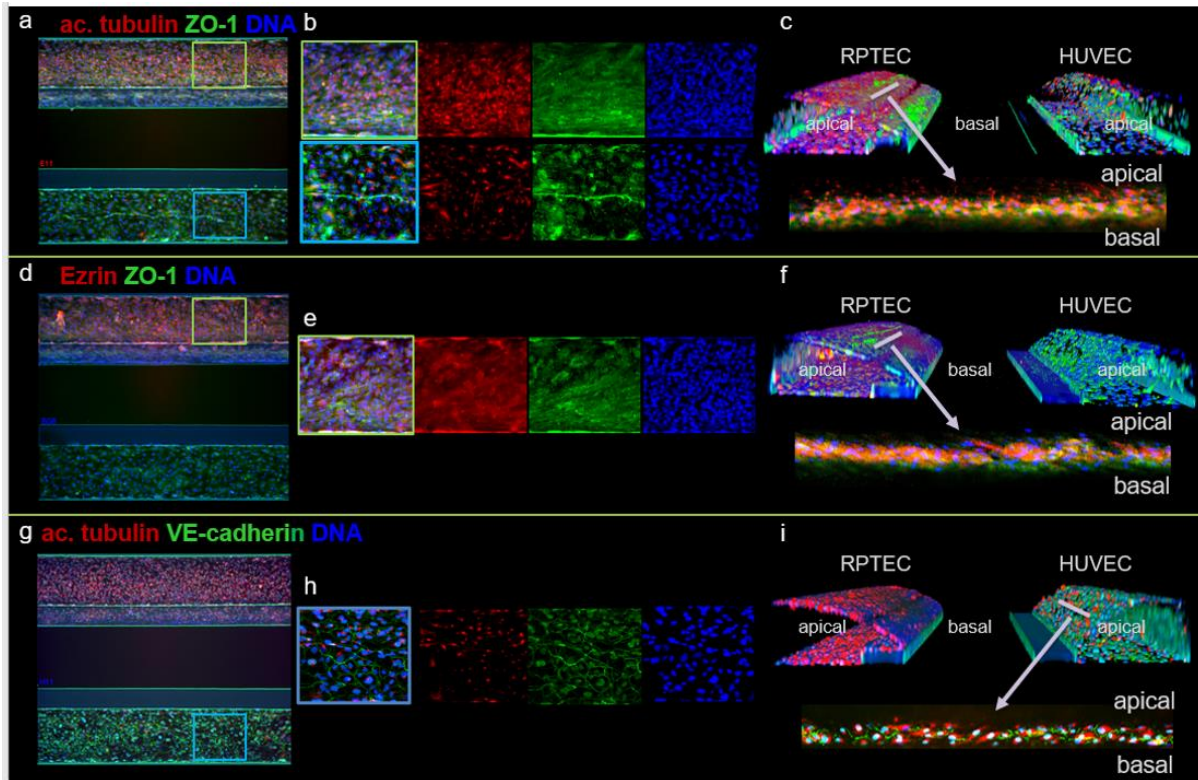
*Figure 2: **Marker expression of the kidney model shows polarized epithelium and endothelium. a, d, g** z-projections of the coculture with the RPTEC tubule in the top channel and the HUVEC vessel in the bottom channel. **b, e, h** Zoom of the z-projections in **a, d, g**. **c, f, i** 3D reconstructions showing a view into the lumen of the tubules. **a-c** Primary cilia were visualized by acetylated tubulin staining (red), present on the apical side of the RPTEC tubule. Tight junction protein ZO-1 (green) was present in both cell types. **d-f** Epithelial marker and brush border protein Ezrin (red) was exclusively present on the apical side of the RPTEC tubule. **g-i** Endothelial tight junction protein VE-cadherin (green) was expressed by the HUVEC vessel at the cell border and primary cilia located on the apical side of the membrane were stained using acetylated tubulin.*

DNA staining (Fig. 3b) and activated caspase 3/7 staining [46] (Fig. 3c) confirmed these observations, showing visible damage for concentration of 27 µM cisplatin or 28.1 mM tobramycin and higher. Tubules exposed to the highest concentration of CysA showed a slight increase in the number of caspase 3/7 positive cells, though this effect was less dominant compared with the other two compounds.

LDH activity released into the medium was measured at the luminal side of RPTEC as an indicator of cell damage [47]. A trend of dose-dependent increase in LDH release was observed after treatment with cisplatin and tobramycin, whereas such a trend was not observed with CysA (Fig. 3d).

Dehydrogenase activity was measured as a representation of cell viability through a WST-8 assay (Fig. 3e, [48], [49]). Cisplatin and tobramycin exhibited a dose-dependent reduction while CysA did not affect the cell viability.

HUVEC were damaged to a similar level as RPTEC when exposed to cisplatin and tobramycin, but more severely after an exposure to CysA (data not shown). Ischemia can be induced through non-flow, low glucose and/or low oxygen.

To model rIRI in the proximal tubule-on-a-chip with blood vessel, cultures were exposed to combinations of three different ischemic assaults: low oxygen (5% O2, termed 'L'), no perfusion (static, termed 'S') and glucose free and nutrient poor medium (termed '-glu') (see Table 2 for an overview of ischemic parameter combinations). After a 24-hour exposure, cultures were reperfused under normoxic conditions (21% oxygen, termed 'N', perfusion on the rocker, termed 'P', and glucose and nutrient rich medium, (5% fetal bovine serum), termed '+glu' for another 24 hours) (Fig. 4).

Phase-contrast images of the proximal tubule after 24-hour exposure are shown in figure 4c. Among the 8 different combinations of ischemic parameters, N+S-glu, L+P-glu, and L+S-glu conditions showed rounded-up and clustered morphology. Endothelial vessels showed less severe or no damage under these conditions (S1a, top). Following the reperfusion, the damage to the proximal tubules had worsened (Fig. 4c bottom). RPTEC exposed to N+S-glu and L+S-glu were washed out of most parts of the channels during reperfusion, whereas HUVEC stayed attached even after the washing steps involved in the staining process (Fig. 4d and S1b, respectively).

Caspase 3/7 activity was determined directly after the reperfusion and showed clear activation in RPTEC when exposed to L+S-glu (Fig. 4e). A fainter staining was detected in the HUVEC in the same condition (S1c). In addition to the L+S-glu condition, caspase 3/7 activation of a few cells was detected in the L+P-glu condition in both cell types, again with a much lower activation in HUVEC.
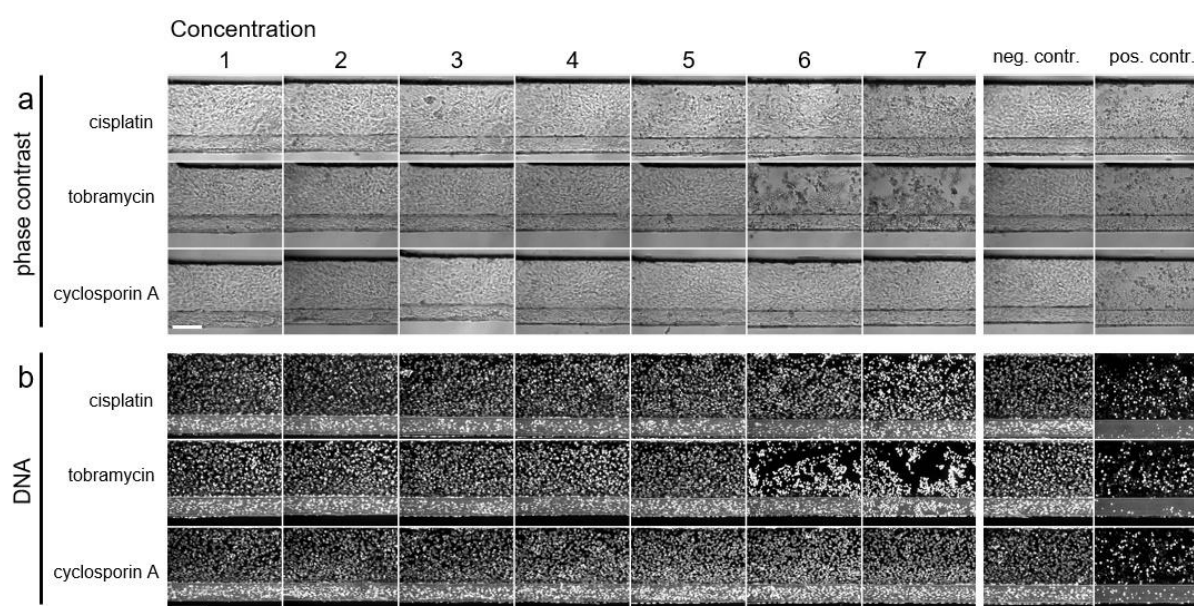
Representative images. Scalebar = 200 μm. Experiment 2, n=4 chips.
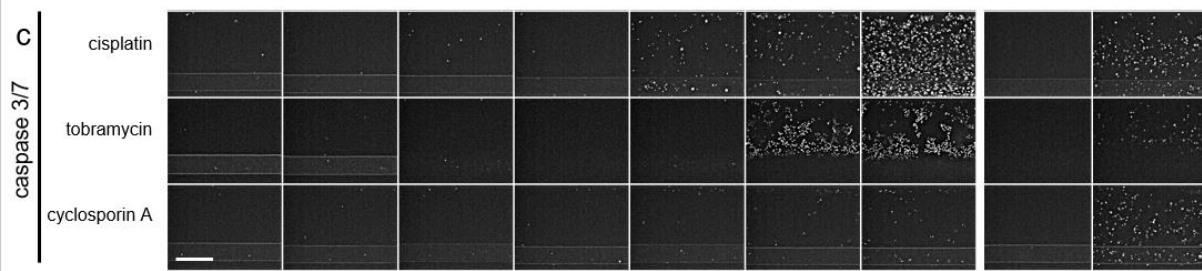
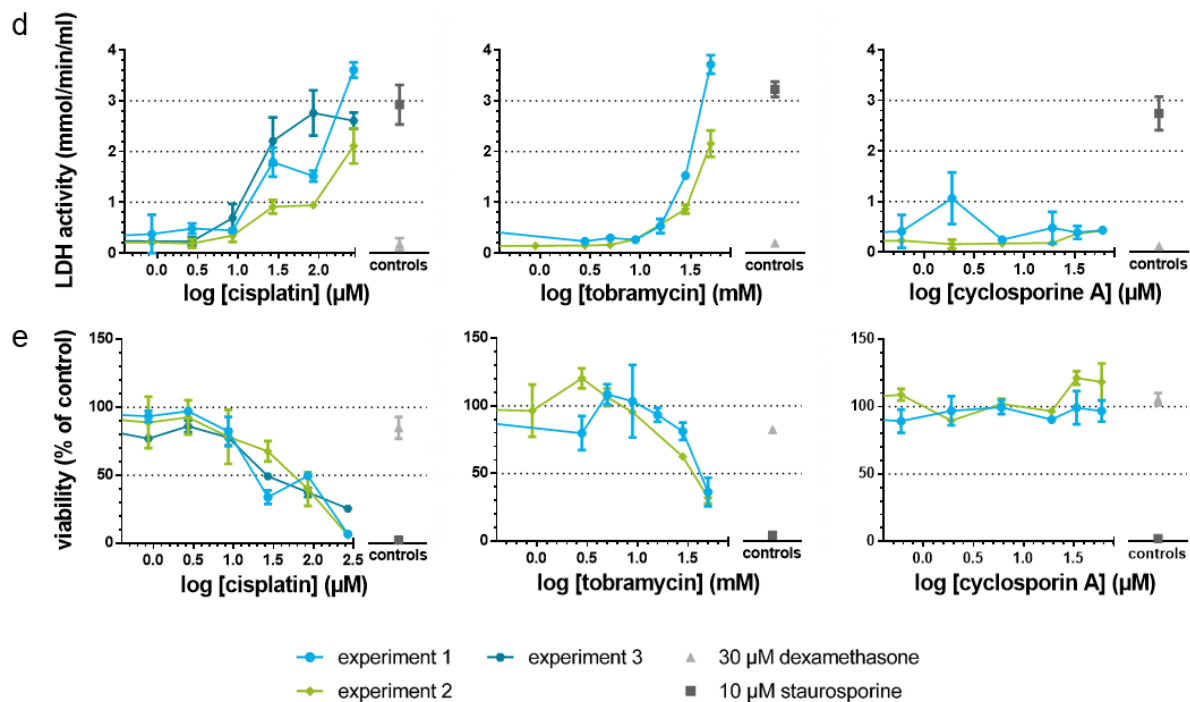Representative images. Scalebar = 200 µm. Experiment 2, n=4 chips.

*Figure 3: **A panel of assays shows susceptibility of the proximal tubule to AKI in response to nephrotoxic drugs**. Cocultures were exposed to concentrations ranges of cisplatin, tobramycin and cyclosporin A for 48 hours. **a-c** Phase-contrast imaging (a), DNA staining (b) and caspase 3/7 staining (c) showed cell damage after cisplatin and tobramycin exposure in a dose dependent manner. Representative images. Scalebar = 200µm. **d** LDH release in the medium was measured and showed cell damage after cisplatin and tobramycin exposure in a dose dependent manner. **e** Assessment of the viability relative to the corresponding vehicle control using a WST-8 assay showed a dose-dependent decrease in viability after cisplatin and tobramycin exposure. Dexamethasone (30µM) was included as a negative control, staurosporine (10µM) was included as a positive control. Error bars represent standard deviation. Experiment 1-3 are independent repeats of the experiment, n=2-4 chips per condition.*

Figure 4f displays the LDH activity in culture medium from the RPTEC tubule after 24 hours ischemia (left panel) and subsequent reperfusion (right panel). Overall, change of LDH activity was limited in comparison to the positive control staurosporine. Under this premise, N+S-glu, L+P-glu, and L+S-glu conditions increased LDH activity, while N+P-glu condition decreased LDH activity.

After 24 hours reperfusion, N+S+glu and L+S+glu treated cultures also displayed increased LDH activity.

Assessment of the dehydrogenase activity as an index of viability showed a significant decrease of 50% in all RPTEC tubules which had been exposed to N+P-glu, N+S-glu, L+P-glu and L+S-glu. Remarkably also the cultures exposed to the condition N+P-glu showed an 50% decrease of dehydrogenase activity, which was not reflected in the LDH release. Dehydrogenase activity measured in the HUVEC cultures was 60% reduced for all conditions exposed to -glu independent from the other parameters (fig. S1).

Adenosine prevented degradation of proximal tubules under ischemic conditions.

We assessed the protective effect of adenosine, nicotinamide, and NAC in our rIRI model. Cultures were subjected to the two ischemic conditions L+P-glu and L+S-glu during 12- or 24-hour exposure, both followed by 24-hour reperfusion.

In phase-contrast imaging, obvious damage of RPTEC was observed in the L+S-glu condition after 12-hour ischemia with 24-hour reperfusion (Fig. 5a). More severe damage was observed after 24-hour ischemia with 24-hour reperfusion (Fig. 5b). Treatment with 1 mM adenosine retained RPTEC in the channel (Fig. 5 a, b, red squares), whereas disrupted RPTEC were observed when treated with 10 mM nicotinamide or 1 mM NAC. The protective effect of adenosine was confirmed by visualization of the DNA (Fig. 5 c, d). In addition, co-incubation with adenosine limited the increase of caspase 3/7 activity while in the control condition all remaining RPTEC were caspase 3/7 positive.

LDH activity in the culture medium is shown in figures 5g and 5i. Co-incubation with adenosine led to a statistically significant LDH activity reduction in four of the ischemic conditions. Unexpectedly, 10 mM nicotinamide tended to lower LDH activity at any condition including the control (Fig. 5g). We hypothesize that nicotinamide interferes with the LDH assay as nicotinamide is part of the LDH coenzyme nicotinamide-adenine dinucleotide (NAD+) [50] and can bind to the active site of LDH, thereby lowering the LDH activity [51]. To test this hypothesis, nicotinamide was co-incubated with staurosporine, a potent inducer of apoptosis (Fig. S3). Staurosporine exhibited renotoxicity as increase of LDH in culture media and decreased cell viability. However, co-treatment with nicotinamide decreased only LDH activity in culture media but had no influence on the WST-8 assay. This finding suggests that the LDH assay is not suitable for evaluating a renoprotective effect of nicotinamide.

Analysis of the viability by quantifying WST-8 reduction showed a decreased viability upon the ischemic event, to approximately 60% of the normoxic control condition after 12-hour exposure to L+S-glu and 35% after the exposure for 24 hours to L+S-glu. No compound appeared to be protective against ischemic damage in the WST-8 assay (Fig. 5 h, j). Results of repetition of the

experiments can be found in the supplemental figure S2. Results indicate the reproducibility of the experiments after both exposure durations, 12 and 24 hours.
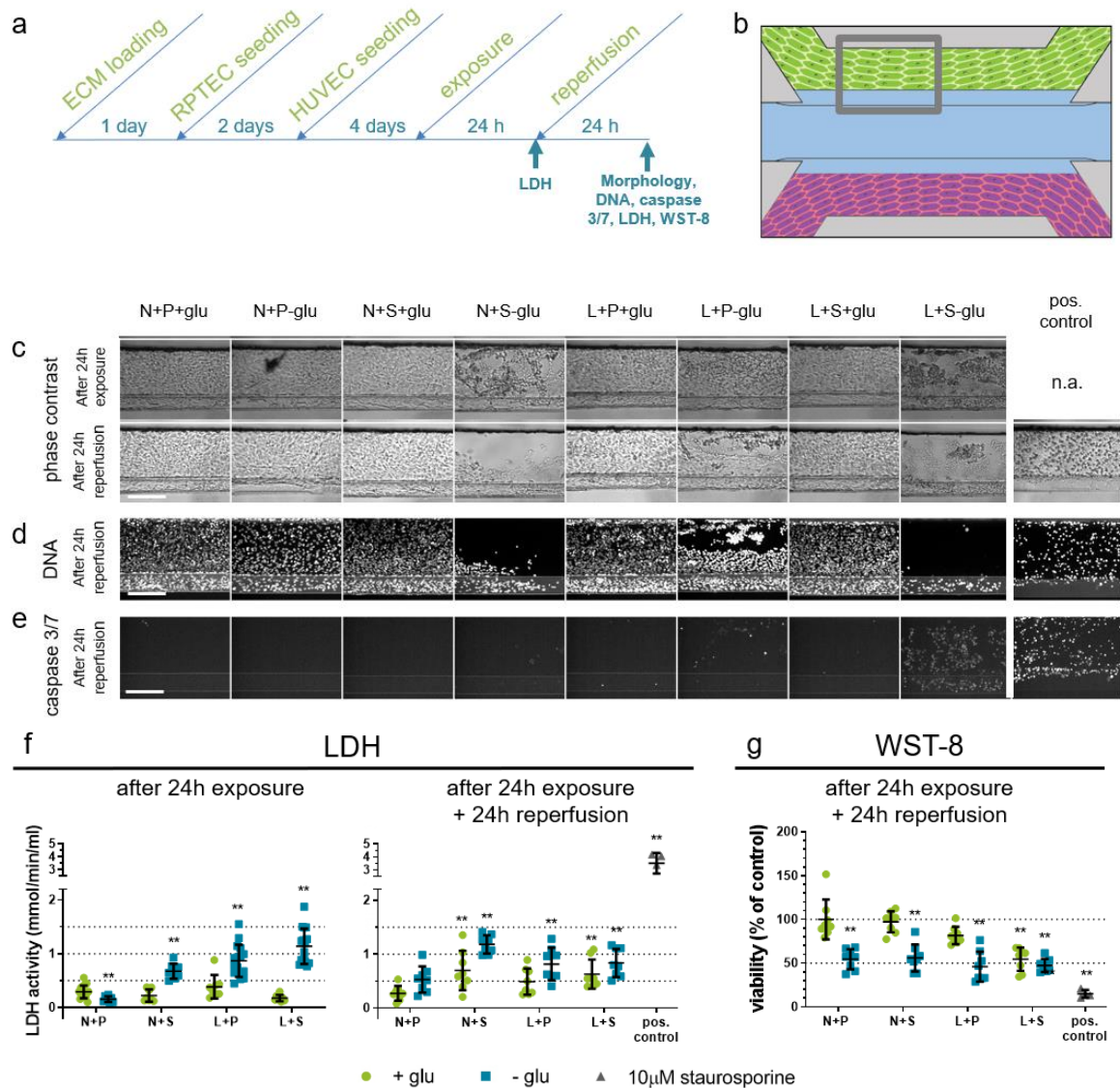

*Figure 4: **Ischemic conditions lead to AKI in the proximal tubule.** Ischemia was modelled on the OrganoPlate coculture through a combination of low oxygen (L), static incubation (S), and glucose and nutrient poor medium (-glu) for 24-hours, followed by a 24h reperfusion in normoxia (N), perfusion on the rocker (P), and in glucose and nutrient rich medium (+glu). **a** Timeline of the experiment. **b** Region of the RPTEC tubule (GREY square) that is used for the images shown in c-e. **c** Representative phase-contrast images after 24-hour exposure (top) and subsequent 24-hour reperfusion (bottom). Different ischemia inducing conditions were tested (columns) and compared to the normal condition N+P+glu. n.a.= not available. **d** DNA staining after 24h reperfusion. **e** Caspase 3-7 staining after 24 hour reperfusion. Scalebar = 200 µm. **f** LDH release in the medium was measured after 24 hour exposure (left) and 24 hour exposure plus 24 hour reperfusion (right) respectively. **g** WST-8 viability relative to the normal condition N+P+glu was assessed after 24h reperfusion. 10 µM staurosporine was included as a positive control. Error bars represent standard deviation. One-way ANOVA compares the conditions to the N+P+glu control condition, ** p<0.01 n=8-16 chips per condition.*

12-hour exposure + reperfusion   **24-hour exposure + reperfusion**

a / b — phase contrast: medium, adenosine, nicotine amide, N-acetyl cysteine, pos. control; rows N+P+glu, L+P-glu, L+S-glu

c / d — DNA

12-hour exposure + 24h reperfusion   **24-hour exposure + reperfusion**

e / f — Caspase 3/7

LDH   **WST-8**

g, h — 12h exposure
i, j — 24h exposure

after exposure | after exposure + 24h reperfusion | after exposure + 24h reperfusion

LDH activity (mmol/min/ml); viability (% of control)

● medium control   ▲ 10 mM nicotinamide   ● 10 µM staurosporine
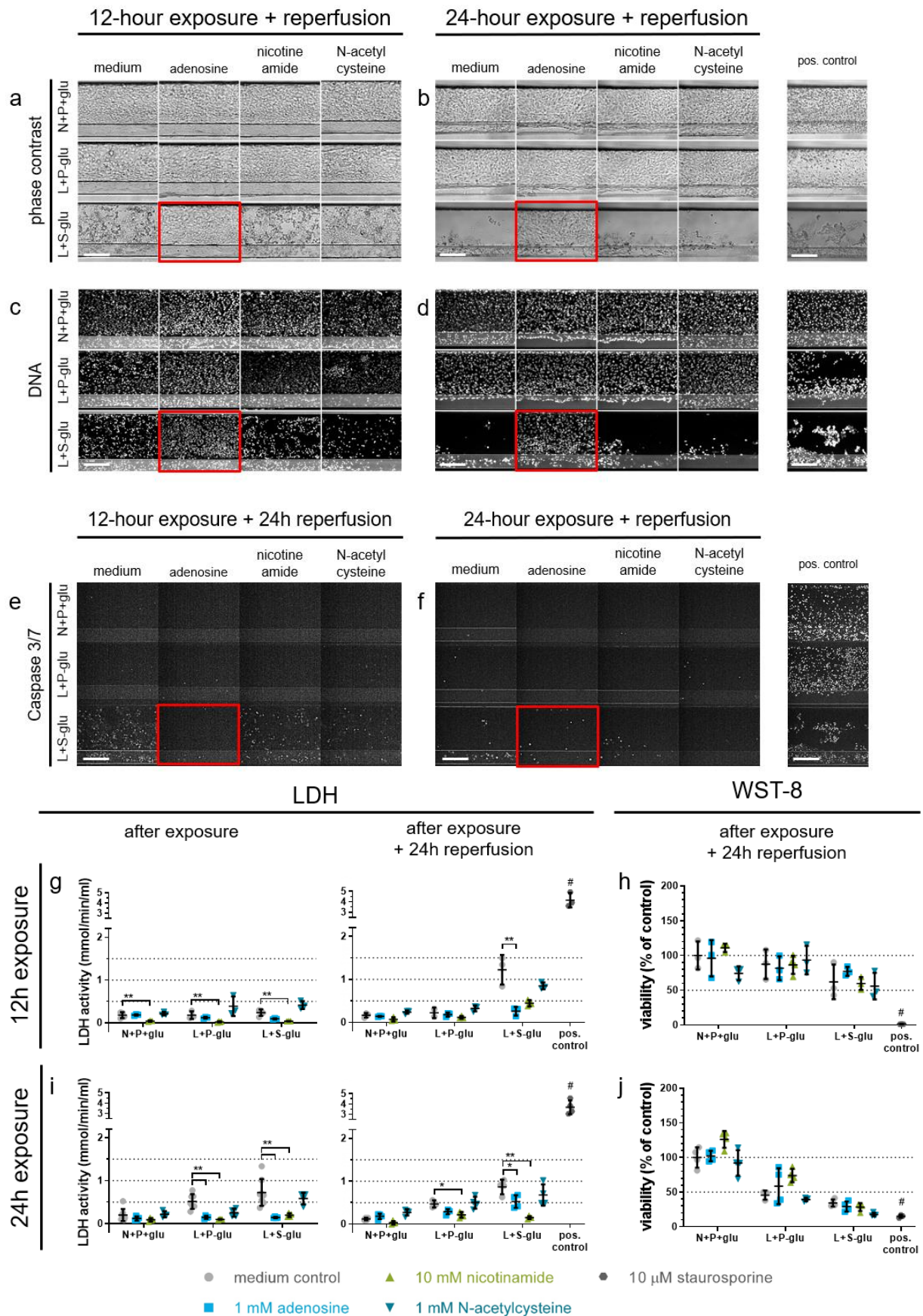■ 1 mM adenosine   ▼ 1 mM N-acetylcysteine

5

137

*Figure 5: **Co-incubation with adenosine decreases ischemia-induced AKI**. Cultures were exposed to the selected ischemic conditions L+P-glu and L+S-glu for either 12 or 24 hours, followed by a 24 hour reperfusion, in the presence of adenosine, nicotinamide or N-acetylcysteine. N+P+glu medium only is the normoxic control condition. **a-f** Images of a region of the RPTEC tubule (see Fig. 4b) after 12-hour exposure and reperfusion (**a, c, e**) or after 24-hour exposure and reperfusion (**b, d, f**). Red squares indicate a protective effect of adenosine compared to the medium control of the same ischemic condition in phase-contrast imaging (**e, f**), DNA staining (**g**, h) and caspase 3/7 staining (**i, j**). Scalebar = 200µm. **g-j** LDH activity (**g ,i**) and WST-8 viability relative to the N+P+glu medium control (**h, j**) after exposure to ischemic for 12 hours (**g, h**) or 24 hours (**i, j**) followed by reperfusion for 24 hours for both conditions. One-way ANOVA compares the co-incubations to the medium control of the same ischemic condition, * p < 0.05, ** p<0.01. # indicates the positive control differs significantly with all medium controls (p<0.01). Error bars represent the standard deviation. 10 µM staurosporine was included as a positive control. n=3-8 chips per condition. Both experiments (12 & 24 hour exposure) were repeated (Fig. S2).*

Real time caspase 3/7 imaging confirms adenosine is protective against rIRI.

The activation of caspase 3/7 during the ischemia and reperfusion process was investigated through time-lapse fluorescent microscopy (Fig. 6, and supplemental movie).

While exposed to ischemia (L+S-glu), caspase 3/7 activity increased over time in the medium control and adenosine treated conditions (Fig. 6a). Upon reperfusion with fresh medium, severe damage to the RPTEC in the medium control was observed because of cells being washed away (Fig. 6 b, top left panel), whereas proximal tubules treated with adenosine remained (Fig. 6b top right panel). After 12 and 24 hours of the reperfusion process, detached RPTEC, as well as an increase of activated caspase 3/7 in the remaining RPTEC, were observed in the medium control, while there were no severely disturbed RPTEC observed with adenosine treatment. HUVEC vessels recovered from the ischemic event, independent of adenosine co-incubation.

Discussion

In this study, we presented a human renal proximal tubule-on-a-chip in coculture with a perfused blood vessel separated by an ECM with the purpose to model rIRI-induced AKI (Fig. 1). A 3D reconstruction of histochemical stainings of the cocultures obtained by confocal microscopy showed that RPTEC and HUVEC adhere to the ECM and the side walls in the shape of tubular/vessel structures with lumen formation (Fig. 2). Correct polarization of the RPTEC was shown by a staining against the brush border marker ezrin. Primary cilia labeled with acetylated tubulin were observed on the apical surface of RPTEC and ZO-1, which is a key molecule of tight junctions, was found at the borders of the cells. Consistent with prior work [24] RPTEC formed barriers with limited diffusion of large molecules such as fluorescein labeled dextran (4.4 kDa and 150 kDa; data not shown) suggesting that the barrier function is well maintained. While this model is used in the present study, there is abundant room for further modifications. For instance, immune cells could be added to the lumen of the endothelial vessel, allowing the investigation of

translocation of immune cells by the endothelium, and their role in inflammation of the kidney microenvironment.
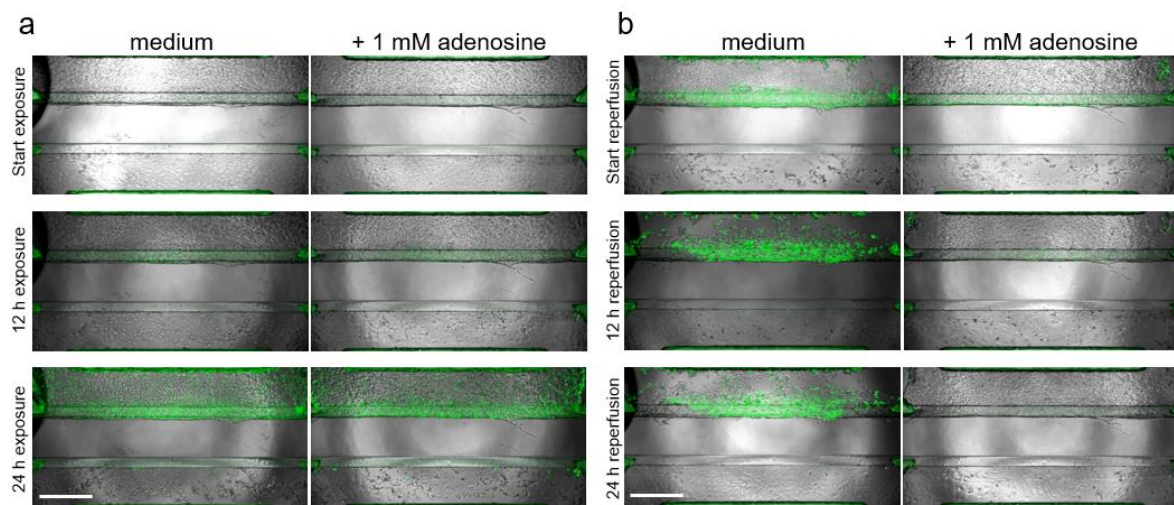

*Figure 6: **Real time caspase 3/7 activation and phase contrast imaging shows protective effect of adenosine upon ischemic exposure**. **a** Cultures, co-incubated with and without 1 mM adenosine were exposed to ischemic conditions (L+S-glu) for 24 hours and caspase 3/7 activity was monitored over time. **b** Medium was refreshed to standard culture medium and cocultures were reperfused under normal conditions (N+P+glu) for 24 hours. Green = activated caspase 3/7. Scalebar = 500 μm. Representative images of n=3 chips per condition. A corresponding time lapse movie can be viewed in the supplemental movie.*

To apply this new culture setup to *in vitro* AKI disease modeling, the response of the model to several renotoxicants was tested and the feasibility to measure cellular damage was assessed using several assays. Cisplatin, tobramycin, and CysA were capable to affect RPTEC in the advanced model as shown in figure 3. Tobramycin is an aminoglycoside antibiotic which causes nephrotoxicity in clinical settings [52]. Our model detected its toxicity from 28.1 mM, which is higher than concentrations used clinically (around 2 μg/mL) [52]. In clinical settings, nephrotoxicity of tobramycin is observed after multiple ingestions [52], while in the present study tobramycin exposure was performed at a single dosing for 48 hours. Using a longer time frame with repeated dosing a toxic effect might be detected at lower concentrations. CysA treatment resulted in increased caspase 3/7 activity at 60 μM. Li et al [53] reported caspase 3/7 activation by CysA with an EC50 of 11 μM in a two-dimensional culture setting of the same cell source (RPTEC SA7K clone). It would be interesting to compare the expression levels of P-glycoprotein, a ABC-transporter, between these culture settings as CysA is a substrate of P-glycoprotein [54]. Different levels could potentially cause a change of the intracellular concentration of CysA. In conclusion, all assays were suitable to detect reasonable cellular responses and we decided to use the model for disease modeling of rIRI.

We modelled an ischemic event on the kidney-on-a-chip by exposing the culture to a combination of three ischemic parameters: low oxygen (5%) (L), no perfusion (S), nutrient/glucose-poor medium (-glu), and combinations of the three. After exposure, reperfusion was reinstated under normal conditions (N+P+glu). When exposed to combined culture conditions (summarized in Table 2), N+S-glu, L+P-glu, and L+S-glu let to damage after the 24-hour exposure followed the reperfusion (Fig. 4). A significant change was observed in tubular morphology: cells appeared as rounded and detached cells were observed. Moreover, increased caspase 3/7 activity was observed in remaining epithelial cells after ischemia-reperfusion (L+S-glu or L+P-glu). These observations are in line with clinical observations as the loss of the brush border and detached epithelium were reported to be found in biopsy samples from AKI patients [8].

We investigated the potential renoprotective effects of adenosine, nicotinamide, and NAC when co-treated during the rIRI event of the two selected ischemic conditions L+P-glu and L+S-glu. A protective effect of the co-incubation with adenosine was observed in the morphology and DNA assessment, caspase 3/7 activation, and LDH release. However, dehydrogenase activity measured with the WST-8 viability assay showed no effect of adenosine. Based on these results we hypothesize that adenosine exerts its protection by lowering the cell metabolism [55], including the dehydrogenase activity. By putting the cells in a resting phase with low metabolism, the oxygen demand of the cells is minimal, which could prevent damage from ischemic condition. Overall, our results suggest that adenosine protects death of RPTEC through reduction of caspase 3/7 activation.

In contrast to adenosine, NAC did not show a renoprotective effect. There are positive reports of NAC being protective in animal rIRI models. Our observation that we did not see a protective effect in our human rIRI model could point towards a species-to-species difference, and that NAC in fact does not have a protective effect in humans. In fact, the KDIGO Clinical Practice Guideline for AKI [56] does not recommend using NAC for prevention of postsurgical AKI. We recommend follow-up research to further validate this hypothesis.

Nicotinamide is one of the precursors of nicotinamide adenine dinucleotide (NAD+), lately considered for its therapeutic potential as an NAD booster [57]. Recently, results of a phase 1 pilot study administrating nicotinamide was reported [31], [58]. In patients undergoing cardiac surgery, an increase of precursors for NAD+ was observed in their serum and urine accompanied by a decrease of serum creatinine. In contrast to our expectations, nicotinamide did not prevent tubular damage in our *in vitro* rIRI model. A decrease of LDH activity after nicotinamide treatment, was contributed to the interference of nicotinamide with the assay as described in result section. Follow-up studies will also help to better understand the translatability of this model to humans. In this regard, time-lapse imaging (Fig. 6 and supplemental movie) can be a powerful tool for monitoring the changes of cellular appearance. We selected a 12-hour or 24-hour duration for mimicking the ischemic exposure, while this duration might be too long to observe the

renoprotective effect of nicotinamide. Further assay optimization facilitated by such live imaging should be undertaken to investigate a broader range of various ischemic conditions and treatments at multiple evaluation time-points.

Endothelium seemed to be more tolerant to ischemia compared to the epithelium, and showed recovery during reperfusion, independent of the treatment condition (Figs. 4 and 6, Fig. S2). Further investigation will be needed to investigate the effect of rIRI on endothelial cells including further readouts such as endothelial marker expression, barrier integrity of the endothelial cell layer, and release of cytokines.

In an earlier study, it was shown that glomerular specific endothelium is key to mimic specific aspects of the glomerulus, including glomerular specific extracellular matrix components [59]. We therefore expect that translatability of our model could be further increased by replacing HUVEC with endothelial cells of the kidney. Alternatively, inclusion of induced pluripotent stem cell-derived cells could be done to study different genetic backgrounds and predispositions. We also anticipate of usage of urine derived tubuloids [60] to capture patient specific responses to ischemic events.

The current model is sufficiently robust to push forward to a high throughput phenotypic screen for finding novel protective compounds that protect the kidney during ischemia and reperfusion. The OrganoPlate platform used in this study is compatible, next to general laboratory equipment, with high content (fluorescent) microscopes and robotics. Kane *et al*. have already reported automation of the system for neuronal cultures [61]. Importantly, we showed that we could measure response to these effects with various orthogonal assays. This allows internal hit verification in a single run.

In conclusion, we successfully expanded our human renal proximal tubule-on-a-chip to a coculture setting with endothelial cells. We were able to study the effect of ischemic conditions and their role in AKI induction by adjustment of various culture settings (nutrient composition, oxygen tension, and perfusion flow). We found that ischemic conditions had a strong detrimental effect on the proximal tubule, but only mildly impacted the endothelium. We furthermore confirmed that adenosine had a protective effect. We thus conclude that we have established a powerful platform to study AKI *in vitro* that will prove useful to advance our understanding of the pathophysiological nature of rIRI and support development of novel therapies for preventing AKI.

Author contributions

Conception and design: MK Vormann, M Ohbuchi, F Kiyonaga, HL Lanz, K Tetsuka
Acquisition of data: MK Vormann, LM Tool, L Gijzen
Analysis and interpretation of data: MK Vormann, LM Tool, M Ohbuchi, R van Vught, T Hankemeier, F Kiyonaga, T Kawabe, T Goto, A Fujimori, HL Lanz, K Tetsuka

Supervision: P Vulto, HL Lanz, K Tetsuka

Drafting the manuscript: MK Vormann, HL Lanz, P Vulto, K Tetsuka

Revising the manuscript: All authors commented on the draft manuscript.

References

[1]   A. Zuk and J. V. Bonventre, "Acute Kidney Injury," *Annu. Rev. Med.*, vol. 67, no. 1, pp. 293–307, Jan. 2016, doi: 10.1146/annurev-med-050214-013407.

[2]   A. J. P. Lewington, J. Cerdá, and R. L. Mehta, "Raising awareness of acute kidney injury: a global perspective of a silent killer," *Kidney Int.*, vol. 84, no. 3, pp. 457–467, Sep. 2013, doi: 10.1038/ki.2013.153.

[3]   D. P. Basile, M. D. Anderson, and T. A. Sutton, "Pathophysiology of acute kidney injury," *Compr. Physiol.*, vol. 2, no. 2, pp. 1303–1353, 2012, doi: 10.1002/cphy.c110041.

[4]   M. A. Perazella, "Renal vulnerability to drug toxicity," *Clin. J. Am. Soc. Nephrol.*, vol. 4, no. 7, pp. 1275–1283, 2009, doi: 10.2215/CJN.02050309.

[5]   S. P. Soltoff, "ATP and the Regulation of Renal Cell Function," *Annu. Rev. Physiol.*, vol. 48, no. 1, pp. 9–31, Oct. 1986, doi: 10.1146/annurev.ph.48.030186.000301.

[6]   P. Hansell, W. J. Welch, R. C. Blantz, and F. Palm, "Determinants of kidney oxygen consumption and their relationship to tissue oxygen tension in diabetes and hypertension," *Clin. Exp. Pharmacol. Physiol.*, vol. 40, no. 2, pp. 123–137, 2013, doi: 10.1111/1440-1681.12034.

[7]   K. Makris and L. Spanou, "Acute Kidney Injury: Definition, Pathophysiology and Clinical Phenotypes," *Clin. Biochem. Rev.*, vol. 37, no. 2, pp. 85–98, 2016, [Online]. Available: https://www.ncbi.nlm.nih.gov/pmc/articles/PMC5198510/.

[8]   J. V Bonventre and L. Yang, "Cellular pathophysiology of ischemic acute kidney injury," *J. Clin. Invest.*, vol. 121, no. 11, pp. 4210–4221, Nov. 2011, doi: 10.1172/JCI45161.

[9]   M. Malek and M. Nematbakhsh, "Renal ischemia/reperfusion injury; from pathophysiology to treatment.," *J. Ren. Inj. Prev.*, vol. 4, no. 2, pp. 20–27, 2015, doi: 10.12861/jrip.2015.06.

[10]   G. R. Kinsey, L. Li, and M. D. Okusa, "Inflammation in acute kidney injury," *Nephron - Exp. Nephrol.*, vol. 109, no. 4, 2008, doi: 10.1159/000142934.

[11]   M. K. Nadim *et al.*, "COVID-19-associated acute kidney injury: consensus report of the 25th Acute Disease Quality Initiative (ADQI) Workgroup," *Nat. Rev. Nephrol.*, Oct. 2020, doi: 10.1038/s41581-020-00356-5.

[12]   W. Lieberthal and S. K. Nigam, "Acute renal failure. II. Experimental models of acute renal

failure: imperfect but indispensable," *Am. J. Ren. Physiol.*, vol. 278, no. 1, pp. F1–F12, 2000.

[13]   N. I. Skrypnyk, L. J. Siskind, S. Faube, and M. P. de Caestecker, "Bridging translation for acute kidney injury with better preclinical modeling of human disease," *Am. J. Physiol. - Ren. Physiol.*, vol. 310, no. 10, pp. F972–F984, 2016, doi: 10.1152/ajprenal.00552.2015.

[14]   A. L. Russ, K. M. Haberstroh, and A. E. Rundell, "Experimental strategies to improve *in vitro* models of renal ischemia," *Exp. Mol. Pathol.*, vol. 83, no. 2, pp. 143–159, 2007, doi: 10.1016/j.yexmp.2007.03.002.

[15]   V. van Duinen, S. J. Trietsch, J. Joore, P. Vulto, and T. Hankemeier, "Microfluidic 3D cell culture: From tools to tissue models," *Curr. Opin. Biotechnol.*, vol. 35, pp. 118–126, 2015, doi: 10.1016/j.copbio.2015.05.002.

[16]   M. J. Wilmer, C. P. Ng, H. L. Lanz, P. Vulto, L. Suter-Dick, and R. Masereeuw, "Kidney-on-a-Chip Technology for Drug-Induced Nephrotoxicity Screening," *Trends Biotechnol.*, vol. 34, no. 2, pp. 156–170, 2016, doi: 10.1016/j.tibtech.2015.11.001.

[17]   G. A. Van Norman, "Limitations of Animal Studies for Predicting Toxicity in Clinical Trials: Is it Time to Rethink Our Current Approach?," *JACC Basic to Transl. Sci.*, vol. 4, no. 7, pp. 845–854, 2019, doi: 10.1016/j.jacbts.2019.10.008.

[18]   U. Marx *et al.*, "Biology-inspired microphysiological systems to advance patient benefit and animal welfare in drug development," *ALTEX*, vol. 37, no. 3, pp. 364–394, 2020, doi: 10.14573/altex.2001241.

[19]   K. Tetsuka *et al.*, "Reconstituted human organ models as a translational tool for human organ response: Definition, expectations, cases, and strategies for implementation in drug discovery and development," *Biol. Pharm. Bull.*, vol. 43, no. 3, pp. 375–383, 2020, doi: 10.1248/bpb.b19-01070.

[20]   S. G. Lloyd, P. Wang, H. Zeng, and J. C. Chatham, "Impact of low-flow ischemia on substrate oxidation and glycolysis in the isolated perfused rat heart," *Am. J. Physiol. - Hear. Circ. Physiol.*, vol. 287, no. 1 56-1, 2004, doi: 10.1152/ajpheart.00983.2003.

[21]   K. J. Jang *et al.*, "Human kidney proximal tubule-on-a-chip for drug transport and nephrotoxicity assessment," *Integr. Biol. (United Kingdom)*, vol. 5, no. 9, pp. 1119–1129, 2013, doi: 10.1039/c3ib40049b.

[22]   J. Jansen *et al.*, "Human proximal tubule epithelial cells cultured on hollow fibers: Living membranes that actively transport organic cations," *Sci. Rep.*, vol. 5, no. November, pp. 1–12, 2015, doi: 10.1038/srep16702.

[23]   K. A. Homan *et al.*, "Bioprinting of 3D Convoluted Renal Proximal Tubules on Perfusable Chips," *Sci. Rep.*, vol. 6, pp. 1–13, 2016, doi: 10.1038/srep34845.

[24]   M. K. Vormann *et al.*, "Nephrotoxicity and Kidney Transport Assessment on 3D Perfused Proximal Tubules," *AAPS J.*, vol. 20, no. 5, pp. 1–11, 2018, doi: 10.1208/s12248-018-0248-z.

[25]   Y. Duan *et al.*, "Shear-induced reorganization of renal proximal tubule cell actin cytoskeleton and apical junctional complexes," *Proc. Natl. Acad. Sci. U. S. A.*, vol. 105, no. 32, pp. 11418–11423, 2008, doi: 10.1073/pnas.0804954105.

[26]   V. Raghavan, Y. Rbaibi, N. M. Pastor-Soler, M. D. Carattino, and O. A. Weisz, "Shear stress-

dependent regulation of apical endocytosis in renal proximal tubule cells mediated by primary cilia," *Proc. Natl. Acad. Sci. U. S. A.*, vol. 111, no. 23, pp. 8506–8511, 2014, doi: 10.1073/pnas.1402195111.

[27]   S. Weinbaum, Y. Duan, L. M. Satlin, T. Wang, and A. M. Weinstein, "Mechanotransduction in the renal tubule," *Am. J. Physiol. - Ren. Physiol.*, vol. 299, no. 6, pp. 1220–1236, 2010, doi: 10.1152/ajprenal.00453.2010.

[28]   A. A. McDonough, "Mechanisms of proximal tubule sodium transport regulation that link extracellular fluid volume and blood pressure," *Am. J. Physiol. Integr. Comp. Physiol.*, vol. 298, no. 4, pp. R851–R861, Apr. 2010, doi: 10.1152/ajpregu.00002.2010.

[29]   J. Vriend *et al.*, "Screening of Drug-Transporter Interactions in a 3D Microfluidic Renal Proximal Tubule on a Chip," *AAPS J.*, vol. 20, no. 5, 2018, doi: 10.1208/s12248-018-0247-0.

[30]   L. Suter-Dick *et al.*, "Combining Extracellular miRNA Determination with Microfluidic 3D Cell Cultures for the Assessment of Nephrotoxicity: a Proof of Concept Study," *AAPS J.*, vol. 20, no. 5, pp. 1–9, 2018, doi: 10.1208/s12248-018-0245-2.

[31]   A. Poyan Mehr *et al.*, "De novo NAD+ biosynthetic impairment in acute kidney injury in humans," *Nat. Med.*, vol. 24, no. 9, pp. 1351–1359, 2018, doi: 10.1038/s41591-018-0138-z.

[32]   A. C. Seguro, L. F. Poli De Figueiredo, and M. H. M. Shimizu, "N-acetylcysteine (NAC) protects against acute kidney injury (AKI) following prolonged pneumoperitoneum in the rat," *J. Surg. Res.*, vol. 175, no. 2, pp. 312–315, 2012, doi: 10.1016/j.jss.2011.05.052.

[33]   M. H. M. Shimizu *et al.*, "N-acetylcysteine protects against renal injury following bilateral ureteral obstruction," *Nephrol. Dial. Transplant.*, vol. 23, no. 10, pp. 3067–3073, Jun. 2008, doi: 10.1093/ndt/gfn237.

[34]   T. M. DesRochers, L. Suter, A. Roth, and D. L. Kaplan, "Bioengineered 3D Human Kidney Tissue, a Platform for the Determination of Nephrotoxicity," *PLoS One*, vol. 8, no. 3, 2013, doi: 10.1371/journal.pone.0059219.

[35]   H. T. Lee and C. W. Emala, "Protective effects of renal ischemic preconditioning and adenosine pretreatment: Role of A1 and A3 receptors," *Am. J. Physiol. - Ren. Physiol.*, vol. 278, no. 3 47-3, pp. 380–387, 2000, doi: 10.1152/ajprenal.2000.278.3.f380.

[36]   P. Vulto, S. Podszun, P. Meyer, C. Hermann, A. Manz, and G. A. Urban, "Phaseguides: A paradigm shift in microfluidic priming and emptying," *Lab Chip*, vol. 11, no. 9, pp. 1596–1602, 2011, doi: 10.1039/c0lc00643b.

[37]   J. Schindelin *et al.*, "Fiji: An open-source platform for biological-image analysis," *Nat. Methods*, vol. 9, no. 7, pp. 676–682, 2012, doi: 10.1038/nmeth.2019.

[38]   S. Raju, S. Kavimani, V. Uma Maheshwara Rao, and K. Sriramulu Reddy, "Nephrotoxicants and nephrotoxicity testing: An outline of *In vitro* alternatives," *J. Pharm. Sci. Res.*, vol. 3, no. 3, pp. 1110–1116, 2011.

[39]   C. A. Belmokhtar, J. Hillion, and E. Ségal-Bendirdjian, "Staurosporine induces apoptosis through both caspase-dependent and caspase-independent mechanisms," *Oncogene*, vol. 20, no. 26, pp. 3354–3362, 2001, doi: 10.1038/sj.onc.1204436.

[40]   K. A. Jacob *et al.*, "Intraoperative high-dose dexamethasone and severe AKI after cardiac

surgery," *J. Am. Soc. Nephrol.*, vol. 26, no. 12, pp. 2947–2951, 2015, doi: 10.1681/ASN.2014080840.

[41]   B. R. Stevenson, J. D. Siliciano, M. S. Mooseker, and D. A. Goodenough, "Identification of ZO-1: A high molecular weight polypeptide associated with the tight junction (Zonula Occludens) in a variety of epithelia," *J. Cell Biol.*, vol. 103, no. 3, pp. 755–766, 1986, doi: 10.1083/jcb.103.3.755.

[42]   A. D. Egorova, K. van der Heiden, R. E. Poelmann, and B. P. Hierck, "Primary cilia as biomechanical sensors in regulating endothelial function," *Differentiation*, vol. 83, no. 2, pp. S56–S61, 2012, doi: 10.1016/j.diff.2011.11.007.

[43]   V. Raghavan and O. A. Weisz, "Flow stimulated endocytosis in the proximal tubule," *Curr. Opin. Nephrol. Hypertens.*, vol. 24, no. 4, pp. 359–365, 2015, doi: 10.1097/MNH.0000000000000135.

[44]   M. Berryman, Z. Franck, and A. Bretscher, "Ezrin is concentrated in the apical microvilli of a wide variety of epithelial cells whereas moesin is found primarily in endothelial cells," *J. Cell Sci.*, vol. 105, no. 4, pp. 1025–1043, 1993.

[45]   M. Giannotta, M. Trani, and E. Dejana, "Review VE-Cadherin and Endothelial Adherens Junctions : Active Guardians of Vascular Integrity," *Dev. Cell*, vol. 26, no. 5, pp. 441–454, 2013, doi: 10.1016/j.devcel.2013.08.020.

[46]   K. M. Hanson and J. N. Finkelstein, "An accessible and high-throughput strategy of continuously monitoring apoptosis by fluorescent detection of caspase activation," *Anal. Biochem.*, vol. 564–565, no. September 2018, pp. 96–101, 2019, doi: 10.1016/j.ab.2018.10.022.

[47]   C. Legrand *et al.*, "Lactate dehydrogenase (LDH) activity of the number of dead cells in the medium of cultured eukaryotic cells as marker," *J. Biotechnol.*, vol. 25, no. 3, pp. 231–243, 1992, doi: 10.1016/0168-1656(92)90158-6.

[48]   H. Tominaga *et al.*, "A water-soluble tetrazolium salt useful for colorimetric cell viability assay," *Anal. Commun.*, vol. 36, no. 2, pp. 47–50, 1999, doi: 10.1039/a809656b.

[49]   K. Chamchoy, D. Pakotiprapha, P. Pumirat, U. Leartsakulpanich, and U. Boonyuen, "Application of WST-8 based colorimetric NAD(P)H detection for quantitative dehydrogenase assays," *BMC Biochem.*, vol. 20, no. 1, pp. 1–14, 2019, doi: 10.1186/s12858-019-0108-1.

[50]   A. McPherson, "Interaction of lactate dehydrogenase with its coenzyme, nicotinamide-adenine dinucleotide," *J. Mol. Biol.*, vol. 51, no. 1, pp. 39–46, 1970, doi: 10.1016/0022-2836(70)90268-8.

[51]   A. J. Forlano, "Effect of the component parts of nicotinamide adenine dinucleotide (NAD⊕) as inhibitors of lactic dehydrogenase," *J. Pharm. Sci.*, vol. 56, no. 6, pp. 763–5, 1967.

[52]   F. Paquette *et al.*, "Acute Kidney Injury and Renal Recovery with the Use of Aminoglycosides: A Large Retrospective Study," *Nephron*, vol. 131, no. 3, pp. 153–160, 2015, doi: 10.1159/000440867.

[53]   S. Li *et al.*, "Development and Application of Human Renal Proximal Tubule Epithelial Cells for Assessment of Compound Toxicity," *Curr. Chem. Genomics Transl. Med.*, vol. 11, no. 1, pp. 19–30, Feb. 2017, doi: 10.2174/2213988501711010019.

[54] T. Saeki, K. Ueda, Y. Tanigawara, R. Hori, and T. Komano, "Human P-glycoprotein transports cyclosporin A and FK506," *J. Biol. Chem.*, vol. 268, no. 9, pp. 6077–6080, 1993.

[55] S. C. Yap and H. Thomas Lee, "Adenosine and protection from acute kidney injury," *Curr. Opin. Nephrol. Hypertens.*, vol. 21, no. 1, pp. 24–32, 2012, doi: 10.1097/MNH.0b013e32834d2ec9.

[56] Acute Kidney Injury Work Group. KDIGO Clinical Practice Guideline for Acute Kidney Injury, "Kidney Disease: Improving Global Outcomes (KDIGO)," *Kidney Int. Suppl.*, vol. 2, pp. 1–138, Mar. 2012, doi: 10.1038/kisup.2012.1.

[57] L. Rajman, K. Chwalek, and D. A. Sinclair, "Therapeutic Potential of NAD-Boosting Molecules: The *In vivo* Evidence," *Cell Metab.*, vol. 27, no. 3, pp. 529–547, Mar. 2018, doi: 10.1016/j.cmet.2018.02.011.

[58] H. Bulluck and D. J. Hausenloy, "Modulating NAD+ metabolism to prevent acute kidney injury," *Nat. Med.*, vol. 24, no. 9, pp. 1306–1307, 2018, doi: 10.1038/s41591-018-0181-9.

[59] A. Petrosyan *et al.*, "A glomerulus-on-a-chip to recapitulate the human glomerular filtration barrier," *Nat. Commun.*, vol. 10, no. 1, 2019, doi: 10.1038/s41467-019-11577-z.

[60] F. Schutgens *et al.*, "Tubuloids derived from human adult kidney and urine for personalized disease modeling," *Nat. Biotechnol.*, vol. 37, no. 3, pp. 303–313, 2019, doi: 10.1038/s41587-019-0048-8.

[61] K. I. W. Kane *et al.*, "Automated microfluidic cell culture of stem cell derived dopaminergic neurons," *Sci. Rep.*, vol. 9, no. 1, pp. 1–12, 2019, doi: 10.1038/s41598-018-34828-3.
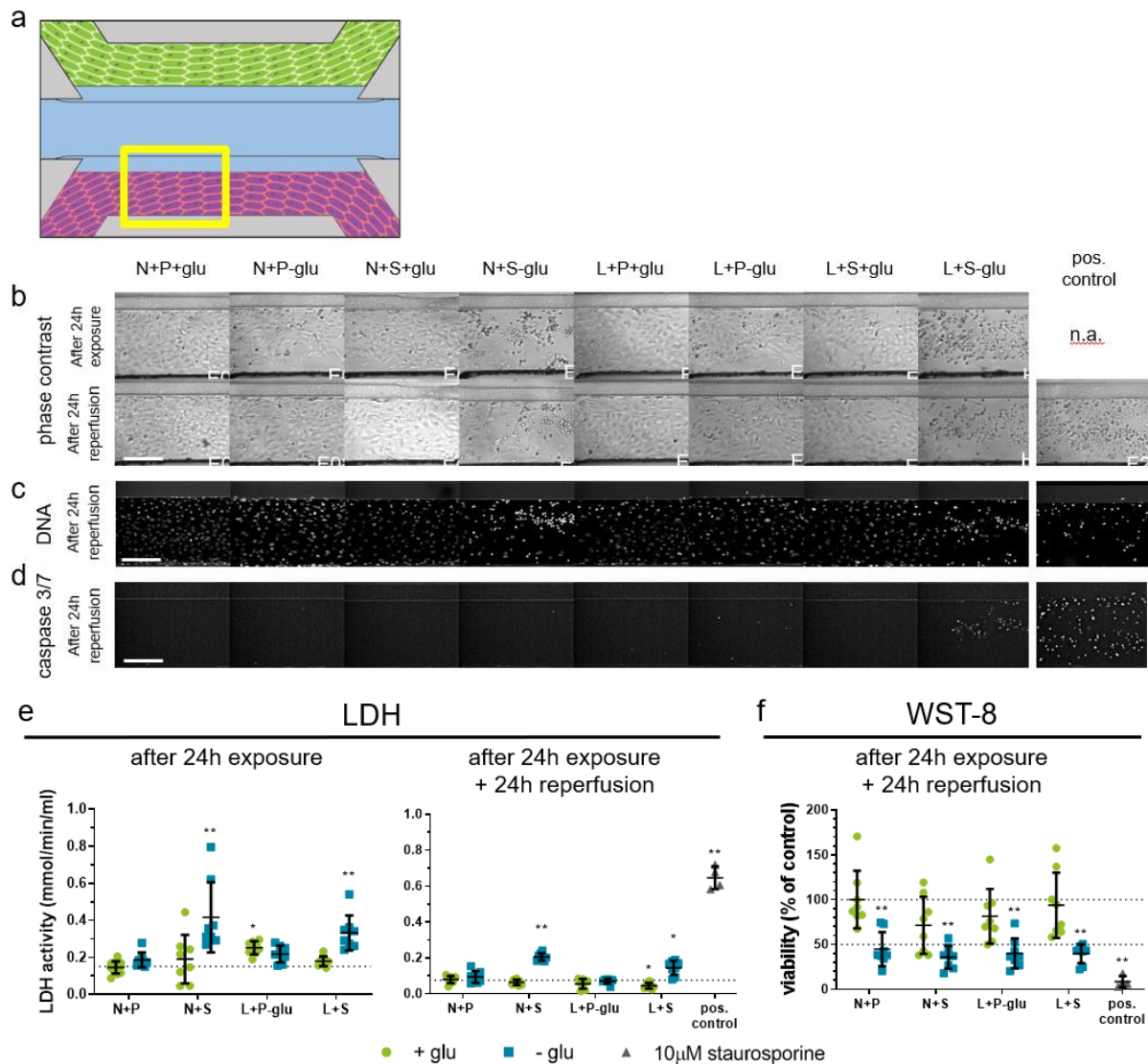
5

Supplementary Data

Figure S1: **Modelling AKI upon ischemic parameter exposure showing results of HUVEC.** *Ischemia was modelled on the OrganoPlate by exposing the coculture to a combination of low oxygen (L), static incubation (S), and glucose and nutrient poor medium (-glu) for 24-hours, followed by a 24h reperfusion in normoxia (N), perfusion on the rocker (P), and in glucose and nutrient rich medium (+glu).* **a** *Region of the HUVEC vessel (yellow square) that is used for the images shown in b-d.* **b** *Representative phase-contrast images after 24-hour exposure (top) and subsequent 24-hour reperfusion (bottom). Different ischemia inducing conditions were tested (columns) and compared to the normal condition N+P+glu. N.a.= not available.* **c** *DNA staining after 24h reperfusion.* **d** *Caspase 3-7 staining after 24h reperfusion. Scalebar = 200µm.* **e** *LDH release in the medium was measured after 24h exposure (left) and 24h exposure plus 24h reperfusion (right) respectively.* **f** *WST-8 viability relative to the normal condition N+P+glu was assessed after 24h reperfusion. 10µM staurosporine was included as a positive control. Error bars represent standard deviation. One-way ANOVA compares the conditions to the N+P+glu control condition, ** p<0.01 n=8-16 chips per condition.*
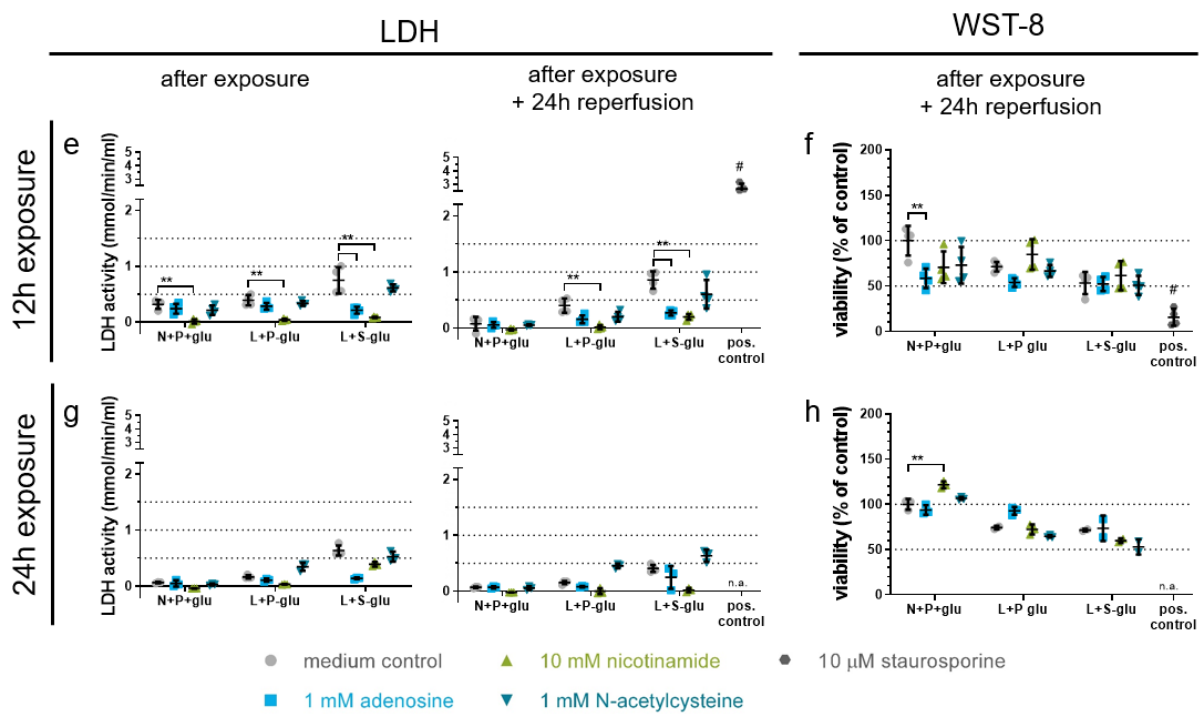
12-hour exposure + re-perfusion

24-hour exposure + re-perfusion

a

b

phase contrast

Medium | Adenosine | Nicotine amide | N-acetyl cysteine

N+P+glu | L+P-glu | L+S-glu

c

d

DNA

n=4

n=3

Representative images. Scalebar = 200 μm.
N=normoxia, H=5% O2, R=rocker (perfusion), S=static (no perfusion), glu=glucose.

LDH

WST-8

after exposure

after exposure + 24h reperfusion

after exposure + 24h reperfusion

e

f

12h exposure

g

h

24h exposure

● medium control   ▲ 10 mM nicotinamide   ● 10 μM staurosporine
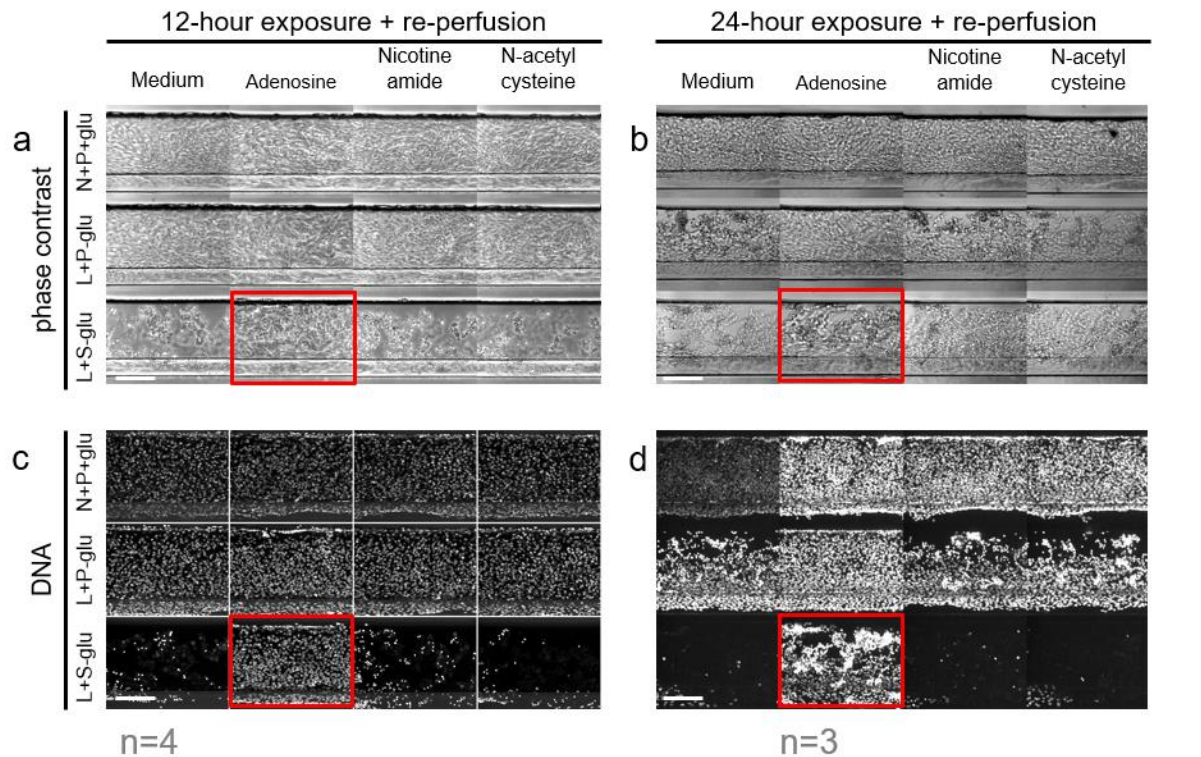
■ 1 mM adenosine   ▼ 1 mM N-acetylcysteine

148

*Figure S2: **Repetition of experimental data presented in figure 5 of the main text. Cultures were exposed to the selected ischemic conditions L+P-glu and L+S-glu for either 12 or 24 hours, followed by a 24 hour reperfusion, in the presence of adenosine, nicotinamide or N-acetylcysteine. N+P+glu medium only is the normoxic control condition. a-d** A zoom of the RPTEC tubule (see Fig. 4b) was imaged after 12-hour exposure and reperfusion (**a, c**) or after 24-hour exposure and reperfusion (**b, d**). Red squares indicate a protective effect of adenosine compared to the medium control of the same ischemic condition in phase contrast imaging and DNA staining. Scalebar = 200µm. **e-h** After the ischemic exposure of either 12 hours (**e, f**) or 24 hours (**g, h**) and a reperfusion of 24 hours for both, medium from the RPTEC channel was sampled and analyzed for LDH activity (**e, g**) and WST-8 viability relative to the N+P+glu medium control (**f, h**) was determined. One-way ANOVA compares the co-incubations to the medium control of the same ischemic condition, * p < 0.05, ** p<0.01. # indicates the positive control differs significantly with all medium controls (p<0.01). Error bars represent the standard deviation. 10 µM staurosporine was included as a positive control. n=3-4 chips per condition.*
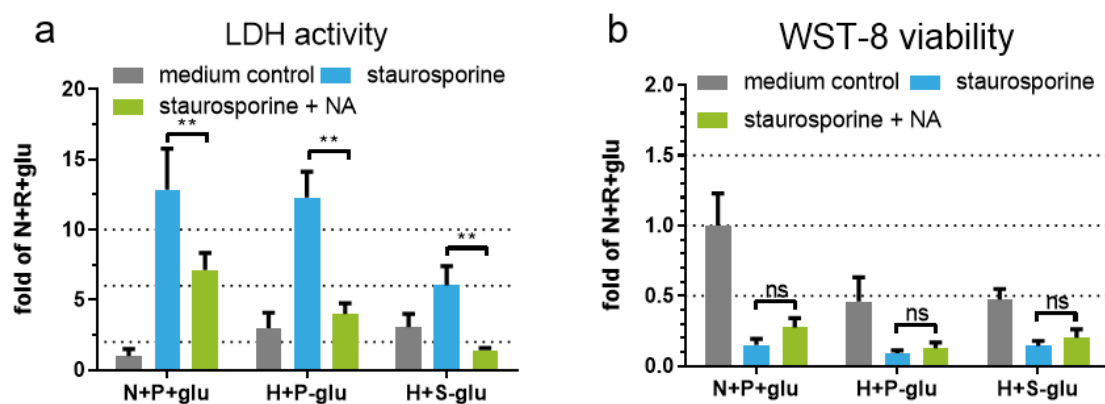

*Figure S3: **LDH activity and WST-viability measured on cocultures exposed to staurosporine with and without co-incubation of nicotinamide (NA). a** LDH activity was significant lower when cocultures exposed to staurosporine were co-incubated with NA. **b** WST-8 viability was not significant higher when cocultures exposed to staurosporine were co-incubated with NA, indicating no protective effect of NA. ** p<0.01. ns: not significant. Error bars represent the standard deviation. n=4-8 chips per condition.*

Supplemental movie for figure 6 will be available online when published

5

Chapter 6

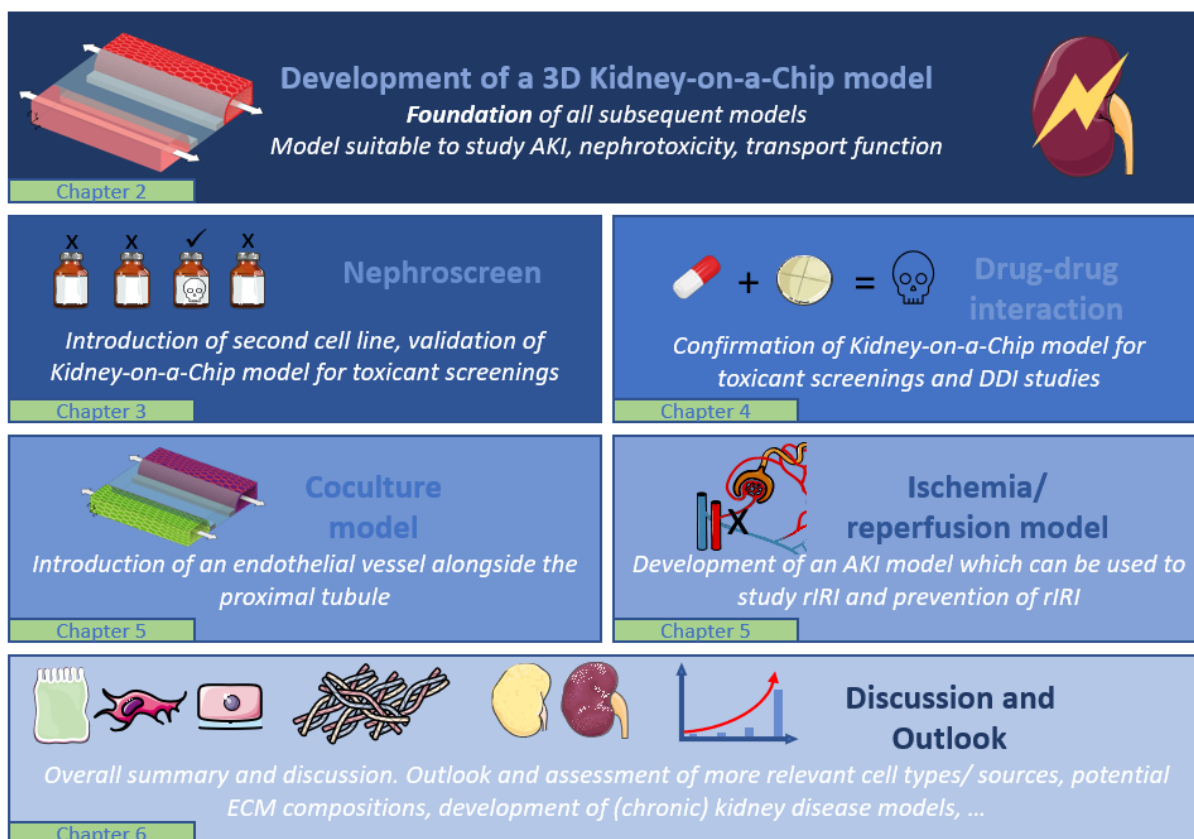## Overall Discussion, Future Perspectives, and Summary

Figure 1: Development of the Kidney-on-a-Chip, the initial model (chapter 2), which was a general foundation for all subsequent models developed over the course of this thesis. The initial model was validated as a screening platform through a panel of 12 different compounds on 2 proximal tubule cell sources (chapter 3). To be able to broaden the sensitivity of the system a second proximal tubule cell source, ciPTEC-OAT1 was introduced. Using knowledge obtained in the toxicant study a Drug-drug-interaction (DDI) study was performed which confirmed the stability of the model for testing nephrotoxic drugs (chapter 4) and their interaction. In Chapter 5 a coculture model was introduced by adding an endothelial vessel adjacent to the proximal tubule. This model was subsequently used to study renal ischemia reperfusion injury of the tubule and the vessel. In chapter 6 a summary of the thesis including a general conclusion is provided. Suggestions for new research areas are discussed which can be undertaken using the model developed here.

Development of a kidney-on-a-chip platform

The number of 3D human tissue models increased remarkably during the last years. This has been a development driven by the limitations of 2D cell culture, the strive to reduce and replace animal testing, and the small percentage of new drug compounds which enter clinical trials. 2D cell culture models of the kidney have not accurately predicted nephrotoxicity, as cells lack some physiologically-relevant characteristics. These characteristics include correct polarization and the possibility to culture on a permeable surface which resembles the extracellular matrix (ECM) with its interstitial fluid on the basal side and the exposure of the cells to shear stress on the apical side of the cell membrane [1], [2]. There are both ethical and physiological reasons to reduce animal testing in drug research. Pressure from society, but also rising costs of animal studies, support the aim to develop alternatives [3]. In addition to that, there are significant differences between physiology of humans and animals, as example for the kidney there is a difference in expression of important drug transporters [4], [5]. Finally, when animal models incorrectly predict human response to the tested drugs and toxicity is only detected subsequently in clinical testing this can lead to high costs or even worse to health-threatening problems in humans [6].

The aim of this thesis was to develop an *in vitro* model with which it is possible to study safety and efficacy of a range of drugs. We hypothesize that such an *in vitro* model at the very least has to offer the following key aspects which we consider crucial for a successful nephrotoxicity-predicting test platform:

- 3D culture of epithelial cells
- Fluid shear stress
- Correct polarization of cells
- Leak tight barrier formation against a natural surface
- No artificial membranes
- Apical and basal access
- High-throughput platform
- Renal cell source expressing key transporters of proximal tubule cells
- Coculture possibilities
- High reproducibility of experimental outcomes
- Commercial availability

The aim was to characterize the model by testing the safety and efficiency of known drugs. In **chapter 2** we describe the development of a model which combines most of the listed points. Human renal proximal tubule cells (RPTEC) were seeded to form tubular structures against a collagen 1 gel into the OrganoPlate® 3-lane. Fluid shear stress was resembled by introducing a gravity-driven flow through the system after placing the OrganoPlate on top of an interval rocker system. In the supplementary data set of **chapter 2** we showed that perfusion is crucial for tube

formation. However, the importance of flow is not only important for the tube formation, but it was also shown that fluid shear stress increased the transport capability of proximal tubule cells grown in the OrganoPlate [7]. Similar observations were published by several other authors, showing that shear stress indeed affects the phenotype and transport function of proximal tubule cells [8]–[13].

For the development of our model, we used a commercially available kidney RPTEC control cell line (SA7K clone). We could demonstrate that these cells exhibit correct polarization and formed leak tight barriers. Polarization of cells was confirmed by immunofluorescence staining depicting one primary cilium per cell pointing to the lumen of the tubules. Cilia function as sensors for fluid flow and as a controlling unit for cell proliferation [14]. Moreover, microvilli, which are covering the brush boarder of the epithelial cells, were exclusively present on the apical surface. Microvilli are responsible for mechanosensing the flow [15] and they play an important role increasing the apical surface for better re-absorption capabilities [16].

Using an immunofluorescent staining and a barrier integrity assay, it was demonstrated that the RPTEC formed leak tight barriers. Tight junctions were found at cell-cell connections, which were visualized using the tight junction marker zonula occludens (ZO)-1 [17]. The tightness of these junctions was validated by a barrier integrity assay which we developed [18], [19] in the course of this thesis for the OrganoPlate system. The tubules were flushed with a medium which contained fluorescent dextran dyes of different sizes. The apparent permeability of the different sizes of dextran could be calculated by measuring the intensity of the dyes at both sides of the epithelial barrier, followed by calculating the ratio of the receiving ECM compartment behind the barrier and the perfused channel. The barrier integrity assay opened a vast array of possibilities which we could use to analyze our model. We used it to determine at which time point after seeding the tubules grew tight barriers against the collagen 1 gel and exposures could start. Furthermore, we could use the barrier integrity assay for time-to-leak experiments by monitoring real-time when the barrier function was affected by a toxic compound [20]. For the analysis of the proximal tubules, we mainly used the assay as an endpoint assay after a toxicant exposure. Just recently, a new device to measure the tightness of barriers was developed for use in the OrganoPlate: A machine which is able to measure trans-epithelial/endothelial electrical resistance (TEER) of the cell barriers formed against the collagen 1, called the OrganoTEER® [21]. The OrganoTEER can already be successfully used to study the differences in tightness of cell barriers with high TEER values. Proximal tubules are known to be a comparably leaky epithelium with very low TEER values of 6-10 ohm/cm^2 [22]. In the first experiments we could already measure values which fall into this range, though we could not use the device for analyzing the barrier function after toxicant exposures, as these values are around the detection limit of the analyzing software. However, further work which will ensure that the OrganoTEER will be able to pick up differences

in barrier tightness of even small TEER values in the near future is ongoing, and promising results to this end are already achieved.

The proximal tubule-on-a-chip model was set up in the OrganoPlate 3-lane, which enables access to the tubule from the basal and the apical side. Combining this important specification with the characteristics of correct polarization and leak tight barriers as described above, the platform can be used as an ideal model for trans-epithelial transport experiments. Two different methods were used to show active transport of cationic compounds : measuring the compound concentration intra-cellular and trans-epithelial transport across the cell membrane. The transport function could be successfully inhibited, proving the existence of active transport. Even though the transport function of cations by the RPTEC (SA7K clone) could be shown, these cells lack some of the key transporters which are crucial for transporting anions. In **chapter 3** a second epithelial cell source was introduced to overcome this problem: conditionally immortalized proximal tubule epithelial cells overexpressing xenobiotic organic anion transporter 1 (ciPTEC-OAT1) [23]. Using ciPTEC-OAT1 we were able to set up a test platform which we could use to detect the toxicity of both active transport dependent drug types; cations and anions. By combining the two cell types with a broader panel of compounds and readout assays a screening platform was developed, called the nephroscreen. We could show that the platform and the protocols are robust and reproducible. In parallel with the development of the nephroscreen a drug-drug interaction (DDI) study was performed on RPTEC, as described in **chapter 4**. The study in **chapter 4** was designed to determine if we can use our proximal tubule-on-a-chip model in a DDI study using a panel of multiplexed assays to examine the toxicity of single and combined dosages of human immunodeficiency virus (HIV)-targeting drugs. HIV-patients are commonly treated with the drug Genvoya which replaced Stribild in the recent years. Both are tenofovir-containing medications and are supplied as pills with a combination of active compounds, namely emtricitabine, elvitegravir and cobicistat, and one of the prodrugs of tenofovir, tenofovir disoproxil fumarate (TDF) or tenofovir alafenamide (TAF). Of all the ingredients in these pharmaceutical formulations, in particular the drug-related nephrotoxicity of tenofovir is widely accepted. Our goal was to investigate if we are able to detect a toxic effect on the proximal tubule cells by one of the two tenofovir prodrugs, especially when combined with one of the additive compounds. One major difference between these two prodrugs is that TDF is not stable when in contact with human plasma, where it quickly undergoes hydrolysis into parent tenofovir, whereas TAF has a much higher stability which results in a higher antiviral activity and reduced dosages compared to TDF. In **chapter 3** we could show that the parent form of tenofovir had a cytotoxic effect on ciPTEC-OAT1 whereas no effect could be measured on RPTEC. As the parent form of tenofovir is transported via the anion pathway (mainly via OAT1) into the cells this was an expected result. However, in the present study we used RPTEC. When we tested the two prodrugs, TDF did not lead to a damaging effect on the proximal tubules, which was expected considering that TDF is hydrolyzed into the parent form of tenofovir when in contact with culture medium. Interestingly,

TAF showed a damaging effect to the proximal tubules at similar concentrations which we found to be toxic for parent tenofovir in the OAT1 expressing cells. These results showed us, that the compound TAF is indeed stable when in contact with serum and is not hydrolyzed into the parent form of tenofovir. Moreover, it is very likely that TAF is not assimilated by the cells via OAT1 transport, which was already suggested before by Bam et al. [24]. Inside of the cells TAF is then converted to parent tenofovir via hydrolysis by intracellular proteases [24], [25].

The two prodrugs of tenofovir are not administered on their own, but in combination with three other antiretroviral agents, namely elvitegravir, cobicistat, and emtricitabine [26], [27]. Next to testing the two prodrugs in single dosages we performed a co-treatment of the prodrugs with the goal to assess if any of them amplifies the cytotoxic effect of the two tenofovir prodrugs. Our results suggest, that even at high concentrations emtricitabine did not have a damaging effect on the proximal tubules, in isolation or in combination with one of the two prodrugs of tenofovir. Elvitegravir did not have an enhancing effect on the cytotoxicity when dosed in combination with TDF. However, when dosed together with TAF elvitegravir strongly enhanced its damaging effect, and super-additive synergistic effects were measured. This result was surprising as elvitegravir is thought to not affect the kidneys but is mainly eliminated via hepatobiliary excretion [28]. To develop a full picture of the toxicity of the co-administration of tenofovir and cobicistat additional research could be undertaken by combining the proximal tubule model with a liver model. When cobicistat was dosed alone, a damaging effect could be already be detected. A combination with TDF led to an increased damage which could be picked up in all assays. A combination of cobicistat and TAF led to an increased cytotoxicity which was detected for the low as well as the high dosed combinations.

The study in chapter 4 indicates that in future studies drugs should be tested in the cocktail they will be administered clinically. However, during *in vitro* experiments some of the drugs might be incorrectly dosed, as *in vivo* they would be metabolized quickly by the liver or cleared via the gut. To overcome this problem a possible solution could be to connect the present model with a liver-on-the-chip system and/or a gut-on-a-chip system. Or, include pharmacokinetic modeling to choose proper concentrations for experiments.

In **chapters 2-4** we mainly focused on acute kidney injury (AKI) as a result of an acute reaction to a nephrotoxicant. Next to these toxicant models we were also interested if we are able to develop a disease model for treatment related toxicity which we can use to screen the protective effect of drugs. To achieve this, we added 3 new aspects to our model which we described in **chapter 5**: coculture with an endothelial vessel, induction of AKI caused by an ischemic insult, and the assessment of compounds that have a protective effect during the ischemic event leading to AKI. For the development of the coculture model, we expanded the kidney on a chip developed in **chapter 2** by introducing endothelial cells to the second perfusion channel. We characterized the culture using immunostaining for cell type specific markers and ensured correct polarization. We

validated AKI-associated read-outs through exposure of the coculture to known nephrotoxicants. To study ischemic events in the kidney the coculture was exposed to ischemia through a combination of low oxygen, reduced glucose, and flow interruption conditions. Subsequently, cultures were reperfused under normal conditions to trigger reperfusion damage. Injury was quantified through morphological assessment, caspase-3/7 activation, viability assessment, and lactate dehydrogenase release. Low oxygen, reduced glucose and interrupted flow were detrimental to the tubules in any combination of two, whereas the combination of all three led to the most severe damage. This effect was strongly amplified upon reperfusion. The effect of ischemic conditions on the endothelium was less severe than on the epithelium.

For the assessment of protective compounds adenosine, nicotinamide, or N-acetylcysteine were added to the culture medium of the proximal tubule and the endothelial vessel during the exposure and reperfusion. Adenosine was shown to have a significant protective effect, whereas no such effect was found for nicotinamide, and N-acetylcysteine.

In **chapter 5** we were able to show that AKI induced by Renal ischemia/reperfusion injury (rIRI) can be effectively modelled in this perfused 3D kidney coculture setup. The robustness of the model and assays in combination with the throughput of the platform make it ideal to study the effect of AKI-preventing compounds and enable development of novel therapeutic modalities.

One unique aspect of the system developed in this study is the commercial availability of the platform, which was also one of the conditions of the crack-IT challenge described in **chapter 3**. This opens the possibility that the platform is not only used and improved by our research team, but it can be rapidly improved, similar to open source software, by an unlimited number of research groups.

Towards a functional nephroscreen

The model which we developed in **chapter 2** as part of a NC3R crack-IT challenge was called the nephroscreen. The development of the nephroscreen was a joint project of a consortium consisting of 4 different parties: Mimetas, Fachhochschule Nordwestschweiz, Radboud University Medical Center Nijmegen, and Utrecht University. The goal of the nephroscreen project was to develop a proximal tubule-on-a-chip platform capable of accurately identifying nephrotoxic effects using human cells (**chapter 3**). The nephroscreen was primarily designed to fulfill the requirements of the sponsors, which were exclusively pharmaceutical companies: developing a platform which can be used to reduce the costs and increase the predictability of pre-clinical studies. During the development of the nephroscreen a second proximal tubule cell source was used: ciPTEC-OAT1 developed by one of the consortium partners. ciPTEC-OAT1 showed a significantly higher sensitivity during transport studies while RPTEC were used when the barrier function of the tubules was of interest. By combining these two cells sources, a compound panel of the proximal tubule of in total 12 compounds was screened for its toxicity. Four of these

compounds were known nephrotoxicants which were also used to set up the different assays. Eight compounds were unknown as they were provided by the sponsors of the study. We could show that the majority of the provided compounds did have a nephrotoxic effect on the nephroscreen. The effect of one compound on the nephroscreen could only be detected during the transport studies as this compound did not have an effect in any other of the other assays. A second compound showed an interaction with P-glycoprotein (P-gp) and a mild effect on an increased level of microRNAs (miRNAs), but again no damaging effect on the viability of tubular integrity of the tubules. One of the compounds did not show any cytotoxicity during the initial study, therefore we tested it in a long-term experiment where the exposure was performed for 11 days instead of 48 hours. This study showed that for some compounds a long term study is able to demonstrate toxicity, which was not picked up in the 48 hour experiment. For future experiments using the nephroscreen it would be recommended to divide the experiments performed on the nephroscreen into 2 phases. In phase 1, a 48-hour long initial testing of a broad panel of compounds should take place, followed by a second phase where only compounds are tested which did not show an effect in the initial phase.

To ultimately install the nephroscreen as a screening platform for drug research at pharmaceutical companies, steps have to be taken to ensure the reproducibility of the experiments. This can be done by implementing standard operating procedures which are in line with the guidelines of Good *In vitro* Method Practices, which were published by the Organization for Economic Co-operation and Development in 2018 [29]. If these guidelines are followed, the platform is ready to be used in short term to test compounds prior to testing them *in vivo*. Here, it would be important to carefully compare the results of each study, *in vitro* on the nephroscreen, *in vivo* on animals and ultimately *in vivo* in humans in clinical studies to investigate the predictive potential of the nephroscreen compared to animal studies. We hope that this will ultimately result in omitting animal tests for drug development and replacing them by *in vitro* models.

As mentioned before, the nephroscreen, including the protocols, the platform, and the cells are commercially available. This will help to improve the suitability of the nephroscreen towards a widely accepted platform during pre-clinical studies. Just recently our system was used to set up a glomerulus-on-a-chip model [30] which shows that our system aligns with the current research interests.

Development of an ischemia model which can be used to study the preventive effect of compounds

Renal ischemia/reperfusion injury, together with nephrotoxicity, is one of the major causes of AKI caused by tubular damage after an insult. In **chapter 5** we continued to develop our model so it could be used to study renal ischemia. Ischemia is a sudden restriction of blood supply of an organ. With our model we could show that not only the exposure to renal ischemia caused damage to the tubules, but also that more severe damage was seen after the reperfusion. During the

exposure and reperfusion, a co-incubation with potential protective compounds was performed. One of the compounds – adenosine – showed strong protective capabilities with tubules nearly completely recovering, whereas the control without adenosine was highly damaged after the reperfusion period. The protective effect of adenosine was also observed in an *in vivo* study by Lee and Emala [31]. Here, rats were preconditioned with adenosine before hypoxia exposure and reperfusion, which was favorable for renal function and morphology. In addition, Lee and Emala investigated which of the adenosine receptors (AR) were involved in this effect. By administering AR agonists and antagonists, they discovered that AR1 is most likely involved in protecting against ischemic AKI. An interesting follow-up study would be to analyze the gene expression in our kidney-on-a-chip model, to see if it can be confirmed that AR1 signaling is the pathway which is responsible for protecting against ischemic AKI.

The most severe scenario of rIRI is when perfusion is stopped completely, radically reducing nutrient and glucose supply, and applying low oxygen. But it is also possible to test one of these conditions separately. Hypoxia for example can be caused by multiple events which lower the oxygen concentration in the blood. Hypoxia is associated with moderate-to-severe pneumonia which can be a result of an infection with a respiratory virus like the novel acute respiratory syndrome coronavirus 2 (SARS-CoV-2) [32]. Here the platform could possibly be used to study compounds which have a potential protective effect. Our kidney-on-a-chip platform which we developed in **chapter 2** was already recognized as a potential platform to study AKI associated with SARS-CoV-2 [33]. The results obtained in **chapter 5** suggest that the use of the kidney-on-a-chip platform for these types of research could be feasible on short term.

Adding more complexity: Cocultures of the proximal tubule

In **chapter 5** the development of a coculture of proximal tubule cells with endothelium is described. For future investigations of the drug safety, cocultures will play a crucial role during the development of test models. The developed model could nicely show the suitability of even a quite simple model using a RPTEC cell line in combination with Human umbilical vein endothelial cells (HUVECs). Both cell types are not the perfect cell types to be used for the end model. For future optimization it would be better to use more relevant proximal tubule cells in combination with endothelium from the kidney. When the model was set up in 2017, endothelial cells from the kidney were used. Unfortunately, these cells did not form vessel structures and were therefore not sufficient to be used for setting up the ischemia model. With more companies offering new cell lines, among others induced pluripotent stem cells (iPSc), new cell sources will bring the current model to a new stage of predicting nephrotoxicity.

The combination of the kidney model with other organs like the liver or the gut system will likely be an important research area in the future. These organs also play an important role in the elimination of waste products from the body. Several systems can be studied: systems which offer the possibility to connect the different organ systems with each other, so-called body-on-a-chip

systems, or even simpler systems which are cultured in parallel and where only the conditioned medium is exchanged.

Future directions for model optimization

Optimization of the proximal tubule-on-a-chip using a more physiologically-relevant cell type

For this thesis two renal proximal cell types were used – RPTEC from Sigma-Aldrich and ciPTEC-OAT1 developed at Radboud University in Nijmegen. Only the combination of both cell lines was an adequate model for the validation of the nephroscreen model. RPTEC from Sigma are a pseudo-immortalized human kidney proximal tubule cell line (SA7K clone) generated via zinc finger nuclease-mediated knockout of a cell cycle protein [34]. ciPTEC are proximal tubule cells which were derived from human urine. These cells contain the temperature-sensitive vector SV40tsA58, allowing the cells to proliferate at 33 °C and differentiate at 37 °C [35]. This cell model was further optimized by Nieskens et al. [23] who were able to establish two additional cell lines from ciPTEC which express stable xenobiotic transporters organic anion transporter 1 and 3 (OAT1 and OAT3). OAT1 and OAT3 are the most abundant influx transporters of the proximal tubules mediating the anion transport into the pre-urine. When we compared the gene expression levels of the OAT1 expression, expression RPTEC was close to the detection limit and expression of OAT1 in ciPTEC-OAT1 was more than 150 times higher than in RPTEC . However, when ciPTEC-OAT1 are cultured in the OrganoPlate against collagen 1 cells do not form a barrier against the ECM which makes them unsuitable for use in barrier assessment.

In Table 1 available cell types and cell sources which have a potential to be cultured in the OrganoPlate similarly to the RPTEC and ciPTEC-OAT1 are summarized. For seeding cells to the 3-lane system it is of importance that the cells are added as a single cell solution to the perfusion channel. In the following paragraphs some of the most promising cell sources for future models are described in more detail.

In collaboration with the Hubrecht Institute tubuloid-derived adult stem cells from mouse kidney organoids were cultured in the OrganoPlate 3-lane system [46]. It could be shown that these cells form polarized tubular structures with clear distinction of the apical and basal side of the cells. Barrier formation of the cells against the ECM was confirmed by perfusing the lumen of the tubes with dextran dyes added to the culture medium [18]. We assessed transport function of the formed tubuloids on a chip using the assay developed in **chapter 2** of this thesis by exposing the cells to calcein-AM in presence or absence of PSC833, a non-immunosuppressant cyclosporine analogue that functionally inhibits P-gp [47]. Intracellular accumulation of calcein was significantly higher in the presence of PSC833, demonstrating activity of P-gp [46].

Table 1: Cell types and cell sources that are available for modeling of (future) Kidney-on-a-Chip models and their pros and cons, including some examples (content of table partly adapted from [36])

Cell type	Pros	Cons	Examples	References
Primary cells	*In vivo* morphology of the tissue source is usually maintained Allows donor specific analysis (personalized toxicity prediction) Easy to isolate Compatible with high-throughput screening and advanced imaging techniques	Differences between donors Limited availability Low throughput (because of limited lifespan) Inter-donor variability Functional changes during passages	Primary RPTEC	[37]–[39]
(Immortalized) Cell lines	High proliferation rate High reproducibility (homogenous population) Ease of use Decent amount of data available Cost-effective	Crucial transporters are absent Do not represent the complete spectrum of proximal tubule characteristics	RPTEC (SAK7 clone), HK-2, HEK 293, ciPTEC OAT1, ciPTEC-OAt3, RPTEC/TERT1	[23], [34], [40]–[44]
Human iPSCs	Easy to isolate Allows donor specific analysis (personalized toxicity prediction) Disease-specific *in vitro* cell-based models Expression of (all) relevant drug transporters?	Not completely characterized Complexity of culture protocol Genetic instability during long culture periods	iPSC differentiated into human primary renal proximal tubular cells	[45]
Derived adult stem cells from organoids	Allows donor specific analysis (personalized toxicity prediction) Direct expansion of patient-derived renal tissue	Heterogenous population (proximal, distal, loop of Henle, collecting duct) Culture conditions usually biased for one cell population (e.g. proximal tubule)	Tubuloid-derived adult stem cells from mouse kidney organoids	[46]

6

161

The trans-epithelial transport function of the cells could be demonstrated using rhodamine 123, which is transported into the cells from the basal side by organic cation transporters [48] and released to the lumen by P-gp [49]. Rhodamine 123 was added to the basal side of the tubes in the presence or absence of the P-gp inhibitor PSC833. In presence of PSC833 the apparent permeability was reduced significantly, suggesting a P-gp dependent efflux inhibition of rhodamine 123. Next to using cell lines with defined characteristics like the above introduced RPTEC, this model has a high potential to also be used with pluripotent stem cell-derived organoids, which would allow personalized studies on transporter-function and drug-interaction studies [46] and ultimately replace the RPTEC cell line in the future.

Recently a new promising cell source of RPTEC got commercially available on the market – RPTEC-tert1 [42], [44]. In addition to the parent version of the cells ATCC offers three modified versions which either overexpress transporter genes OAT1, OAT3, or OCT2. The parent version of RPTEC-tert1 was already used in a kidney-on-a-chip platform with promising results resulting in confluent tubules growing tight barriers against an ECM [50]. This makes them an interesting cell source to test in the OrganoPlate.

The market of renal proximal tubule cells is slowly growing and offering various newly developed proximal cell tubules sources. First studies by K. Kandasamy *et al.* [45] which use human iPSC from the kidney suggest a higher accuracy in predicting nephrotoxicity induced by drugs compared with using primary human proximal tubule cells.

In conclusion, we can say that new proximal tubule cell sources have a high potential. They may be of assistance to further develop the proximal tubule-on-a-chip model which to its end can reliably predict renal toxicity and can be used for a broad variety of pre-clinical drug studies and ultimately for complex disease studies.

ECM composition investigation of the proximal tubule-on-a-chip

3D cell cultures require an environment which is as similar as possible to the *in vivo* situation. This environment can be modeled on a huge number of different 3D culture platforms. In the last 15 years the number of publications describing 3D systems grew rapidly [51]. However, the first studies on 3D culture were already conducted 50-60 years ago, as summarized by Mina Bissell in 1982 [52] who was one of the first researchers studying the importance of the ECM on the cell behavior in *in vitro* systems. What all of these culture platforms have in common is that they all make use of an ECM environment. The ECM in the human body is a non-cellular component, which serves as a scaffold for diversity of different cell structures but also plays a huge role in the tissue morphogenesis, differentiation and homeostasis [53]. The ECM is comprised of water, proteins, and polysaccharides. However, the composition of the ECM is unique for each tissue. In the tubulointerstitium of the kidney collagen type I and collagen type III are the most abundant proteins, whereas in the basement membrane of the proximal tubule collagen type IV and laminin

are predominant, which networks are connected via perlecan and nidogen [54], [55]. Collagen of the interstitial space is produced by fibroblasts [56], whereas the basal laminar is produced by the epithelial cells themselves [55]. With fluorescent immunohistochemical stainings we could show that our RPTEC model was positive for the basal membrane proteins laminin, perlecan, and nidogen. This suggests that the basement membrane is indeed remodeled by the cells (figure 2). When developing our kidney on a chip model which was eventually used in thesis, we ended up successfully using an ECM gel made from rat tail collagen 1. We could show that collagen 1 imitates the tubulointerstitium of the kidney quite accurately. Here, it could be of high interest to investigate if an addition of collagen type III to the mixture would offer advantages. Another important aspect to consider when using ECM is their origin. All ECM components which we used originated from animal material. Therefore, future studies on animal-free ECMs are highly recommended. For general research synthetic ECMs could be a solution to overcome batch to batch variances and pave the way for standardized and reproducible compound investigations.

6
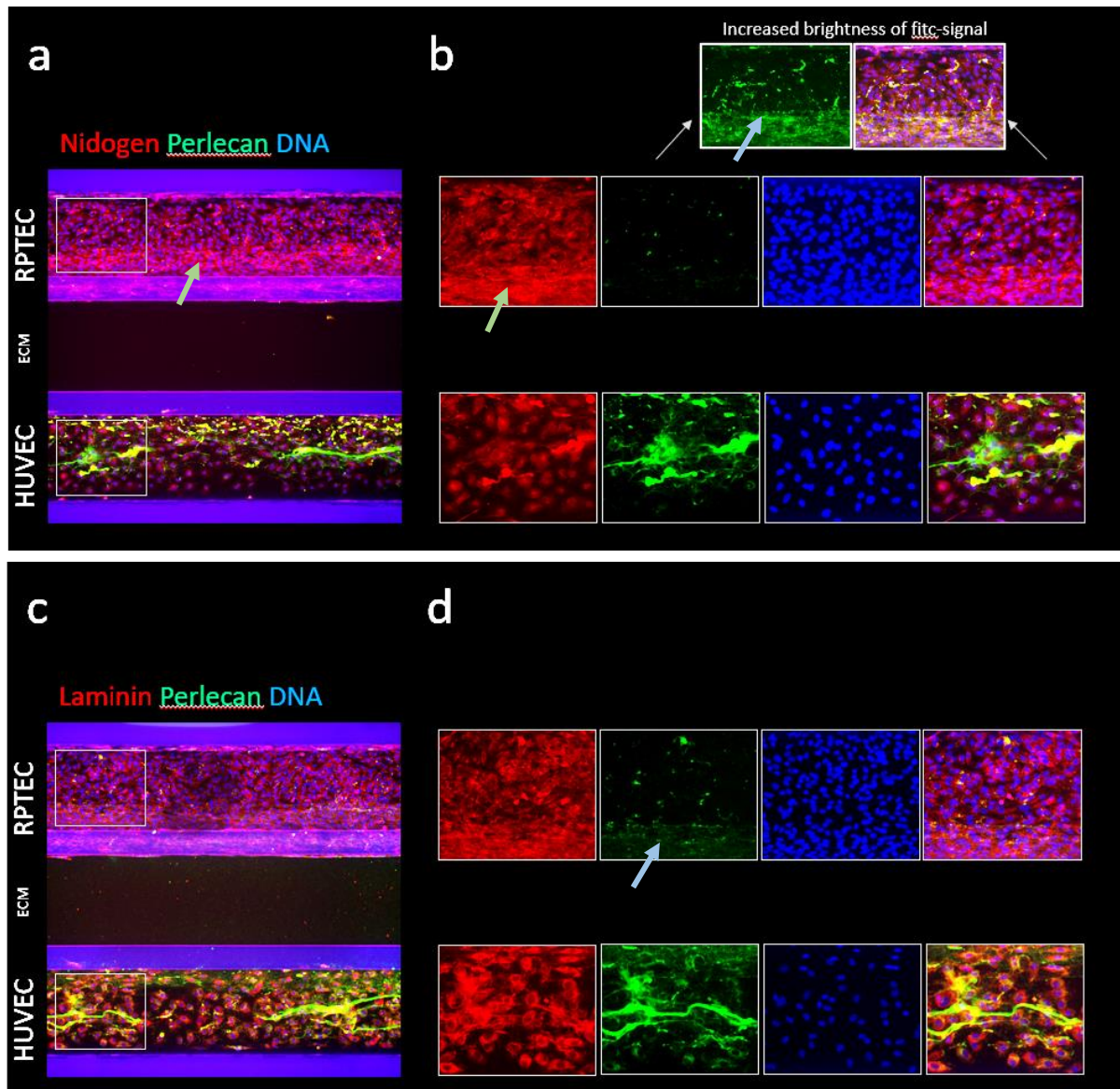
*Figure 2: **Marker expression of the kidney model shows presence of basal membrane proteins laminin, nidogen and perlecan of the coculture of RPTEC and HUVEC. A, C** z-projections of the coculture with the RPTEC tubule in the top channel and the HUVEC vessel in the bottom channel. **B, D** Zoom-in of the z-projections. **A, B** Nidogen (red) is expressed by both cell types, though the expression is more dominant in the epithelium with a higher expression at the cell/ECM interface. **A-C** Perlecan (green) expression is significantly higher expressed in HUVEC, though this appearance is dominated by strings. These strings appeared to be atypical staining. Perlecan was less expressed by the epithelial cells than endothelial cells. Expression is almost exclusively found at the cell/ECM interface with an even higher difference compared to Nidogen. **A, C** Laminin (red) is expressed equally by both cell types, with no significantly higher expression at the cell/ECM interface.*

The use of human derived ECMs could open possibilities to study donor-specific medical conditions, for instance matrix metalloproteinases which are suggested to play a role in tubulointerstitial fibrosis [57].

Conclusion

Pharmaceutical companies, governments and the general public have become increasingly aware that animal models used in drug testing lack some vital aspects in the endeavor to serve as an accurate representation of human biology. As these models of the human body should be more physiologically relevant, animal models no longer suffice because the response of animal cells often differs from the response of human cells. In their place, *in vitro* cell culture models with 3D architecture, microfluidics and high throughput capabilities are a promising technology and are currently getting in the limelight of drug research. These 3D models can be developed in such ways that they will likely surpass animal models on important aspects like resemblance to a human body, predicting safety and efficacy of compounds, high throughput testing capabilities, ethical aspects, and costs.

To demonstrate the feasibility of such an advanced 3D invitro model, we used a microfluidic *in vitro* platform to develop a kidney-on-a-chip platform which possess the ability to reproduce the tubular response to known and unknown nephrotoxicants and compounds as seen in *in vitro* and in clinical studies. Furthermore, we assessed the response of the model to renal ischemia/reperfusion injury and could measure the prevention of tubular damage when adding protective compounds.

These findings show that 3D tissue models are able to compete with alternatives like animal models and 2D models. We actually expect that 3D tissue models are the test platforms of the future for developing new drugs.

Since research on 3D tissue models is a relatively new research field there remains a large scope for improvement. For example, the endeavor to use *in vitro* findings to confidently predict *in vivo* behavior is an area of research where 3D tissue models can play an important role. Ways of replicating different human organs on 3D chips are likely to greatly improve in the coming years, combining different chips and creating interactions between them can test the effectiveness of drugs at a whole new level. In this way the complexity of the *in vitro* 3D models can be increased, in ways which better resemble tissue responses in humans.

This could lead to testing a drug simultaneously on different organs while connecting them in ways resembling real structures in the human body and measuring responses of each different organ singularly. When these 3D tissue models are cultured in a high throughput environment huge amounts of data can be produced in short time. These data can serve as a foundation for mechanistic models using big data approaches that can be ultimately used to rapidly predict *in vivo* drug efficacy and safety.

Interesting examples of complex future applications of 3D tissue models are for instance complete *in vitro* vascularized organoids, 'body-on-a-chip' systems which can be designed for a specific test

6

to combine all relevant tissues and their interactions in order to resemble *in vivo* responses. Another example is the creation of complex disease models where the response of tissue and their interactions can be tested in a realistic way. Another potential future application of 3D tissue models is personalized medicine, where a high number of replicates of patient cell samples can be cultured in 3D on the microfluidic chips to create patient derived *in vitro* models. These cell samples can be subsequently screened for the most effective treatment for this individual patient using his own cells. In time, the further development of 3D tissue models could mean that these examples are no longer dreams but become reality.

6

References

[1] P. Y. W. Dankers *et al.*, "Bioengineering of living renal membranes consisting of hierarchical, bioactive supramolecular meshes and human tubular cells," *Biomaterials*, vol. 32, no. 3, pp. 723–733, 2011, doi: 10.1016/j.biomaterials.2010.09.020.

[2] K. J. Jang *et al.*, "Human kidney proximal tubule-on-a-chip for drug transport and nephrotoxicity assessment," *Integrative Biology (United Kingdom)*, vol. 5, no. 9, pp. 1119–1129, 2013, doi: 10.1039/c3ib40049b.

[3] M. Balls, "Replacement of animal procedures: Alternatives in research, education and testing," *Laboratory Animals*, vol. 28, no. 3, pp. 193–211, 1994, doi: 10.1258/002367794780681714.

[4] H. Kusuhara and Y. Sugiyama, "Role of transporters in the tissue-selective distribution and elimination of drugs: Transporters in the liver, small intestine, brain and kidney," *Journal of Controlled Release*, vol. 78, no. 1–3, pp. 43–54, 2002, doi: 10.1016/S0168-3659(01)00480-1.

[5] M. Aoki *et al.*, "Kidney-specific expression of human organic cation transporter 2 (OCT2/SLC22A2) is regulated by DNA methylation," *American Journal of Physiology - Renal Physiology*, vol. 295, no. 1, pp. 165–170, 2008, doi: 10.1152/ajprenal.90257.2008.

[6] G. A. Van Norman, "Limitations of Animal Studies for Predicting Toxicity in Clinical Trials: Is it Time to Rethink Our Current Approach?," *JACC: Basic to Translational Science*, vol. 4, no. 7, pp. 845–854, 2019, doi: 10.1016/j.jacbts.2019.10.008.

[7] J. Vriend *et al.*, "Flow stimulates drug transport in a human kidney proximal tubule-on-a-chip independent of primary cilia," *Biochimica et Biophysica Acta - General Subjects*, vol. 1864, no. 1, 2020, doi: 10.1016/j.bbagen.2019.129433.

[8] E. M. Frohlich, X. Zhang, and J. L. Charest, "The use of controlled surface topography and flow-induced shear stress to influence renal epithelial cell function," *Integrative Biology*, vol. 4, no. 1, pp. 75–83, 2012, doi: 10.1039/c1ib00096a.

[9] M. Essig and G. Friedlander, "Tubular shear stress and phenotype of renal proximal tubular cells," *Journal of the American Society of Nephrology*, vol. 14, no. SUPPL. 1, pp. 33–35, 2003, doi: 10.1097/01.ASN.0000067650.43083.DF.

[10] M. Essig, F. Terzi, M. Burtin, and G. Friedlander, "Mechanical strains induced by tubular flow affect the phenotype of proximal tubular cells," *American Journal of Physiology - Renal Physiology*, vol. 281, no. 4 50-4, pp. 751–762, 2001, doi: 10.1152/ajprenal.2001.281.4.f751.

[11] Y. Duan *et al.*, "Shear-induced reorganization of renal proximal tubule cell actin cytoskeleton and apical junctional complexes," *Proceedings of the National Academy of Sciences of the United States of America*, vol. 105, no. 32, pp. 11418–11423, 2008, doi: 10.1073/pnas.0804954105.

[12] S. Weinbaum, Y. Duan, L. M. Satlin, T. Wang, and A. M. Weinstein, "Mechanotransduction in the renal tubule," *American Journal of Physiology - Renal Physiology*, vol. 299, no. 6, pp. 1220–1236, 2010, doi: 10.1152/ajprenal.00453.2010.

[13] E. J. Weber *et al.*, "Development of a microphysiological model of human kidney proximal tubule function," *Kidney International*, vol. 90, no. 3, pp. 627–637, 2016, doi: 10.1016/j.kint.2016.06.011.

[14] V. Singla and J. F. Reiter, "The primary cilium as the cell's antenna: Signaling at a sensory organelle," *Science*, vol. 313, no. 5787. pp. 629–633, 2006. doi: 10.1126/science.1124534.

6

[15] Z. Du, Y. Duan, Q. S. Yan, A. M. Weinstein, S. Weinbaum, and T. Wang, "Mechanosensory function of microvilli of the kidney proximal tubule," *Proceedings of the National Academy of Sciences of the United States of America*, vol. 101, no. 35, pp. 13068–13073, 2004, doi: 10.1073/pnas.0405179101.

[16] B. A. Molitoris and M. C. Wagner, "Surface membrane polarity of proximal tubular cells: Alterations as a basis for malfunction," *Kidney International*, vol. 49, no. 6, pp. 1592–1597, 1996, doi: 10.1038/ki.1996.231.

[17] B. R. Stevenson, J. D. Siliciano, M. S. Mooseker, and D. A. Goodenough, "Identification of ZO-1: A high molecular weight polypeptide associated with the tight junction (Zonula Occludens) in a variety of epithelia," *Journal of Cell Biology*, vol. 103, no. 3, pp. 755–766, 1986, doi: 10.1083/jcb.103.3.755.

[18] M. K. Vormann *et al.*, "Nephrotoxicity and Kidney Transport Assessment on 3D Perfused Proximal Tubules," *AAPS Journal*, vol. 20, no. 5, pp. 1–11, 2018, doi: 10.1208/s12248-018-0248-z.

[19] P. Vulto, S. J. Trietsch, H. L. Lanz, and M. K. Vormann, "Barrier Function Measurements," WO 2017/007325 Al, 2017

[20] S. J. Trietsch *et al.*, "Membrane-free culture and real-time barrier integrity assessment of perfused intestinal epithelium tubes," *Nature Communications*, vol. 8, no. 1, pp. 1–7, 2017, doi: 10.1038/s41467-017-00259-3.

[21] A. Nicolas *et al.*, "High throughput transepithelial electrical resistance (TEER) measurements on perfused membrane-free epithelia," *Lab on a Chip*, vol. 21, no. 9, pp. 1676–1685, May 2021, doi: 10.1039/d0lc00770f.

[22] B. M. Denker and E. Sabath, "The biology of epithelial cell tight junctions in the kidney," *Journal of the American Society of Nephrology*, vol. 22, no. 4, pp. 622–625, 2011, doi: 10.1681/ASN.2010090922.

[23] T. T. G. Nieskens *et al.*, "A Human Renal Proximal Tubule Cell Line with Stable Organic Anion Transporter 1 and 3 Expression Predictive for Antiviral-Induced Toxicity," *AAPS Journal*, vol. 18, no. 2, pp. 465–475, 2016, doi: 10.1208/s12248-016-9871-8.

[24] R. A. Bam, S. R. Yant, and T. Cihlar, "Tenofovir alafenamide is not a substrate for renal organic anion transporters (OATs) and does not exhibit OAT-dependent cytotoxicity," *Antiviral Therapy*, vol. 19, no. 7, pp. 687–692, 2014, doi: 10.3851/IMP2770.

[25] G. Birkus *et al.*, "Cathepsin A Is the Major Hydrolase Catalyzing the Intracellular Hydrolysis of the Antiretroviral Nucleotide Phosphonoamidate Prodrugs GS-7340 and GS-9131," *Antimicrobial Agents and Chemotherapy*, vol. 51, no. 2, pp. 543–550, Feb. 2007, doi: 10.1128/AAC.00968-06.

[26] U.S. Food & Drug Administration, "Drug Approval Package, Stribild, Fixed Dose," 2012. https://www.accessdata.fda.gov/drugsatfda_docs/nda/2012/203100Orig1s000TOC.cfm#:~:text =Approval Date%3A 08%2F27%2F2012 (accessed Oct. 29, 2020).

[27] U.S. Food & Drug Administration, "GENVOYA (elvitegravir, cobicistat, emtricitabine, and tenofovir alafenamide) fixed-dose combination tablet.," 2015. https://www.accessdata.fda.gov/drugsatfda_docs/nda/2015/207561Orig1s000Approv.pdf (accessed Oct. 29, 2020).

6

[28] S. Ramanathan, A. A. Mathias, P. German, and B. P. Kearney, "Clinical pharmacokinetic and pharmacodynamic profile of the HIV integrase inhibitor elvitegravir," *Clinical Pharmacokinetics*, vol. 50, no. 4, pp. 229–244, 2011, doi: 10.2165/11584570-000000000-00000.

[29] OECD, *Guidance Document on Good In vitro Method Practices (GIVIMP)*. OECD, 2018. doi: 10.1787/9789264304796-en.

[30] A. Petrosyan *et al.*, "A glomerulus-on-a-chip to recapitulate the human glomerular filtration barrier," *Nature Communications*, vol. 10, no. 1, 2019, doi: 10.1038/s41467-019-11577-z.

[31] H. T. Lee and C. W. Emala, "Protective effects of renal ischemic preconditioning and adenosine pretreatment: Role of A1 and A3 receptors," *American Journal of Physiology - Renal Physiology*, vol. 278, no. 3 47-3, pp. 380–387, 2000, doi: 10.1152/ajprenal.2000.278.3.f380.

[32] L. Del Vecchio and F. Locatelli, "Hypoxia response and acute lung and kidney injury: possible implications for therapy of COVID-19," *Clinical Kidney Journal*, vol. 13, no. 4, pp. 494–499, 2020, doi: 10.1093/ckj/sfaa149.

[33] H. Ryan and C. S. Simmons, "Potential Applications of Microfluidics to Acute Kidney Injury Associated with Viral Infection," *Cellular and Molecular Bioengineering*, vol. 13, no. 4, pp. 305–311, 2020, doi: 10.1007/s12195-020-00649-6.

[34] S. Li *et al.*, "Development and Application of Human Renal Proximal Tubule Epithelial Cells for Assessment of Compound Toxicity," *Current Chemical Genomics and Translational Medicine*, vol. 11, no. 1, pp. 19–30, Feb. 2017, doi: 10.2174/2213988501711010019.

[35] M. J. Wilmer *et al.*, "Novel conditionally immortalized human proximal tubule cell line expressing functional influx and efflux transporters," *Cell and Tissue Research*, vol. 339, no. 2, pp. 449–457, 2010, doi: 10.1007/s00441-009-0882-y.

[36] J. Faria, S. Ahmed, K. G. F. Gerritsen, S. M. Mihaila, and R. Masereeuw, "Kidney-based *in vitro* models for drug-induced toxicity testing," *Archives of Toxicology*, vol. 93, no. 12, pp. 3397–3418, 2019, doi: 10.1007/s00204-019-02598-0.

[37] K. M. Stray *et al.*, "Evaluation of the effect of cobicistat on the *in vitro* renal transport and cytotoxicity potential of tenofovir," *Antimicrobial Agents and Chemotherapy*, vol. 57, no. 10, pp. 4982–4989, 2013, doi: 10.1128/AAC.00712-13.

[38] P. C. Breda *et al.*, "Renal proximal tubular epithelial cells exert immunomodulatory function by driving inflammatory CD4 T cell responses," *Am J Physiol Renal Physiol*, vol. 317, pp. 77–89, 2019, doi: 10.1152/ajpre.

[39] C. Sakolish *et al.*, "Technology Transfer of the Microphysiological Systems: A Case Study of the Human Proximal Tubule Tissue Chip," *Scientific Reports*, vol. 8, no. 1, Dec. 2018, doi: 10.1038/s41598-018-33099-2.

[40] M. J. Ryan, G. Johnson, J. Kirk, S. M. Fuerstenberg, R. A. Zager, and B. Torok-Storb, "HK-2: An immortalized proximal tubule epithelial cell line from normal adult human kidney," *Kidney International*, vol. 45, no. 1, pp. 48–57, 1994, doi: 10.1038/ki.1994.6.

[41] J. Jansen *et al.*, "A morphological and functional comparison of proximal tubule cell lines established from human urine and kidney tissue," *Experimental Cell Research*, vol. 323, no. 1, pp. 87–99, 2014, doi: 10.1016/j.yexcr.2014.02.011.

6

[42] M. Wieser *et al.*, "hTERT alone immortalizes epithelial cells of renal proximal tubules without changing their functional characteristics," *American Journal of Physiology - Renal Physiology*, vol. 295, no. 5, pp. 1365–1375, 2008, doi: 10.1152/ajprenal.90405.2008.

[43] M. K. Vormann *et al.*, "Implementation of a Human Renal Proximal Tubule on a Chip for Nephrotoxicity and Drug Interaction Studies," *Journal of Pharmaceutical Sciences*, pp. 1–14, 2021, doi: 10.1016/j.xphs.2021.01.028.

[44] R. Voglauer *et al.*, "Establishment of human fibroma cell lines from a MEN1 patient by introduction of either hTERT or SV40 early region.," *International journal of oncology*, vol. 26, no. 4, pp. 961–970, 2005, doi: 10.3892/ijo.26.4.961.

[45] K. Kandasamy *et al.*, "Prediction of drug-induced nephrotoxicity and injury mechanisms with human induced pluripotent stem cell-derived cells and machine learning methods," *Scientific Reports*, vol. 5, no. January, pp. 1–15, 2015, doi: 10.1038/srep12337.

[46] F. Schutgens *et al.*, "Tubuloids derived from human adult kidney and urine for personalized disease modeling," *Nature Biotechnology*, vol. 37, no. 3, pp. 303–313, 2019, doi: 10.1038/s41587-019-0048-8.

[47] H. Bark and C. H. Choi, "Psc833, cyclosporine analogue, downregulates MDR1 expression by activating JNK/c-Jun/AP-1 and suppressing NF-κB," *Cancer Chemotherapy and Pharmacology*, vol. 65, no. 6, pp. 1131–1136, 2010, doi: 10.1007/s00280-009-1121-7.

[48] E. Jouan, M. Le Vee, C. Denizot, G. Da Violante, and O. Fardel, "The mitochondrial fluorescent dye rhodamine 123 is a high-affinity substrate for organic cation transporters (OCTs) 1 and 2," *Fundamental and Clinical Pharmacology*, vol. 28, no. 1, pp. 65–77, 2014, doi: 10.1111/j.1472-8206.2012.01071.x.

[49] R. Yumoto, T. Murakami, Y. Nakamoto, R. Hasegawa, J. Nagai, and M. Takano, "Transport of Rhodamine 123, a P-glycoprotein substrate, across rat intestine and Caco-2 cell monolayers in the presence of cytochrome P-450 3A- related compounds," *Journal of Pharmacology and Experimental Therapeutics*, vol. 289, no. 1. pp. 149–155, 1999.

[50] K. A. Homan *et al.*, "Bioprinting of 3D Convoluted Renal Proximal Tubules on Perfusable Chips," *Scientific Reports*, vol. 6, pp. 1–13, 2016, doi: 10.1038/srep34845.

[51] C. Jensen and Y. Teng, "Is It Time to Start Transitioning From 2D to 3D Cell Culture?," *Frontiers in Molecular Biosciences*, vol. 7, no. March, pp. 1–15, 2020, doi: 10.3389/fmolb.2020.00033.

[52] M. J. Bissell, H. G. Hall, and G. Parry, "How does the extracellular matrix direct gene expression?," *Journal of Theoretical Biology*, vol. 99, no. 1, pp. 31–68, 1982, doi: 10.1016/0022-5193(82)90388-5.

[53] C. Frantz, K. M. Stewart, and V. M. Weaver, "The extracellular matrix at a glance," *Journal of Cell Science*, vol. 123, no. 24, pp. 4195–4200, 2010, doi: 10.1242/jcs.023820.

[54] C. Alexakis, P. Maxwell, and G. Bou-Gharios, "Organ-specific collagen expression: Implications for renal disease," *Nephron - Experimental Nephrology*, vol. 102, no. 3–4, pp. 71–75, 2006, doi: 10.1159/000089684.

[55] B. Singh, C. Fleury, F. Jalalvand, and K. Riesbeck, "Human pathogens utilize host extracellular matrix proteins laminin and collagen for adhesion and invasion of the host," *FEMS Microbiology Reviews*, vol. 36, no. 6, pp. 1122–1180, 2012, doi: 10.1111/j.1574-6976.2012.00340.x.

[56] C. Kaya and B. Sahin, "The Role of Extracellular Matrix Proteins in the Urinary Tract: A Literature Review," in *Composition and Function of the Extracellular Matrix in the Human Body*, vol. i, no. tourism, InTech, 2016, p. 38. doi: 10.5772/62807.

[57] J. M. Catania, G. Chen, and A. R. Parrish, "Role of matrix metalloproteinases in renal pathophysiologies," *American Journal of Physiology - Renal Physiology*, vol. 292, no. 3, 2007, doi: 10.1152/ajprenal.00421.2006.

6

6

Addendum

Nederlandse Samenvatting

Curriculum Vitae

List of Publications

Acknowledgements

A

Nederlandse Samenvatting

Ontwikkeling van een Kidney-on-a-Chip platform

Het aantal verschillende 3D-modellen van menselijk weefsel gebruikt voor medisch onderzoek is de laatste jaren opmerkelijk toegenomen. Dit is een ontwikkeling die wordt voortgestuwd door de beperkingen van 2D-celkweek, het streven om dierproeven te verminderen en te vervangen, en het kleine percentage geneesmiddelen in ontwikkeling dat in klinische proeven wordt opgenomen. 2D-celkweekmodellen van de nier kunnen nefrotoxiciteit niet nauwkeurig voorspellen, omdat de cellen die worden gekweekt in deze modellen enkele fysiologisch relevante kenmerken missen. Deze kenmerken omvatten correcte polarisatie van de cellen en de mogelijkheid om te kweken op een permeabel oppervlak dat lijkt op de extracellulaire matrix (ECM) met zijn interstitiële vloeistof aan de basale zijde en de blootstelling van de cellen aan schuifspanning aan de apicale zijde van het celmembraan. Er zijn zowel ethische als fysiologische redenen om dierproeven in geneesmiddelenonderzoek te verminderen. Druk vanuit de samenleving, maar ook de almaar stijgende kosten van dierproeven, ondersteunen het streven om alternatieven te ontwikkelen. Daarnaast zijn er significante verschillen tussen fysiologie van mens en dier, bijvoorbeeld voor de nier is er een verschil in expressie van belangrijke transporteiwitten van chemische verbindingen zo als medicijnen. Ten slotte, wanneer diermodellen de menselijke reactie op de geteste geneesmiddelen onjuist voorspellen en toxiciteit pas achteraf kan worden gedetecteerd tijdens klinische tests, kan dit leiden tot hoge kosten of zelfs erger tot gezondheidsbedreigende problemen bij de mens.

Het doel van dit proefschrift was om een *in vitro* model te ontwikkelen waarmee het mogelijk is om de veiligheid en werkzaamheid van een reeks geneesmiddelen te bestuderen.

In hoofdstuk 2 beschrijven we de ontwikkeling van een model dat de meeste van de hierboven genoemde punten combineert. Humane Renal Proximal Tubule Epithelial Cells (RPTEC) werden gezaaid om buisvormige structuren te vormen tegen een collageen 1-gel in de OrganoPlate® 3-lane. Vloeistofschuifspanning werd vergeleken door het introduceren van een bidirectionele, door zwaartekracht aangedreven stroming door het systeem na plaatsing van de OrganoPlate bovenop een interval rocker systeem. In de aanvullende dataset van hoofdstuk 2 lieten we zien dat perfusie cruciaal is voor buisvorming. Voor de ontwikkeling van ons model hebben we een commercieel verkrijgbare RPTEC-controlecellijn (SA7K-clone) gebruikt. We konden aantonen dat deze cellen de juiste polarisatie vertonen en lekdichte barrières vormen. Polarisatie van cellen werd bevestigd door immunofluorescentiekleuring die één primaire cilium per cel afbeeldde, wijzend naar het lumen van de tubulus. Bovendien waren microvilli, die de borstelrand van de epitheelcellen bedekken, uitsluitend aanwezig op het apicale oppervlak. Met behulp van een immunofluorescente kleuring en een barrière-integriteitstest werd aangetoond dat de RPTEC lekdichte barrières vormden. Er werden tight junctions gevonden bij cel-cel verbindingen, die werden gevisualiseerd met behulp van de tight junction marker zonula occludens (ZO)-1. De

dichtheid van deze verbindingen werd gevalideerd door een barrière-integriteitstest die we ontwikkelden in de loop van dit proefschrift voor het OrganoPlate-systeem. De tubuli werden gespoeld met een medium dat fluorescerende dextrankleurstoffen van verschillende groottes bevatte. De barrièretest opende een breed scala aan mogelijkheden dat we konden gebruiken om ons model te analyseren. We gebruikten deze barrièretest om te bepalen op welk tijdstip na het zaaien de tubuli een lekdichte barrière tegen de collageen 1-gel groeiden en de blootstelling kon beginnen. Verder evalueerden we het nefrotoxische effect van cisplatine, een geneesmiddel waarvan bekend is dat het een schadelijk effect heeft op de proximale tubuli, zowel *in vivo* als *in vitro*. Dosisafhankelijke effecten van de blootstelling aan cisplatine kunnen worden gedetecteerd in een breed scala aan testen.

Het model werd opgezet in de OrganoPlate 3-lane, die toegang tot de tubulus vanaf de basale en de apicale zijde mogelijk maakt. Door deze belangrijke specificatie te combineren met de kenmerken van correcte polarisatie en lekdichte barrières zoals hierboven beschreven, werd het platform gebruikt voor trans-epitheliale transportexperimenten. Er werden twee verschillende methoden gebruikt om actief transport van kationische verbindingen aan te tonen: het meten van de concentratie van de verbinding intracellulair en trans-epitheliaal transport door het celmembraan. De transportfunctie kon met succes worden geremd, wat het bestaan van actief transport aantoont. Hoewel de transportfunctie van kationen door de RPTEC (SA7K-kloon) kon worden aangetoond, missen deze cellen enkele van de belangrijkste transporters die cruciaal zijn voor het transport van anionen. In hoofdstuk 3 werd een tweede epitheelcelbron geïntroduceerd om dit probleem te verhelpen: conditioneel onsterfelijk gemaakte epitheelcellen van de proximale tubulus die xenobiotische organische aniontransporter 1 (ciPTEC-OAT1) tot overexpressie brengen. Met behulp van ciPTEC-OAT1 konden we een testplatform opzetten dat we konden gebruiken om de toxiciteit van beide actieve transportafhankelijke medicijnen te detecteren; kationen en anionen. Door de twee celtypen te combineren met een breder spectrum van verbindingen en uitleesassays, werd een screeningplatform ontwikkeld, de Nephroscreen. De ontwikkeling van de Nephroscreen was onderdeel van de Nephrotube challenge crackIT die werd georganiseerd door het National Center for the Replacement Refinement & Reduction of Animals in Research (NC3R's). De Nephroscreen was een gezamenlijk project van een consortium bestaande uit 4 verschillende partijen: Mimetas, Fachhochschule Nordwestschweiz, Radboud Universitair Medisch Centrum Nijmegen en Universiteit Utrecht. Het doel van het Nephroscreen-project was om een Proximal Tubulus-on-a-Chip te ontwikkelen dat in staat is om nefrotoxische effecten nauwkeurig te identificeren met behulp van menselijke cellen in een 3D-microfluïdisch platform met hoge doorvoer.

Hiertoe werd de proximale tubuli op in totaal 12 verbindingen gescreend en de toxiciteit hiervan word bepaald. Vier van deze verbindingen waren bekende nefrotoxische middelen die ook werden gebruikt om de verschillende testen op te zetten. Acht verbindingen waren onbekend

omdat ze werden geleverd door de sponsors van het onderzoek. We konden aantonen dat het merendeel van de geleverde verbindingen een nefrotoxisch effect had op de Nephroscreen. Het effect van één verbinding op de Nephroscreen kon alleen worden gedetecteerd tijdens de transportonderzoeken, omdat deze verbinding geen effect had in een van de andere testen. Een tweede verbinding vertoonde een interactie met P-glycoproteïne (P-gp) en een mild effect op een verhoogd niveau van microRNA's (miRNA's), maar wederom geen schadelijk effect op de levensvatbaarheid van de tubulaire integriteit van de tubuli. Een van de verbindingen vertoonde tijdens het eerste onderzoek geen cytotoxiciteit, daarom hebben we het getest in een langdurig experiment waarbij de blootstelling gedurende 11 dagen werd uitgevoerd in plaats van 48 uur. Deze studie toonde aan dat voor sommige verbindingen een langetermijnstudie toxiciteit kan aantonen, die niet werd gedetecteerd in het 48-uursexperiment.

Parallel aan de ontwikkeling van de Nephroscreen is een drug-drug interaction (DDI) studie uitgevoerd op de RPTEC, zoals beschreven in hoofdstuk 4. De studie in hoofdstuk 4 was bedoeld om te bepalen of we onze Proximale Tubulus-on-a-Chip konden gebruiken in een DDI-onderzoek. Met behulp van enkele multiplex-assays konden wij de toxiciteit van enkelvoudige en gecombineerde doseringen van op het humaan immunodeficiëntievirus (HIV) gerichte geneesmiddelen onderzoeken. HIV-patiënten worden vaak behandeld met het medicijn Genvoya dat haar voorganger Stribild de afgelopen jaren heeft vervangen. Beide zijn geneesmiddelen die tenofovir bevatten en worden geleverd in pilvorm. Ze bevatten een combinatie van werkzame stoffen, namelijk emtricitabine, elvitegravir en cobicistat, en een van de prodrugs van tenofovir, tenofovirdisoproxilfumaraat (TDF) of tenofoviralafenamide (TAF). Van alle ingrediënten in deze combinaties wordt met name de nefrotoxiciteit van tenofovir algemeen aanvaard. Ons doel was om te onderzoeken of we een toxisch effect op de proximale tubuluscellen konden detecteren door een van de twee tenofovir-prodrugs, vooral in combinatie met een van de additieve verbindingen. Een belangrijk verschil tussen deze twee prodrugs is dat TDF niet stabiel is wanneer het in contact komt met menselijk plasma, waar het snel hydrolyse ondergaat tot tenofovir, terwijl TAF een veel hogere stabiliteit heeft, wat resulteert in een hogere antivirale activiteit en lagere doseringen in vergelijking met TDF. In hoofdstuk 3 konden we aantonen dat de oorspronkelijke vorm van tenofovir een cytotoxisch effect had op ciPTEC-OAT1 terwijl er geen effect kon worden gemeten op RPTEC. Aangezien de oorspronkelijke vorm van tenofovir via de anionroute (voornamelijk via OAT1) in de cellen wordt getransporteerd, was dit een verwacht resultaat. In de huidige studie hebben we echter RPTEC gebruikt. Toen we de twee prodrugs testten, leidde TDF niet tot een schadelijk effect op de proximale tubuli, wat verwacht werd gezien het feit dat TDF in tenofovir wordt gehydrolyseerd wanneer het in contact komt met kweekmedium. Interessant genoeg vertoonde TAF een schadelijk effect op de proximale tubuli bij vergelijkbare concentraties waarvan we maten dat deze toxisch waren voor tenofovir in de OAT1-expressiecellen. Deze resultaten lieten ons zien dat de verbinding TAF inderdaad stabiel is in contact met serum en geen hydrolyse ondergaat in de oorspronkelijke vorm van tenofovir.

De twee prodrugs van tenofovir worden niet afzonderlijk toegediend, maar in combinatie met drie andere antiretrovirale middelen, namelijk elvitegravir, cobicistat en emtricitabine. Naast het testen van de twee prodrugs in enkelvoudige doseringen, voerden we een gelijktijdige behandeling van de prodrugs uit met als doel te beoordelen of een van hen het cytotoxische effect van de twee tenofovir-prodrugs versterkt. Onze resultaten suggereren dat zelfs bij hoge concentraties emtricitabine geen schadelijk effect had op de proximale tubuli, afzonderlijk of in combinatie met een van de twee prodrugs van tenofovir. Elvitegravir had geen versterkend effect op de cytotoxiciteit bij toediening in combinatie met TDF. Wanneer het echter samen met TAF werd gedoseerd, versterkte elvitegravir het schadelijke effect ervan sterk en werden superadditieve synergetische effecten gemeten. Een combinatie met TDF leidde tot een verhoogde schade die in alle testen kon worden gedetecteerd. Een combinatie van cobicistat en TAF leidde tot een verhoogde cytotoxiciteit die werd gedetecteerd voor zowel de laag als de hoog gedoseerde combinaties.

In hoofdstukken 2-4 hebben we ons vooral gericht op acuut nierletsel (AKI) als gevolg van een acute reactie op een nefrotoxisch middel. Naast deze toxische modellen waren we ook geïnteresseerd in het ontwikkelen van een ziektemodel voor behandelingsgerelateerde toxiciteit waarmee we de beschermende werking van medicijnen kunnen screenen. Om dit te bereiken hebben we 3 nieuwe aspecten aan ons model toegevoegd die we beschreven in hoofdstuk 5: co-cultuur met een bloedvat, inductie van AKI veroorzaakt door een ischemische gebeurtenis, en de beoordeling van verbindingen die een beschermend effect hebben tijdens de ischemische gebeurtenis die leidt tot AKI. Voor de ontwikkeling van het co-cultuurmodel hebben we het Kidney-on-a-Chip model dat ontwikkeld is in hoofdstuk 2 uitgebreid door endotheelcellen in het tweede perfusiekanaal te introduceren. We karakteriseerden de cultuur met behulp van immunokleuring voor celtype-specifieke markers en zorgden voor correcte polarisatie. We hebben AKI-geassocieerde uitlezingen gevalideerd door blootstelling van de co-cultuur aan bekende nefrotoxische stoffen. Om ischemische gebeurtenissen in de nier te bestuderen, werd de co-kweek blootgesteld aan ischemie door een combinatie van lage zuurstof, verminderde glucose en het stoppen van de perfusie. Vervolgens werden kweken onder normale omstandigheden opnieuw geperfuseerd om reperfusieschade te veroorzaken. De schade werd gekwantificeerd door middel van morfologische beoordeling, caspase-3/7-activering, beoordeling van de levensvatbaarheid en afgifte van lactaatdehydrogenase. Lage zuurstof, verminderde glucose en onderbroken doorstroming waren schadelijk voor de tubuli in elke combinatie van twee, terwijl de combinatie van alle drie tot de meest ernstige schade leidde. Dit effect werd flink versterkt na reperfusie. Het effect van ischemische aandoeningen op het endotheel was minder ernstig dan op het epitheel.

Voor de beoordeling van beschermende verbindingen werden adenosine, nicotinamide of N-acetylcysteïne toegevoegd aan het kweekmedium van de proximale tubulus en het bloedvat

tijdens de blootstelling en reperfusie. Adenosine bleek een significant beschermend effect te hebben, terwijl een dergelijk effect niet werd gevonden voor nicotinamide en N-acetylcysteïne.

In hoofdstuk 5 waren we in staat om aan te tonen dat AKI geïnduceerd door nierischemie/reperfusieschade (rIRI) effectief kan worden gemodelleerd in deze geperfuseerde 3D nier-cokweek. De robuustheid van het model en de testen in combinatie met de doorvoer van het platform maken het ideaal om het effect van AKI-voorkomende verbindingen te bestuderen en de ontwikkeling van nieuwe therapeutische behandelingsmethodes mogelijk te maken.

Conclusie

Farmaceutische bedrijven, regeringen en het grote publiek zijn zich er steeds meer van bewust dat diermodellen die worden gebruikt bij het testen van geneesmiddelen een aantal essentiële aspecten missen om te dienen als een nauwkeurige weergave van de menselijke biologie. Omdat deze modellen van het menselijk lichaam fysiologisch relevanter zouden moeten zijn, voldoen diermodellen niet meer omdat de reactie van dierlijke cellen vaak verschilt van de reactie van menselijke cellen. In plaats daarvan zijn *in vitro* celkweekmodellen die beschikken over 3D-architectuur, microfluïdica en hoge doorvoercapaciteiten een veelbelovende technologie en treden ze momenteel steeds meer op de voorgrond van geneesmiddelenonderzoek. Deze 3D-modellen kunnen op zo'n manier worden ontwikkeld dat ze waarschijnlijk diermodellen zullen overtreffen op belangrijke aspecten zoals gelijkenis met het menselijk lichaam, het voorspellen van veiligheid en werkzaamheid van verbindingen, testmogelijkheden met hoge doorvoer, ethische aspecten en kosten.

Om de haalbaarheid van zo'n geavanceerd 3D-invitromodel aan te tonen, hebben we een microfluïdisch *in vitro*-platform gebruikt om een Kidney-on-a-Chip platform te ontwikkelen dat het vermogen heeft om de tubulaire respons op bekende en onbekende nefrotoxische stoffen en verbindingen te reproduceren, zoals gezien in *in vitro* en in klinische studies. Verder hebben we de respons van het model op nierischemie/reperfusieschade beoordeeld en konden we de preventie van tubulaire schade meten bij het toevoegen van beschermende verbindingen.

Deze bevindingen laten zien dat 3D-weefselmodellen kunnen concurreren met alternatieven zoals diermodellen en 2D-modellen. We verwachten dat 3D-weefselmodellen de testplatforms van de toekomst zijn voor het ontwikkelen van nieuwe medicijnen.

Aangezien onderzoek naar 3D-weefselmodellen een relatief nieuw onderzoeksgebied is, blijft er veel ruimte voor verbetering. Het streven om *in vitro* bevindingen te gebruiken om in vivo gedrag met vertrouwen te voorspellen, is bijvoorbeeld een onderzoeksgebied waar 3D-weefselmodellen een belangrijke rol kunnen spelen. Manieren om verschillende menselijke organen op 3D-chips te repliceren, zullen de komende jaren waarschijnlijk sterk verbeteren. Door verschillende chips te combineren en interacties tussen hen te creëren, kan de effectiviteit van medicijnen op een

geheel nieuw niveau worden getest. Op deze manier kan de complexiteit van de *in vitro* 3D-modellen worden vergroot, op manieren die beter lijken op weefselreacties bij mensen.

Dit zou kunnen leiden tot het gelijktijdig testen van een medicijn op verschillende organen, terwijl ze worden verbonden op manieren die lijken op echte structuren in het menselijk lichaam en terwijl de reacties van elk afzonderlijk orgaan worden gemeten. Wanneer deze 3D-weefselmodellen worden gekweekt in een omgeving met hoge doorvoer, kunnen in korte tijd enorme hoeveelheden gegevens worden geproduceerd. Deze gegevens kunnen dienen als basis voor mechanistische modellen met behulp van big data-benaderingen die uiteindelijk kunnen worden gebruikt om de werkzaamheid en veiligheid van geneesmiddelen in vivo snel te voorspellen.

Interessante voorbeelden van complexe toekomstige toepassingen van 3D-weefselmodellen zijn bijvoorbeeld complete *in vitro* gevasculariseerde organoïden, 'body-on-a-chip'-systemen die voor een specifieke test kunnen worden ontworpen om alle relevante weefsels en hun interacties te combineren zodat ze zo goed mogelijk lijken op in vivo reacties. Een ander voorbeeld is het maken van complexe ziektemodellen waarbij de respons van weefsel en hun interacties op een realistische manier kunnen worden getest. Een andere mogelijke toekomstige toepassing van 3D-weefselmodellen is gepersonaliseerde geneeskunde, waarbij een groot aantal replica's van monsters van patiënten in 3D op de microfluïdische chips kunnen worden gekweekt om van deze patiënt afgeleide *in vitro*-modellen te maken. Deze celmonsters kunnen vervolgens worden gescreend op de meest effectieve behandeling voor deze individuele patiënt. Op termijn zou de verdere ontwikkeling van 3D-weefselmodellen kunnen betekenen dat deze voorbeelden geen droom meer zijn, maar werkelijkheid worden.

A

Curriculum Vitae

Marianne Katharina Vormann was born on December 8th 1986 in Gräfelfing, a municipality in the district of Munich, in Bavaria, Germany. After graduating from the pre-university education at Marienschule in Münster (Westfalen) she started with her bachelor studies General Engineering Science at Hamburg University of Technology (TUHH) in 2006. During her bachelor studies she followed the specialization biomedical engineering. She wrote her Bachelor thesis about how to optimize the calculation of radiation doses during radiotherapy of head and neck cancers. Her bachelor studies were followed by a master study in biomedical engineering, also at TUHH. The first year of her master studies she participated in the European exchange program Erasmus and conducted her studies at Chalmers University of Technology in Gothenburg. During her studies in Gothenburg she got fascinated in the field of tissue engineering, in which field she received the opportunity to visit courses and perform small practical projects. Back in Hamburg she continued to work in the field of tissue engineering by conducting her project thesis focusing on cytotoxicity testing on cell cultures at the Institute of Bioprocess and Biosystems Engineering. Realizing that tissue engineering might be an important way to replace animal testing in long term she conducted an 8 months internship under the supervision of Matthias Brandenburg at Fraunhofer Research Institution for Marine Biotechnology EMB in Lübeck. During this internship she worked on a method to prepare stem cells which were isolated from human sweat glands for clinical translation meeting the GMP guidelines.

After obtaining her master's degree in 2013 she started working as a scientist at Mimetas in 2014. In parallel to her work at Mimetas she started in 2015 a PhD at the division of Analytical BioSciences at the LACDR, Leiden University under the supervision of Thomas Hankemeier in collaboration with Mimetas where she was supervised by Henriette Lanz. The project was focused on developing a 3D Kidney-on-a-chip model which can be used for toxicity screenings, transport studies, and disease modeling.

Currently Marianne is still employed at Mimetas as a Scientist. However, she is at this moment on parental leave discovering Europe with a camper together with her family.

A

List of publications

In this thesis - published

MK Vormann, L Gijzen, S Hutter, L Boot, A Nicolas, A van den Heuvel, J Vriend, CP Ng, TTG Nieskens, V van Duinen, B de Wagenaar, R Masereeuw, L Suter-Dick, SJ Trietsch, MJ Wilmer, J Joore, P Vulto, and HL Lanz. 2018. "*Nephrotoxicity and Kidney Transport Assessment on 3D Perfused Proximal Tubules*." AAPS J. Doi: 10.1208/s12248-018-0248-z

MK Vormann*, J Vriend*, HL Lanz, L Gijzen, A van den Heuvel, S Hutter, J Joore, SJ Trietsch, C Stuut, TTG Nieskens, JGP Peters, D Ramp, M Caj, FGM Russel, B Jacobsen, A Roth, S Lu, JW Polli, AA Naidoo, P Vulto, R Masereeuw, MJ Wilmer, L Suter-Dick. 2021. *"Implementation of a Human Renal Proximal Tubule on a Chip for Nephrotoxicity and Drug Interaction Studies."* J Pharm Sci. Doi: 10.1016/j.xphs.2021.01.028. *Authors contributed equally.

In this thesis - Submitted

MK Vormann, LM Tool, M Ohbuchi, L Gijzen, R van Vught, T Hankemeier, F Kiyonaga, T Kawabe, T Goto, A Fujimori, P Vulto, HL Lanz & K Tetsuka. 2021. *"Modelling and prevention of acute kidney injury through ischemia and reperfusion in a combined human renal proximal tubule/blood vessel-on-a-chip."* Kidney360 - In submission.

Other publications

SJ Trietsch, E Naumovska, D Kurek, MC Setyawati, **MK Vormann**, KJ Wilschut, HL Lanz, A Nicolas, CP Ng, J Joore, S Kustermann, A Roth, T Hankemeier, A Moisan, and P Vulto. 2017. "*Membrane-Free Culture and Real-Time Barrier Integrity Assessment of Perfused Intestinal Epithelium Tubes.*" Nat Commun. Doi: 10.1038/s41467-017-00259-3

L Suter-Dick, L Mauch, D Ramp, M Caj, **MK Vormann**, S Hutter, HL Lanz, J Vriend, R Masereeuw, and MJ Wilmer. 2018. "*Combining Extracellular MiRNA Determination with Microfluidic 3D Cell Cultures for the Assessment of Nephrotoxicity: A Proof of Concept Study.*" AAPS J. Doi: 10.1208/s12248-018-0245-2

J Vriend, TTG Nieskens, **MK Vormann**, BT van den Berge, A van den Heuvel, FGM Russel, L Suter-Dick, HL Lanz, P Vulto, R Masereeuw, and MJ Wilmer. 2018. "*Screening of Drug-Transporter Interactions in a 3D Microfluidic Renal Proximal Tubule on a Chip*." The AAPS Journal. Doi: 10.1208/s12248-018-0247-0

F Schutgens, MB Rookmaaker, T Margaritis, A Rios, C Ammerlaan, J Jansen, L Gijzen, **MK Vormann**, A Vonk, M Viveen, FY Yengej, S Derakhshan, KM de Winter-de Groot, B Artegiani, R van Boxtel, E Cuppen, APA Hendrickx, MM van den Heuvel-Eibrink, E Heitzer, HL Lanz, J Beekman, JL Murk, R Masereeuw, F Holstege, J Drost, MC Verhaar and H Clevers. 2019. "*Tubuloids derived from human adult kidney and urine for personalized disease modeling."* Nat Biotechnol. Doi: 10.1038/s41587-019-0048-8

A

J Vriend*, **MK Vormann***, HL. Lanz, J Joore, SJ Trietsch, FGM Russel, B Jacobsen, AB Roth, S Lu, JW Polli, AA Naidoo; R Masereeuw, MJ Wilmer, L Suter-Dick. 2021. "Nephroscreen: a robust and versatile renal tubule-on-a-chip platform for nephrotoxicity assessment." Current Opinion in Toxicology. Doi: 10.1016/j.cotox.2021.03.001. *Authors contributed equally.

L Gijzen, FAY Yengej, F Schutgens, **MK Vormann**, CME Ammerlaan, A Nicolas, D Kurek, P Vulto, MB Rookmaaker, HL Lanz, MC Verhaar & H Clevers. 2021. *"Culture and analysis of kidney tubuloids and perfused tubuloid cells-on-a-chip."* Nat Protoc. Doi: 10.1038/s41596-020-00479-w

Patents

P Vulto, SJ Trietsch, HL Lanz, **MK Vormann**. Barrier Function Measurements. 2017

A

A